# Modifications to gravitational waves due to matter shells

A thesis submitted in fulfilment of the requirements
for the degree of

Doctor of Philosophy (Science)

Rhodes University

Department of Mathematics (Pure & Applied)

by

**Monogaran Naidoo**

Supervised by: Prof. Nigel T. Bishop

April 2021

# Abstract

As detections of gravitational waves (GWs) mount, the need to investigate various effects on the propagation of these waves from the time of emission until detection also grows. We investigate how a thin low density dust shell surrounding a gravitational wave source affects the propagation of GWs. The Bondi-Sachs (BS) formalism for the Einstein equations is used for the problem of a gravitational wave (GW) source surrounded by a spherical dust shell. Using linearised perturbation theory, we find the geometry of the regions exterior to, interior to and within the shell. We find that the dust shell causes the gravitational wave to be modified both in magnitude and phase, but without any energy being transferred to or from the dust. This finding is novel. In the context of cosmology, apart from the gravitational redshift, the effects are too small to be measurable; but the effect would be measurable if a GW event were to occur with a source surrounded by a massive shell and with the radius of the shell and the wavelength of the GWs of the same order. We extended our investigation to astrophysical scenarios such as binary black hole (BBH) mergers, binary neutron star (BNS) mergers, and core collapse supernovae (CCSNe). In these scenarios, instead of a monochromatic GW source, as we used in our initial investigation, we consider burst-like GW sources. The thin density shell approach is modified to include thick shells by considering concentric thin shells and integrating. Solutions are then found for these burst-like GW sources using Fourier transforms. We show that GW echoes that are claimed to be present in the Laser Interferometer Gravitational-Wave Observatory (LIGO) data of certain events, could not have been caused by a matter shell. We do find, however, that matter shells surrounding BBH mergers, BNS mergers, and CCSNe could make modifications of order a few percent to a GW signal. These modifications are expected to be measurable in GW data with current detectors if the event is close enough and at a detectable frequency; or in future detectors with increased frequency range and amplitude sensitivity. Substantial use is made of computer algebra in these investigations. In setting the scene for our investigations, we trace the evolution of general relativity (GR) from Einstein's postulation in 1915 to vindication of his theory with the confirmation of the existence of GWs a century later. We discuss the implications of our results to current and future considerations. Calculations of GWs, both analytical and numerical, have normally assumed their propagation from source to a detector on Earth in a vacuum spacetime, and so discounted the effect of intervening matter. As we enter an era of precision GW measurements, it becomes important to quantify any effects due to propagation of GWs through a non-vacuum spacetime Observational confirmation of the modification effect that we find in astrophysical scenarios involving black holes (BHs), neutron stars (NSs) and CCSNe, would also enhance our understanding of the details of the physics of these bodies.

# Acknowledgements

Prof. Nigel Bishop has been instrumental in seeing this doctoral work through to fruition. Apart from his capacity as supervisor, he has provided encouragement, support and fruitful discussions on general relativity, numerical relativity and cosmology. He has both length and breadth in his subject matter and through this has provided valuable insight into this study. He has also helped with the many administrative tasks that form a part of the completion of this thesis. Furthermore, through his assistance in arranging funding, I have been privileged to attend many local and international conferences and workshops in the field of study.

Dr Peet van der Walt has collaborated on both papers that resulted from this study. His help on these papers, his guidance on the thesis and the many discussions held over lunches have helped immeasurably. His keen interest in the field has kept my interest topical and up to date and his expert code-writing skills were invaluable in this project.

I would like to dedicate this thesis to my mother and to my late-father for this and all other opportunities they made possible. My mother continues to be an inspiration for all that she has achieved.

# Contents

# Chapter 1

# Introduction

*"I was sitting in a chair in the patent office at Bern. Suddenly an idea dawned on me: 'If a man falls freely he will not feel his weight himself.' I felt startled at once. This simple thought left me with a deep impression indeed. It was this deep impression that drove me to the theory of gravitation. "*

Einstein in his Kyoto address (14 December 1922) [1]

In November 1915, on each of the Thursdays of that month, Albert Einstein presented the culmination of a decade of intense work on gravitation to the Prussian Academy of Sciences [2, 3, 4, 5]. The core of his theory of general relativity (GR), were his equations relating the geometry of space and time to matter and radiation [5], which he delivered in his lecture on the final of the four consecutive Thursdays, the 25th of November 1915. Einstein, in his papers, proposed three tests of GR: the precession of Mercury's orbit; the bending of starlight near the Sun and the gravitational redshift of light. The precession of the perihelion of Mercury was already known at that stage, as 574 seconds of arc (arcsec) per century. However, according to Newtonian gravitation, based on the gravitational forces exerted by the planets, the predicted value was 531 arcsec per century. Einstein's calculations, using GR, accounted for this discrepancy, by predicting that the curvature of spacetime around the Sun, would advance the perihelion of Mercury 43 arcsec per century more than that predicted by Newtonian gravity. Einstein's theory of GR provided the best calculated match for the observed value for the precession, where the Newtonian theory of gravity fell short, and put to a rest a decades-old mystery and the search for any elusive planet in the vicinity of Mercury. In spite of this, in the initial years of its existence, the theory did not enjoy wide acceptance. This was compounded by the Great War of 1914 to 1918, which meant that the theory was virtually unknown outside of Germany at that time. The British astronomer Arthur S. Eddington, the Plumian Professor at Cambridge and officer of the Royal Astronomical Society (RAS), did much to popularise Einstein's work on GR to the English-speaking world [6, 7]. Backed by Frank W. Dyson, the Astronomer Royal, Eddington set about convincing the RAS to fund the investigation to corroborate (or disprove) the second of Einstein's proposed tests of GR: that starlight just grazing

the Sun's surface should be deflected by an angle of 1.75 arcsec as calculated using GR. For such a test where one would have to measure the 'deflection' of light rays from a star, whose light rays just graze the sun, a total solar eclipse would be necessary in order to photograph the event. To measure the undeflected light rays from the same star, readings would have to be taken at the same position of the star relative to earth and so would have to be 6 months before or after the solar eclipse (or anytime annually, corresponding to that location). Having secured funding to observe the eclipse of 29 May 1919, two teams were commissioned to observe the eclipse in two different regions where the total eclipse would occur. One expedition was sent to Sobral in Brazil and the other, led by Eddington, to Príncipe, in West Africa. Both teams produced results consistent with Einstein's predictions. Einstein, himself, was very impressed with the results of the expedition. Hendrik Lorentz, who shared the 1902 Nobel prize in Physics, described the results as "*one of the most brilliant confirmations of a theory ever achieved*" [8]. Still, many critics of the theory remained unconvinced. This was clearly reflected by even the Swedish Academy of Sciences, in their reluctance to acknowledge this aspect of Einstein's work in their deliberations on the awarding of the Nobel Prize for Physics to Einstein. Christopher Aurivillius, secretary of the academy, wrote to Einstein: "*...the Royal Academy of Sciences decided to award you last year's [1921] Nobel prize for physics, in consideration of your work in theoretical physics and in particular for your discovery of the law of the photoelectric effect, but without taking into account the value which will be accorded your relativity and gravitation theories after these are confirmed in the future*" [8].

The third of Einstein's tests of GR was only verified in 1960 [9], a few years after his death in 1955. Aside from the three tests of GR proposed by Einstein, which are regarded as the three classical tests of GR, several modern tests of GR were developed. The modern tests include the Shapiro delay (often referred to as the fourth classical test), gravitational time dilation, 'frame dragging' of spacetime, the 'geodetic effect', gravitational lensing and tests of cosmology. However, there was one prediction of Einstein's GR which grew to capture the imagination of the entire world. In 1916, Einstein postulated that a consequence of GR would be the existence of ripples in spacetime: gravitational waves (GWs) [10]. There were certain errors in his paper [10] including an incorrect formula for gravitational radiation and the conclusion that an oscillating spherical mass would produce gravitational radiation in a form known as *monopole radiation*. These were then amended and Einstein presented the correct equation for gravitational radiation in his 1918 paper [11], laying the foundation for the field of GWs. Although the theory predicted it, Einstein had his doubts on whether GWs could ever be detected and even on whether they existed at all. Two decades later, however, together with his assistant Nathan Rosen, he presented further calculations in support of the existence of GWs [12], correcting an error the year before which had initially led to him believing otherwise [13]. According to the theory, GWs, would travel as ripples in space at the speed of light and as they encounter an object (on Earth, for example) would deform the object temporarily through stretching it in one direction and squeezing it in another. The inherent weakness of the gravitational force meant that the detection of the distortion would fall far outside the range of instruments available at the time or even imagined over the coming century. The search for GWs only began in earnestness a couple of years after Einstein's death. Progress on GW research was hampered by Einstein's own ambivalence around the existence of GWs together with the slow acceptance that BHs could exist. It is ironic that, for the latter, Eddington was the culprit for this slow acceptance. In the 1930's, Subrahmanyan Chandraskekhar, who was then an emerging astro-

physicist, through combining consideration in GR and quantum mechanics (QM), theorised a critical mass now called the **Chandrasekhar limit** $\sim 1.4M_{\odot}$ [14]. In the case where the 'gravitational' forces cause a star to collapse onto itself, this critical mass of the star determines whether the outward electron degeneracy pressure, a QM effect which is reached when the star reaches a certain density, would be adequate to 'balance' the inward gravitational collapse. Below the Chandrasekhar limit, an imploding star could continue to exist in the form of a white dwarf (WD) in this stable "balancing act." However, if the final mass is above this critical mass then the star would not be able to exist as a stable WD and this collapse with a BH being a possible result. Strong theoretical evidence for the existence of such highly compact bodies as BHs would have reignited the waning interest in GWs. Eddington openly criticised Chandrasekhar's work on the critical mass of WD's [15] and given the stature of Eddington compared with the young Indian astrophysicist, Chandrasekhar's work received little support from the scientific community at large. Arthur Miller's biography on Chandrasekhar, entitled *Empire of the Stars: Obsession, Friendship, and Betrayal in the Quest for Black Holes*, encapsulates this prejudice:
"*Chandra's discovery might well have transformed and accelerated developments in both physics and astrophysics in the 1930s. Instead, Eddington's heavy-handed intervention lent weighty support to the conservative community astrophysicists, who steadfastly refused even to consider the idea that stars might collapse to nothing. As a result, Chandra's work was almost forgotten.* [16]. It was only in the 1950's that a revival in the interest in GWs surfaced. The first in a series of international conferences exclusively for GR began in Bern, Switzerland in 1955 followed by the 1957 conference held at the University of North Carolina at Chapel Hill, USA entitled "*The role of gravitation in Physics*" [17]. These conferences were later to be referred to retrospectively as **GR0** and **GR1**, the series of Gravitation and General Relativity conferences, referred to as GR conferences, that continue to be held, the most recently being the 22nd edition, GR22, held in Valencia, Spain. Both these conferences reignited the interest in GR and GWs in particular and were the catalyst for the building of GW detectors to search for GWs.

At the North Chapel conference, held from 18 to 23 January 1957, the newly appointed head of the institute, DeWitt, provided a catalyst for the growth of NR by tackling the subject of electronic computers being used to solve gravitation equations and the issues likely to be faced in scheduling them for calculations. Hermann Bondi, the King's College physicist, led discussions on the question of whether or not a gravitational pulse passing through/by a particle would transmit energy to the particle. Caltech Physicist Richard Feynman (who had Wheeler as his doctoral adviser at Princeton) produced a compelling argument based on a thought experiment in the tradition Einstein was famous for ("gedankenexperiment") supporting the argument that GWs carry energy. Joseph Weber, who was then an engineer at the University of Maryland, intrigued by these discussions would go on, together with his students Robert Forward and David Zipoy, to build the first GW Detector [18]. Years later, Weber's student Robert Forward, working at the Hughes Research Laboratory in Malibu, California, and encouraged by Rainer Weiss, designed the first interferometer prototype in 1971, referred to as a "Transducer Laser", with arms of 8.5 m. Rainer Weiss was the first to suggest that the arms of the interferometer needed to be several kilometres long in order to be able to detect GWs. This idea propelled the development of prototype GW detectors and formed the basis of configurations of current day detectors and those planned for the coming decades. Several different groups, built on Weber's and Forward's designs, testing interferometers of various armlength prototypes. Plans for full-

sized interferometers gained momentum in the 1980's from other groups, one in in Germany [19] and another in Glasgow, UK, which had initially been led by Ronald Drever [20] (who remained actively involved in the group after his leadership ended). Both the British and German groups, struggling to obtain funding for their projects, joined forces and, in 1994, proposed a 600-m detector [21] which eventually resulted in the GW detector GEO600. A Franco-Italian group based in Orsay and Pisa proposed the idea of a single European detector to the German team, which was German group, leading to the French and Italian group pursuing their own collaborative effort, the VIRGO Interferometer. In the USA, physicist Kip Thorne had set up an interferometer group at Caltech, recruiting Drever to work on the construction of an interferometer, whilst Weiss set up a team at MIT. By 1983, Drever had succeeded in building a 40 m interferometer. At MIT, the team led by Weiss, embarked on a study of a interferometer on the scale of kilometres. The result of their study was presented to the National Science Foundation (NSF) in October 1983, in which they proposed the construction of two separate interferometers in the USA. The joint project by the Caltech and MIT teams was named the "Laser Interferometer Gravitational-Wave Observatory" (LIGO) and was to be led by Thorne, Weiss, and Drever, with project leadership eventually falling solely to Barry Barrish. He proposed the construction of an "initial LIGO" (iLIGO), for testing and data gathering, with the remote possibility of a GW detection and an evolved, refined, enhanced version "advanced LIGO" (aLIGO) to be built at the second stage [22]. LIGO would consist of two interferometers one in Hanford, Washington, the other 1900km away in Livingston, Louisiana. Detection runs took place from 2002 to 2010 without any detections and the second phase construction began in 2010 and was completed five years later in 2015. aLIGO began operating in test mode starting in February 2015 in preparation for scientific observations scheduled to start on 18 September 2015. Whilst still in test mode, undergoing the last preparations days before the scientific runs were to begin, aLIGO made the first detection of a GW at around 4:50 am local time on 14 September 2015. The event was referred to as GW150914 [23], reflecting the date of detection and that the event was that of a GW. The source for this signal was the merger of two BHs and the signal had travelled for over a billion years before impinging on each of the detectors of aLIGO.

Subsequent to this initial discovery, the twin aLIGO observatories responsible for the first discovery made several further detections of GW signals from coalescing compact binaries [24, 25]. Detection with two interferometers, separated geographically, help filter local disturbances and corroborate the extra-terrestrial origin of a signal. However, a third detector would be needed to triangulate the signal, providing a better guide to the location of the source of the gravitational waves detected. aVIRGO located near Pisa, Italy, provided this opportunity when it came online in 2016. The aLIGO and aVIRGO detectors, on 14 August 2017, jointly observed the GW event GW170814, which was the BBH merger. Three days later, on 17 August, the first detection of a BNS merger was made, the GW event GW170817. This was profound for the era of Multi-messenger Astronomy (MMA). While BH mergers do not produce currently discernible electromagnetic (EM) signals, the same is not true for BNS mergers. The detection of GW170817 by aVIRGO, together with the two aLIGO detectors, allowed triangulation of the signal leading to pinpointing the location of the signal. This allowed other terrestrial and space-based detectors to train their focus in the direction of GW170817, to lie in wait for signals of trailing events in the EM spectrum [26, 27]. The subsequent signals provided a wealth of information on the BNS merger, on the compositions of the compact bodies and on population

synthesis. As detections of mergers of compact bodies begin to flow in, our understanding of compact bodies, their physics and that of the surrounding astrophysical environment, will continue to grow and at times even challenge previously long held notions. The GW event, GW190814, involving a BH, of mass 23 $M_\odot$ and a smaller compact body, of mass 2.6 $M_\odot$ challenged previously expected mass limits for BHs and NSs. The 2.6 $M_\odot$ body falls outside the expected lower bound for a BH and above the expected upper bound for a NS, placing questions on the previously thought of upper limit of mass of a NS. The object would then either be an extremely heavy NS (beyond the upper bound mass of NSs predicted by theory) or it could be a BH that is too light (lighter than the lower bound expected by theory).

On the other hand, the GW event, GW190521, reported by aLIGO and aVIRGO, seems to suggest a pre-merger candidate in the pair-instability supernova (PISN) gap. The short GW signal detected has been postulated to be the consequence of the merger of a quasi-circular BBH, with a remnant BH of mass $\mathrm{M}_f \sim 142\ \mathrm{M}_\odot$. This is the first ever observed intermediate-mass black hole (IMBH) [28]. Dark matter candidates have been postulated as alternatives in this scenario [29].

As we fully immerse into this era of GW detection, we will need to prepare for other expected (and unexpected) challenges. An extended discussion on GW detectors and detections will be found in Chapter 5.

Calculations of GWs, both analytical and numerical, normally assume that they propagate from source to a detector on Earth in a vacuum spacetime. Although the average cosmological density of baryonic plus dark matter is small, of order $10^{-29}\mathrm{g/cm}^3$, a detected GW event may be a considerable distance away from its source, up to order 1 Gpc, and the quantity of intervening matter is not negligible. Further, it is possible that the astrophysical environment of a source event could be such that the source is surrounded by a substantial amount of matter. Thus, as we move into an era of precision GW measurements, it is important to quantify any effects due to propagation of GWs through a non-vacuum spacetime. In Chapter 6 we consider the problem of a GW source in a spacetime that is empty apart from matter contained in a thin shell around the source (then, results for a thick matter shell can be modelled by adding up, i.e. integrating, over thin shells). As a first step, the shell is given the simplest equation of state, i.e., that of dust. It is found that the effect of the shell is to modify the outgoing GWs in both phase and magnitude, although in a way that does not contradict previous results about energy transfer. The modification of the GW is small, and in a cosmological context is not expected to be measurable; but it is possible that a GW event could occur in which the local astrophysical environment is such that the effect would be measurable. Further, there is a view that LIGO data for BBH mergers may contain echoes, and explanations investigated, using numerical simulations, have included new physics near the event horizon, and the astrophysical environment such as a shell around the system; see, e.g., [30, 31]; this matter is discussed further in Sec. 7.6. In any case, the results are certainly of interest to the theory of GWs propagating in matter.

At the quantum level, Hawking's information paradox suggests Planck-scale modifications of BH horizons (firewalls [32]) and other modifications to BH structure (fuzzballs [33]). Dark matter particles have been suggested surrounding star-like objects [34]. Other postulations include stars with interiors consisting of self-repulsive, de Sitter spacetime, surrounded by a

shell of ordinary matter (gravastars [35]). Then there are Boson stars, which are macroscopic objects made up of scalar fields [36]. All these objects may be classified as Exotic Compact Objects (ECOs), compact bodies mimicking BH, but without a horizon. One consequence of these horizonless structures is that ingoing gravitational waves produced in a merger may reflect multiple times off effective radial potential barriers. The gravitational waves may be, in effect, trapped between effective radial potential barriers causing the waves to be 'bounced' off these barriers several times with wave packets leaking out to infinity at regular times. These gravitational wave signals, 'trailing' the main (outward bound) signal are referred to as echoes. [37, 38, 39].

There have already been tentative claims of the detection of GW echoes such as those from [40] asserting that LIGO has observed echoes in the binary BH waveforms. These claims have been contested [41, 42], sparking a debate and responses in defence of the claims [43, 44] with further substantiations [45, 46]. In Sec. 7.5, we discuss these claims and the arguments contesting them, together with the elaborations in the defence of the claims.

Whilst this debate around GW echoes revolves suggests 'new physics', the likelihood that the echoes may be a consequence of the astrophysical environment, needs to be investigated further. One such scenario is the effect of a matter shell surrounding the GW source, In Chapter 6 and as published in [47], we show that a thin spherical dust shell surrounding a GW source, causes the GW to be modified both in magnitude and phase, but without any energy being transferred to or from the dust. In Chapter 6 we describe the problem considered in the given scenario, the assumptions made and the key results. These considerations are extended in Chapter 7 to investigate whether matter shells can lead to GW echoes and if they do, whether they will be detectable within current instrumentation sensitivity or expected increased sensitivity in the next decade or two. We extend the discussion to various astrophysical scenarios such as those involving BBHs, BNSs and CCSNe.

We arrange this thesis by first giving a background to the theory of GR and providing the important equations to the theory in Chapter 2. The theory of GWs, as a consequence of GR, is also discussed in Chapter 2. Next, in Chapter 3 we discuss some important formalisms of the theory, especially the BS formalism. Astrophysical scenarios that are likely to produce GWs are discussed in more detail in Chapter 4. In Chapter 5, we describe the development of GW detectors and the detections that have been successfully made. The effect of a shell of matter surrounding a gravitational source is discussed in Chapter 6 which is an extension of the discussion in [47]. The model in Chapter 6 is then adapted in Chapter 7, to include astrophysical scenarios where matter shells may surround events such as compact binary mergers and CCSNe. Parts of Chapter 7 have been presented in [48]. Chapters 6 and 7 represent original work with the two collaborators mentioned in Ref. [47] and [48]. All results are summarised in Chapter 8 and prospects for further investigation are discussed. All code that is used is provided in the Appendices so that any of the results in this thesis may be reproduced by the reader.

## 1.1 Some preliminaries: conventions, units, abbreviations

Notation in GR varies from author to author and this thesis tries to remain faithful to the conventions most consistent in the literature. This thesis uses notation in texts widely accepted as providing foundations in GR such as [49, 50, 51, 52]. For the BS formalism in NR, preference is given to the notation used in the widely cited [53, 54].

Any changes in symbols that may create confusion are clearly pointed out in the text. Furthermore, a list of symbols used is given in Appendix B together with their specific contexts. Occasionally, where the use of symbol in its common form may clash with another, an alternative form is given. For differentiation, partial derivatives are denoted by $\partial$ or a comma "," and covariant derivatives by $\nabla$ or a semi-colon ";". Spatial derivative are indicated as $A' = A_{,r}$ and temporal derivatives $\dot{A} = A_{,t}$. The choice of convention used is based on the prominence in literature. For units we will confine ourselves to geometrised units, $G = c = 1$, where $G$ is the gravitational constant and $c$ is the speed of light, unless specified otherwise. In the few instances where the values of these constants have significance in providing the appreciation of the scale of a quantity then these are given in their usual units. For the metric $g_{\alpha\beta}$, the signature $(-,+,+,+)$ is exclusively used. The conventions used in Chapter 2 are:

- Greek letters $\alpha, \beta, \gamma, \ldots$ denote spacetime indices 0,1,2,3.
- Small Latin letters $i, j, k, \ldots$ denote spatial indices 1,2,3.
- Capital Latin letters $A, B, C, ...$ denote angular indices 2,3.

The summation rule for tensors is followed where the $\Sigma$ symbol is implied when superscript and subscript indices are repeated.

Regarding the use of abbreviations: commonly used abbreviations are given with the first instance of their use written in full. A summary of the abbreviations used is given in Appendix A. Where an abbreviation refers to an object, that may take on a plural form, then only the singular instance is given in the Appendix and the plural use should be obvious in the text. The plural form will take on an 's' (or an 'e'), such as **BH** in the Appendix, for a **black hole** will occur as **BHs** for **black holes** in the text.

# Chapter 2

# Einstein's general relativity

*"The theory of relativity marks all in all one term: it is the achievement of a physics of cartesian spirit that gives an account of the phenomena by figures and by motions... One hears today the saying that we live in the atomic era. Should we not also speak of the relativistic era?"*

André Mercier, secretary of the Berne Conference (later known as the GR0 Conference), in his foreword to the proceedings [55] as translated in Ref. [56].

Albert Einstein presented the culmination of a decade of intense work on gravitation to the Prussian Academy of Sciences in November 1915. Core to the theory was his equations relating the geometry of space and time to matter and radiation. These equations, which have subsequently come to be aptly named the Einstein Field Equations (EFEs), are non-linear and have proved extremely difficult to solve. Even though solutions exist locally, the equations can still be regarded as unsolved at a global level. In a century since their introduction, for most astrophysical scenarios of interest, brute force remains the primary means of solution and even then, current resources do not allow a full simulation. However, the Theory of General Relativity is widely accepted and with the recent proof of the existence of gravitational waves, the theory may be considered to be finally vindicated. This was hardly the case in the initial years of the theory's existence as reflected by even the Swedish Academy of Sciences in their reluctance to acknowledge this aspect of Einstein's work in their deliberations on the awarding of the Nobel Prize for Physics. This was in spite of the results of the 1919 eclipse expeditions [57] which confirmed one of the predictions of Einstein's General Relativity (the bending of light). Niels Bohr, a previous recipient of the Nobel Prize in Physics, strongly supported the recognition by the academy of Einstein's work in relativity by writing that "one faces here an advance of decisive significance for the development of physical research" [8]. Despite the growing support for Einstein's Theory of Relativity (special and general), the Nobel Committee member tasked with drawing a report on Einstein's work in this area, Allvar Gullstrand, was highly critical of Einstein's work in Relativity. His report contained several misconceptions on his part and is generally considered a bad piece of work [8]. Until his death in 1955, Einstein never received recognition by the Nobel Committee for his work in Relativity.

According to the theory of GR, as formulated by Einstein [5], the force of gravity is due to curvature of spacetime caused by the presence of massive objects. The curvature is more pronounced the greater the mass of the object, which in turn increases the gravity. A decade earlier Einstein had presented his Special Theory of Relativity (SR), where he postulated that the laws of physics are the same for all non-accelerating observers, and that the speed of light in a vacuum was independent of the motion of all observers [58, 59]. The General Theory (GR) extends SR by further incorporating the phenomenon of gravity absent from the considerations of SR. Instead of treating gravity as a force as in Newton's Law, it is regarded as a manifestation of the curvature of spacetime, the curvature being caused by the presence of mass (and also energy and momentum of an object). Put differently the equations of Einstein in GR match, on the one side, the curvature of local spacetime with, on the other side of the equation, local energy and momentum within that spacetime. [60]. We discuss elements of the mathematical basis of the GR in Section 2.1

The motion of massive objects in spacetime produces changes to the curvature and if this motion occurs in a particular way, ripples in the curvature of spacetime can be produced, which are referred to as GWs. Einstein, himself, showed this was a consequence of his GR theory in the years immediately following his first presentation of GR [10, 11]. However, he remained doubtful of his own work. These waves are produced for accelerating masses, provided that the motion is not spherically symmetrical. Mathematically, for gravitational radiation to occur, the second time derivative of the quadrupole moment (or the $l$-th time derivative of the $l$-th multipole moment) of the stress-energy tensor (of an isolated system) must be non-zero. For this reason we do not expect gravitational radiation from an isolated non-spinning object moving at constant speed nor from a spherical star pulsating spherically. However, for non-spherical rotating masses, gravitational radiation will be produced. So too in the case of two masses orbiting each other. The corresponding power loss for two orbiting masses $m_a$ and $m_b$ with separation $r$ is given by

$$P = \frac{dE}{dt} = N\frac{G(\eta M)^2 r^4 \omega^6}{c^5} \tag{2.1}$$

where, $\eta = m_a m_b/(m_a + m_b)^2$ is the dimensionless ratio of the masses, N is a numerical factor depending on the details of the theory used to derive the result, which for GR is 32/5, $M = m_a + m_b$, $r = r_a + r_b$, the sum of the radial distances to the centre of mass, and $\omega$ is the orbital angular frequency.
For the Earth-Sun system, this power loss is only about 300 watts. Compare this with the electromagnetic radiation of the sun of about $3.86 \times 10^{26}$ watts or to the kinetic energy of the Earth orbiting the Sun of about $2.7 \times 10^{33}$ joules. The power-loss is far greater for close compact binaries. We will use geometrised units, $c = G = 1$, unless otherwise stated and so Eq. (2.1) would instead, appear as

$$P = \frac{dE}{dt} = N(\eta M)^2 r^4 \omega^6. \tag{2.2}$$

## 2.1 The theory of general relativity

We make a note here, of some preliminaries, regarding the notation and definitions that will be used in discussing Einstein's GR.

A co-ordinate change $x^a \to x^{a'}(x^b)$ on space time, has inverse $x^{a'} \to x^a(x^{b'})$.

We define

$$p_a^{a'} = \frac{\partial x^{a'}}{\partial x^a}, \tag{2.3}$$

$$p_{a'}^{a} = \frac{\partial x^{a}}{\partial x^{a'}}. \tag{2.4}$$

We then obtain on using the chain rule

- $p_{a'}^a p_b^{b'} = \delta_a^b$,

  where the Kronecker delta; $\delta_a^b = \begin{cases} 1 & \text{if } a = b \\ 0 & \text{if } a \neq b \end{cases}$

- for repeated co-ordinate change, $x^a \to x^{a'} \to x^b$, we have the group property

$$p_{a'}^a p_b^{a'} = \delta_a^b. \tag{2.5}$$

A **covariant tensor** of $n^{th}$ rank, with components $\mathrm{T}_{a_1 \ldots a_n}$ with respect to co-ordinates $\mathrm{x}^a$, at a point P, satisfies the transformation law $T_{a_1 \ldots a_n} \to T_{a'_1 \ldots a'_n} = p_{a'_1}^{a_1} \ldots p_{a'_n}^{a_n} T_{a_1 \ldots a_n}$.

A **contravariant tensor** satisfies $T^{a_1 \ldots a_n} \to T^{a'_1 \ldots a'_n} = p_{a_1}^{a'_1} \ldots p_{a_n}^{a'_n} T^{a_1 \ldots a_n}$.

A **mixed tensor** may transform as , for example

$T_a^b = T_{a'}^{b'} p_a^{a'} p_{b'}^b T_a^b$.

The differential line element $ds$ at a space-time point $\mathbf{x}$, may be described by:

$$ds^2 = g_{\alpha\beta}(\mathbf{x})\, dx^\alpha\, dx^\beta, \tag{2.6}$$

with $g_{\alpha\beta}$, the symmetric metric tensor, repeated indices implying summation.

First, consider the flat Cartesian-coordinate metric ($x = (t, x, y, z)$):

$$g_{\alpha\beta}^{\mathrm{Cart.}}(\mathbf{x}) = \begin{pmatrix} -1 & 0 & 0 & 0 \\ 0 & 1 & 0 & 0 \\ 0 & 0 & 1 & 0 \\ 0 & 0 & 0 & 1 \end{pmatrix}, \tag{2.7}$$

and then a curved, spherical-coordinate Schwarzschild metric ($x = (t, r, \theta, \phi)$) exterior to a

spherically symmetric mass distribution of total mass $M$,

$$g_{\alpha\beta}^{\text{Schwarz.}}(\mathbf{x}) = \begin{pmatrix} -(1-2\,GM/c^2r) & 0 & 0 & 0 \\ 0 & (1+2GM/c^2r)^{-1} & 0 & 0 \\ 0 & 0 & r^2 & 0 \\ 0 & 0 & 0 & r^2\sin^2(\theta) \end{pmatrix}, \tag{2.8}$$

or in geometrised units, where $c = G = 1$

$$g_{\alpha\beta}^{\text{Schwarz.}}(\mathbf{x}) = \begin{pmatrix} -(1-2\,M/r) & 0 & 0 & 0 \\ 0 & (1+2\,M/r)^{-1} & 0 & 0 \\ 0 & 0 & r^2 & 0 \\ 0 & 0 & 0 & r^2\sin^2(\theta) \end{pmatrix}. \tag{2.9}$$

The geodesic equation of motion for a test particle is given by:

$$\frac{d^2x^\alpha}{d\tau^2} \quad = \quad -\Gamma^\alpha_{\beta\gamma}\,\frac{dx^\beta}{d\tau}\,\frac{dx^\gamma}{d\tau}, \tag{2.10}$$

with $\tau$, the proper time and $\Gamma^\alpha_{\beta\gamma}$, the Christoffel symbol or affine connection defined as:

$$g_{\alpha\delta}\,\Gamma^\delta_{\beta\gamma} \quad = \quad \frac{1}{2}\left(\frac{\partial g_{\alpha\beta}}{\partial x^\gamma} + \frac{\partial g_{\alpha\gamma}}{\partial x^\beta} - \frac{\partial g_{\beta\gamma}}{\partial x^\alpha}\right), \tag{2.11}$$

otherwise written as:

$$g_{\alpha\delta}\,\Gamma^\delta_{\beta\gamma} \quad = \quad \frac{1}{2}\left(\partial_\gamma g_{\alpha\beta} + \partial_\beta g_{\alpha\gamma} - \partial_\alpha g_{\beta\gamma}\right), \tag{2.12}$$

or sometimes written as:

$$g_{\alpha\delta}\,\Gamma^\delta_{\beta\gamma} \quad = \quad \frac{1}{2}\left(g_{\alpha\beta,\gamma} + g_{\alpha\gamma,\beta} - g_{\beta\gamma,\alpha}\right). \tag{2.13}$$

The Riemann curvature tensor is defined as:

$$R^\alpha_{\beta\gamma\delta} \quad = \quad \frac{\partial\Gamma^\alpha_{\delta\beta}}{\partial x^\gamma} - \frac{\partial\Gamma^\alpha_{\gamma\beta}}{\partial x^\delta} + \Gamma^\alpha_{\gamma\epsilon}\Gamma^\epsilon_{\delta\beta} - \Gamma^\alpha_{\delta\epsilon}\Gamma^\epsilon_{\gamma\beta}\,, \tag{2.14}$$

otherwise written as

$$R^\alpha_{\beta\gamma\delta} \quad = \quad \partial_\gamma\Gamma^\alpha_{\delta\beta} - \partial_\delta\Gamma^\alpha_{\gamma\beta} + \Gamma^\alpha_{\gamma\epsilon}\Gamma^\epsilon_{\delta\beta} - \Gamma^\alpha_{\delta\epsilon}\Gamma^\epsilon_{\gamma\beta}\,. \tag{2.15}$$

We may lower the index in Eq. (2.15) by

$$R_{\rho\beta\gamma\delta} \quad = g_{\rho\alpha} R^{\alpha}_{\beta\gamma\delta}. \tag{2.16}$$

$R_{\rho\beta\gamma\delta}$ is invariant under interchange of the first pair of indices with the second

$$R_{\rho\beta\gamma\delta} \quad = R_{\gamma\delta\rho\beta}. \tag{2.17}$$

and it is antisymmetric in its first two indices, or last two, for that matter

$$R_{\rho\beta\gamma\delta} \quad = -R_{\beta\rho\gamma\delta} = -R_{\rho\beta\delta\gamma} \tag{2.18}$$

Some useful consequences of these properties are the cyclic permutations

$$R_{\rho\beta\gamma\delta} \quad + R_{\rho\gamma\delta\beta} + R_{\rho\delta\beta\gamma} = R_{\rho[\beta\gamma\delta]} = 0, \tag{2.19}$$

and the **Bianchi identity** involving the covariant derivative of the Riemann tensor in Riemann normal coordinates (following Ref. [61])

$$\nabla_{[\lambda} R_{\rho\beta]\gamma\delta} = 0. \tag{2.20}$$

Note that the square brackets, [ ], indicate antisymmetrisation which are, in effect, cyclic permutations of the indices in the brackets as illustrated in Eq. (2.19). Antisymmetrisation, is where odd number of exchanges between indices are given a minus sign, such as,

$$T_{[\mu\nu\rho]\sigma} = \frac{1}{6} \left( T_{\mu\nu\rho\sigma} - T_{\mu\rho\nu\sigma} + T_{\rho\mu\nu\sigma} - T_{\nu\mu\rho\sigma} + T_{\nu\rho\mu\sigma} - T_{\rho\nu\mu\sigma} \right) \ . \tag{2.21}$$

The Ricci tensor is obtained by contracting two of the indices of the Riemann tensor in Eq. (2.15) giving:

$$R_{\beta\delta} \quad = \quad R^{\alpha}_{\beta\alpha\delta} \, , \tag{2.22}$$

and a further contraction leads to the Ricci scalar

$$R \quad = \quad R^{\beta}_{\beta} = g^{\beta\delta} R_{\beta\delta}. \tag{2.23}$$

This then leads to the well-known **equation of Einstein**,

$$G_{\alpha\beta} = R_{\alpha\beta} - \frac{1}{2} g_{\alpha\beta} R \quad = \quad 8\pi \, T_{\alpha\beta}, \tag{2.24}$$

with $T_{\alpha\beta}$, the stress-energy tensor,

$$T_{\alpha\beta} = \left( \begin{array}{c|c} \text{Energy Density} & \text{Energy Flux} \\ \hline \text{Momentum Density} & \text{Stress Tensor} \end{array} \right) . \tag{2.25}$$

where, $T^{tt}(\mathbf{x})$ is the local energy density, $T^{ti}(\mathbf{x})$ is the flux of energy in the $x^i$ direction, $T^{it}$ is the density of momentum in the $x^i$ direction (with $T^{it} = T^{ti}$), diagonal elements $T^{ii}$ represent pressure components, off-diagonal elements represent shear stresses.

Local energy and momentum conservation may be described by:

$$\frac{\partial T_{\alpha\beta}}{\partial x_\beta} \quad = \quad 0\,. \tag{2.26}$$

For a region far from a source, and nearly flat, a GW will produce only small perturbations by an amount $h_{\alpha\beta}$, which we will investigate in Section 2.2. The Bianchi identity, described in Eq. (2.20), may also be written, in what is referred to as the **contracted Bianchi identities**, as

$$\nabla^\lambda R_{\rho\gamma} = \frac{1}{2}\nabla_\rho R, \tag{2.27}$$

which is, in comparison with Eq. (2.24), equivalent to

$$\nabla^\alpha G_{\alpha\beta} = 0. \tag{2.28}$$

## 2.2 The weak-field approximation of gravitation

We will consider the following approximations:

- The gravitational field is weak but not static.
- There are no restrictions on the motion of particles in the gravitational field.
- In the absence of any gravitational perturbance, space-time is flat and is characterised by the Minkowski metric. $\eta_{\mu\nu}$.

With these considerations, a weak-field gravitational approximation may be thought of as a small 'perturbation', $h_{\mu\nu}$ , on the flat Minkowski metric, $\eta_{\mu\nu}$, which is diag(-1,1,1,1) in Cartesian coordinates $(t, x, y, z)$.

$$g_{\mu\nu} = \eta_{\mu\nu} + h_{\mu\nu}, \quad |h_{\mu\nu}| \ll 1 \tag{2.29}$$

where on raising the indices, the contravariant metric is written as:

$$g^{\mu\nu} = \eta^{\mu\nu} - h^{\mu\nu}, \tag{2.30}$$

with

$$h^{\mu\nu} = \eta^{\mu\rho}\eta^{\nu\sigma}h_{\rho\sigma}, \tag{2.31}$$

on neglecting the corrections which are of higher order in the perturbation.

The perturbation transforms as a second-rank tensor under a Lorentz transformation $x^\alpha = \Lambda_\mu{}^\alpha x^\mu$ (and $x^\alpha = \Lambda^T x^\alpha \Lambda$), where the matrices $\Lambda_\mu^\alpha$(x) represent position-dependent transformations which (at each point) leave the canonical form of the metric unaltered [61]

$$h_{\alpha\beta} = \Lambda_\alpha{}^\mu \Lambda_\beta{}^\nu \; h_{\mu\nu}. \tag{2.32}$$

The Christoffel symbols, are given by

$$\Gamma^\lambda_{\mu\nu} \;=\; \frac{1}{2} g^{\lambda\rho}(\partial_\mu g_{\nu\rho} + \partial_\nu g_{\rho\mu} - \partial_\rho g_{\mu\nu}). \tag{2.33}$$

To first order, the affine connection is,

$$\begin{aligned} \Gamma^\lambda_{\mu\nu} &= \frac{1}{2}\eta^{\lambda\rho}[\partial_\mu h_{\rho\nu} + \partial_\nu h_{\mu\rho} - \partial_\rho h_{\mu\nu}] + \mathcal{O}(h^2) \\ &= \frac{1}{2}[\partial_\mu h^\lambda_\nu + \partial_\nu h^\lambda_\mu - \partial^\lambda h_{\mu\nu}] + \mathcal{O}(h^2). \end{aligned} \tag{2.34}$$

The Riemann curvature tensor may then be written, on lowering an index, as :

$$R_{\mu\nu\rho\sigma} = \eta_{\mu\lambda}\partial_\rho \Gamma^\lambda{}_{\nu\sigma} - \eta_{\mu\lambda}\partial_\sigma \Gamma^\lambda{}_{\nu\rho}. \tag{2.35}$$

The D'Alembertian in flat space-time, is defined as :

$$\Box \equiv \eta^{\lambda\rho}\partial_\lambda\partial_\rho. \tag{2.36}$$

and so using Eq. (2.36), and contracting over $\mu$ and $\lambda$, we obtain, to first order, the Ricci tensor:

$$\begin{aligned} R_{\mu\nu} \approx R^{(1)}_{\mu\nu} &= \frac{1}{2}\left[\partial_\lambda\partial_\nu h^\lambda{}_\mu + \partial_\lambda\partial_\mu h^\lambda{}_\nu - \partial_\mu\partial_\nu h - \Box h_{\mu\nu}\right] \\ &= \frac{1}{2}\left[\partial^\lambda\partial_\nu h_{\mu\lambda} + \partial^\lambda\partial_\mu h_{\nu\lambda} - \partial_\mu\partial_\nu h - \partial_\lambda\partial^\lambda h_{\mu\nu}\right], \end{aligned} \tag{2.37}$$

where $h = h^\mu_\mu = \eta^{\mu\nu}h_{\mu\nu}$, the trace of the metric perturbations.

By performing a contraction with $\eta^{\mu\nu}$, we obtain the Ricci scalar as:

$$R = \partial_\lambda\partial_\mu h^{\lambda\mu} - \Box h \tag{2.38a}$$

$$= \partial_\lambda\partial_\mu h^{\lambda\mu} - \partial_\lambda\partial^\lambda h \tag{2.38b}$$

$$= \partial^\lambda\partial^\mu h_{\lambda\mu} - \partial_\lambda\partial^\lambda h. \tag{2.38c}$$

In this weak-field, limit of gravitation, the Einstein tensor, $G_{\mu\nu}$, is given as:

$$G_{\mu\nu} = R_{\mu\nu} - \frac{1}{2}\eta_{\mu\nu}R \tag{2.39}$$

$$= \frac{1}{2}[\left(\partial^\lambda\partial_\nu h_{\mu\lambda} + \partial^\lambda\partial_\mu h_{\nu\lambda} - \partial_\mu\partial_\nu h - \partial_\lambda\partial^\lambda h_{\mu\nu}\right) - \eta_{\mu\nu}\left(\partial^\lambda\partial^\rho h_{\lambda\rho} - \partial_\lambda\partial^\lambda h\right)]. \tag{2.40}$$

This leads to the linearised Einstein field equations (EFE) written as

$$G_{\mu\nu} = 8\pi T_{\mu\nu}. \tag{2.41}$$

We define the *trace-reversed* perturbation, $\bar{h}_{\mu\nu}$, as (see, for instance, [49]),

$$\bar{h}_{\mu\nu} = h_{\mu\nu} - \frac{1}{2}\eta_{\mu\nu}h, \tag{2.42}$$

with

$$\bar{h}^\mu{}_\mu = -h^\mu{}_\mu, \tag{2.43}$$

meaning that the Einstein tensor is the trace-reversed Ricci tensor and

$$h_{\mu\nu} = \bar{h}_{\mu\nu} - \frac{1}{2}\eta_{\mu\nu}\bar{h}. \tag{2.44}$$

Hence, we may rewrite Eq. (2.40) as

$$G_{\mu\nu} = -\frac{1}{2}\left[\partial_\lambda\partial^\lambda\bar{h}_{\mu\nu} + \eta_{\mu\nu}\partial^\lambda\partial^\rho\bar{h}_{\lambda\rho} - \partial_\nu\partial^\lambda\bar{h}_{\mu\lambda} - \partial_\mu\partial^\lambda\bar{h}_{\nu\lambda}\right], \tag{2.45}$$

and then from Eq. (2.41), we may write Eq. (2.45) as

$$G_{\mu\nu} = -\frac{1}{2}\left[\partial_\lambda\partial^\lambda\bar{h}_{\mu\nu} + \eta_{\mu\nu}\partial^\lambda\partial^\rho\bar{h}_{\lambda\rho} - \partial_\nu\partial^\lambda\bar{h}_{\mu\lambda} - \partial_\mu\partial^\lambda\bar{h}_{\nu\lambda}\right] = 8\pi T_{\mu\nu}. \tag{2.46}$$

This equation is covariant in that there is no "preferred" notion of time. There are 16 second-order differential equations (DEs) describing how the spacetime reacts in the presence of energy-momentum. Both sides are symmetric two-index tensors, reducing the set of equations, then, to ten independent equations. The Bianchi identity from Eq. (2.28) on page 13 gives (contracted)

$$\nabla_\mu G^{\mu\nu} = 0. \tag{2.47}$$

The four equations represented by

$$G^{0\nu} = 8\pi T^{0\nu}, \tag{2.48}$$

(see [62] for a detailed explanation) act as constraints reducing the EFEs, $G^{\mu\nu} = 8\pi T^{\mu\nu}$, to six equations in 10 unknowns:

$$G^{ij} = 8\pi T^{ij}. \tag{2.49}$$

These are the dynamical evolution equations for the metric. A way of dealing with the problm

of six equations in 10 unknowns is to *fix* the gauge. This involves fixing the co-ordinate system thus restricting the freedom to perform gauge transformations (see below for an explanation of gauge transformations). We choose, following Ref. [52]), to work in a *harmonic coordinate system*, using the **harmonic gauge**

$$\Box x^{\alpha} = 0 \ . \tag{2.50}$$

where $\Box = \nabla^{\alpha}\nabla_{\alpha}$ is the covariant D'Alembertian.
Now,

$$\Box x^{\alpha} = g^{\mu\nu}\partial_{\mu}\partial_{\nu}x^{\alpha} - g^{\mu\nu}\Gamma^{\lambda}_{\mu\nu}\partial_{\lambda}x^{\alpha} = 0 \tag{2.51}$$

$$\implies g^{\mu\nu}\Gamma^{\lambda}{}_{\mu\nu} = 0 \ . \tag{2.52}$$

This gauge condition reduces, in the weak-field limit, to

$$\partial_{\lambda}h^{\lambda}{}_{\mu} = \frac{1}{2}\partial_{\mu}h. \tag{2.53}$$

This is also referred to as the **Lorentz gauge**.

Now, following [63], a gauge transformation is a coordinate transformation of the form

$$x^{(\mathrm{new})\mu} = x^{(\mathrm{old})\mu} + \xi^{\alpha}(x^{(\mathrm{old})\nu}), \tag{2.54}$$

where $\partial_{\nu}\xi^{\mu}$ is of the same order of smallness as $h_{\mu\nu}$ and terms of order $\mathcal{O}(h_{\mu\nu})^2$, $\mathcal{O}(h_{\mu\nu}\partial_{nu}\xi^{\mu})$, $\mathcal{O}(\partial_{nu}\xi^{\mu})^2$ are neglected.
Then, the coordinate transformation in Eq. (2.54) applied to the metric in Eq. (2.29) on page 13, results in

$$h^{(\mathrm{new})}_{\mu\nu} = h^{(\mathrm{old})}_{\mu\nu} - \partial_{\nu}\xi_{\mu} - \partial_{\mu}\xi_{\nu}, \tag{2.55}$$

inducing a change in the trace reversed perturbation

$$\bar{h}^{(\mathrm{new})}_{\mu\nu} = \bar{h}^{(\mathrm{old})}_{\mu\nu} - \partial_{\nu}\xi_{\mu} - \partial_{\mu}\xi_{\nu} + \eta_{\mu\nu}\partial_{\alpha}\xi^{\alpha}. \tag{2.56}$$

The harmonic gauge condition then leads to

$$\partial_{\mu}\bar{h}^{\mu}{}_{\lambda} = 0. \tag{2.57}$$

Hence, we may express the EFEs in Eq. (2.46) on page 15 as

$$\begin{aligned} G_{\mu\nu} = -\frac{1}{2}\left[\partial_{\lambda}\partial^{\lambda}\bar{h}_{\mu\nu}\right] &= 8\pi T_{\mu\nu} \\ \implies -\frac{1}{2}\Box\bar{h}_{\mu\nu} &= 8\pi T_{\mu\nu}, \end{aligned}$$

leading to

$$\Box\bar{h}_{\mu\nu} = -16\pi T^{\mu\nu}, \tag{2.58}$$

which in a vacuum, becomes

$$\Box\bar{h}_{\mu\nu} = 0. \tag{2.59}$$

For the vacuum equations for $\bar{h}_{\mu\nu}$ we may use plane-wave solutions:

$$\bar{h}_{\mu\nu} = A_{\mu\nu} e^{ik_\sigma x^\sigma} \ , \tag{2.60}$$

with $A_{\mu\nu}$, a constant, symmetric, $(0,2)$ tensor and $k^\sigma$, a constant four-vector vector referred to as the *wave vector*.

A caution from [63] is that the possibility of making gauge transformations means that a metric that appears to be wavelike may not represent a GW and so it is important to confirm that a vacuum spacetime with a wave-like metric does represent GWs by, for example, checking that the Riemann tensor contains some non-zero components.

Substituting from Eq. (2.60) in Eq. (2.59) leads to the condition

$$k_\alpha k^\alpha = 0, \tag{2.61}$$

which means a solution is obtained when $k_\alpha$ is null or tangent to the world line of a photon. Hence, it is evident that GWs propagate at the speed of light. The time-like component of the wave vector is referred to as the *frequency* of the wave, written as the four-vector:

$$k^\sigma = (\omega, k^1, k^2, k^3), \tag{2.62}$$

and with $k_\alpha$ null, leads to

$$\omega^2 = \delta_{ij} k^i k^j \ , \tag{2.63}$$

referred to as the *dispersion relation* for the gravitational wave.

With 10 independent parameters from the coefficients, $A_{\mu\nu}$ and three from the null vector, $k_\mu$, the harmonic gauge condition in Eq. (2.57), then leads to :

$$\begin{aligned} \partial_\mu \bar{h}^{\mu\nu} &= \partial_\mu (A^{\mu\nu} e^{ik_\sigma x^\sigma}) \\ &= iA^{\mu\nu} k_\mu e^{ik_\sigma x^\sigma}, \end{aligned} \tag{2.64}$$

which means that

$$k_\alpha A^{\alpha\beta} = 0, \tag{2.65}$$

thus requiring that $A^{\alpha\beta}$ be orthogonal to $k_\alpha$. The number of independent components of $A_{\mu\nu}$ to is then reduced to six.

Now a coordinate transformation of the form

$$x^{\alpha'} = x^\alpha + \xi^\alpha(x^\beta), \tag{2.66}$$

will satisfy the harmonic coordinate condition

$$\Box x^\mu = 0, \tag{2.67}$$

on condition that

$$\Box\xi^{\alpha} = 0. \tag{2.68}$$

This, again, is a wave equation, this time in $\xi$, where we may choose a solution such as:

$$\xi_{\mu} = B_{\mu} e^{ik_{\sigma}x^{\sigma}} \ , \tag{2.69}$$

with $k_{\sigma}$, the wave vector for the GW and $B_{\mu}$, the constant coefficients.

It is then possible to convert from the old set of constants, $A^{(\mathrm{old})}_{\mu\nu}$, to a new set of constants, $A^{(\mathrm{new})}_{\mu\nu}$ :

$$A^{(\mathrm{new})}_{\mu}{}^{\ \mu} = 0, \tag{2.70}$$

and

$$A_{\mu\nu}U^{\beta} = 0 \tag{2.71}$$

with, $U^{\beta}$, a constant time-like unit four-velocity vector.

Together the Equations (2.65), (2.70) and (2.71) are called the **transverse traceless** (TT) gauge conditions.

Having exhausted all the possible gauge freedom, we have arrived at the subgauge of the harmonic gauge

$$\bar{h}^{\mathrm{TT}}_{\mu\nu} = h^{\mathrm{TT}}_{\mu\nu}. \tag{2.72}$$

We refer to this as the **transverse traceless gauge** or **TT gauge** or "radiation gauge".

In general, following Ref. [63], the transverse property is expressed as

$$\bar{h}'_{\alpha\beta}k^{\alpha} = 0\,, \tag{2.73}$$

so that for the **transverse** metric $\bar{h}_{\alpha\beta}$, the wave travels in the $z$-direction, and its effects are in the $x$- and $y$-directions.

The **traceless** property of the metric perturbation is expressed as

$$\bar{h}'^{\alpha}_{\alpha} = \bar{h}' = 0\,, \tag{2.74}$$

so that the metric and its trace-reverse form are the same, $\bar{h}'_{\alpha\beta} = h'_{\alpha\beta}$.

Any metric satisfying Eqs. (2.73) and (2.74) is said to be in the **Transverse Traceless** or **TT gauge** [63].

So, the metric perturbation is traceless and perpendicular to the wave vector. With $A_{\mu\nu}$ traceless, so is the trace-reversed perturbation $\bar{h}_{\mu\nu}$ which is then equivalent to the perturbation $h_{\mu\nu}$ itself in this gauge.

There is some ambiguity in the definition of the TT gauge common in the literature. This ambiguity has been highlighted and elaborated in [64] and we summarise the discussions therein. There are two conceptually distinct notions of transverse-traceless modes each related to different theoretical paradigms stemming from two different observational techniques or goals, however, with the same notation used to describe both: $h^{\rm TT}_{\alpha\beta}$. The first notion results from the search for GWs as a result of astrophysical sources such as the coalescing compact binaries, which is the most commonly accepted usage, and the meaning taken here. The second results from the search for GWs as a result of primordial BHs with the origin of primordial radiation as cosmological. The first case is described by retarded solutions of Einstein's equations sourced by highly dynamical compact objects in asymptotically flat space-times, whilst the second is is described by source-free solutions of linearised Einstein's equations on a Friedmann-Lemaître-Robertson-Walker background [64]. Confusion may arise in the situation of GWs produced by isolated bodies (which does not arise in this work). Throughout the discussions we will refer to the TT gauge as relevant to astrophysical situations (first kind).

[64] distinguishes between the case where $h^{\rm TT}_{\alpha\beta}$ is extracted from $h_{\alpha\beta}$ by going to the momentum space where the operation is algebraic and hence local as opposed to physical space where the operation is non-local. In the study of retarded fields produced by compact sources, the notion of transverse traceless modes, local in physical space, is used. $h_{ab}$ is projected into a 2-sphere orthogonal to the radial direction in physical space using $P_a^{\ b}$, a projection operator, extracting a new transverse-traceless part of $h_{ab}$, removing the trace. [64] argues for a different notation of the transverse traceless mode in this case, $h^{\rm tt}_{\alpha\beta}$, defined by

$$h^{\rm tt}_{\alpha\beta} = \left( P_a^{\ c} P_b^{\ d} - \frac{1}{2} P_{ab} P^{cd} \right), \tag{2.75}$$

reserving the notation $h^{\rm TT}_{\alpha\beta}$ for the case in momentum space where the operation is algebraic and local. The operation of extracting $h^{\rm tt}_{\alpha\beta}$ local in physical space is generally not gauge invariant. However, as admitted by [64], in practice and tailored to BS type expansions (and behavior of fields near null infinity), $h^{\rm tt}_{\alpha\beta}$ is constructed only in the asymptotic region where its $1/r$-part can be shown to be gauge invariant under a large class of gauge transformations. In the cosmological context, these BS type expansions are not available. We will confine our attention to the case of astrophysical scenarios and so will continue to use $h^{\rm TT}_{\alpha\beta}$ here, to exclusively mean $h^{\rm tt}_{\alpha\beta}$, so as to maintain consistency with the overwhelming occurrence in the literature. In this work the ambiguity will not arise.

Adopting spatial coordinates where the wave is travelling in the $x^3 = z$ direction,

$$k^\mu = (\omega, 0, 0, k^3). \tag{2.76}$$

Since the wave vector is null, $k^3 = \omega$, and so Eq. 2.76 may be written as:

$$k^\mu = (\omega, 0, 0, \omega). \tag{2.77}$$

Now, $k^\mu A_{\mu\nu} = 0$ and $A_{0\nu} = 0$ together imply

$$A_{3\nu} = 0. \tag{2.78}$$

Hence, the only nonzero components of $A\mu\nu$ are $A_{11}$, $A_{12}$, $A_{21}$, and $A_{22}$. Now, $A_{\mu\nu}$ is traceless, so for a plane wave travelling in the $x^3 = z$ direction, in this gauge, the two components $A_{11}$ and $A_{12}$, together with the frequency, $\omega$, completely characterise the wave, and we may write:

$$A^{TT}_{\alpha\beta} = \begin{pmatrix} 0 & 0 & 0 & 0 \\ 0 & A_{11} & A_{12} & 0 \\ 0 & A_{12} & -A_{11} & 0 \\ 0 & 0 & 0 & 0 \end{pmatrix}. \tag{2.79}$$

This metric is in the TT gauge.

Next, we investigate the effect of GWs on free particles. We will use the geodesic deviation equation to consider the relative motion of two particles with four-velocities described by a single vector field, $U^\alpha$ and a separation vector, $\zeta^\alpha$. The separation vector obeys the geodesic equation

$$\frac{d^2\zeta^\alpha}{d\tau^2} = R^\alpha{}_{\beta\gamma\delta} U^\beta U^\gamma \zeta^\delta \tag{2.80}$$

with, $U^\nu = dx^\nu/d\tau$, the four-velocity of the two particles.
For flat space, we take only the lowest-order components of $U^\nu$. Corrections to $U^\nu$ that depend on $h_{\mu\nu}$ lead to terms second order in the perturbation in Equation (2.80). So,

$$U^\nu = (1, 0, 0, 0). \tag{2.81}$$

Initially $\zeta^\nu = (0, \epsilon, 0, 0)$. Now, to first order in $h_{\mu\nu}$, Equation (2.80) leads to

$$\frac{d^2\zeta^\alpha}{d\tau^2} = \frac{\partial^2\zeta^\alpha}{\partial t^2} = \epsilon R^\alpha{}_{00x} = -\epsilon R^\alpha{}_{0x0}. \tag{2.82}$$

In the TT gauge, from the definition of the Riemann tensor, we arrive at:

$$\begin{aligned} R^x{}_{0x0} = \quad R_{x0x0} = \quad & -\frac{1}{2} h^{TT}_{xx,00}; \\ R^y{}_{0x0} = \quad R_{y0x0} = \quad & -\frac{1}{2} h^{TT}_{xy,00}; \\ R^y{}_{0y0} = \quad R_{y0y0} = \quad & -\frac{1}{2} h^{TT}_{yy,00} = -R^x{}_{0x0}. \end{aligned} \tag{2.83}$$

All other independent components vanish. This means that two particles initially separated in the x-direction have a separation vector which obeys the equation

$$\begin{aligned} \frac{\partial^2\zeta^x}{\partial t^2} \quad &= \quad \frac{1}{2}\epsilon\frac{\partial^2}{\partial t^2} h^{TT}_{xx}, \\ \frac{\partial^2\zeta^y}{\partial t^2} \quad &= \quad \frac{1}{2}\epsilon\frac{\partial^2}{\partial t^2} h^{TT}_{xy}. \end{aligned} \tag{2.84}$$

In the same way, two particles initially separated by $\epsilon$ in the y-direction obey the equations

$$\begin{aligned} \frac{\partial^2 \zeta^y}{\partial t^2} &= \frac{1}{2}\epsilon \frac{\partial^2}{\partial t^2} h^{TT}_{yy} = -\frac{1}{2}\epsilon \frac{\partial^2}{\partial t^2} h^{TT}_{xx}, \\ \frac{\partial^2 \zeta^x}{\partial t^2} &= \frac{1}{2}\epsilon \frac{\partial^2}{\partial t^2} h^{TT}_{xy}. \end{aligned} \tag{2.85}$$

Next, using these equations, we will describe the polarisation of a GW. First, we consider a ring of particles initially at rest. Then, suppose a wave with: $h^{TT}_{xx} \neq 0$ and $h^{TT}_{xy} = 0$ impacts on them. This results in opposite effects on proper distance on the two transverse axes. First, one will contract, say, the x-axis while the other, the y, expands. Then, as $h^{TT}_{xx}$ reverses sign, the x-axis will expand and the y-axis contracts and the process will alternate. So, the particles along the x-axis alternately come towards each other and then move away from each other. The alternation produces a shape resembling the $\oplus$ sign . Hence, this type of polarisation is referred to as $\oplus$ polarization.

Now, suppose, that the wave had $h^{TT}_{xy} \neq 0$, and $h^{TT}_{xx} = h^{TT}_{yy} = 0$, instead. Then we have what is referred to as pure $\otimes$ polarisation, with $h_\times$ obtained from the previous case by a simple $45^\circ$ rotation. The alternation produces a shape resembling the $\otimes$ sign. Since $h^{TT}_{xy}$ and $h^{TT}_{xx}$ are independent, two different states of polarisation exist. So, the wave is characterised by two numbers, from the matrix in Eq. (2.79):

$$A_+ = A_{11} \tag{2.86}$$

and

$$A_\times = A_{12}. \tag{2.87}$$

The effect of a pure $A_R$ wave would be to rotate the particles in a right-handed sense. It is important to note that the individual particles do not travel around the ring but just move in little epicycles [61]. Since the wave equation and TT conditions are linear, a general wave will be a linear combination of the two polarisation tensors. We could consider right- and left-handed circularly polarised modes by defining :

$$\begin{aligned} A_R &= \frac{1}{\sqrt{2}}(A_+ + iA_\times); \\ A_L &= \frac{1}{\sqrt{2}}(A_+ - iA_\times)\ . \end{aligned} \tag{2.88}$$

These are the plane wave solutions to the linearised Einstein's equations in vacuum, Eq (2.59). Ref. [63] makes some important notes to such an analysis. First, it is important to recognise that the spacetime is not Minkoskian because we have $R^\alpha{}_{\beta\gamma\delta} \neq 0$. Secondly, if the two particles we considered are massive and are connected by a damping system, then relative motion and acceleration implies that work is done on the damping system. This in turn means an increase in temperature and hence a transfer in energy. For that to be possible, the GWs contain energy

originating from some source are hence are real physical effects [63].

## 2.3 Generation of gravitational radiation by sources

We now turn our attention to obtaining the solution of the linearised Einstein equations coupled with matter, i.e. in the presence of a source:

$$\Box\bar{h}_{\mu\nu} = -16\pi T_{\mu\nu}. \tag{2.89}$$

We will use the Green's function method to obtain the solution.
In the presence of a delta-function source, a solution of Eq. (2.89) is given by the Green's function, $G(x^\sigma - y^\sigma)$, of the D'Alembertian operator $\Box$

$$\Box_x G(x^\sigma - y^\sigma) = \delta^{(4)}(x^\sigma - y^\sigma) \ , \tag{2.90}$$

with $\delta^{(4)}$, the four-dimensional Dirac delta function, and $\Box_x$, the D'Alembertian with respect to the coordinates $x^\sigma$.

Then, the general solution to Eq. (2.89) may be represented by:

$$\bar{h}_{\mu\nu}(x^\sigma) = -16\pi \int G(x^\sigma - y^\sigma) T_{\mu\nu}(y^\sigma)\ d^4y \ . \tag{2.91}$$

These well-known solutions are then either **advanced**, representing waves travelling forward in time or **retarded**, representing waves travelling backward in time. We will consider the latter case, representing the accumulated effects of signals to the past of the point being considered. Using the retarded Green's function,

$$G(x^\sigma - y^\sigma) = -\frac{1}{4\pi|\mathbf{x}-\mathbf{y}|}\delta[|\mathbf{x}-\mathbf{y}| - (x^0 - y^0)] \times \ \theta(x^0 - y^0) \ . \tag{2.92}$$

with, $\mathbf{x} = (x^1, x^2, x^3)$, $\mathbf{y} = (y^1, y^2, y^3)$, the norm, $|\mathbf{x}-\mathbf{y}| = [\delta_{ij}(x^i - y^i)(x^j - y^j)]^{1/2}$ and the Heaviside unit step function, $\theta(x^0 - y^0) = \begin{cases} 1 & \text{if } x^0 > y^0 \\ 0 & \text{otherwise .} \end{cases}$

Substituting from Eq (2.92) into Eq (2.91), we perform the integral over $y^0$ using the delta function, to obtain

$$\bar{h}^{\mu\nu}(t, \mathbf{x}) = 4 \int \ \frac{1}{|\mathbf{x}-\mathbf{y}|} T^{\mu\nu}(t - |\mathbf{x}-\mathbf{y}|, \mathbf{y}) d^3y, \tag{2.93}$$

where, $t = x^0$, $(t, x^i)$ is the event at which the metric perturbation $\bar{h}^{\mu\nu}$ is evaluated, $y^i$ represents a spatial point inside the source, $|x^i - y^i|$ is the Euclidean distance, $r$ between $x^i$ and $y^i$ and the **retarded time** is,

$$t_r = t - |\mathbf{x}-\mathbf{y}|. \tag{2.94}$$

From the Eq. (2.93) for $\bar{h}_{\mu\nu}$, note that the disturbance in the gravitational field at $(t, \mathbf{x})$ is a

sum of the influences from the energy and momentum sources at the point $(t_r, \mathbf{y})$ on the past light cone [61].

Now, we recall from Eq. (2.49) on page 15 that there are only six independent equations of the EFEs, these being the spatial components. Hence, determining only the spatial components of $\bar{h}^{ij}$ would be adequate. From our conditions of constraint in Eqs. (2.47) and (2.48), we may write, on separating time and spatial components,

$$\partial_t T^{00} + \partial_i T^{0i} = 0. \tag{2.95}$$

Taking the covariant derivative,

$$\partial_i \partial_j T^{ij} = \partial_t^2 T^{00}\,. \tag{2.96}$$

Now,

$$\begin{aligned} \partial_k \partial_\ell (T^{k\ell} x^i x^j) &= \partial_k \left[ (\partial_\ell T^{k\ell}) x^i x^j + (T^{ki} x^j + T^{kj} x^i) \right] \\ &= \partial_k \left[ (\partial_\ell T^{k\ell}) x^i x^j \right] + \partial_k (T^{ki} x^j + T^{kj} x^i). \end{aligned} \tag{2.97}$$

For the first term on the right of Eq. (2.97)

$$\begin{aligned} \partial_k \left[ (\partial_\ell T^{k\ell}) x^i x^j \right] &= (\partial_k \partial_\ell T^{k\ell}) x^i x^j + (\partial_\ell T^{i\ell}) x^j + (\partial_\ell T^{j\ell}) x^i \\ &= (\partial_k \partial_\ell T^{k\ell}) x^i x^j + 2(\partial_k T^{ik}) x^j. \end{aligned} \tag{2.98}$$

For the second term on the right of Eq. (2.97)

$$\begin{aligned} \partial_k (T^{ki} x^j + T^{kj} x^i) &= [(\partial_k T^{ik}) x^j + T^{ik} \delta^j_k] + [(\partial_k T^{jk}) x^i + T^{kj} \delta^i_k] \\ &= \\ &= 2(\partial_k T^{ik}) x^j + 2T^{ij}. \end{aligned} \tag{2.99}$$

We may then eliminate the $2(\partial_k T^{ik}) x^j$ term by subtracting Eq. (2.99) from Eq. (2.98)

$$\partial_k \left[ (\partial_\ell T^{k\ell}) x^i x^j \right] - \partial_k (T^{ki} x^j + T^{kj} x^i) = (\partial_k \partial_\ell T^{k\ell}) x^i x^j - 2T^{ij}, \tag{2.100}$$

and so comparing Eqs. (2.97) and (2.100) we may rewrite Eq. (2.97) as

$$\partial_k \partial_\ell (T^{k\ell} x^i x^j) - 2\partial_k (T^{ki} x^j + T^{kj} x^i) = (\partial_k \partial_\ell T^{k\ell}) x^i x^j - 2T^{ij} \tag{2.101}$$

and rearrange as

$$\begin{aligned}
\partial_k\partial_\ell(T^{k\ell}x^ix^j) - 2\partial_k(T^{ki}x^j + T^{kj}x^i) + 2T^{ij} &= (\partial_k\partial_\ell T^{k\ell})x^ix^j, \\
\partial_k\left[\partial_\ell(T^{k\ell}x^ix^j) - 2(T^{ki}x^j + T^{kj}x^i)\right] + 2T^{ij} &= \partial_t^2(T^{00})x^ix^j, \\
\int T^{ij}d^3x &= \frac{1}{2}\partial_t^2\int T^{00}x^ix^jd^3x\,, \qquad (2.102)
\end{aligned}$$

where we have used the relation in Eq. (2.96) on the right-hand side of Eq. (2.102) and the term on the left-hand side of Eq. (2.102) $\partial_k\left[\partial_\ell(T^{k\ell}x^ix^j) - 2(T^{ki}x^j + T^{kj}x^i)\right]$ may be transformed by the divergence theorem taking the surface integral over the boundary of the volume of integration where $T^{\alpha\beta} = 0$ following [63].

We make the following assumptions about the source:

- It is at a large distance, $R \gg 1$, away from the point of observation.
- It is spread around a region $R + \delta R$, where $\delta R \ll R$.
- It is slowly moving, i.e. the velocities of the components of the source $\ll c$ (non-relativistic).

From Eq. (2.93) we have

$$\bar{h}^{\mu\nu}(t, \mathbf{x}) = \frac{4}{r}\int T^{\mu\nu}(t - r, \mathbf{y})d^3y, \qquad (2.103)$$

where the matter density $\rho$ may replace $T^{00}$ leading to

$$\bar{h}^{ij}(t, x^i) = \frac{2}{r}\frac{d^2I^{ij}(t - r)}{dt^2}\,, \qquad (2.104)$$

with the 3-dimensional tensor, the second moment of the mass distribution, also referred to as the **quadrupole moment**, given by

$$I^{ij}(t) = \int \rho(t, x'^k)x'^ix'^jd^3x. \qquad (2.105)$$

Or if the matter distribution is instead considered as a system of $N$ particles, then

$$I^{ij}(t) = \sum_{a=1}^{N} M_a y_a^i y_a^j. \qquad (2.106)$$

For two particles, each of mass $M$ in circular orbit around each other with orbital diameter $r_0$,

and angular velocity of each particle, $\omega$, from Ref. [63]

$$\bar{h}^{ij} = \frac{Mr_0^2\omega^2}{r}\begin{pmatrix} -\cos 2\omega(t-r) & 0 & 0 \\ 0 & \cos 2\omega(t-r) & 0 \\ 0 & 0 & 0 \end{pmatrix}. \tag{2.107}$$

So,

$$h_+ = -\frac{M\omega^2 r_0^2}{r}\cos(2\omega(t-r)), \tag{2.108}$$

and hence, the wave is linearly polarised.

Generalising for masses $M_1$ and $M_2$, also in a circular orbital, and using spherical polars $(r, \theta, \phi)$ we have from Ref. [63]

$$h_+ = -\frac{2\omega^2\mu r_0^2}{r}(1+\cos^2\theta)\cos(2\omega(t-r)-2\phi) \tag{2.109}$$

$$h_\times = -\frac{4\omega^2\mu r_0^2}{r}\cos\theta\sin(2\omega(t-r)-2\phi), \tag{2.110}$$

where the reduced mass of the binary $\mu$ is given by $\mu = M_1M_2/(M_1+M_2)$. For equal mass, $M_1 = M_2 = M$, so $\mu = M/2$ and for the particles confined to the x-y plane, $\theta = \pi/2$ and $\phi = 0$, so we recover Eq. (2.108).

For $\theta = 0$ or $theta = \pi$, $\cos^2\theta = 1$ gives

$$h_+ = -\frac{4\omega^2\mu r_0^2}{r}\cos(2\omega(t-r)-2\phi) = h_\times, \tag{2.111}$$

where both components are maximum and equal and the GW is then circularly polarised. This would be the case for an observer exactly perpendicular to the plane of the binary and so "head-on" with the binary.

At $\theta = \pi/2$, the minimum values are reached, with only the "plus" component non-zero, and the observer in the same plane as the binary, with the GW linearly polarised

$$h_+ = -\frac{2\omega^2\mu r_0^2}{r}\cos(2\omega(t-r)-2\phi). \tag{2.112}$$

In the general case for $h_+$ from Eq. 2.109 and $h_\times$ from Eq. 2.109 the power loss for the binary is following Ref. [63],

$$L^{[GW]} = \frac{32}{5}\mu^2 r_0^4\omega^6. \tag{2.113}$$

and for an equal mass binary, this would be

$$L^{[GW]} = \frac{8}{5}M^2 r_0^4\omega^6. \tag{2.114}$$

Consequently, for an isolated, monochromatic, non-relativistic source, the GW is proportional to the second derivative of the quadrupole moment of the energy density at the point where the past light cone of the observer intersects the source. In general, the dipole moment is significantly larger than the quadrupole moment for a system, implying that GWs are significantly weaker than electromagnetic waves.

The linearised theory of GWs has enjoyed extensive study, however a non-linear approach will be crucial as some of the properties of the gravitational field may only be evident through the non-linear terms. For a qualitative understanding linearised-gravity approximations will suffice and in number of cases be be accurate, however, for highly relativistic sources, such as the merger of two rapidly spinning black holes, detailed numerical calculation is unavoidable. For cases of even mildly relativistic systems, linearised gravitational approximations will also not suffice and at the very least post-Newtonian perturbative approaches will be required.

# Chapter 3

# The Bondi-Sachs formalism for the Einstein equations

*"the problem of gravitational waves is ready for solution, and you are the person to solve it."*

Remark to Hermann Bondi in 1955 by Marcus Fierz, Professor at the Eidgenössische Technische Hochschule (Swiss Federal Institute of Technology)

as recounted by Herman Bondi in "*Science, Churchill and Me* " [65]

Encouraged by discussions with Marcus Fierz (quotation above) and others at the Bern Conference in July 1955 (later known as GR0), Herman Bondi dedicated a significant part of his scientific work, thereafter, to the study of gravitational waves. He joined King's College in London in October of that same year starting up a group working on the theory of GR. Five years later, in 1960, he proposed a new approach to the study of GWs in Einstein's GR in his article in *Nature* [66]. This opened the door to a fifteen paper series on GWs, the first of which appeared two years later, in 1962. Collaborating with Metzner and van der Burg, he produced the details of this new approach to GWs based on outgoing null rays along which the GWs travelled. Their paper was confined to the case of axisymmetric spacetimes, however later that very year, the formalism was generalised, for non-axisymmetric spacetimes by Rainer Sachs [67]. The approach subsequently came to be referenced as the Bondi-Sachs (BS) formalism based on outgoing null rays with the fundamental quantity of the formalism being the metric. Independently of this work, Ezra Newman and Roger Penrose presented, also in the same year, 1962, their approach to tackling Einstein's equations which was based on null hypersurfaces, with the fundamental quantity of their formalism based on a null tetrad and its curvature components [68].

This chapter will discuss these seminal papers of Bondi [69] and Sachs [67], published in 1962, which led to the Bondi-Sachs formalism for the Einstein equations. Our discussions will extend to the interpretations of Newman and Penrose [68] in their equally ground-breaking paper of

that same year. We will also make reference to and follow the modern-day reviews [70, 71, 72], where the Bondi-Sachs formalism enjoys particular attention.

The BS formalism is based on the characteristic initial value problem (CIVP) (for a description see [73, 74, 75, 76]). Typically, characteristics have been a central feature of the analysis of hyperbolic partial differential equations (PDEs). However, the development of computational physics focused mainly on hydrodynamics, where the characteristics do not define useful coordinate surfaces and there is no generic outer boundary behaviour comparable to null infinity [77]. In the BS formalism asymptotic flatness is formulated in terms of characteristic hypersurfaces extending to infinity. This enabled the reconstruction, of the basic properties of GWs which had been developed in linearised theory on a Minkowski background, (as we outlined in Section 2.2), to a nonlinear geometric setting. The BS formalism led to the first unambiguous description of gravitational radiation in a fully nonlinear context, with its main nonlinear features being the *Bondi mass* and *Bondi news function*, and the mass loss formula relating them. The Bondi news function is an invariantly defined complex radiation amplitude $N = N_{\oplus} + iN_{\otimes}$, with real and imaginary parts corresponding to the time derivatives $\partial_t h_{\oplus}$ and $\partial_t h_{\otimes}$ of the "plus" and "cross" polarisation modes of the strain $h$, as described earlier in 2.2, incident on a GW antenna. The work presented by Bondi, his collaborators and Sachs in 1962 provided the strongest theoretical framework for the existence of GWs ending decades of doubt since first being postulated as a consequence of GR in 1916 [10]. It provided the first convincing evidence that mass loss due to gravitational radiation is a nonlinear effect of GR and that the emission of GWs from an isolated system is accompanied by a mass loss from the system [72].

## 3.1 The Bondi–Sachs metric

We follow the description as given in these references together with the extensive discussions of the formalism in [72, 71, 77] in presenting a summary of the salient features of the BS formalism below.

In setting up the BS metric, we will begin with the BS spacetime coordinates, $x^a (a = 0, 1, 2, 3)$, where:

- $x^0 = u = const$ are the outgoing null hypersurfaces, characterising the BS formalism;
- $x^1 = r$ is a surface area radial co-ordinate and
- $x^A$, $(A, B, C, ... = 2, 3)$ can be taken to be angular coordinates, such as spherical polars $(\theta, \phi)$, which are constant along the null rays.

As we have seen in Chapter 2, linear perturbations $h_{ab}$ of the Minkowski metric $\eta_{ab} = \text{diag}(-1, 1, 1, 1)$ in Eq, (2.29) obey the wave equation

$$\Big( - \frac{\partial^2}{\partial t^2} + \delta^{ij} \frac{\partial^2}{\partial x^i \partial x^j} \Big) h_{ab} = 0 \,, \tag{3.1}$$

with the standard Cartesian coordinates $x^i = (x, y, z)$ satisfying the harmonic coordinate condition to linear order. The retarded time $u$ described as

$$u = t - r \ , \ \ r^2 = \delta_{ij} x^i x^j \ , \tag{3.2}$$

define characteristic hypersurfaces of the hyperbolic equations Eq. (3.1), along which wavefronts can travel. A feature of these characteristic hypersurfaces is that they are also null hypersurfaces. By this we mean that their normals are null,

$$g^{ab}(\partial_a u)(\partial_b u) = 0 \rightarrow g^{uu} = 0, \tag{3.3}$$

implying that the hypersurfaces are constant:

$$k_a = -\nabla_a u = 0 \rightarrow u = const. \tag{3.4}$$

Another property of null hypersurfaces is that their normal direction, $k^a = \eta^{ab} k_b$, is also tangent to the hypersurface, $u = const$. Curves tangent to $k^a$ are null geodesics, called null rays, and generate the $u = const$ outgoing null hypersurfaces. The corresponding future pointing vector $k^a = -g^{ab}\partial_b u$ is tangent to the null rays. The angular coordinates $x^A$, $(A, B, C, ... = 2, 3)$, are constant along the null rays,

$$k^a \partial_a x^A = -g^{ab}(\partial_a u)\partial_b x^A = 0 \rightarrow g^{uA} = 0. \tag{3.5}$$

The surface area radial co-ordinate, $x^1 = r$, varies along the null rays, such that

$$\det[g_{AB}] = r^4 \mathfrak{q}, \tag{3.6}$$

where $\mathfrak{q}(x^A)$ is the determinant of the unit 2-sphere metric $q_{AB}$, embedded in flat Euclidean 3-space, associated with the angular coordinates $x^A$.
Taken in standard spherical coordinates, for example, $x^A = (\theta, \phi)$, we have

$$q_{AB} = \begin{pmatrix} 1 & 0 \\ 0 & \sin^2\theta \end{pmatrix} . \tag{3.7}$$

or

$$q_{AB} = \mathrm{diag}(1, \sin^2\theta) \tag{3.8}$$

so that $q = \sin^2\theta$.
The contravariant components $g^{ab}$ and covariant components $g_{ab}$ are related by

$$g^{ac} g_{cb} = \delta^a_b. \tag{3.9}$$

From Eq. (3.9)

$$\begin{aligned} \delta^u_r = 0 \ \ &\rightarrow \ \ g_{rr} = 0, \\ \delta^u_A = 0 \ \ &\rightarrow \ \ g_{rA} = 0. \end{aligned} \tag{3.10}$$

Hence the metric can be written in the BS form,

$$g_{ab}dx^a dx^b = -\frac{V}{r}e^{2\beta}du^2 - 2e^{2\beta}dudr + r^2 h_{AB}\Big(dx^A - U^A du\Big)\Big(dx^B - U^B du\Big), \tag{3.11}$$

where

$$g_{AB} = r^2 h_{AB}, \tag{3.12}$$

$$\det[h_{AB}] = \mathfrak{q}(x^A). \tag{3.13}$$

Consequently, the conformal 2-metric $h_{AB}$ only has two degrees of freedom.

On expanding Eq. (3.11), we obtain

$$\begin{aligned} ds^2 &= -\left[e^{2\beta}\left(1+\frac{W}{r}\right) - r^2 h_{AB}U^A U^B\right]du^2 \\ &\quad -2e^{2\beta}dudr - 2r^2 h_{AB}U^B dudx^A + r^2 h_{AB}dx^A dx^B, \end{aligned} \tag{3.14}$$

where the non-zero contravariant components are

$$g^{ur} = -e^{-2\beta}, \tag{3.15}$$

$$g^{rr} = \left(1+\frac{W}{r}\right)e^{-2\beta}, \tag{3.16}$$

$$g^{rA} = -U^A e^{-2\beta}, \tag{3.17}$$

$$g^{AB} = \frac{1}{r^2}h^{AB}. \tag{3.18}$$

where $h^{AC}h_{CB} = \delta^A_B$.
In the original papers, Ref [78] used V instead of W, with V=r+W. The Minkowski spacetime is recovered on setting $\beta = J = U = W = 0$, with J defined in Eq. (3.28) and U defined in Eq. (3.30) on page 32. In numerical simulations $V = r + r^2 W_c$ with $W_c$ bounded as $r \to \infty$.

In the 1962 paper [78], the Bondi metric was given for the axisymmetric case with rotational symmetry and with $\gamma = \gamma(u, r, \theta)$, as described by

$$\begin{aligned} g^{(B)}_{ab}dx^a dx^b &= \Big(-\frac{V}{r}e^{2\beta} + r^2 U e^{2\gamma}\Big)du^2 \\ &\quad -2e^{2\beta}dudr - r^2 U e^{2\gamma}dud\theta + r^2\Big(e^{2\gamma}d\theta^2 + e^{-2\gamma}\sin^2\theta d\phi^2\Big), \end{aligned} \tag{3.19}$$

with $U \equiv U^\theta$.

The original Bondi metric has the reflection symmetry $\phi \to -\phi$ which is not suitable for

describing an axisymmetric rotating star [72].
Also, in the original work, the areal coordinate $r$ becomes singular when the expansion $\Theta$ of the null hypersurface vanishes, where [79, 67]

$$\Theta = \nabla_a(e^{-2\beta}k^a) = \frac{2}{r}e^{-2\beta}, \tag{3.20}$$

$$k^a\partial_a = -g^{ur}\partial_r. \tag{3.21}$$

In the Newman-Penrose formalism [80], the affine parameter $\lambda$, is the standard radial coordinate along the null rays. This remains regular when $\Theta = 0$. $\Theta = 0$ occurs in cosmology on the past null cone, and codes with an affine radial parameter are used [81, 82, 83]. The areal distance and affine parameter are related by $\partial_r\lambda = e^{2\beta}$, so that as long as $\beta$ is finite, the areal coordinate is non-singular [84]. As mentioned, whilst the BS formalism was based on outgoing null rays with the fundamental quantity of the formalism being the metric, the Newman-Penrose formalism was based on null hypersurfaces, with the fundamental quantity of their formalism based on a null tetrad and its curvature components [68]. Whilst the Newman-Penrose formalism involved more variables it led to a more geometric treatment of gravitational radiation, culminating in the description in terms of the conformal compactification of future null infinity, denoted by $\mathcal{I}^+$. We will next look at elements of the Newman-Penrose formalism.

## 3.2 The complex dyad and the complex differential angular operators

The Newman-Penrose formalism introduced a convenient way to represent vector and tensor quantities over the unit 2-sphere, $q_{AB}$, embedded in flat Euclidean 3-space as well as their covariant derivatives. This was by way of introducing spin-weighted quantities and the *eth* operator, $\eth$ [85, 86].

Here, following [87, 71, 88] we will represent $q_{AB}$ by means of a complex dyad $q^A$, a 2-vector, whose real and imaginary parts are unit vectors that are orthogonal to each other and which has the properties

$$\begin{aligned} q^Aq_A &= 0, \\ q^A\bar{q}_A &= 2, \\ q_{AB} &= \frac{1}{2}(q_A\bar{q}_B + \bar{q}_Aq_B). \end{aligned} \tag{3.22}$$

$q_A$ is not unique, up to a unitary factor, meaning that if $q_A$ represents a given 2-metric, then so does $q'_A = e^{i\alpha}q_A$. It is convenient to write the dyad in a way that is natural to the coordinates being used [71], which for spherical polar coordinates

$$q^{^A} = \left(1, \frac{i}{\sin\theta}\right), \text{ and } q_{_A} = (1, i\sin\theta). \tag{3.23}$$

Embedding the sphere into Euclidean space with coordinates $(r, \phi^2, \phi^3)$ that are always *right-handed*, avoids the complication of different parities such as reflection [71].

With the dyad defined, complex quantities may be constructed representing tensorial ob-

jects, such as

$$\begin{aligned} X_1 &= T_A q^A, \\ X_2 &= T^{AB} q_A \bar{q}_B, \text{ and} \\ X_3 &= T^{AB}_C \bar{q}_A \bar{q}_B \bar{q}^C. \end{aligned} \tag{3.24}$$

Each object has no free indices, and has associated with it a spin-weight $s$ . Following [71], we do this by, for instance, taking a spin-weighted field, $\mu(\phi^2, \phi^3)$, with spin-weight $s = 0$. Now, given a vector field $v_{_A}(\phi^2, \phi^3)$, we define

$$V = q^{_A} v_{_A} \tag{3.25}$$

to be a field with spin-weight $s = 1$. $V$ is a complex quantity containing two independent fields and so uniquely represents the two components of $v_{_A}$. The quantity $\bar{V}$ may also be defined as $\bar{V} = \bar{q}^{_A} v_{_A}$ with spin-weight $s = -1$ (but is not independent of $V$).
Now, consider a second-rank tensor $t_{_{AB}}$. We may then construct two independent fields

$$\begin{aligned} T &= q^{_A} q^{_B} t_{_{AB}}, \qquad \text{with spin-weight } s = 2, \\ \tau &= q^{_A} \bar{q}^{_B} t_{_{AB}}, \qquad \text{with spin-weight } s = 0. \end{aligned} \tag{3.26}$$

Together $T$ and $\tau$ have 4 independent fields to represent the 4 components of $t_{_{AB}}$. For any tensor field $w_{A\cdots D}$,

$$F = f_{_{A\cdots BC\cdots D}} q^{_A} \cdots q^{_B} \bar{q}^{_C} \cdots \bar{q}^{_D}, \tag{3.27}$$

with $m$ factors $q$ and $n$ factors $\bar{q}$ is defined to be a quantity with spin-weight $s = m - n$.

An arbitrary BS metric, $h_{AB}$ may be represented by its dyad component

$$J = \frac{1}{2} h_{AB} q^A q^B, \tag{3.28}$$

with the spherically symmetric case characterised by $J = 0$.
We also introduce the fields

$$K = \sqrt{1 + J\bar{J}}, \tag{3.29}$$

and

$$U = U^A q_A. \tag{3.30}$$

Next, we consider the complex differential angular operators (eth operators) $\eth$ and $\bar{\eth}$ [87], following [71].

With $F$ defined in Eq. (3.27), we require

$$\begin{aligned} \eth F &= \nabla_{_E} f_{_{A\cdots BC\cdots D}} q^{_A} \cdots q^{_B} \bar{q}^{_C} \cdots \bar{q}^{_D} q^{_E}, \\ \bar{\eth} F &= \nabla_{_E} f_{_{A\cdots BC\cdots D}} \cdots q^{_B} \bar{q}^{_C} \cdots \bar{q}^{_D} \bar{q}^{_E}. \end{aligned} \tag{3.31}$$

where it is evident that if $F$ has spin-weight $s$, then $\eth F$ has spin-weight $s+1$ and $\bar{\eth}F$ has spin-weight $s-1$. Hence, we define

$$\begin{aligned} \eth F &= q^{A}\,\partial_{A} F + s\Upsilon F, \\ \bar{\eth} F &= \bar{q}^{A}\,\partial_{A} F - s\bar{\Upsilon} F, \end{aligned} \tag{3.32}$$

where

$$\Upsilon = -\frac{1}{2} q^{A}\,\bar{q}^{B}\,\nabla_{A} q_{B}. \tag{3.33}$$

For spherical polar coordinates,

$$\Upsilon = -\cot\theta \tag{3.34}$$

Now, consider, for example, the spin-weight 1 field

$$V = q^{A} v_{A}. \tag{3.35}$$

From Eqs. (3.32) and (3.33), we obtain

$$q^{A}\,\partial_{A}(q^{B} v_{B}) + \Upsilon q^{C} v_{C} = q^{A} q^{B}\,\partial_{B} v_{A} - q^{A} q^{B} v_{C} \Gamma^{C}_{AB}, \tag{3.36}$$

leading to

$$v_{C}\left[q^{C}\Upsilon + q^{A}\left(\partial_{A} q^{C} + q^{B}\,\Gamma^{C}_{AB}\right)\right] = 0. \tag{3.37}$$

This will be valid for all $v_{C}$. The bracketed term is a covariant derivative. Hence, we may write

$$q^{C}\,\Upsilon + q^{A}\,\nabla_{A} q^{C} = 0\,. \tag{3.38}$$

To recover $\Upsilon$, lower the free superscript $^{C}$, then contract with $\bar{q}^{C}$.
The commutator is

$$(\bar{\eth}\eth - \eth\bar{\eth})F = 2sF, \tag{3.39}$$

so unless the spin-weight is $s = 0$, $\eth$ and $\bar{\eth}$ do not commute.

## 3.3 The Einstein equations

Returning to the Einstein equations given in Eqs.(2.39) on page 15, we write

$$E_{ab} := R_{ab} - \frac{1}{2} g_{ab} R^{c}{}_{c} - 8\pi T_{ab} = 0\ , \tag{3.40}$$

where $R_{ab}$ is the Ricci tensor, $R^{c}{}_{c}$ its trace and $T_{ab}$ the matter stress-energy tensor.

The spin-weight $s$ of the quantities in Eqs. (3.28), (3.29), (3.30) on page 32 are then eval-

uated for the metric (3.14) on page 3.14 as previously outlined,

$$\begin{aligned} s(V) = s(\beta) = 0\,, \qquad & s(J) = 2\,, \qquad & s(\bar{J}) = -2\,, \\ & s(U) = 1\,, \qquad & s(\bar{U}) = -1\,. \end{aligned} \tag{3.41}$$

We may classify the 10 Einstein equations as:

- *hypersurface equations* $R_{11}, q^A R_{1A}, h^{AB} R_{AB}$ (these form a hierarchical set for $\beta, U$ and $W_c$);
- *evolution equation* $q^A q^B R_{AB}$ for $J$;
- *constraints* $R_{0\alpha}$.

In numerical simulations an evolution problem is formulated in the region of spacetime between a time-like or null world-tube, $\Gamma$, and future null infinity ($\mathcal{J}^+$), with free initial data, $J$, given on $u = 0$, and with boundary data for $\beta, U, W_c, J$ satisfying the constraints given on the inner world-tube [89]. It is possible to include $\mathcal{J}^+$ in the computational grid by compactifying the radial coordinate, $r$. This may be done by means of a transformation, for example, of the form

$$r \to x = \frac{r}{r + r_\Gamma}\,. \tag{3.42}$$

which maps $r \in (0, \infty)$ to $x \in (0, 1)$. The Einstein equations remain regular at $\mathcal{J}^+$ under such a transformation in characteristic coordinates but not in general coordinates [89]. However, in analytic work it is normal practice to compactify using

$$r \to \rho = 1/r\,. \tag{3.43}$$

The BS metric is manifestly asymptotically flat in the Bondi gauge, with the metric tending to Minkowskian form as $r \to \infty$. Following [71], we take the Minkowski metric in spherical coordinates $(t, r, \phi^A)$, and then write in compactified BS coordinates, by applying the coordinate transformation $(t, r) \to (u, \rho)$, where

$$u = t - r, \quad \rho = \frac{1}{r}. \tag{3.44}$$

This results in the metric form

$$ds^2 = \rho^{-2} \left( -\rho^2 du^2 + 2du\, d\rho + q_{_{AB}} d\phi^A\, d\phi^B \right)\,. \tag{3.45}$$

Quantities in the Bondi gauge will be represented by notation $\tilde{}$. As $\tilde{\rho} \to 0$,

$$\tilde{J} = 0\,, \quad \tilde{K} = 1\,, \quad \tilde{\beta} = 0\,, \quad \tilde{U} = 0\,, \quad \tilde{W} = 0\,. \tag{3.46}$$

The **gravitational news** as defined by Bondi *et al.* [69], is

$$\mathcal{N} = \frac{1}{2}\partial_{\tilde{u}}\partial_{\tilde{\rho}}\tilde{J}\,, \tag{3.47}$$

evaluated in the limit $\tilde{\rho} \to 0$.
This is related to the strain in the TT gauge by

$$\mathcal{N} = \frac{1}{2}\partial_{\tilde{u}} \lim_{\tilde{r}\to\infty} \tilde{r}\,(h_+ + ih_\times) = \frac{1}{2}\partial_{\tilde{u}}\mathcal{H}\,, \tag{3.48}$$

The rescaled strain $\mathcal{H}$ is

$$\mathcal{H} \coloneqq \lim_{\tilde{r}\to\infty} \tilde{r}(h_+ + ih_\times) = \partial_{\tilde{\rho}}\tilde{J}\,, \tag{3.49}$$

In many cases it is not possible to choose the coordinates so that the Bondi gauge applies. So, in order to determine the GW emission, a coordinate transformation to the Bondi gauge coordinates must be made. This procedure is quite complicated and is described in the general case in Refs. [90, 91] .

## 3.4 Einstein equations linearised about Minkowski space

We evaluate the Einstein equations (2.39) on page 15 for the metric Eq. 3.14 on page 30 in the case of small perturbations in vacuum, neglecting second-order terms in $J, \beta, U, W$. Then, the hypersurface equations are

$$E_{11}: \qquad \frac{4}{r}\partial_r\beta = 0\,, \tag{3.50}$$

$$q^A E_{1A}: \qquad \frac{1}{2r}\left(4\eth\beta + r\bar{\eth}\partial_r J + r^3\partial_r^2 U + 4r^2\partial_r U\right) = 0\,, \tag{3.51}$$

$$h^{AB}E_{AB}: \qquad (4 - 2\eth\bar{\eth})\beta + \frac{1}{2}(\bar{\eth}^2 J + \eth^2\bar{J}) + \frac{1}{2r^2}\partial_r(r^4\eth\bar{U} + r^4\bar{\eth}U) - 2r^2\partial_r W - 4rW = 0\,. \tag{3.52}$$

The evolution equation is

$$q^A q^B E_{AB}: \quad -2\eth^2\beta + \partial_r(r^2\eth U) - 2r\partial_r J - r^2\partial_r^2 J + 2r\partial_r\partial_u(rJ) = 0\,. \tag{3.53}$$

The constraint equations are [92]

$$E_{00}: \quad \frac{1}{2r^2}\Big(r^3\partial_r^2 W + 4r^2\partial_r W + 2rW + r\eth\bar{\eth}W + 2\eth\bar{\eth}\beta \\ -4r\partial_u\beta - r^2\partial_u(\eth\bar{U} + \bar{\eth}U) + 2r^2\partial_u W\Big) = 0\,, \tag{3.54}$$

$$E_{01}: \quad \frac{1}{4r^2}\Big(2r^3\partial_r^2 W + 8r^2\partial_r W + 4rW + 4\eth\bar{\eth}\beta - \partial_r(r^2\eth\bar{U} + r^2\bar{\eth}U)\Big) = 0\,, \tag{3.55}$$

$$q^A E_{0A}: \quad \frac{1}{4}\Big(2r\eth\partial_r W + 2\eth W + 2r(4\partial_r U + r\partial_r^2 U) + 4U \\ +(\eth\bar{\eth}U - \eth^2\bar{U}) + 2\bar{\eth}\partial_u J - 2r^2\partial_r\partial_u U - 4\eth\partial_u\beta\Big) = 0\,. \tag{3.56}$$

The required ansatz for the quantities $\beta^{[e]}, U^{[e]}, W^{[e]}, J^{[e]}$, is

$$\beta^{[e]} = \Re(\beta^{[2,2]}(r)e^{i\nu u})_0 Z_{2,2}\,,\ \ U^{[e]} = \Re(U^{[2,2]}(r)e^{i\nu u})_1 Z_{2,2}\,,\ \ W^{[e]} = \Re(W^{[2,2]}(r)e^{i\nu u})_0 Z_{2,2}\,, \\ J^{[e]} = \Re(J^{[2,2]}(r)e^{i\nu u})_2 Z_{2,2}\,, \tag{3.57}$$

with the superfix $^{[2,2]}$ indicating a coefficient of ${}_sZ_{2,2}$.
The perturbations oscillate in time with frequency $\nu/(2\pi)$. The quantities ${}_sZ_{\ell,m}$ are spin-weighted spherical harmonic basis functions related to the usual ${}_sY_{\ell,m}$ as specified in [54, 71]. They have the property that ${}_0Z_{\ell,m}$ are real, enabling the description of the metric quantities $\beta, W$ (which are real) without mode-mixing; however, for $s \neq 0$ ${}_sZ_{2,2}$ is, in general, complex. A general solution may be constructed by summing over the $(\ell, m)$ modes, but that is not needed here, since we are considering a source that is continuously emitting GWs at constant frequency dominated by the $\ell = 2$ (quadrupolar) components (Of course, the wave frequency changes with inspiral, and we are assuming that this timescale is much longer than the wave period). We substitute the ansatz Eqs. (3.57) into Eqs. (3.52) with $\ell = 2$, leading to a system of ordinary differential equations (ODEs) in $r$:

$$E_{11}: \frac{4}{r}\frac{d}{dr}\beta^{[2,2]} = 0; \tag{3.58}$$

$$q^A E_{1A}: -\frac{1}{2r^2}\frac{d}{dr}\left(r^4\frac{d}{dr}U^{[2,2]}\right) + \frac{d}{dr}J^{[2,2]} = 0; \tag{3.59}$$

$$h^{AB}E_{AB}: 16\,\beta^{[2,2]} + 2\sqrt{6}\,J^{[2,2]} - 2\sqrt{6}\,r\,U^{[2,2]} - \sqrt{6}\,\frac{d}{dr}\left(r^2\,U^{[2,2]}\right) - 2\,\frac{d}{dr}W^{[2,2]} = 0; \tag{3.60}$$

$$E_J: \ 4\sqrt{6}\beta^{[2,2]} - 2\,\frac{d}{dr}\left(r^2\,U^{[2,2]}\right) + \frac{d}{dr}\left(r^2\frac{d}{dr}J^{[2,2]}\right) - 2\,i\,\nu\,r\,\frac{d}{dr}\left(r\,J^{[2,2]}\right) = 0\,. \tag{3.61}$$

### 3.4.1 Solution Procedure

Eqs. (3.58) to (3.61) may be solved in the following way. First, note that from Eq. (3.58) $\beta^{[2,2]}$ takes a constant value. We can take the constant value as, say, $b_0$. Eqs. (3.59) and (3.61) constitute a coupled system of ordinary differential equations (ODEs) in $U^{[2,2]}$ and $J^{[2,2]}$ only. Once they have been solved, then we can solve Eq (3.60) for $W^{[2,2]}$. Now, following Ref. [54],

the equations for $q^A E_{1A}$ and $E_J$ may be manipulated to give

$$-2J_2(2\rho + i\nu) + 2\frac{dJ_2}{d\rho}\left(2\rho^2 + i\nu\rho\right) + \rho^3\frac{d^2J_2}{d\rho^2} = 0, \tag{3.62}$$

where $\rho = 1/r$ and in the reference, Ref. [54], $J_2(\rho) \equiv d^2J^{[2,2]}/d\rho^2$.
Eq. (3.62) has solution

$$C_1\rho + C_2\exp\left(\frac{2i\nu}{\rho}\right)\left(2\nu^4 + 4i\nu^3\rho - 6\nu^2\rho^2 - 6i\rho^3\nu + 3\rho^4\right)/\rho^3. \tag{3.63}$$

We then integrate twice with respect to $\rho$, then replace $\rho$ by 1/r, and rename the integration constants to find

$$J^{[2,2]} = 2\sqrt{6}C_{10} + \frac{2\sqrt{6}C_{30}}{r} + \frac{2\sqrt{6}C_{40}}{r^3} + C_{in0}\exp(2ir\nu)\sqrt{6}\left(\frac{1}{r^3} - 2i\frac{\nu}{r^2} - \frac{\nu^2}{r}\right). \tag{3.64}$$

The procedure leading to Eq. (3.62) gives an expression for $U^{[2,2]}$ in terms of $J^{[2,2]}$:

$$U^{[2,2]} = -\sqrt{6}i\nu C_{10} + \frac{2\sqrt{6}b_0}{r} + \frac{2\sqrt{6}C_{30}}{r^2} - \frac{4i\nu\sqrt{6}C_{40}}{r^4} - \frac{3\sqrt{6}C_{40}}{r^4}. \tag{3.65}$$

Finally, integration of Eq. (3.60) on page 36 leads to

$$W^{[2,2]} = 6i\nu r^2C_{10} + r(12C_{10} - 10b_0) + C_{50} - \frac{12i\nu C_{40}}{r} - \frac{6C_{40}}{r^2} - C_{in0}\exp(2ir\nu)\frac{3}{r^2}. \tag{3.66}$$

The solution includes constants of integration $b_0, C_{in0}, C_{10}, C_{30}, C_{40}, C_{50}$, two of which are fixed on applying the constraints $E_{00}, q^A E_{0A}$ giving

$$C_{50} = 12\nu^2C_{40}\,,\quad C_{10} = \frac{2b_0 + i\nu C_{30} + i\nu^3C_{40}}{3}\,. \tag{3.67}$$

The remaining Einstein equation $E_{01}$ is known as the trivial equation, since it is automatically satisfied provided all the other Einstein equations are satisfied [69]. An expression for the GWs for the above solution is given in Sec. 6.2 on page 80.

# Chapter 4

# Astrophysics of gravitational wave sources

GW sources may be broadly categorised into 4 types for the purposes of detection, [28]:

- **short-lived and well defined**. Here, compact binary coalescence (CBC) is the canonical example.
- **short-lived and** *a priori* **poorly known**. The supernova explosion is the canonical example in this case.
- **long-lived and well defined**. Continuous waves from spinning neutron stars are examples of this type.
- **long-lived and stochastic**. Primordial gravitational waves from the Big Bang belong to this category.

In the case of terrestrial detection, for current and pipeline detectors, the first category is the most prolific, with all of the current confirmed detections falling into this category.

For future spaced-based detectors, such as LISA, able to operate in the milliHz regime, the pre-coalescence phase of galactic binaries BNS, will be accessible, as will the coalescence of binary super-massive black holes (SMBHs), such as those from galaxy mergers [93]. Pulsar timing arrays (PTAs) may be able to detect a stochastic astrophysical background from the superposition of cosmologically distant SMBH binary systems at even lower frequencies in the $\sim$nHz regime.

## 4.1 Compact binaries and compact body mergers

Compact objects such as NS and BH may exist in binary configurations such as BBH, NSBH and BNS. In tight enough orbits the evolution of the system could lead to a CBC. In the case that one of the compact bodies is a NS or even both, tidal forces will come into play. We shall refer to any compact body merger where at least one of the compact bodies is a NS, that is

either a BNS or a NSBH, as a NS merger. A NS that is tidally perturbed, may suffer tidal disruption and loss of mass, leading to eventual coalescence. However, the evolution will not lead to coalescence if the NS loses mass at a rate that leads to it becoming unbound or if it undergoes a "birth kick" that disrupts the bound orbit [94]

For a compact binary (BBH, NSBH or BNS) that evolves to coalescence resulting in a single BH, three distinctive stages occur: **inspiral**; **merger** and **ringdown**. The last stable orbit or innermost stable circular orbit (ISCO) is the innermost complete orbit before the transition from inspiral to merger. Perturbative post-Newtonian approximations may be used to obtain the gravitational waveforms quite accurately for the inspiral stage. However, for the merger, NR is required because of the strong relativistic effects. The first NR calculation to model the merger of compact bodies for inspiral, merger, and ringdown was completed by Frans Pretorius in 2005 [95] and was for the case of a BBH. In that same year, independent efforts by other groups also presented templates for the merger of a BBH [96, 97] Providing these templates were critical for GW detection efforts. Simulations for NS mergers have proved more difficult to complete in full GR. This is partly due to the shock formation and degeneracy at the stellar surface. These are both sources of nonsmoothness which make the numerical calculations less accurate. Around the same time as Pretorius completed the case for BBH in full GR, many other groups, including the group of Shibata and co-workers in Kyoto and Tokyo were setting the stage for BNS mergers [98, 99, 100, 101, 102]. The reason for the difficulties in generating full GR simulations for NS mergers is the uncertainty of the EOS and internal composition of NSs.

There are several routes for the formation of compact binaries, however not all will lead to merger. In order for a merger to occur the binaries need to be sufficiently close as orbital energy loss through GW emission is not efficient at wide separations [103].

Compact binary orbital decay induced by GW decay may be estimated by "*Peters' timescale*" who used the quadrupole formula to calculate how the semimajor axis and the eccentricity of a Keplerian ellipse evolve in time [104]. This was the first successful quantitative description of the relationship between gravitational radiation and the decay of binary orbits. The calculation is based on two point masses and is exact for circular orbits, essentially giving the timescale of orbital decay scaling as a power of 4 to the orbital separation.

This places upper limits on the orbital separation of binaries to occur within Hubble time. Improved gravitational radiation time-scales involving corrections to "Peters'" formula have been given recently by Zwick, *et. al* in [105], using the quadrupole formula to the energy of a PN orbit rather than a Keplerian orbit.

Peters' timescale is often used in the estimation of the probability of a population of compact objects producing GWs detectable by GW observatories. A fractional increase in the timescale of gravitational decay corresponds to a fractional increase in the time that any signal remains in the optimal frequency band of the observatory, impacting on how many and what potential sources of GWs are considered promising for both LISA and LIGO-Virgo observatories [105].

Ref. [106] provides the gravitational radiation merger timescale, $\tau_{\rm GW}$, for a BNS merger as

$$\begin{aligned}\tau_{\rm GW} &= \frac{5}{64}\frac{a^4}{\mu M^2} = \frac{5}{64}\frac{a^4}{q(1+q)M_1^3} \\ &= 2.2\times 10^8 q^{-1}(1+q)^{-1}\left(\frac{a}{R_\odot}\right)^4\left(\frac{M_1}{1.4\,M_\odot}\right)^{-3}\ \text{yr},\end{aligned} \tag{4.1}$$

where $M_1$, $M_2$, and $M \equiv M_1 + M_2$ are the individual NS masses and the total mass of the binary, $\mu = M_1 M_2/M$ is the reduced mass, $q = M_2/M_1$ is the binary mass ratio and the separation distance is given by $a$.

### 4.1.1 Binary black holes

In what is referred to as the "populations paper" [107]' the LIGO VIRGO Collaboration (LVC) researchers reconstructed the distribution of masses and spins of the BH population and estimated the merger rate for BNSs. These results will contribute to the understanding of the detailed astrophysical processes shaping the formation of these systems. The mass distribution of BHs and knowledge that BH spins can be misaligned suggests multiple scenarios for BH formation.

In the classical **isolated binary evolution**, the formation of the ultra-compact binary leading to the BBH merger, is driven through an unstable mass-transfer phase where a common-envelope (CE) is ejected [108]. **Dynamical formation** BBHs are produced by three-body encounters in stellar clusters. Less than a few percent of all observed events of BBH formation are expected to be formed in globular clusters whilst a magnitude higher is expected from open and young star clusters from this type of formation [109]. In the **chemically homogeneous evolutionary channel**, rapidly rotating stars in near contact binaries that experience efficient internal mixing, may result in the formation of compact BBHs [103]. These would be for situations of massive stars in low metallicity environments where strong losses of angular-momentum due to winds are not present [110]. In this scenario, however, low-mass BBHs with M$\lesssim$ 10M$\odot$ are not produced. The classical isolated evolutionary channel for BBH begins with massive stellar-binary systems that evolve starting from zero-age main sequence (ZAMS). Atmospheric transfer or mass transfer (MT) must occur, leading to Roche lobe overflow (RLO) for one of the stars, the donor. The accretor acquires enough mass for BH formation either through direct core collapse, bypassing a SN, or through a SN explosion with the remnant being a BH. Section 4.2 for a description of BH formation. The BH formation may be modelled according to [111]. In the event that the second star also evolves to a BH, leading to a BBH, the merger time, $t_{\rm merger}$, may be estimated from "Peters' timescale" based on the component masses ($M_{\rm BH}$), their mutual separation and eccentricity [103]. For BBH formation, the following are factors in attaining the proper target BH

- **metallicity**. The higher the metallicity, the more massive both primary and secondary masses need to be, because initial-mass distributions widen.

- **initial binary separation**. Stellar interactions occur later in initially wide binaries than in close binaries. Depending on the initial separation, the total mass loss due to stellar

winds can operate on different time-scales.

- **MT efficiency**. Inefficient MT process, will require more massive progenitors in order to reach the target BH masses.

### 4.1.2 Neutron star mergers

NS mergers refer to both BNS and NSBH mergers. They have been detected across the EM spectrum, and are likely to produce neutrinos over several decades in energy [112]. Distinct insights into the physics of NS mergers are provided by the non-thermal prompt and afterglow emission of short gamma ray bursts (SGRBs) and the quasi-thermal emission from the radioactively powered kilonovae.

The addition of information emerging from GW detection of NS mergers, to MMA is expected to:

- lead to a better understanding of sources of GWs;
- lead to a better understanding of sources astrophysical neutrinos;
- enable precision cosmology;
- create the opportunity for unique tests of fundamental physics;
- shed light on the origin of heavy elements;
- improve the understanding of the behavior of relativistic jets and
- provide information on the EOS of supranuclear matter.

There are a number of good reviews on NS mergers emerging at the turn of this decade as a precursor to upcoming runs of terrestrial GW detectors , such as those on NS Mergers [113, 112], the challenges ahead for multimessenger analyses of GWs [114], modelling NSBH binaries [115], modelling DNSs radio and GWs [116] and NSBH mergers [117]
We will provide a reflection on NS mergers referencing these and other relevant sources such as those on binary and millisecond pulsars [118] and on BNS mergers [119].
Following [118], the favoured route for BNS formation is sketched in Fig. 4.1.

We begin with a configuration of a binary star system, with one of the companions more massive than the other. The more massive companion, the primary, would have a shorter main sequence lifetime than its companion, the secondary. The resulting core collapse may lead to a SN explosion for a stellar mass of $\gtrsim 8M_{\odot}$. The resulting remnant could be a BH or NS. The binary itself may or may not survive the SN explosion, with disruption occurring if more than half the total pre-supernova mass is ejected from the system Survival of the binary is also

dependent on the magnitude and direction of any impulsive "kick" velocity the NS receives when created in the SN explosion. There is a small percentage of binaries that do survive and, in these cases, when the companion, the secondary, is sufficiently massive it will evolve into a giant. It will undergo tidal deformation and overflow of its Roche lobe may occur. In this case, the NS accretes matter and therefore angular momentum at the expense of its companion. Infalling matter onto the NS will produce X-rays as a result of the liberation of gravitational energy, rendering the system visible as an X-ray binary system.

For high-mass companions, onset of core collapse may be reached and a second supernova may occur. If the binary system is fortunate enough to survive the second explosion, and the SN leaves a compact remnant, which is NS, then we will have a BNS as the result.
It is possible that in either the formation of either the first or second compact body a BH could be formed. This could be from direct core-collapse with the SN stage bypassed. The formation of a BH is discussed in [111]. Progenitor masses govern the routes the evolution of a star could take if a compact body were to be the final result. If core collapse is not halted, then only a BH could be formed. In the case where core collapse is halted and the evolution proceeds to a SN with a compact remnant, then either a NS or BH is formed. If the primary compact object is a NS the second is most often also a NS. This likely forms a BNS system, but could form a NSBH system if the primary accretes sufficient mass to collapse into a BH during the CE phase. If the primary collapses directly to a BH the system becomes an NSBH if the secondary is light enough to form a NS, otherwise it is a BBH system.

The 2–5 M$\odot$ range corresponds to the mass gap [120] which NS and BH are not expected to populate. The highest expected mass of a NS is expected to be $\lesssim$ 2M $\odot$, whilst the BHs are expected to have mass $\gtrsim$ 5m $\odot$.

Ideal conditions have to exist for a DNS to form in the scenario above and given that it is the favoured scenario, it is no surprise that they are the very rare in the Galaxy. There are more routes to the formation of NSBHs, so they occur more frequently.

A very small percentage of systems can be formed dynamically, where two compact objects form separately but become gravitationally bound when they travel close enough to each other.

Most binaries are likely to be disrupted when one of the components explodes in a supernova. Conditions will still have to be favourable for a NS to be a remnant of the first SN instead of a BH and the scenario will have to be repeated for the companion.

An example of such a formation is the Hulse-Taylor binary system [121], consisting of a pulsar, PSR B1913+16, a 59-ms radio pulsar with a characteristic age of $\sim 10^8$ yr, orbiting its companion every 7.75 hr. In the binary, the pulsar is the older, first-born, NS of the two NSs both formed as described above by SN explosions.

For BNS to be driven to merger within Hubble time, through GW radiation only, the initial separation is required to be $\lesssim 5\,R_\odot$ according to [122]. For this to happen requires a CE stage, where the two massive stars are not distinct. Alternatively, the primary may form a compact object before being enveloped by the secondary during its supergiant phase, hastening the inspiral and resulting in a smaller initial separation [112].

NS mergers have been detected across the EM spectrum, and are likely to produce neutrinos over several decades in energy. The non-thermal prompt and afterglow emission of SGRBs and the quasi-thermal emission from the radioactively powered kilonovae provide distinct insights into the physics of NS mergers. When combined with direct information on coalescence from

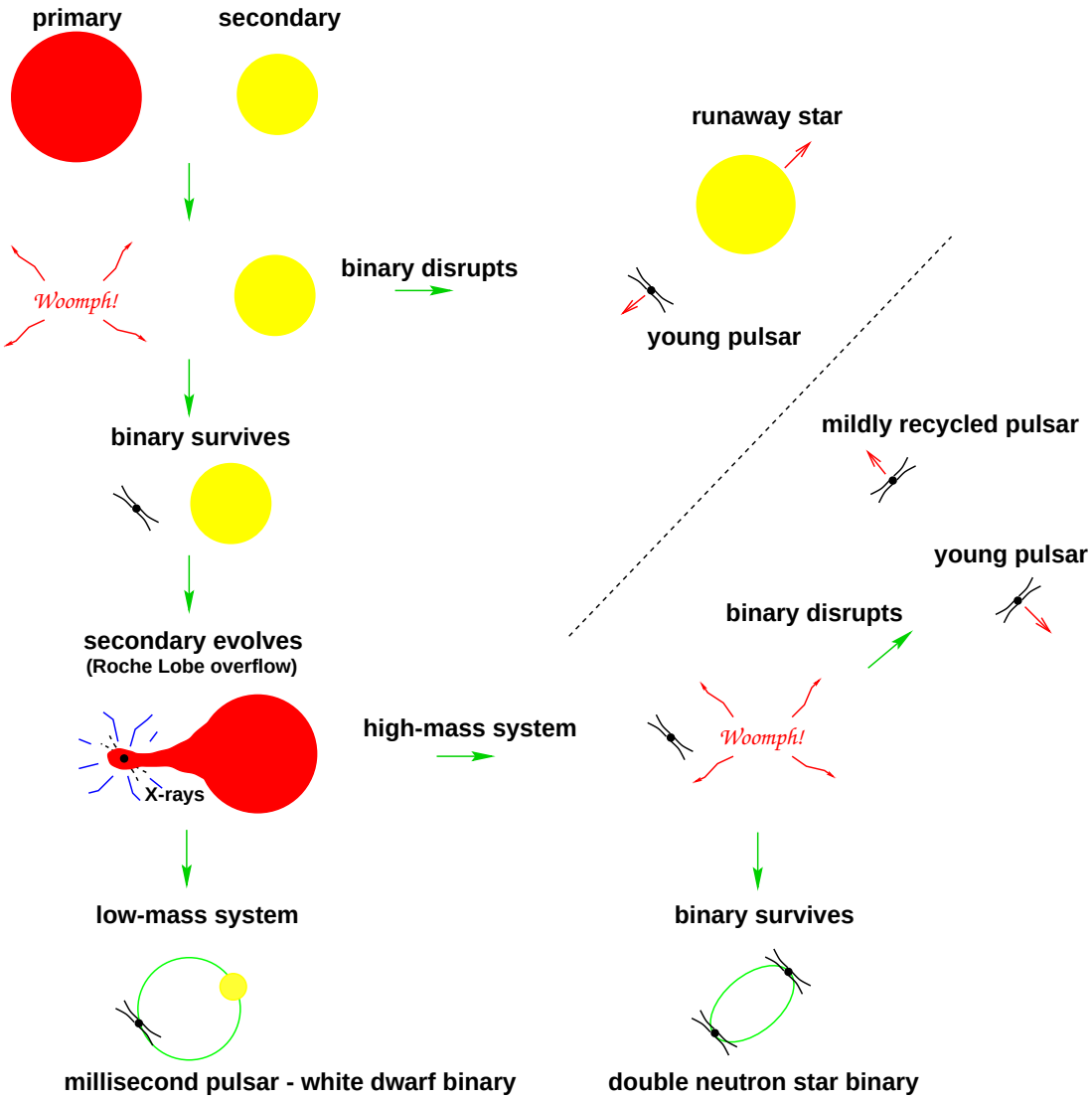


Figure 4.1: Cartoon showing various evolutionary scenarios involving binary pulsars. From [118].

GWs and neutrinos these sources may become the best understood astrophysical transients. Multimessenger observations of these cataclysmic events will determine sources of GWs and astrophysical neutrinos, enable precision cosmology, and unique tests of fundamental physics, the origin of heavy elements, the behaviour of relativistic jets, and the EOS of supranuclear matter.

## 4.2 Supernovae

We next turn our attention to another progenitor of detectable GW waves. Whilst no detection has taken place yet, SN are expected to produce, under certain conditions, GW waves detectable by the current generation of interferometers or those on the horizon.

### 4.2.1 The astrophysics of supernovae

Whilst the central engines and inner regions of Core-collapse supernovae (CCSNe) have yet to be fully understood, there exist several studies of their progenitors and the subsequent evolution and detection [123, 124, 125, 126, 127, 128]. We will follow these discussions in summarising the evolution of CCSNe. Whilst supernovae are touted as one of the possible detectable sources of GW's, none have led to resultant detected GW's. BBH and BNS mergers are currently the only GW events picked up by LIGO and VIRGO. For now, all detection of SN have been confined to EM detection. The photons originate at the outer edge of the star and hence provide only limited information on the interior regions of the star. The detection of GW's, which are the result of the aspherical motion of the inner regions, will provide a wealth of information on these regions and the mechanism leading to the SN explosion, where all the four fundamental forces of nature are involved.

### 4.2.2 Star evolution leading to core collapse

The majority of stars spend their life in the main sequence, in the hydrogen burning phase which in the case of the star in our solar system is of the order of $\sim 10^{10}$ years. For stars of mass, M, this time is scaled by a factor of $(M/M_{\odot})^{-2.5}$. The larger the star the quicker the hydrogen burning phase. The hydrogen is converted to helium and once the hydrogen is depleted, nuclear burning proceeds to produce heavier and more bound nuclei. The rate of the nuclear burning process increases after the hydrogen burning face. The initial mass of the star dictates the evolution of the stars, with the least massive stars not reaching the higher core burning phases. These result in stars where the nuclear burning phase does not proceed beyond the carbon (C) and oxygen (O) stage resulting in carbon oxygen white dwarfs (WD). Typically these stars would have initial mass $\lesssim 8{-}9M_{\odot}$. Slightly more massive stars of mass $8M_{\odot} \lesssim M \lesssim 9M_{\odot}$ may terminate their burning phases with residual oxygen, neon (Ne), and Magnesium (Mg) leading to oxygen-neon-magnesium (ONeMg) WDs. Still heavier stars, with masses, $9M_{\odot} \lesssim M \lesssim 10M_{\odot}$, whilst terminating their evolution as ONeMg WDs, may be able to trigger core collapse leading to a supernova. We will consider the mechanisms for this in the next section 4.2.3. If the core collapse cannot be counteracted by the thermonuclear burning, this leads to a Protoneutron star (PNS). At the bounce, the shock launched expels the stellar envelope producing what is known as an electron-capture supernova (ECSN). If, on the other

hand, the nuclear burning phase reignites and is strong enough to counter the infall, nuclear burning proceeds to the final stage of nuclear burning stoppin at an iron (Fe) core leaving an iron-rich white dwarf.

For initial masses of $9M_\odot \lesssim M \lesssim 100M_\odot$, such massive stars terminate the nuclear burning process at silicon burning, resulting in an iron core.

Further contractions of the core will occur as a result of the high temperatures of the order $T \sim 10^{10}\,\mathrm{K}$. At these temperatures, the iron nuclei dissociate into alpha particles and free nucleons, colliding with high-energy photons, leading to the absorption of thermal energy and hence the reduction in pressure. The capture of electrons by nuclei and free protons contribute to the reduction in pressure, triggering. dynamical core collapse.

Stars with mass $\gtrsim 100M_\odot$ have a different evolution. The temperature reached after the central carbon burning phase is high enough (for the photons) to allow $e^+$ and $e^-$ pair production converting thermal energy to rest mass. Gravitational collapse is triggered as the adiabatic index falls below 4/3. For stars of initial mass $M \gtrsim 260M_\odot$, this loss proceeds unabated leading to a BH. However, this gravitational collapse may be countered by thermonuclear reactions in stars of intermediate mass in the range $(100M_\odot - 200M_\odot)$. These may then power what may be referred to as pair-instability supernovae (PISN). These SN explosions may have energies up to $\sim 10^{53}$ erg.

For stars of mass larger than $8M_\odot$, the evolution proceeds to several stages of core burning. After each stage of burning, shells with lighter nuclei are forced outward as burning proceeds in the next heavier shell which in turn will be forced outward as a heavier shell develops in the subsequent burning phases. This leads to a series of concentric shells with the lightest shell, outermost at the edge of the envelope and shells arranged with progressively heavier burning components towards the core. At the C-O core left by He-burning, the nuclear burning increases rapidly to go through the remaining stages to produce an Fe core. At the Fe core, nuclear fusion halts rendering the core inert. With no further burning processes to balance the gravitational attraction, the core begins to collapse. The core has the radius and density of an iron white dwarf, with the circumnuclear shells decreasing in density away from this core, with a density profile that is a power law going as $\rho \propto r^{-n}$ Typically n ranges from 1.5 to 3 just above the core and is around n=3 at the outer layers, with sometimes steep, shelf-like decline in the density between the shells such as between carbon and helium. The He envelope is normally radiative just before the explosion. Above the helium envelope sits whatever hydrogen-rich envelope has survived the stellar mass loss, which may be none at all (as is often the case for stars of initial mass $\geqq 40M_\odot$). The pressure and temperature of the H shell is relatively negligible when compared with the interior and so the structure of the interior of the star is not affected by the presence of a H shell or lack thereof. For the instances where an H shell is present, the density drop-off at the juncture of the H and He shells is even steeper that that at the juncture of the He and C shells. Blue supergiants (BSGs), are pre-supernova stars with H envelopes, where the H envelope is radiative, whilst red supergiants RSGs have convective hydrogen envelopes Helium or carbon stars do not contain H envelopes.

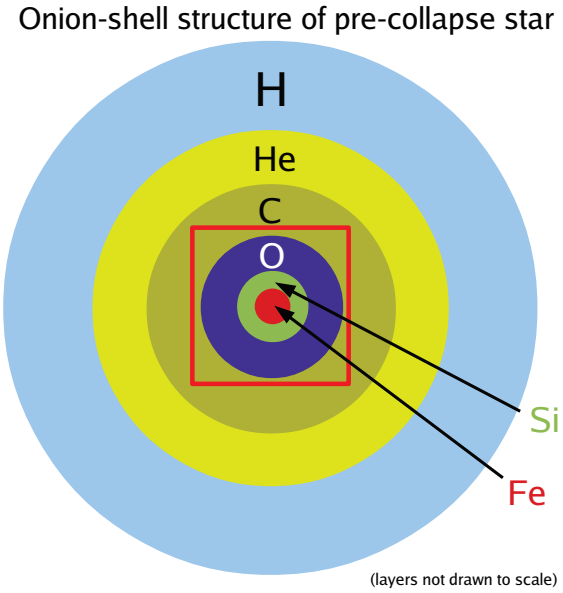


Figure 4.2: The "*onion-skin*" layered concentric shells of nuclear burning remnants for a progenitor of a SN. The density distribution can be described by a power law of radius, going as $\rho \propto r^{-n}$, with n about 1.5 in the immediate layers above the core and increasing up to 3 in the outer layers. From [129].

| burning stage | $\rho(g/cm^3)$ | fuel | products |
|---|---|---|---|
| H | 5.8 | H | He |
| He | $1.4 \times 10^3$ | He | C, O |
| C | $2.4 \times 10^5$ | C | O, Ne |
| Ne | $7.2 \times 10^6$ | Ne | O, Mg |
| O | $6.7 \times 10^6$ | O, Mg | Si, S |
| Si | $4.3 \times 10^7$ | Si, S | Fe, Ni |

Table 4.1: Table of typical densities

The radii of the outer edge of shells for each layer may be calculated by first integrating over each shell using the density profile to find the total mass and match with the expected mass of the corresponding shell:

$$\int_{r_{i-1}}^{r_i} 4\pi\rho(r)r^2 = m_i\,, \qquad i = 1, 2, 3, ... \tag{4.2}$$

where $m_i$ is the expected mass of the shell, with $r_i$, the radius of outer edge of the shell and $r_{i-1}$, the radius of inner edge of the shell of the $i$th shell.

We can associate the radius of the outer edge of the shell as the radius corresponding to the $i$th shell containing the mass $m_i$. For the core, the outer edge of shell is at $r_0$, and the mass is given by $m_0$, Now, the profile density for the matter in the shells in the envelope is given as power law of the radius, i.e. $\rho \propto r^{-n}$ or $\rho(r) = \frac{k}{r^n}$, $k > 0$, where $n$ ranges from 1.5 (shells

immediately above the core) to 3 (outermost shells).

Given values of the density profile, total mass and radius of the core we can then, by starting with the core, calculate the radius of the subsequent shells (given the expected masses of those shells).

$m_i = 4\pi \int_{r_{i-1}}^{r_i} \rho(r) dr = 4\pi \int_{r_{i-1}}^{r_i} \frac{k}{r^n} dr = 4\pi k n \left[ (r_{i-1})^{-1-n} - (r_i)^{-1-n} \right]$

So, the radius $r_i$, for the $i$th shell containing the mass $m_i$ is:

$$r_i = \left[ \frac{1}{(r_{i-1})^{n+1}} - \frac{m_i}{4\pi k n} \right]^{-\frac{1}{n+1}} \tag{4.3}$$

Starting with the radius of the core we may recursively solve for the shells in the envelope. For example the first shell immediately outside the core is given by:

$$r_1 = \left[ \frac{1}{(r_0)^{n+1}} - \frac{m_i}{4\pi k n} \right]^{-\frac{1}{n+1}} \tag{4.4}$$

Alternatively, we can use the stellar evolution code, Modules for Experiments in Stellar Astrophysics (MESA) code [130] to evolve progenitors from pre main-sequence to the white dwarf just before collapse of the iron-core. The MESA code runs up until the point where any location of the iron core reaches an infall velocity of greater than 1000 km $s^{-1}$. This corresponds to about 424s before iron collapse. From iron collapse to bounce is of the order of a few hundred ms and the GW wave generation following that is also of similar order. We conduct the simulation for a 15 $M_\odot$ star with metallicity $Z = 0.0134$ (equivalent to the solar metallicity). The results replicate the calculation done in [131] for the same conditions. The mass of the iron core is $\approx 1.44 M_\odot$. The first shell in the envelope is the Si-shell, with radii, $r_{i-1} \approx 2220$ km to $r_i \approx 3760$ km as described in our formulation above (i=1, in this case) The mass coordinate of the Si-shell corresponds to $m \approx 1.53 - 1.68\ M_\odot$. The outer edge of the Si-shell approximately meets the inner edge of the O-shell which then extends to an outer shell with mass coordinate $m \approx 2.26\ M_\odot$. The O-shell limits are $r_{i-1} \approx 3770$ km to $r_i \approx 26{,}620$ km (i=2).

### 4.2.3 Core collapse and the outer shells of stellar matter

The timescale of the core collapse is of the order of ∼0.3 s. The collapse of the core splits into two parts, with an outer part plunging supersonically, and the inner core collapsing at subsonic speed. The inner core will halt collapse on reaching supranuclear densities where the nuclear matter stiffens. this results in a bounce of the inner core. The resulting shock wave is launched into the collapsing outer core. However, the shock loses energy to dissociation of iron nuclei, stalling at ∼150 km within ∼10 ms after formation. The infalling shells of stellar matter then pile on the PNS, driving the evolution of the PNS to a BH. However, if there is a "revival" of the shock within a few hundred milliseconds, the resulting outward shock will lead to the expulsion of the infalling outer shells, leaving behind a stable neutron star. Whilst these outer shells will be proceeding at high velocity outwards, there may be conditions leading to stable outer shells existing at constant distance away from the GW event at the centre. These would

then be typical of the scenario we have postulated leading to an echo of a GW signal produced by a shell of matter.

Many computationally demanding multi-dimensional simulations exist [132, 133, 134] for generation of GW's from CCSNe. [134] provides models producing GW strains for supernovae characterised by GW strains where the GW signal starts with a burst shortly after bounce. They found that this burst is then followed by a $\sim$ 100 ms phase of quiescence. The next phase begins when the neutrino-driven convection or the standing accretion shock instability become fully developed. Following this, the GW emission is maintained by non-spherical, intermittent accretion streams hitting the resultant PNS, exciting its quadrupolar oscillation modes. The GW models of these scenarios are tested against our code in this thesis. Currently, template-based search methods for CCSNe, such as those used for the range of compact binary coalescences detected so far, are not realistic, analytically. The interplay of general relativity, particle physics, and nuclear physics, suggest the need for alternative parameter estimation routines. The authors of [135] conduct a full general relativistic three-dimensional hydrodynamics simulation of rapidly rotating core-collapse of a 70 $M_{\odot}$, finding strong GW emission. They find the bounce shock propagates outward to reach $\sim$ 200 km at $t_{pb} \sim 70$ ms (for post bounce time, $t_{pb}$). The bounce shock is then affected by the growth of non-axisymmetric rotational instabilities which will then accelerate the shock further outward, until the instability end. Thereafter the shock propagation decelerates, stagnating at $\sim$ 300 km at $t_{pb} \sim 85$ ms. This is then followed by the shock surface shrinking, stopping at $t_{pb} \sim 100$ ms. The average shock radius then keeps $\sim$ 200 km until the end of their simulation at $t_{pb} \sim 270$ ms. The frequency grows from f $\approx$ 450 Hz at $t_{pb} \sim 120$ ms to f $\approx$ 800 Hz at $t_{pb} \sim 270$ ms. Schematic representation of the evolution stages from the onset of stellar core collapse (*top left*) to the development of a SN explosion, on a scale of several 1000 kilometres, are given in Fig. 4.3 from Ref. [129] The displayed intermediate stages show the moment of core bounce and shock formation (*top right*), shock stagnation and onset of quasi-stationary accretion (*middle left*), beginning of the re-expansion of the shock wave ("shock revival", *middle right*), and acceleration of the explosion (*bottom left*). Nickel formation is indicated in the matter heated by the outgoing shock, but also the rising bubbles of neutrino-heated ejecta and the essentially spherically symmetric neutrino-driven wind (*bottom right*) are interesting sites for nucleosynthesis.

## 4.3 Pulsars, spinning neutron stars

Strong indirect evidence for GW emission first came from the famous Hulse-Taylor binary system [121] we described above. Taylor and Hulse first detected the radio pulses of PSR B1913+16 in 1974 as a 17 Hz radio emission. By noticing variations in the arrival times of the pulses, they were able to infer the existence of a second star in a binary orbital. The second star was later indentified to be a NS. They also discovered that the system suffered from a small but unmistakable quadratic decrease in orbital period that agreed with predictions made from GW energy loss [136, 137, 138]. For their discovery and use of the PSR B1913+16 system to test GR and, in particular, for the verification of an orbital decay rate consistent with that expected from GW energy emission as given in Eq. 4.1, Taylor and Hulse were awarded the 1993 Nobel Prize in Physics. The presumed GW emission frequency of $\sim$70 $\mu$Hz) is outside the range of current terrestrial GW detectors and even first generation space-detectors such as LISA. Ultimately, in $\sim$ 300 million years, the system would spiral into a coalescence and this

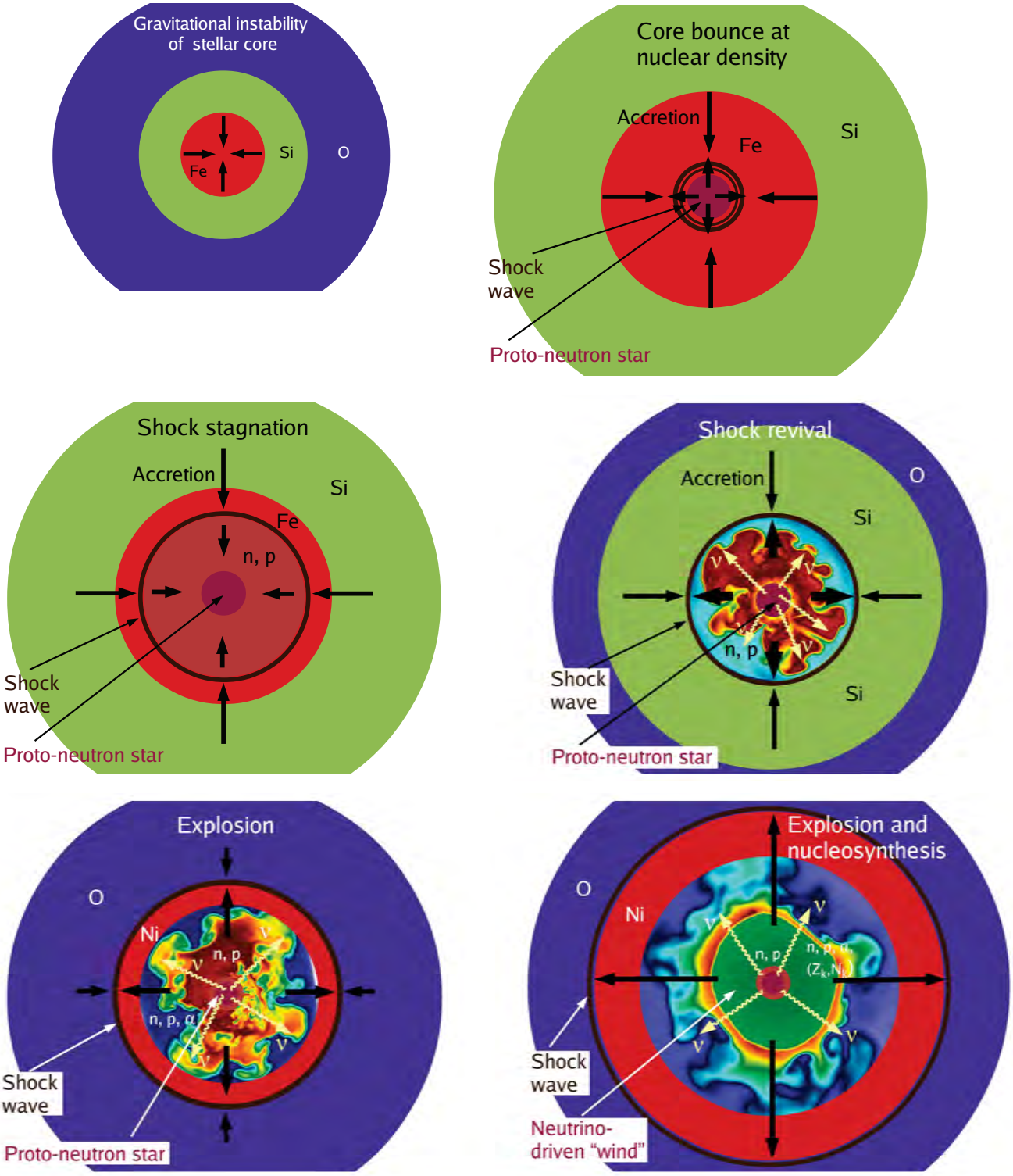


Figure 4.3: Schematic representation of the evolution stages of a SN explosion. From [129].

event would fall well within the net of terrestrial GWDs. In the meantime, pulsars may well provide an avenue as GW detectors themselves as we outline in Section 4.4.

**Continuous gravitational waves** are GWs that are nearly monochromatic, and, as the name suggests, long-lasting. Sources for these types of GWs, that would be detectable by current and pipeline GW detectors, are galactic, non-axisymmetric NSs, spinning fast enough that twice their rotation frequency is in the detectable band [94]. The early stages of coalescing binaries, where the orbital decay leads to only a small secular departure from monochromaticity, would be another continuous-wave source. However, these would be outside the range of terrestrial GW detectors but well within the range of future space-based GW detectors such as LISA. There are several mechanisms by which spinning NSs could generate detectable GWs. In isolated NSs, cooling and cracking of the crust may lead to residual crustal deformation leading to intrinsic non-axisymmetry of the NS [139] . Non-axisymmetric distribution of magnetic field energy trapped beneath the crust may also cause this [140]. An isolated star may also exhibit normal modes of oscillations, including r-modes in which quadrupole mass currents emit GWs [141, 142].

## 4.4 Stochastic gravitational waves

In the same way as Hulse and Taylor were able to infer the existence of a second star existing in a binary orbit with the pulsar PSR B1913+16, so too would it be possible to detect a persistent, noise-like, GW "background", the result of the combination of GWs created over billions of years by countless pairs of SMBHs orbiting one another across the universe. These objects produce GWs with much longer wavelengths than those detectable by aLIGO and aVIRGO.

According to Einstein's GR, the effect of the GW background should influence the timing of the pulsars slightly differently based on their positions relative to one another.

If GWs pass between a pulsar and Earth, the subtle stretching and squeezing of space-time would appear to introduce a small deviation in the pulsar's otherwise regular timing. However, this effect is subtle, and a number of other factors are known to influence pulsar timing also.

The North American Nanohertz Observatory for Gravitational Waves (NANOGrav) as part of the International Pulsar Timing Array (IPTA) collaboration, has, over the past 12 and a half years, monitored the timing of 47 pulsars spread across the sky, using ground-based radio telescopes. By subtracting contributions from other known factors, from the timing data for each pulsar, the NANOGrav project now reports the detection of unexplained fluctuations, consistent with the effects of GWs [143].

# Chapter 5

# Gravitational wave detectors and detection

Currently operational GW detectors include the two Advanced LIGO instruments, Advanced Virgo, GEO 600 and, KAGRA, the underground GW detector in Japan which began observation runs in 2020. LIGO-India, to be built near Aundha Nagnath in the Indian state of Maharashtra, is anticipated to come online in 2027. We review the development of GW detectors, including the status of current detectors and those expected to come online in the coming decades, terrestrial and space-based. We discuss the first detection of GWs and subsequent detections, contextualising GW detection in the evolution of multi-messenger astronomy (MMA). A number of reviews of GW astronomy have appeared in the last decade or so [94, 144, 145, 146, 147, 148], which we have used in compiling this summary together with the publicly available information and data for the GW projects themselves.

## 5.1 Gravitational wave detectors

The route from the initial conceptualisation of the construction of GW detectors to the operation of a detector with sensitivity within a realistic range of detecting a GW is one that is six decades long. It could be said that first realistic efforts theorising a route to a GW detector had its roots at what retrospectively came to be known as GR1, the first meeting in the series of Gravitation and General Relativity conferences. Hosted by the then newly formed Institute of Field Physics (IOFP), GR1 took place on 18-23 January, 1957, at the University of North Carolina at Chapel Hill, USA [17]. The precursor to this conference occurred two years earlier in Bern as we discussed in Chapter 3, at a time when not many were convinced of the existence of GWs. This lack of support for the existence of GWs was compounded by Einstein's earlier ambivalence on the matter, his collaborator, Rosen's belief that the phenomenon was merely an artefact of the mathematics [60], widespread uncertainty on whether GWs carried energy and the difficulties presented by GR in choosing appropriate coordinate systems in which to measure observables.

In his ground-breaking 1956 paper [149], Pirani demonstrated a mathematical formalism for the

deduction of physical observable quantities applicable to gravitational waves. This work was inspired by talks held in Poland with Leopold Infield who had been Einstein's assistant. Infield had been instrumental in getting Einstein to review his initial repudiation of GWs in the 1930's, which had been based on erroneous calculations [150], and again he played an instrumental intervening role in the evolution of the GR theory two decades later. Pirani had been forced to travel to Poland as Infield's return to his native Poland had resulted in him being stripped of his Canadian citizenship in the wave of anti-communist sentiment of the time. This resulted in the article, itself, being published in a lesser-known Polish journal and so Pirani's ground-breaking efforts remained hidden from the mainstream community involved in gravitational physics [60]. The Chapel conference provided Pirani the opportunity to present his findings in his scheduled talk. The session in which Pirani presented his talk was chaired by none other than Hermann Bondi who prefaced the session by the cautionary note that researchers "still do not know if a transmitter transmits energy radiation..." [17] Whilst it was still several years before Bondi's seminal work in the 1960's, as discussed in Chapter 3 would finally lay to rest this doubt, Pirani's talk laid a convincing path to the eventual theoretical framework of GWs and it swayed the belief of many sceptics including Bondi [60]. Although, we credited Caltech physicist Richard Feynman, earlier in our discussion (see Chapter 1), for the "*sticky bead argument*", it was actually the brainchild of Felix Pirani. Bondi, himself, took part credit for this analogy by providing his version of it in his paper in *Nature* later that year [151]. In the "sticky bead argument", two rings of beads are considered to be sliding freely on either side of a bar placed transversely to the propagation of a GW. Tidal forces on the midpoint of the bar created by the GW would mean the rings would slide toward the outer ends of the bar. In the case that the bar is "sticky", then friction would heat both the bar and beads implying the transfer of energy, an illustration that GWs could transmit energy to a particle it passed through. The conference was also a catalyst for the advent of NR, with the newly elected head of the IOFP, Bryce DeWitt, raising the possibility of using electronic computers to solve gravitation equations and the issues likely to be faced in scheduling them for calculations. Bryce DeWitt had won a 1953 essay competition on gravitation funded by millionaire businessman Roger Babson as part of the activities of the Gravity Research Foundation (GRF) founded by Babson, himself. It was DeWitt's essay which further motivated Babson and he, together with fellow millionaire Agnew Bahnson, set about initiating the creation of the IOFP with the academic backing of Johan Archibald Wheeler, the illustrious physicist at Princeton.

Another attendee at the conference, Joseph Weber, inspired by the discussions at GR1, set about conceptualising an instrument for GW detection and presented his ideas in his 1960 paper [18]. Weber would go on to construct what could be considered the first GW detector in 1966, setting the bar for GW detector construction. Whilst his results, published in a paper entitled "Evidence for the Discovery of Gravitational Radiation" [152] were widely criticised and his methods questioned, he did create the momentum that would lead to GW detector construction with sensitivity to obtain the actual evidence of GWs a half century after his premature assertion.

Weber, together with his students Robert Forward and David Zipoy, began efforts to assemble a GW "antenna". Weber subsequently built two detectors, one at the University of Maryland and another 950 km away, in Argonne National Laboratory near Chicago, with both detectors connected via a high-speed phone line to a registration centre. The notion of using two anten-

nae separated by a large distance was to eliminate spurious local noise. Years later, Weber's student Robert Forward, working at the Hughes Research Laboratory in Malibu, California, and encouraged by Rainer Weiss, designed the first interferometer prototype in 1971, which he referred to as a "Transducer Laser", with arms of 8.5 m. Rainer Weiss was the first to suggest that the arms of the interferometer needed to be several kilometres long in order to be able to detect GWs. This idea propelled the development of prototype GW detectors and formed the basis of configurations of current day detectors and those planned for the coming decades.

A proposal by a German group to build a full-sized interferemeter of 3km ("*Plans for a large Gravitational wave antenna in Germany*") was presented at the fourth edition of the Marcel Grossman meetings, (MG4), which was held in Rome in June 1985 [19]. Around the same time, a group in Glasgow, UK, began plans to design their Long Baseline Gravitational Wave Observatory [20]. This group, initially led by Ronald Drever, had successfully completed a 10-m interferometer under his leadership in the 1970's. Both the British and German groups, struggling to obtain funding for their projects, joined forces and, in 1994, proposed a 600-m detector [153]. Successful with their proposal, construction of a 600-m detector, GEO600, began on 4 September 1995 in Germany, 20km south of the city of Hanover. These were not the only efforts to build a GW observatory.

In 1983, two years before the Germans first made their proposal at MG4, the French scientist, Allain Brillet, delivered a lecture at a meeting on Relativity and Gravitation (organized by the Direction des Etudes Recherches et Techniques de la Délégation Générale pour l'Armement), where he campaigned for the use of interferometers as the best method of confirming the existence of GWs. Brillet, who was working with a group at Orsay in France, had established strong ties with Weiss who he had visited in 1980 and 1981 at MIT. He had also previously done a postdoc at the Laboratory of Astrophysics, University of Colorado, Boulder under Peter L. Bender, who, together with his colleague, Jim Faller, first proposed the notion of a space-based interferometer. Despite Brillet's campaigns at the 1983 meeting and for several years after that, he struggled to secure funding from French agencies and academic department. At MG4, Brillet met the Italian scientist Adalberto Giazotto who was based at the Universita di Pisa and an agreement was reached that their groups in Orsay and Pisa would work together. They then proposed the idea of a single European detector to the German team. The German group rejected this collaboration as they were of the opinion that the late inclusion would delay their project proposal, which they believed was then close to approval for funding.

The French and Italian groups then opted to pursue their own collaborative effort, the VIRGO Interferometer. Eventually, they successfully secured funding from their respective national scientific institutes, the French CNRS (Le Centre National de la Recherche Scientifique) in 1993, and the Italian INFN (Istituto Nazionale di Fisica Nucleare, Italy) in 1994. Construction at the VIRGO site, in Cascina near Pisa, began in 1996. The collaboration of the French and Italian teams grew to include laboratories from the Netherlands, Poland, Hungary and Spain into the European Gravitational Observatory (EGO) consortium. By June 2003, construction was completed on the initial VIRGO detector. Four years later, the VIRGO and LIGO consortiums finally joined forces in a collaborative effort in the search for GWs. The initial VIRGO detector would later be decommissioned in 2011 to be upgraded to Advanced Virgo, which came online in 2016 [154].

Separate to the developments in Europe, efforts in the USA had also progressed, led by initial discussions in 1975, between Weiss and Caltech physicist Kip Thorne. Thorne set up an interferometer group at Caltech, recruiting Drever to work on the construction of an interferometer, whilst Weiss set up a team at MIT. By 1983, Drever had succeeded in building a 40 m interferometer. At MIT, the team led by Weiss, embarked on a study of a interferometer on the scale of kilometres. The result of their study was presented to the National Science Foundation (NSF) in October 1983, in which they proposed the construction of two separate interferometers in the USA. The joint project by the Caltech and MIT teams was named the "Laser Interferometer Gravitational-Wave Observatory" (LIGO) and was to be led by Thorne, Weiss, and Drever. NSF provided funding to the project in 1988. The project went through project management difficulties and eventually Barry Barrish was recruited to lead the efforts. He proposed the construction of LIGO in two stages. First would be the construction of an "initial LIGO" (iLIGO), which would test the concept. This stage would be mainly for data gathering on refining the system with the possibility of a GW detection. Subsequently, a refined and enhanced version would be built, an "advanced LIGO" (aLIGO), where GW detection would be very likely [22]. LIGO itself would consist of two interferometers as initially proposed. In 1994, construction began on the first observatory based in Hanford, Washington state with construction on the second site in Livingston, Louisiana beginning a year later. The constructions were completed in 1997. Detection runs took place from 2002 to 2010 with iLIGO but were unsuccessful. However, these runs were critical in providing clues to the refinement required for aLIGO. The upgrade to aLIGO started in 2010 and was completed five years later, with aLIGO operating in test mode starting in February 2015 in preparation for scientific observations scheduled to start on 18 September 2015. In preparation for the start date, a series of last-minute tests were performed on the 13th of September with all but one completed by 4 am local time (Louisiana) the next morning. The team elected to leave for home at 4am and return to resume the last test later that day. At 4:50 am local time, a signal arrived at each of the detectors, the detection by each detector separated by 10 milliseconds, the time it takes light to travel between the detectors. No-one was present at either detector to witness this event. Instead, the honour of the detection fell to postdoctoral student, Marco Drago, at the Max Planck Institute for Gravitational Physics in Hanover, Germany, where he, as member of the LIGO team, worked on data analysis. His responsibilities included monitoring automated data pipelines which sent alerts when any anomalous signals were received by the LIGO detectors. He received an email alerting him to the signal and after checking and double-checking, he in turn sent a broadcast email to the entire LIGO collaboration. The teams still needed to measure background noise, estimate the statistical significance of the signal, and corroborate the readings from both detectors and by 15 October had concluded that the first detection of a GW had taken place.

The event, referred to as GW150914 [23], reflecting the date of detection and that the event was that of a GW, was emphatic vindication of Einstein's GR, a century after he introduced it in November 1915. The source for this signal was the merger of two black holes and the signal had travelled for over a billion years before impinging on each of the detectors of aLIGO.

Subsequent to this initial discovery, the twin Advanced LIGO observatories responsible for the first discovery made several further detections of GW signals from coalescing compact binaries [24, 25]. Detection with two interferometers, separated geographically, are necessary to

discern the direction the GW is coming from and to filter out acoustic noise. This was the case for the LIGO detectors with one located in Hanford, Washington and the other some 3,000 km away in Livingstone, Louisiana. However, a third detector would be needed to triangulate the signal, providing a better guide to the location of the source of the gravitational waves detected. Advanced Virgo provided this opportunity, when it came online in 2016. The LIGO and VIRGO detectors, on 14 August 2017, jointly observed the GW event GW170814, which was the binary black hole (BBH) merger. Three days later, on 17 August, the first detection of a (Binary Neutron Star) BNS merger was made, the GW event GW170817. This was profound for the era of Multi-messenger Astronomy. While Black Hole mergers do not produce currently discernible electromagnetic signals, the same is not true for BNS mergers. The detection of GW170817 by VIRGO, together with the two LIGO detectors, allowed triangulation of the signal leading to pinpointing the location of the signal. 70 other detectors, terrestrial and space-based, were able to train their focus in the direction of GW170817. This global (and extra-terrestrial) network of detectors, detecting electromagnetic radiation in various frequency bands, was able to lie in wait for signals of trailing events in the electromagnetic spectrum. These signals came in the following seconds, hours and days of the GW signal, which itself lasted for 100s. [26, 27]. The subsequent signals provided a wealth of information on the BNS merger, on the compositions of the compact bodies and on population synthesis. As detections of mergers of compact bodies begin to flow in, our understanding of compact bodies, their physics and that of the surrounding astrophysical environment, will continue to grow and at times even challenge previously long held notions.

### 5.1.1 Electromagnetic radiation vs gravitational radiation

Electromagnetic (EM) radiation forms the basis for much of our present understanding of the universe. GWs are set to revolutionise that understanding in that they are significantly different from electromagnetic waves. These differences will define the era of MMA. We have had an extensive discussion on the theory of GWs in Chapter 2 and here, only highlight some key distinctions between EM radiation and GWs:

| **Electromagnetic Waves** | **Gravitational Waves** |
|---|---|
| Typical sources of electromagnetic waves are stellar atmospheres, accretion discs and clouds of interstellar dust, none of which emit significant gravitational waves. | Sources of GWs are BHs and other exotic objects which emit no EM radiation at all; also the cores of SN which are hidden from EM view by dense layers of surrounding stellar gas. |
| They propagate through spacetime as oscillating fields of coexisting electric and magnetic fields. | They propagate as oscillations of the 'fabric' of spacetime itself. |
| They are almost always incoherent superpositions of emission from individual electrons, atoms, or molecules. | GWs are produced by coherent, bulk motions of huge amounts of mass-energy - either material mass, or the energy of vibrating, nonlinear spacetime curvature. |

| | |
|---|---|
| The wavelengths of EM waves are small compared to their sources (gas clouds, stellar atmospheres, accretion disks, ...), so from the waves we can make pictures of the sources. | The wavelengths of cosmic gravitational waves are comparable to or larger than their coherent, bulk-moving sources, so we cannot make pictures from them. Instead, the GWs are like sound; they carry, in two independent waveforms, a stereophonic, symphony-like description of their sources. |
| EM waves are easily absorbed, scattered, and dispersed by matter. | GWs are suggested to travel nearly unscathed through all forms and amounts of intervening matter, which we will investigate in this thesis. |
| Their frequencies range from about $10^7$ Hz *upwards* by around 20 orders of magnitude. | The frequencies of GWs range from around $10^4$ Hz *downwards* by about 20 orders of magnitude. |
| Information brought to us by EM waves show us the thermodynamic state of optically thin concentrations of matter. | GWs will show us details of the bulk motion of dense concentrations of energy. |

### 5.1.2 The frequency range of gravitational waves

GW spectrum indicating wavelength and frequency together with some anticipated sources and range of GW detectors is illustrated in Fig 5.1. The frequency range of the gravitational waves may be broken into four frequency bands:

- The **Extremely Low Frequency Band** (ELF)
  range : $10^{-15}$ to $10^{-18}$ Hz.
  The measured anisotropy of the cosmic microwave background radiation places strong limits on GW strengths and may, in fact, have detected waves.
  The only waves expected in this band are relics of the big bang.

- The **Very Low Frequency Band** (VLF).
  range: $10^{-7}$ to $10^{-9}$ Hz.
  The only expected strong sources in this band are processes in the very early universe: the big bang; phase transitions of the vacuum states of quantum fields; and vibrating or colliding defects in the structure of spacetime, such as monopoles, cosmic strings, domain walls, textures, and combinations thereof.
  Joseph Taylor [121] and others have achieved remarkable gravity-wave sensitivities by the timing of millisecond pulsars.

- The **Low-Frequency Band** (LF).
  range : $10^{-4}$ to 1 Hz.
  The Laser Interferometer Space Antenna, LISA will operate in this frequency range.
  This is the band of massive black holes ($1000M_\odot \sim 10^8 M_\odot$) in the distant universe, and of other hypothetical massive exotic objects (naked singularities, soliton stars), as well of

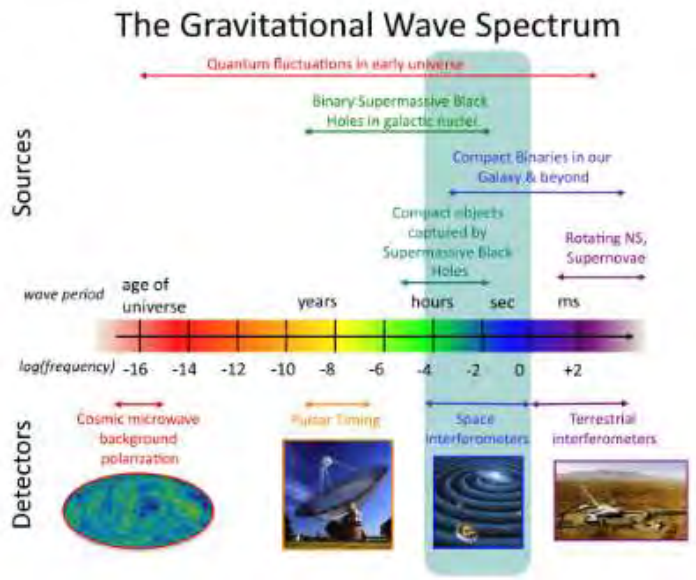


Figure 5.1: Gravitational wave spectrum indicating wavelength and frequency together with with some anticipated sources and range of GW detectors. Figure credit: NASA Goddard Space Flight Center. As referenced from [155]

as binary stars (ordinary, WDs, NSs, and BHs). For NSBH binary mergers, LISA will see them weeks or months before the actual merger.

- The **High-Frequency Band** (HF).
  range : 1 to $10^4$ Hz.
  Earth-based gravitational-wave detectors such as aLIGO, aVIRGO and KAGRA operate in this frequency range. This is the band of stellar-mass black holes (M  1 to 1000M. and of other conceivable stellar-mass exotic objects (naked singularities and boson stars) in the distant universe, as well as of supernovae, pulsars, and coalescing and colliding neutron stars. Early universe processes should also have produced waves at these frequencies, as in the ELF, VLF, and LF bands.

### 5.1.3 Gravitational wave detection by interferometers

From GR, as discussed in Chapter 2, a GW has two linear polarisations. These polarisations each have an associated GW field which oscillates in time and propagates at the speed of light. As each wave passes through any object it produces tidal forces. For objects that are

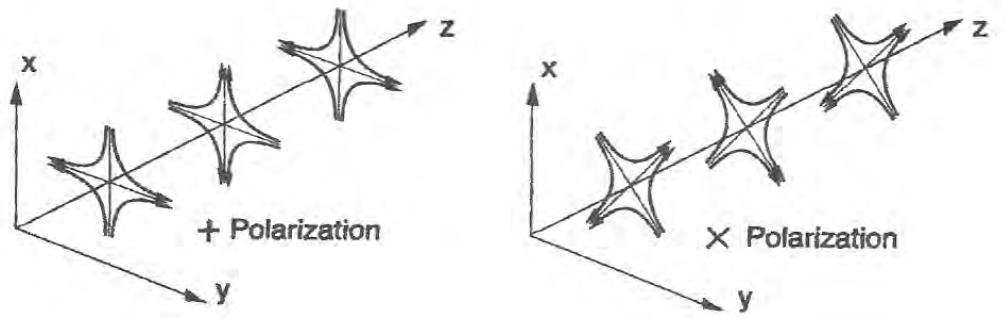


Figure 5.2: The lines of force associated with the two polarisations of a GW. From Abramovici *et. al.* [156]

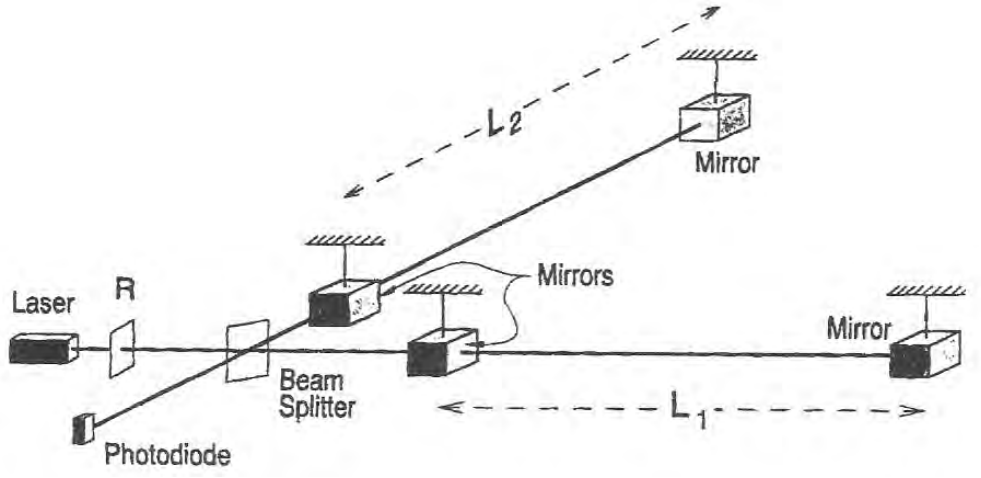


Figure 5.3: Schematic diagram of a laser interferometer GW detector. From Abramovici *et. al.* [156]

comparatively small in relation to the wavelength of these waves, the forces have quadripolar patterns relative to the object's centre. These patterns are shown in Fig. 5.2. From the force patterns characterised by the orientation of the axis, the polarisations have derived the names 'plus'(+) and 'cross' (×). Each of the GW fields are in turn named $h_+$ and $h_\times$.

Currently, GW detectors consist of a laser interferometer with four masses hanging from vibration-isolated supports with an optical system to monitor the separations between the masses. Fig. 5.3 illustrates such a detection system. The device consists of two long arms at right angles to each other meeting each other in such a manner as to form an 'L shape'. A mass is placed at each end of the long arms of the 'L shape', whilst two masses are placed near each other at the corner of the 'L'. The arm lengths are approximately equal, with $L_1 \simeq L_2 = L$. As a GW (with high frequencies in comparison to the masses' $\sim$ 1Hz natural frequency) passes through the detector, the masses are pushed back and forth relative to each other as though they were not connected to their suspension wires. This results in a change in the arm-length difference, i.e. $\Delta L \equiv L_1 - L_2$. Through laser interferometer that change is monitored. The variations

in the output of the photodiode (the output of the interferometer) is directly proportional to $\Delta L$. If the GWs are arriving from above or below the device and the axes of the + polarisation coincide with the arm's directions, then it is the waves' + polarisation that will drive the masses. We may then write:

$$\frac{\Delta L(t)}{L} = h_+(t). \tag{5.1}$$

In general, though, it is more likely that the interferometer's output is a linear combination of the two wave fields :

$$\frac{\Delta L(t)}{L} = F_+ h_+(t) + F_\times h_\times \equiv h(t). \tag{5.2}$$

$h(t)$ is referred to as the gravitational wave-strain acting on the detector. As time can be measured more accurately than distance, it is actually the difference in time that is measured and $\Delta L$ inferred from that measurement. Reliable detection of GWs requires the operation of at least two detectors in coincidence - if the signals coincide with those of a distant detector, local perturbations can be ruled out. In order to obtain the full information about the GWs (source position, polarization), data from at least four detectors have to be compared. For a NSBH binary's inspiral and coalescence, a GW with two components is produced, one for each polarisation. For any compact merger there are the following phases:

- *Inspiral*
- *Merger*
- *Quasinormal mode (QNM) ringdown*

## 5.2 Aspects of interferometer design

### 5.2.1 The components of interferometers

#### 5.2.1.1 Lasers

With the advent of the laser in the 1960s, interferometry design received a boost. Lasers produce monochromatic, high intensity, unidirectional bundled beams of light, ideal for interferometers designed to measure the phase of light accurately. The suitability of the use of lasers in GW detection is based on the power of the light beam together with the stability of the wavelength and amplitude. Currently, laser-diode-pumped solid-state lasers are used designed with a non-planar ring oscillator (NPRO) [157] as its core element and using yttrium aluminum garnet (Nd:YAG) crystals as the lasing medium.

#### 5.2.1.2 Precision optics

A key component of terrestrial laser interferometers is the mirrors and these need to be operating at the highest levels of efficiency, minimising scattering and not contributing to noise themselves. Current mirrors used, operate at an absorption rate below the 1 ppm range, with reflectivities

of around 99.995 %. Figure 5.4 [158] shows the beam splitter of the Virgo interferometer which absorbs scattered light.

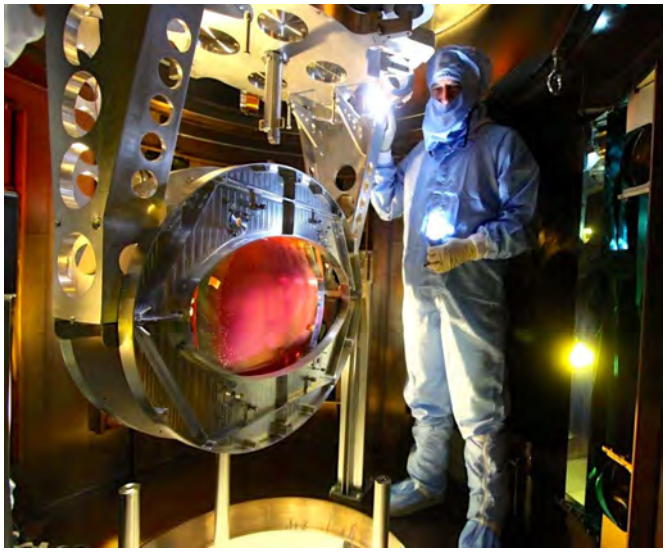

Figure 5.4: The aLIGO beam splitter shown framed by a metal screen. Photo courtesy: EGO/Virgo. Photographer: Maurizio Perciballi. [158]

#### 5.2.1.3 Vacuum systems

Ultra-high vacuum (UHV) systems serve several purposes. Fluctuations in the effective refractive index of residual gas may be mistaken for GW signals. Test masses are shielded from this and acoustic noise by isolation in a vacuum environment. The UHV, composed of chambers connected by kilometre-long beam tubes also maintains a sanitary environment ensuring optimal efficiency of the optical elements. The LIGO Hanford detector is shown in Figure 5.5 [159] with one of its four 4-km long stainless-steel beam tubes leading out of a vacuum chamber housing the optics.

#### 5.2.1.4 Seismic isolation components

The vibrations of the earth, which are typically $10^{-9}\,\mathrm{m}/\sqrt{\mathrm{Hz}}$ at 10 Hz, also need to be taken into account when designing the interferometers. The mirrors need to be seismically isolated from the ground and in LIGO a system of controlled platforms on springs is used to do this. In Virgo seismic isolation is achieved by suspending the mirrors in a series of inverted cascading pendula, as shown in Fig. 5.6 [159], which are in turn housed on isolated platforms. These platforms are equipped with sensors which provide, together with sensors on the ground, constant feedback to counteract seismic activity [160, 161].

#### 5.2.1.5 Simulation and diagnostic methods

Simulation tools are required for the design and commissioning. Codes are split into time-domain and frequency-domain tools, such as for the latter, Finesse[163], Optickle [164] and

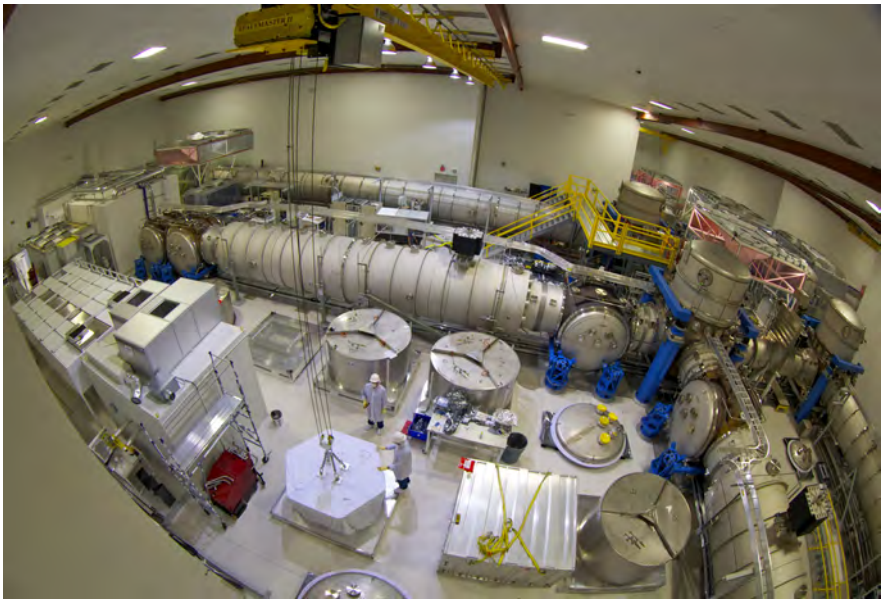

Figure 5.5: The Ultra-high vacuum system at the LIGO Hanford Observatory. Photo courtesy: Caltech/MIT/LIGO Lab. [159]

MIST [165]. Gaussian optical beams based on FFT-methods, estimate the effect of mirror imperfections. These are all numerical based tools whilst analytical modelling tools also exist and are critical in noise mitigation.

#### 5.2.1.6 Calibration

For proper interpretation of the GW strain, calibration of the output signal is required. From the known arm length of the detector, strain sensitivity may be inferred from the known displacement of test masses. This test has to be carried out at multiple frequencies as strain variations are frequency dependent and the instrument calibrated accordingly. In order to achieve sensitivity for certain categories of GW events, accuracy to sub-percent level is targeted [166, 167].

### 5.2.2 Noise sources and noise mitigation strategies

Interferometers are designed to detect GW signals within a certain frequency range. However, within this range there may be a host of competing signals and discerning a GW signal will involve filtering of the competing noise signals. The noise cannot be eliminated completely but can be sufficiently suppressed or filtered to begin to isolate a GW signal. A threshold may be described as the acceptable signal-to-noise ratio (SNR) suitable for detection to occur. We discuss the various noise sources and noise mitigation strategies

We may group noise sources contaminating the output of a detector into two categories:

- *displacement noise* which are those that create real motion of mirror surfaces. Seismic noise and the related gravity gradient noise occur at very low frequencies. Thermal motion

Figure 5.6: A portion of the Virgo detector's 8 m multi-stage pendulum from which the mirror is suspended. Photo courtesy: EGO/Virgo [162].

of the dielectric coatings of the mirrors and of their suspensions, quantum radiation and pressure noise occur at low- to mid-frequency.

- *sensing noise* arises during the process of measuring the positions of the mirrors such as the shot noise arising from the Poisson statistics of photon arrival time at the photodetector [145].

We give a brief description of some of the types of noise sources expected to contaminate the GW signal received by the terrestrial GW detectors.

#### 5.2.2.1 Quantum noise

Quantum noise occurs at frequencies $\gtrsim 50\,\mathrm{Hz}$. *Shot noise*, a sensing noise, is the most dominant form of quantum noise, the manifestation of Poisson statistics for the counting of detected photons. Shot noise limits all position measurements that use classical light.
For frequencies $\lesssim 50\,\mathrm{Hz}$, we have *radiation pressure noise* where momentum transfer from all photons recoiling from the freely suspended test masses gives rise to position noise [145].

A mitigation strategy for shot noise and radiation pressure noise would be to increase laser

power in the interferometer. The measured GW signal is proportional to $n$, the number of photons, whilst the shot noise scales as $\sqrt{n}$. The shot and radiation pressure noise are inversely linked by the laser power in the interferometer, and so increasing the laser power, results in the radiation pressure noise (at low frequencies) increasing. To counteract this, the inertial mass of the test masses may be increased. The test masses are themselves bound by limits to which they may be increased based on their constituent material and manner of production. For a targeted frequency of a GW signal, there would be a maximally efficient power of the laser based on the fixed test mass.

Shot and radiation pressure noise may be understood as the result of the vacuum fluctuations of the electromagnetic field (EMF) entering the interferometer from the output port [168]. By reducing the vacuum fluctuations entering the interferometer, one can reduce one of these noises at the expense of the other. This has led to the use of use of *squeezed vacuum states of light*. GEO 600 set the trend for this feature of noise reduction, implementing this feature in 2010 [169]. In 2019, both LIGO and Virgo incorporated this feature into their detectors also [170, 171].

By reflecting the squeezed beams off suitable optical resonators or so-called filter cavities, quantum noise reduction across the entire frequency band of a GW detectors may be achieved [172].

#### 5.2.2.2 Thermal noise

Thermal noise may be regarded as thermally driven fluctuations of mechanical systems. These would refer to changes in the surface positions of the test masses arising from the internal vibrational modes of the mirrors, the vibrational modes of the fibres suspending the mirrors , and the pendulum motion of the suspended mirrors.

The current method in quantifying this effect for detectors was developed by Yuri Levin [173]

*Thermoelastic dissipation* is a type of thermal noise as a result of temperature fluctuations or temperature gradients. If a suspension fiber bends, dissipative heat flows, generating mechanical noise. Heat dissipation causes statistical fluctuations of temperature, also causing mechanical displacement. Both of these processes may also be referred to as *thermoelastic noise*.

*Thermorefractive* noise is the effect of refractive index fluctuations caused by temperature fluctuations.

Thermoelastic and thermorefractive noises, together, constitute what is known as together as *thermo-optic noise*, relevant to the reflectivity of optical coatings on the mirrors, and they partially cancel each other out when treated coherently [174].

For aLIGO and aVIRGO, operating at room-temperature, thermal noise remains a key contributor to the overall noise suffered by the detectors. Improvements in coating materials and designs will help reduce this noise as would cryogenic operation such as in the case of the operation for KAGRA. The Japanese detector, which was, earlier in its history, referred to as the Large Scale Cryogenic Gravitational Wave Telescope (LCGT), uses cryogenic mirrors in its design.

#### 5.2.2.3 Seismic and gravity gradient noise

As is to be expected, tremors, natural seismic activity and atmospheric disturbances are an impediment to all terrestrial interferometric GW detectors, factors that a space-based detector would enjoy an absence of. In the category of seismic noise, we include ocean and ground water dynamics, earthquakes, wind, human-induced activities, as well as slow gravity drifts and the atmosphere. The consequences include the direct mechanical effect by moving the test masses and mirrors including through gravitational attraction. At frequencies $\lesssim 20\,\mathrm{Hz}$ this category of noise dominates and can even lead to damage of the Fabry-Perot cavities affecting the longevity of the detector in the case of extreme events.

*Gravity gradient noise* or Newtonian noise is the direct coupling of the test masses to density fluctuations in the atmosphere. Accurate models may be used to subtract the effect from the GW detector output [175, 176].

#### 5.2.2.4 Technical noises

*Technical noises*, refer to noise resulting from imperfections of the technologies used. These include

- **Feedback loops**

  To maintain the optical resonators and interferometer of the GW detector at their operating points, feedback control is necessary. This would entail a variety of sensors to detect minor deviations and mechanisms for the relay of this information and appropriate adjustment. This system in itself contributes to the overall noise.

- **Scattered light**

  GW measurement may be contaminated through dust on the test mass surfaces or unevenness of the actual surface. The position of the test masses may also be affected by the radiation pressure scattered light can exert, manifesting as a displacement noise. Reducing the generation of scattered light by improving the optics and the absorption of whatever scattered light through baffles reduces the contribution of this noise.

- **High power** laser light absorbed by the optics, creates thermal distortions, which in turn produce higher order spatial modes of the laser beam which can adversely affect interferometer. performance. To mitigate against this problem thermal compensation systems have been developed [145].

## 5.3 Detectors currently operational

### 5.3.1 aLIGO

Approved for funding by the US government in 1990, construction on LIGO began in 1994. By 1998, one of the key components of the detector, the vacuum system, was completed. Subsequentially, installation of the power-recycled Fabry-Perot resonator Michelson interferometers (PRFPMI) in each arm began. The detector in Livingston, Louisiana housed a single 4 km long

interferometer, whilst Hanford housed a 4 km interferometer and another, 2 km long, which was the first to be locked in 2000 [144]. Figure 5.7 [177] shows an aerial view of the LIGO site in Louisiana in 2015.

Figure 5.7: The LIGO Livingston Observatory in Livingston, Louisiana, USA. Photo courtesy: Caltech/MIT/LIGO Lab. [177]

Over the years that followed, investigations into isolating the various noise contributions were conducted and mitigation strategies developed in order to reach the requisite design sensitivity. As Barry Barish had strategised this phase of iLIGO was to gather data to inform the evolution of the detectors to the next stage: aLIGO.

The construction of aLIGO included the transition to a more powerful 200 W laser, as compared with the 10 W of iLIGO; the increase of the test masses from 10 kg to 40 kg; a change in the welded suspension fibers from stainless steel to glass and replacement of the single stage suspensions for the test masses with quadruple pendulum suspensions. Signal recycling was added leading to the dual-recycled Fabry-Perot Michelson Interferometer (DRFPMI). Construction of the aLIGO DRFPMI was completed in 2014, marking the start of the commissioning phase. The test mode began in February 2015 in preparation for the scientific observation phase that was scheduled to start on 18 September 2015. Whilst still in the stages of fine-tuning the system in preparation for the start of the scientific run, aLIGO made its first GW detection on 14 September 2015.

### 5.3.2 aVIRGO

Construction on iVIRGO, shown in Fig 5.8 [178], was completed in June 2003. In 2007, the VIRGO and LIGO Scientific Collaborations entered into an agreement to share and jointly analyse the data recorded by their detectors and to jointly publish their results [144]. Several science runs took place between 2007 and 2011, and in September 2011, the operation of iVIRGO and the installation of aVIRGO began. In 2016 aVIRGO began its commissioning phase and in May and June 2017 aVirgo joined the two aLIGO detectors for a first "engineering" observing period [145]. On 14 August 2017, aVIRGO made its first GW detection in conjunction with aLIGO: the event GW170814.

Figure 5.8: The Virgo gravitational wave detector near Pisa, Italy. Photo courtesy: Caltech/MIT/LIGO Lab. [178]

### 5.3.3 GEO600

Initially envisaging an interferometer with an arm length of around 3km, this joint German-UK GW detector initiative, constrained by funding difficulties, settled on building an interferometer of arm length 600m, GEO600. Construction began in September 1995 with operations taking place from 2003 to 2009. GEO600 consisted of a Michelson interferometer with dual recycling (combining power and signal recycling). The simultaneous use of arm resonators and dual recycling had not yet been tested then on prototypes and so GEO600 was not able to use the Fabry-Perot resonators. For the same reasons, iLIGO used the Fabry-Perot resonators, but avoided using dual recycling and instead only used power recycling.

Whilst no advanced second generation GEO600 was planned several incremental upgrades took place including one where the technique of squeezed light [168] was first tested, laying the ground-work for its adoption in aLIGO and aVIRGO. Whilst both LIGO and VIRGO were being upgraded between 2010 to 2015, GEO600 continued recording observational data minimised the risk of missing a event with detectable GWs [145].

### 5.3.4 KAGRA

The location of the underground GW detector, KAGRA, is in the Ikenoyama mountain in Kamioka, Japan. The detector is so-named after appending the first two letters of the location to the first three letters of the word "gravity". Kamioka is the same area where the first-ever detection of astrophysical neutrinos took place in 1987 co-incident with Supernova 1987A, leading to Japanese physicist, Masatoshi Koshiba, being awarded the Nobel prize in Physics in 2002. The KAGRA project is headed by another Nobel prize winning physicist, Takaaki Kajita, who was instumental in securing funding for the project. The KAGRA GW detector, part of which is shown in Fig. 5.9 on page 67, is dual-recycled laser interferometer with Fabry-Perot cavities.

Figure 5.9: The 3 km long beam tube of KAGRA underground in the Ikenoyama mountain in Kamioka, Japan. Photo courtesy: KAGRA Observatory, ICRR, The University of Tokyo. [179]

The Japanese project began as an interferometric GW detector of arm length 300 m called TAMA300, with an optical configuration using Fabry-Perot resonators in the arms, as well as power recycling. TAMA operations began with much success in 1999, achieving, at that time, the world's best sensitivity (for strain sensitivity of $10^{-21}$) and the longest accumulated data set during its runs in 2000 and 2001. With the start of the LIGO science run in 2002, TAMA aggressively joined the effort, helping to forge the international collaboration of coincidence analysis by scheduling operation time and sharing analysis methods and data. An upgrade of TAMA300 to a 3 km interferometer with cryogenic mirrors was proposed as the Large-scale Cryogenic Gravitational-wave Telescope (LCGT) project, to be constructed in the Ikenoyama mountain in Kamioka. The Japanese government approved funding for the project which was renamed to KAGRA in 2012.

Table 5.1: Design properties of each of the four GW detectors. DRFPMI stands for dual-recycled Fabry-Perot Michelson. Interferometer. From [145]

| | aLIGO | aVirgo | GEO 600 | KAGRA |
|---|---|---|---|---|
| arm length | 4 km | 3 km | 2×600 m | 3 km |
| power recycling gain | 44 | 39 | 900 | 11 |
| arm power | 800 kW | 700 kW | 20 kW | 400 kW |
| # of pendulum stages | 4 | 8 | 3 | 6 |
| mirror mass | 40 kg | 42 kg | 6 kg | 23 kg |
| mirror material | fused silica | fused silica | fused silica | sapphire |
| temperature | room | room | room | cryogenic |
| topology | DRFPMI | DRFPMI | DRMI | DRFPMI |
| location | surface | surface | surface | underground |

A summary of the design properties of each of the four GW detectors is given in Table 5.1 from Ref. [145].

## 5.4 The next generation of detectors

Both the LIGO and Virgo collaborations are continuously enhancing the detector capabilities of their instruments.

The current upgrade of aLIGO to LIGO A+, scheduled for completion in 2024, will almost double the sensitivity of the device, increasing the volume of space searched by a factor of up to seven. Improvements are scheduled to the mirror suspension systems and larger beam splitter is planned to reduce losses. Mirror reflectivity is to be enhanced with improved coatings with lower mechanical loss. A 300 m long filter cavity is to be installed in each interferometer to create frequency-dependent squeezed light, facilitating simultaneously decreasing radiation pressure noise at low frequencies and shot noise at high frequencies [145].

KAGRA, which only began joint detection searches in 2020, will itself follow the patterns of continuous enhancement with an upgrade later this decade.

Upgrades to aVIRGO are expected to also double its sensitivity. Signal recycling, which is already operational in aLIGO will be introduced to AdV+. This, together with the use of frequency-dependent squeezing and the subtraction of gravity gradient noise, all scheduled for completion by 2022, will result in the two-fold increase in sensitivity. For the three years following that upgrade further upgrades will take place with larger beams to be installed in combination with heavier mirrors (more than 100 kg) and improved coatings to overcome thermal noise. Shot noise is to be tackled by increasing the beam power. Radiation pressure is expected to be reduced by increasing the weight of the mirrors [145].

LIGO-India is expected to be operational by 2027, beginning joint operations in with LIGO A+, AdV+ VIRGO and KAGRA (which should have undergone an upgrade itself by then).

By the next decade LIGO A+ is anticipated for further upgrades to **LIGO Voyager** again with an expected two-fold increase in sensitivity extending the sensitive frequency band to as

low as 10 Hz. This is to be achieved by replacing the current silica mirrors by larger and heavier (160 kg) silicon test masses, cooled to a temperature of 123 K with liquid nitrogen. As silicon is only transparent between 1500 and 2200 nm, the currently used 1064 nm lasers would need to be replaced.

The proposed underground **Einstein Telescope** (ET), has a design of three detectors in a 10 km triangular arrangement with each detector consisting of two distinct interferometers, one for the detection of GWs in the frequency range $2 \sim 20$ Hz, with the other focussing on higher frequencies. Optimal noise reduction is expected to be a key feature of the device with the low-frequency interferometer operating at cryogenic temperatures and the thermal, seismic, gravity gradient and radiation pressure noise sources particularly suppressed [145] The device will also employ frequency-dependent squeezed light technologies and high laser power circulating in the Fabry-Perot cavities. The Einstein Telescope consortium enjoys the support of 40 research institutions and universities in Europe, where it will be built.

The proposed US based surface detector **Cosmic Explorer** is modelled on the LIGO Voyager technology. It would have an L-shaped geometry with arms 40 km in length, operating with conventional room temperature technology. For frequencies beyond 10 Hz, it is expected to have a higher sensitivity than the ET. At frequencies below 10 Hz the ET is expected to have better sensitivity. GWA is expected to receive a boost also from planned transient astronomy instruments such as the Square Kilometre Array (SKA) in South Africa operating in the radio band [115, 180] , and the Large Synoptic Survey Telescope (LSST) in the optical band [181].

## 5.5 Space-based detectors

The Laser Interferometer Space Antenna (LISA), the first dedicated space-based GW observatory is expected to be launched by 2034 [182]. Terrestrial GW detectors, current and even next generational are constrained from GW detections $\lesssim 1$ Hz as at those frequencies, the GW signals would be overwhelmed by the noise of the Earth's gravitational field. LISA is then expected to conduct the first survey of the millihertz GW sky. Although GW searches in space have been made previously, they were conducted for short periods by planetary missions that had other primary science objectives. Some current missions are using microwave Doppler tracking to search for gravitational waves. However, LISA will use an advanced system of laser interferometry for detecting and measuring them. LISA will directly detect the existence of gravitational waves, rather than inferring it from the motion of celestial bodies, as has been done previously. Whilst LISA won't be affected by terrestrial environmental noise, other environmental factors will impact LISA, such as the drift of the spacecraft, charging of the test masses, and buffeting by the solar wind.

The LISA Pathfinder (LPF) mission [183] was launched in December 2015 by the European Space Agency (ESA) with the aim to test and prove the special technologies needed for space-based interferometric detection, including drag-free technology. LPF exceeding its specification on the drag-free system by factors of more than 10, showing that LISA could achieve its design sensitivity or better [144]. With the LPF technology in its three spacecraft, LISA would be able to detect mergers of $10^6 M_\odot$ black holes with SNRs up to 5000, or at redshifts out to $z = 20$

[144]. Such mergers are expected in cosmology, as tracers of the mergers of gas clouds that led to our present-day galaxy population. LISA can help elucidate this process. And LISA can also monitor the year-long signals from stellar-mass black holes that happen to spiral into the $10^6 M_\odot$ holes in relatively nearby galaxies, another process that happens regularly as a result of stellar interactions in the central star clusters of these galaxies. These so-called Extreme Mass-Ratio Inspirals (EMRIs) contain a wealth of information about the geometry of the central black hole and are ideal instruments for performing high-precision tests of general relativity.

Proposals for other space-based GW detectors are being considered in Japan [184] and China [185].

The **Advanced Laser Interferometer Antenna** (ALIA) is a proposed as an intermediate LISA follow-on mission aimed at observing the frequent merger events of 10 $M_\odot$ BHs with Intermediate Mass Black Holes (IMBHs) of 50 to 50,000 $M_\odot$ at redshifts up to z = 10. The data provided form these detections will provide insight into the evolution of BH mass. It is expected that ALIA, consisting of 500,000 km arms, 30 W lasers and 1.0 m mirrors, may attain sensitivities 30-fold that of LISA, with an optimal frequency detection range of 30 mHz to 100 mHz. It would be expected to be launched a few years after LISA.

The **DECi-hertz Interferometer Gravitational wave Observatory** (DECIGO) is expected to have an even higher sensitivity with optimal frequency in the range 1Hz to 10 Hz. It would consist of three drag-free spacecraft, a differential Fabry–Perot (FP) Michelson interferometer, arm lengths of 1,000 km, a 100 kg mirror of diameter 1 m and 0.5 $\mu$m laser light operating at 10 W [184]. There would be three sets of such interferometers all sharing the mirrors with an arm cavity comprising one cluster of DECIGO. The constellation of DECIGO would then be comprised of four clusters of DECIGO each located separately in a heliocentric orbit [184]. The **Big Bang Observer** (BBO) is another proposal as a follow-up to LISA. It would be capable of detecting stochastic gravitational waves from the very early Universe and certain compact binary configurations within a year of coalescence. These would include NSs and stellar mass BHs, with inspirals out to $z < 8$, mergers of IMBHs at any z, rapidly rotating WD explosions from Type 1a SNe at distances less than 1 Mpc and ∼1 Hz pulsars with non-axisymmetric magnetic fields of $B > 310^{14}$ G [144].

## 5.6 The first detection

The first GW detection took place at 14 September 2015 at 09:50:45 Coordinated Universal Time (UTC). Fig. 5.10 on page 71 represents the waveforms from LIGO Hanford (H1) and LIGO Livingston (L1) and their sonograms. For visualisation, all time series are filtered with a 35–350 Hz band-pass filter to suppress large fluctuations outside the detectors' most sensitive frequency band, and band-reject filters to remove the strong instrumental spectral lines [60]. Careful checking of the data and allowing for the discovery article, entitled "**Observation of Gravitational Waves from a Binary Black Hole Merger**" [186], to be accepted for publication, meant that the announcement was only made to the public the next year on 11 February 2016. The data released in the paper confirmed the following:

- The signal swept upwards in frequency from 35 Hz to 250 Hz.

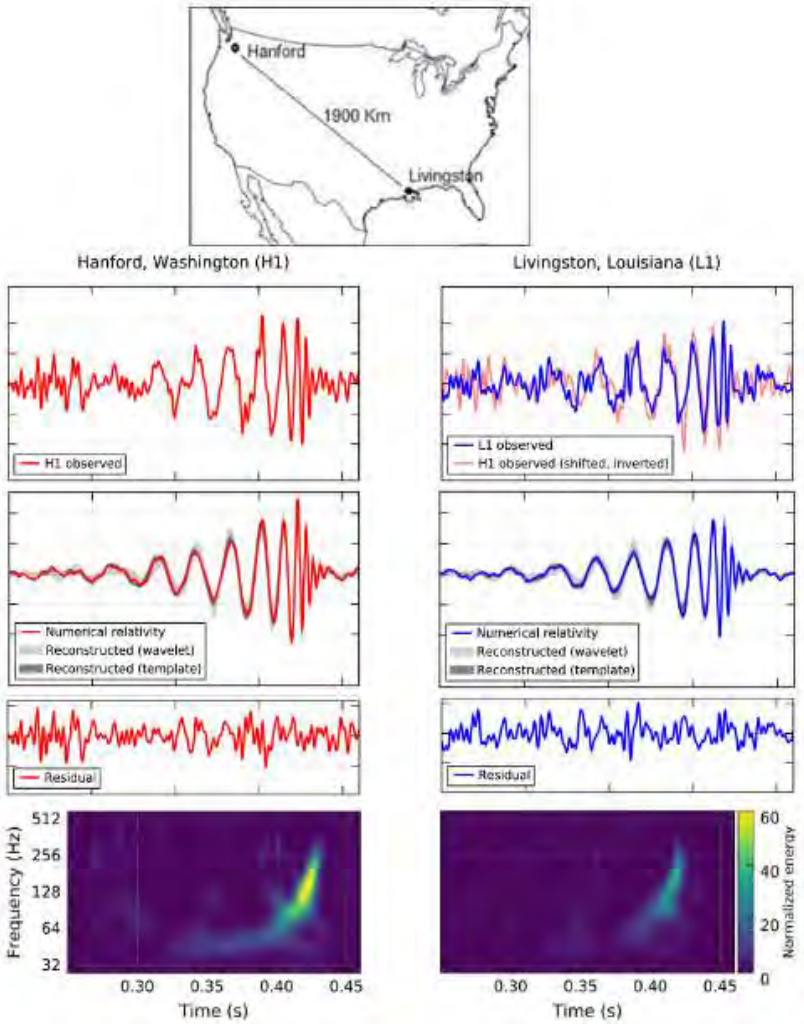


Figure 5.10: (a): Waveforms from LIGO Hanford (H1) and LIGO Livingston (L1) and their location and their sonograms. Figure from https://losc.ligo.org/events/GW150914/. Times shown are relative to 14 September 2015 at 09:50:45 UTC. From Ref. [60]

- The peak GW strain was $1.0 \times 10^{-21}$.
- The signal sweeps matched the waveform predicted by GR for the inspiral and merger of a pair of BHs and the ringdown of the resulting single BH;
- the signal was observed with a matched-filter SNR of 24.
- The false alarm rate was estimated to be less than 1 event per 203 000 years, equivalent to a significance greater than $5.1\sigma$.
- The source was estimated to lie at a luminosity distance of $410^{+160}_{-180}$ Mpc, corresponding to a redshift $z = 0.09^{+0.03}_{-0.04}$.
- In the source frame, the initial BH masses correspond to $36^{+5}_{-4}M_{\odot}$ and $29^{+4}_{-4}M_{\odot}$, and the remnant corresponds to a BH (which is spinning) with mass $m_f = 62^{+4}_{-4}M_{\odot}$.
- The GW radiated was estimated to be $3.0^{+0.5}_{-0.5}M_{\odot}c^2$.
- Uncertainties defined 90% credible intervals.
- The observations demonstrate the existence of binary stellar-mass BH systems.
- The event was "**the first direct detection of gravitational waves and the first observation of a binary black hole merger**" [186].

The majority of the energy released was in the final 0.2s of the event. The luminosity of the event corresponds to $3 \times 10^{48}$W, approximately $10^{22}$ to that of the Sun or to the electromagnetic luminosity of the entire Universe [144]. The probability of a false alarm according to the SNR translates to about $10^{-90}$ and the rates given in the paper [186] are more conservative providing the lower limits of a false alarm rate but not by many orders lower. A summary of some of the key features of the first detection, GW150914, is given in Fig. 5.13 on page 75.

## 5.7 Subsequent detections

There have been three observing runs for the GW detectors, referred to as **O1** [24], **O2** [25] and **O3** [187], with the last run, O3 halted on 27th March 2020. The O3 run yielded 56 GW detections whereas the O1 and O2 collectively made 11 detections, with this comparison illustrated in Fig 5.11 on page 73. The BBH mergers up to the O3 run are shown in Fig. 5.12 on page 74, comparing the BH masses in the mergers with those of known BHs from X-ray binaries, illustrating that they are typically much more massive. The event GW151226 [188] was the only event with both component masses within the range of X-ray selected BHs.

Shortly after the first detection, the event GW151012, was observed. This event, although expected to be a real event, did not fall within the limits set for an event to be classified as a confirmed GW event and so instead of being prefixed by "GW" it was initially referred to as "LVT151012" for Ligo-Virgo-Transient. The glitch co-incidence was calculated to be 5%, however there is a very good match of the event with the templates [144]. LVT151012 was subsequently promoted to a full GW event, GW151012. On 1 August 2017, aVIRGO, in Italy, joined the observation runs of aLIGO. Shortly thereafter, the event GW170814 was the first

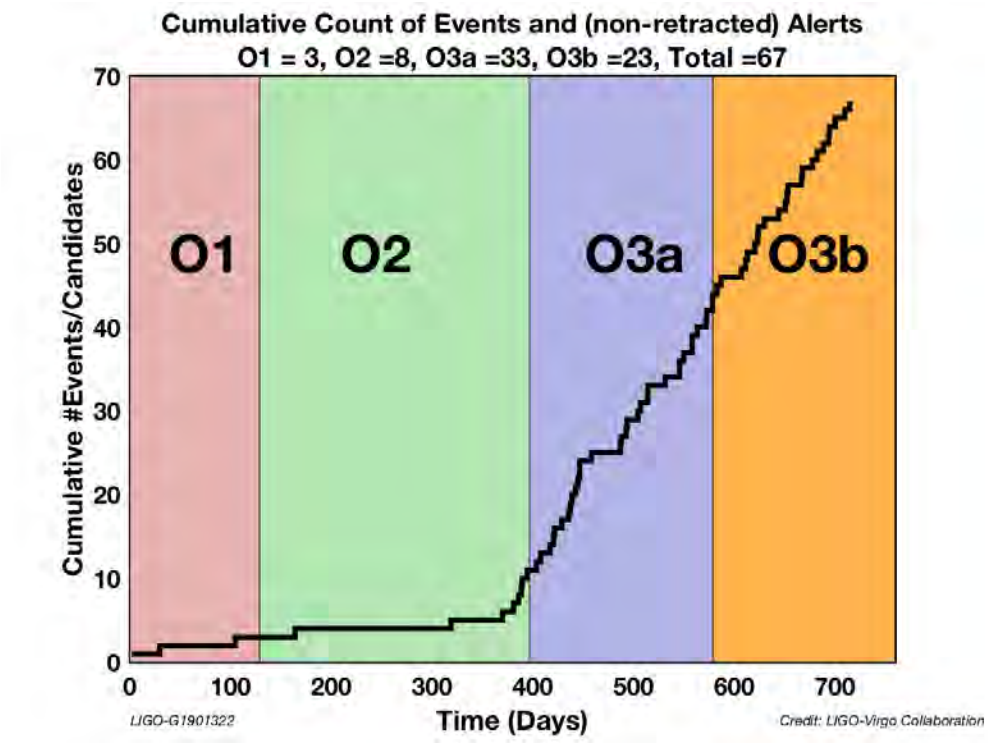


Figure 5.11: Observing runs O1, O2, O3 made by LIGO. Image credit: LVC [190]

event to be jointly observed by three interferometers: aLIGO's two detectors, in Hanford (H1) and Livingston (L1) in the USA, and aVIRGO in Italy. The detection with three detectors allowed greater accuracy in pinpointing the source direction. Three days later, an even more momentous observation was made when the three detectors working in unison all detected the first BNS merger, GW170817. With three detectors working together, the location was able to be determined with greater accuracy. BNS mergers unlike BH mergers are rich in EM and other signals. With the advantage of the three detectors giving a narrower range of location and coupled with the additional advantage that the GW data indicated that the event was close by, at 40Mpc away, the event provided the opportunity for the firt ever MMA GW detection. The Fermi satellite observed a weak GRB 1.7s after the GW signal, transient-astronomy survey telescopes made a host of other detections and in all 70 different partners of aLIGO and aVIRGO all confirmed detection of the event within 12 hours of the GW signal [144]. This led to the first GW MMA observation paper [189]. A summary of some of the key features of the first BNS detection, GW170817, is given in Fig. 5.14 on page 76. A list of the GW detections in the GW detection runs are given in Appendix E.

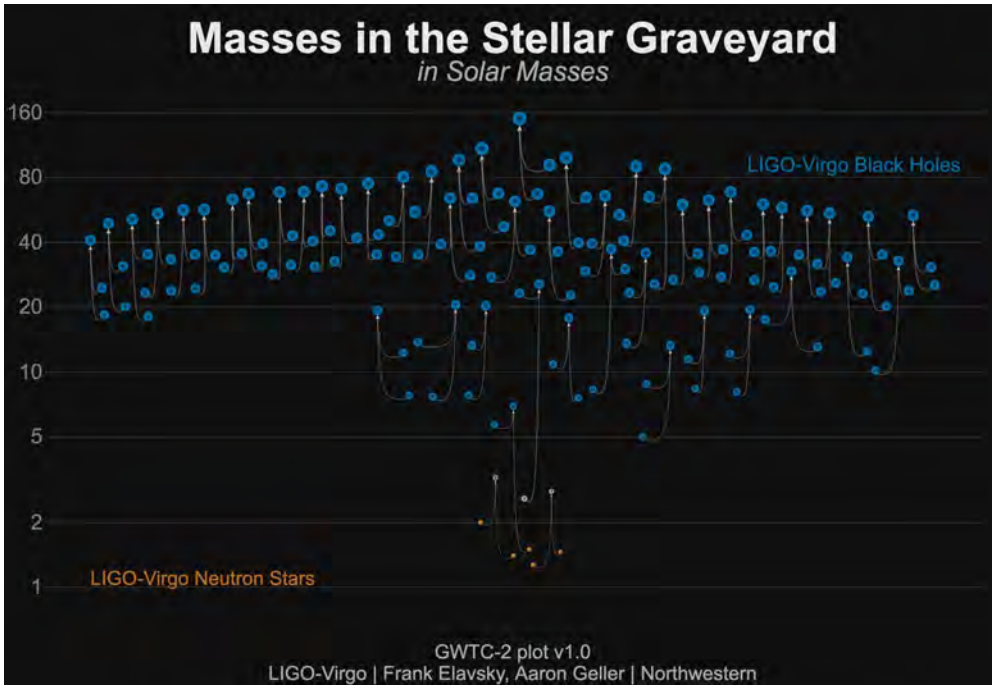


Figure 5.12: masses in BBH mergers up to the O3 run [191]

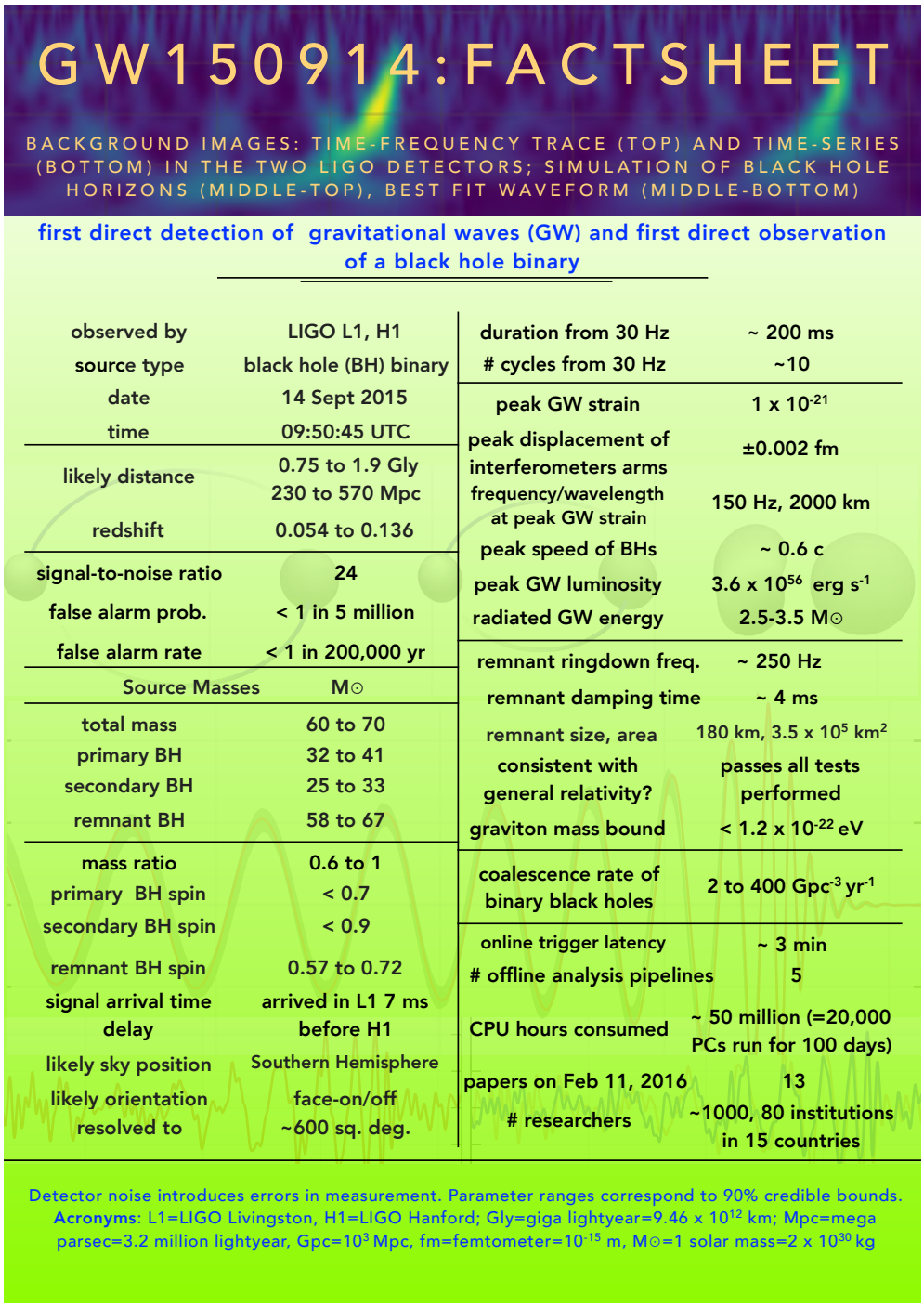


Figure 5.13: GW150914 factsheet [192]

# GW170817 FACTSHEET

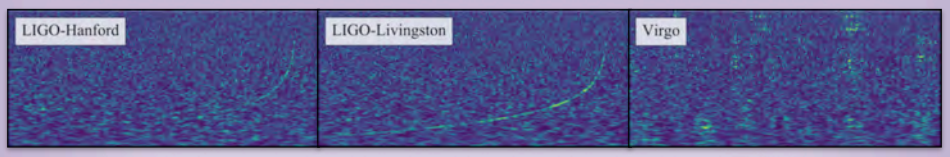


| | | | |
|---|---|---|---|
| observed by | H, L, V | inferred duration from 30 Hz to 2048 Hz** | ~ 60 s |
| source type | binary neutron star (NS) | inferred # of GW cycles from 30 Hz to 2048 Hz** | ~ 3000 |
| date | 17 August 2017 | initial astronomer alert latency* | 27 min |
| time of merger | 12:41:04 UTC | HLV sky map alert latency* | 5 hrs 14 min |
| signal-to-noise ratio | 32.4 | HLV sky area† | 28 deg$^2$ |
| false alarm rate | < 1 in 80 000 years | # of EM observatories that followed the trigger | ~ 70 |
| distance | 85 to 160 million light-years | also observed in | gamma-ray, X-ray, ultraviolet, optical, infrared, radio |
| total mass | 2.73 to 3.29 $M_\odot$ | host galaxy | NGC 4993 |
| primary NS mass | 1.36 to 2.26 $M_\odot$ | source RA, Dec | $13^h09^m48^s$, -23°22'53" |
| secondary NS mass | 0.86 to 1.36 $M_\odot$ | sky location | in Hydra constellation |
| mass ratio | 0.4 to 1.0 | viewing angle (without and with host galaxy identification) | ≤ 56° and ≤ 28° |
| radiated GW energy | > 0.025 $M_\odot c^2$ | Hubble constant inferred from host galaxy identification | 62 to 107 km s$^{-1}$ Mpc$^{-1}$ |
| radius of a 1.4 $M_\odot$ NS | likely ≤ 14 km | | |
| effective spin parameter | -0.01 to 0.17 | | |
| effective precession spin parameter | unconstrained | | |
| GW speed deviation from speed of light | < few parts in $10^{15}$ | | |

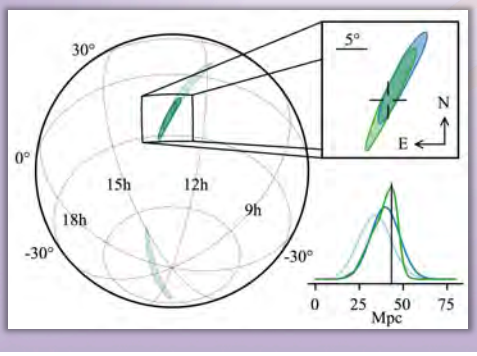


Images: time frequency traces (top), GW sky map (left, HL = light blue, HLV = dark blue, improved HLV = green, optical source location = cross-hair)

GW=gravitational wave, EM = electromagnetic, $M_\odot$=1 solar mass=2x$10^{30}$ kg, H/L=LIGO Hanford/Livingston, V=Virgo

Parameter ranges are 90% credible intervals.
*referenced to the time of merger
**maximum likelihood estimate
†90% credible region

Figure 5.14: GW170817 factsheet [193]

# Chapter 6

# Effect of a low density dust shell on the propagation of gravitational waves

In this chapter we will consider the problem of a GW source surrounded by a spherical dust shell using the BS formalism, which is discussed in Chapter 3; see also the reviews [71, 54, 70]. The geometry is found in the regions: in the shell, exterior to the shell, and interior to the shell. It is found that the dust shell causes the GW to be modified both in magnitude and phase, but without any energy being transferred to or from the dust. This finding is novel and has been published in the journal *General Relativity and Gravitation* [47].

It is possible that the astrophysical environment of a source event could be such that the source is surrounded by a substantial amount of matter. Thus, as we move into an era of precision GW measurements, it is important to quantify any effects due to propagation of GWs through a non-vacuum spacetime. These issues have been investigated previously. There is a simple physical argument that an ideal fluid should not extract energy from a GW, because there is no physical mechanism for it to do so; and this idea has been given a precise expression in the work of Esposito [194], and of Ehlers *et al.* [195, 196]. However, if the matter is dissipative, e.g. through shear viscosity, then one would expect GWs to be attenuated.

We consider small perturbations about a fixed background, which topic was first considered some time ago and known as the "quasi-Newtonian" or "quasi-spherical" approximation [197, 198]; there has also been previous work using this approach in which a dust cloud source was considered [199]. However, this work uses the method of separation of variables to construct, within a BS framework, eigensolutions for linearised perturbations [54]; when the background is Minkowski spacetime, these solutions have a remarkably simple analytic form. This approach has given additional insights in another context, that of GWs propagating in de Sitter spacetime [200]; see also [201, 202].

We model the problem of a GW source in a spacetime that is empty apart from matter con-

tained in a thin shell around the source (then, results for a thick matter shell can be modelled by adding up, i.e. integrating, over thin shells). The shell is given the simplest equation of state, i.e., that of dust. It is found that the effect of the shell is to modify the outgoing GWs in both phase and magnitude, although in a way that does not contradict previous results about energy transfer. The modification of the GW is small, and in a cosmological context is not expected to be measurable; but it is possible that a GW event could occur in which the local astrophysical environment is such that the effect would be measurable. Further, there is a view that LIGO data for black hole mergers may contain echoes, and explanations investigated, using numerical simulations, have included new physics near the event horizon, and the astrophysical environment such as a shell around the system; see, e.g., [30, 31]; this matter is discussed further in Chapter 6. In any case, the results are certainly of interest to the theory of GWs propagating in matter.

Sec. 6.1 specifies the problem, and constructs the background solution, i.e. when the geometry is spherically symmetric. The solution when the source is emitting GWs is then constructed in Sec. 6.2. The physical interpretation of the modified GWs is discussed in Sec. 6.3. A discussion on the results and our conclusions are given in Sec. 6.4, which also includes a discussion of the extension of this investigation and they are applied to astrophysics in Chapter 6. Substantial use of computer algebra; the scripts used are summarised in Appendix C.

## 6.1 The background solution

The BS formalism for the Einstein equations is well-known [69, 67] and discussed in Chapter 3. The coordinates are based on outgoing null hypersurfaces labelled by the coordinate $x^0 = u$. Let $x^A$ $(A = 2, 3)$ be angular coordinates (e.g. spherical polars $(\theta, \phi)$) that label the null ray generators of a hypersurface $u =$ constant, and let $x^1 = r$ be a surface area radial coordinate. The Bondi-Sachs metric describes a general spacetime, and here we write it as

$$\begin{aligned} ds^2 = &-\left(e^{2\beta}\left(1+\frac{W}{r}\right) - r^2 h_{AB}U^A U^B\right) du^2 - 2e^{2\beta} du dr \\ &- 2r^2 h_{AB} U^B du dx^A + r^2 h_{AB} dx^A dx^B \,, \end{aligned} \tag{6.1}$$

where $h^{AB}h_{BC} = \delta^A_C$, and the condition that $r$ is a surface area coordinate implies $\det(h_{AB}) = \det(q_{AB})$ where $q_{AB}$ is a unit sphere metric (e.g. $d\theta^2 + \sin^2\theta d\phi^2$). We represent $q_{AB}$ by a complex dyad (e.g. $q^{AB} = (1, 1/\sin\theta)$) and introduce the complex differential angular operators $\eth, \bar{\eth}$ [85]; see also [87, 71]. Then $h_{AB}$ is represented by the complex quantity $J = q^A q^B h_{AB}/2$ (with $J = 0$ characterizing spherical symmetry), and we also introduce the complex quantity $U = U^A q_A$. Einstein's equations are

$$E_{\alpha\beta} := \quad R_{\alpha\beta} = 8\pi(T_{\alpha\beta} - \frac{1}{2}g_{\alpha\beta}T)\,, \tag{6.2}$$

with: $E_{\alpha\beta}$ representing a set of **equations**, rather than tensor components; $T_{\alpha\beta} = \rho V_\alpha V_\beta$

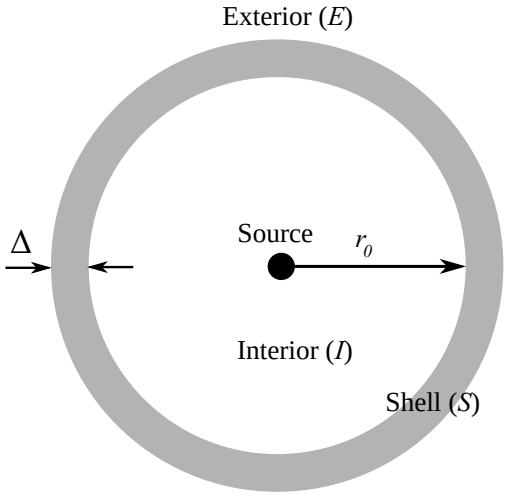


Figure 6.1: Schematic representation: The spacetime is empty apart from a GW source at the origin, and a shell of mass $M_S$ located between $r = r_0$ and $r = r_0 + \Delta$. The spacetime thus comprises three regions as shown: Interior ($I$), Shell ($S$) and Exterior ($E$).

for dust of density $\rho$ and 4-velocity $V_\alpha$; $T = -\rho$. Einstein's equations may be categorized as

$$\begin{aligned} \text{Hypersurface equations: } & E_{11}\,, E_{1A}q^A\,, E_{AB}h^{AB}\,, \\ \text{Evolution equation: } & E_J = E_{AB}(q^Aq^B - Jh^{AB})\,, \\ \text{Constraint equations: } & E_{00}\,, E_{01}\,, E_{0A}q^A\,. \end{aligned} \tag{6.3}$$

Much previous work uses $E_J = E_{AB}q^Aq^B$; in the case that the background is not Minkowskian, the additional term introduced above leads to some simplification of the equation. A characteristic initial value problem may be formulated for the above with $J$ specified on a null hypersurface $u =$ constant [203].

We consider the physical problem of a spacetime that is empty except in a shell located at $r_0 < r < r_0 + \Delta$. where there is a spherically symmetric distribution of dust with a density profile that vanishes at $r = r_0$ and $r = r_0 + \Delta$; see Fig. 6.1. An example density profile is

$$\rho = \rho_c \left(\frac{1}{r^3} - \frac{r_0}{r^4}\right)\left(\frac{r_0+\Delta}{r^4} - \frac{1}{r^3}\right)\,, \tag{6.4}$$

and other density profiles tested are

$$\begin{aligned} &\rho = \rho_c \left(\frac{1}{r^3} - \frac{r_0}{r^4}\right)\left(\frac{(r_0+\Delta)^2}{r^5} - \frac{1}{r^3}\right)\,, \qquad \rho = \rho_c \left(\frac{1}{r^4} - \frac{r_0}{r^5}\right)\left(\frac{r_0+\Delta}{r^4} - \frac{1}{r^3}\right)\,, \\ &\rho = \rho_c \left(\frac{1}{r^2} - \frac{r_0}{r^3}\right)\left(\frac{(r_0+\Delta)}{r^5} - \frac{1}{r^4}\right)\,, \qquad \rho = \rho_c \left(\frac{1}{r^2} - \frac{r_0}{r^3}\right)\left(\frac{r_0+\Delta}{r^6} - \frac{1}{r^5}\right)\,. \end{aligned} \tag{6.5}$$

There is also a source of quadrupolar GWs at the origin, but the first problem that needs

to be solved is the background solution for which this source is neglected. The problem is spherically symmetric so $J = U = 0$. Further, the shell density is small and terms of $\mathcal{O}(\rho^2)$ are neglected. The collapse of the shell under its own gravity is an effect with acceleration $\mathcal{O}(\rho^2)$ and is therefore ignored. Thus, the shell is treated as static, and the only non-zero metric coefficients are $\beta(r), W(r)$. The Einstein equations for $E_{11}, E_{AB}h^{AB}$ then simplify to [203, 204]

$$\partial_r \beta = 2\pi r \rho (V_1)^2 \,, \qquad \partial_r W = e^{2\beta} - 1 - 4\pi e^{2\beta} \rho r^2 \,. \tag{6.6}$$

Here, to $\mathcal{O}(\rho)$, $\rho(V_1^{[B]})^2 = \rho$ and $\beta = \mathcal{O}(\rho)$, so we have

$$\partial_r \beta = 2\pi r \rho \,, \qquad \partial_r W = 2\beta - 4\pi \rho r^2 \,, \tag{6.7}$$

which are solved subject to the boundary conditions $\beta \to 0$ as $r \to \infty$ (so that the background coordinates are asymptotically Minkowskian), and $W = \mathcal{O}(r)$ as $r \to 0$ (so that the $W/r$ is regular at the origin). We find:

$$\begin{aligned} r < r_0 : \ \beta^{[B]} = B_0 \,, \qquad W^{[B]} = 2rB_0, \\ r_0 + \Delta < r : \ \beta^{[B]} = 0 \,, \qquad W^{[B]} = -2M_S \,, \end{aligned} \tag{6.8}$$

with the superfix $^{[B]}$ indicating a quantity in the background depending only on $r$, and where $B_0$ is a constant and $M_S$ is the mass of the shell (see below). The solution for $\beta^{[B]}, W^{[B]}$ in $r_0 \le r \le r_0 + \Delta$ is lengthy and is given in Appendix C. In the case of Eq. (6.4) we find,

$$\begin{aligned} M_S &= \int_{r_0}^{r_0+\Delta} 4\pi \rho r^2 dr = \rho_c \frac{\pi \Delta^3 (10 r_0^2 + 10 r_0 \Delta + 3\Delta^2)}{15 r_0^4 (r_0 + \Delta)^4} \,, \\ B_0 &= -\rho_c \frac{\pi \Delta^3 (2r_0 + \Delta)(5r_0^2 + 5r_0\Delta + 2\Delta^2)}{30 r_0^5 (r_0 + \Delta)^5} = -\frac{M_S}{2r_0} + \mathcal{O}(\Delta) \,, \end{aligned} \tag{6.9}$$

with the result $B_0 = -M_S/2r_0 + \mathcal{O}(\Delta)$ applying to all density profiles tested. The solution in $r > r_0 + \Delta$ is Schwarzschild spacetime in Eddington-Finkelstein coordinates. The solution in $r < r_0$ is Minkowski spacetime (which in standard form has $\beta = W = 0$), and this can be seen upon applying the coordinate transformation

$$u \to u' = (1 + 2B_0) u \,. \tag{6.10}$$

We check, using computer algebra, that for a given density profile, $\beta$ and $W$ and their first derivatives are continuous at the interfaces at $r = r_0$ and $r = r_0 + \Delta$; and also that the solution in the shell satisfies all 10 Einstein equations.

## 6.2 The perturbed solution

Having determined the background solution, which can be regarded as Minkowski plus small spherically symmetric corrections of $\mathcal{O}(\rho)$, we perturb the solution by writing the metric quantities $(\beta, U, W, J)$ as

$$\beta = \beta^{[B]} + \beta^{[e]} \,, \ U = U^{[e]} \,, \ W = W^{[B]} + W^{[e]} \,, \ J = J^{[e]} \,, \tag{6.11}$$

where the superfix $^{[e]}$ indicates the deviation of a quantity about its background value. The metric perturbations are functions of $(u, r, x^A)$ and are treated as $\mathcal{O}(\epsilon)$ with $\epsilon \ll 1$, and with the smallness parameters $\rho_c, \epsilon$ independent of each other. We also introduce the matter field perturbations

$$\rho = \rho^{[B]} + \rho^{[e]}\,,\ V_\alpha = V_\alpha^{[B]} + V_\alpha^{[e]}\,, \tag{6.12}$$

with $V_\alpha^{[e]}$ treated as $\mathcal{O}(\epsilon)$ and $\rho^{[e]}$ treated as $\mathcal{O}(\rho_c\epsilon)$. Linearization about certain backgrounds was described in [54]; using a similar procedure we retain only terms of order $\mathcal{O}(\rho_c, \epsilon, \rho_c\epsilon)$ and find that the hypersurface and evolution equations are

$$\begin{aligned}
E_{11}:\ & \frac{4}{r}\left(\partial_r\beta^{[e]} + \partial_r\beta^{[B]}\right) = 8\pi T_{11}\,,\\
q^a E_{1A}:\ & \frac{1}{2r^2}\left[-2\,r^4\partial_r\left(\frac{\eth\beta^{[e]}}{r^2}\right) - 2\,\partial_r\left(r^4\,\beta^{[B]}\partial_r U^{[e]}\right) + \partial_r\left(r^4\partial_r U^{[e]}\right) + r^2\bar{\eth}\partial_r J^{[e]}\right]\\
& = 8\pi q^A T_{1A}\,,\\
h^{AB}E_{AB}:\ & 4\,\beta^{[B]} - 2\,\eth\bar{\eth}\beta^{[e]} - 2\,\partial_r W^{[B]} + 4\,\beta^{[e]}\partial_r W^{[B]}\\
& - \left(2\,\beta^{[B]} - 1\right)\left[4\,\beta^{[e]} - 2\partial_r W^{[e]} + \frac{1}{r^2}\,\partial_r\left(r^4\eth\bar{U}^{[e]} + r^4\bar{\eth}U^{[e]}\right)\right]\\
& + \frac{1}{2}\left(\bar{\eth}^2 J^{[e]} + \eth^2\bar{J}^{[e]}\right)\\
& = 8\pi\left(h^{AB}T_{AB} - r^2\,T\right)\,,\\
E_J:\ & -2\,\eth^2\beta^{[e]} - \partial_r\left(r\,\partial_r J^{[e]}W^{[B]}\right)\\
& + \left(2\,\beta^{[B]} - 1\right)\left[-\partial_r\left(r^2\eth U^{[e]}\right) + \partial_r\left(r^2\partial_r J^{[e]}\right) - 2\,r\,\partial_r\left(r\partial_u J^{[e]}\right)\right]\\
& = 0\,.
\end{aligned} \tag{6.13}$$

The above equations are tackled using the method of separation of variables, rather than formulation as a characteristic initial value problem. The required ansatz for the quantities $\beta^{[e]}, U^{[e]}, W^{[e]}, J^{[e]}, \rho^{[e]}, V_\alpha^{[e]}$ is

$$\begin{aligned}
\beta^{[e]} =& \Re(\beta^{[2,2]}(r)e^{i\nu u})_0 Z_{2,2}\,,\ \ U^{[e]} = \Re(U^{[2,2]}(r)e^{i\nu u})_1 Z_{2,2}\,,\ \ W^{[e]} = \Re(W^{[2,2]}(r)e^{i\nu u})_0 Z_{2,2}\,,\\
J^{[e]} =& \Re(J^{[2,2]}(r)e^{i\nu u})_2 Z_{2,2}\,,\ \ \rho^{[e]} = \Re(\rho^{[2,2]}(r)e^{i\nu u})_0 Z_{2,2}\,,\ \ V_0^{[e]} = \Re(V_0^{[2,2]}(r)e^{i\nu u})_0 Z_{2,2}\,,\\
V_1^{[e]} =& \Re(V_1^{[2,2]}(r)e^{i\nu u})_0 Z_{2,2}\,,\ \ q^A V_A^{[e]} = \Re(V_{ang}^{[2,2]}(r)e^{i\nu u})_1 Z_{2,2}\,,
\end{aligned} \tag{6.14}$$

with the superfix $^{[2,2]}$ indicating a coefficient of ${}_sZ_{2,2}$. The perturbations oscillate in time with frequency $\nu/(2\pi)$. The quantities ${}_sZ_{\ell,m}$ are spin-weighted spherical harmonic basis functions related to the usual ${}_sY_{\ell,m}$ as specified in [54, 71]. They have the property that ${}_0Z_{\ell,m}$ are real, enabling the description of the metric quantities $\beta, W$ (which are real) without mode-mixing; however, for $s \neq 0$ ${}_sZ_{2,2}$ is, in general, complex. A general solution may be constructed by summing over the $(\ell, m)$ modes, but that is not needed here, since we are considering a source that is continuously emitting GWs at constant frequency dominated by the $\ell = 2$ (quadrupolar) components (Of course, the wave frequency changes with inspiral, and we are assuming that this timescale is much longer than the wave period). We substitute the ansatz Eqs. (6.14) into Eqs. (6.13) with $\ell = 2$ to obtain: (1) On integrating over the sphere, only the $\ell = 0$ part survives and Eqs. (6.7) for the background are obtained; (2) Multiplication by ${}_sZ^*_{2,m}$ (where $^*$ denotes

complex conjugate) followed by integration over the sphere kills the spherically symmetric part, and Eqs. (6.13) transform to a system of ordinary differential equations in $r$

$$
\begin{aligned}
E_{11}: & \frac{4}{r}\frac{d}{dr}\beta^{[2,2]} = 8\,\pi\,\left(\rho^{[2,2]} - 2\,\rho^{[B]}V_1^{[2,2]}\right)\,, \\
q^A E_{1A}: & \frac{1}{r^2}\left[\sqrt{6}\,r^4\,\frac{d}{dr}\left(\frac{\beta^{[2,2]}}{r^2}\right) + \frac{1}{r^2}\frac{d}{dr}\left(r^4\,\beta^{[B]}\frac{d}{dr}U^{[2,2]}\right)\right. \\
& \left. - \frac{1}{2}\frac{d}{dr}\left(r^4\frac{d}{dr}U^{[2,2]}\right) + r^2\frac{d}{dr}J^{[2,2]}\right] \\
& = 8\,\pi\,\rho^{[B]}\,V_{ang}^{[2,2]}\,, \\
h^{AB}E_{AB}: & 12\,\beta^{[2,2]} + 4\,\beta^{[2,2]}\frac{d}{dr}W^{[B]} + 2\,\sqrt{6}\,J^{[2,2]} \\
& - \left(2\,\beta^{[B]} - 1\right)\left[4\,\beta^{[2,2]} - 2\,\sqrt{6}\,r\,U^{[2,2]} - \sqrt{6}\,\frac{d}{dr}\left(r^2\,U^{[2,2]}\right) - 2\,\frac{d}{dr}W^{[2,2]}\right] \\
& = 8\,\pi\,r^2\,\rho^{[2,2]}\,, \\
E_J: & \; 4\,\sqrt{6}\beta^{[2,2]} + \partial_r\left(r\,W^{[B]}\,\frac{d}{dr}J^{[2,2]}\right) \\
& + \left(2\,\beta^{[B]} - 1\right)\left[2\,\frac{d}{dr}\left(r^2\,U^{[2,2]}\right) - \frac{d}{dr}\left(r^2\frac{d}{dr}J^{[2,2]}\right) + 2\,i\,\nu\,r\,\frac{d}{dr}\left(r\,J^{[2,2]}\right)\right] \\
& = 0\,.
\end{aligned}
\tag{6.15}
$$

Eqs. (6.15) contain terms of order $\mathcal{O}(\epsilon, \rho\epsilon)$; terms of $\mathcal{O}(\rho^2)$ may be larger than those of $\mathcal{O}(\rho\epsilon)$, but are excluded by the procedure that kills the spherically symmetric part of Eqs. (6.13). In changing from Eqs. (6.13) to Eqs. (6.15), formulas were used for the effect of the $\eth$ operator on ${}_sZ_{\ell,m}$ [54, 71]

$$
\begin{aligned}
& \eth\,{}_{-1}Z_{2,2} = -\sqrt{6}\,{}_0Z_{2,2}\,, \;\; \eth\,{}_0Z_{2,2} = \sqrt{6}\,{}_1Z_{2,2}\,, \;\; \bar{\eth}\,{}_1Z_{2,2} = -\sqrt{6}\,{}_0Z_{2,2}\,, \;\; \eth\,{}_1Z_{2,2} = 2\,{}_2Z_{2,2}\,, \\
& \bar{\eth}\,{}_2Z_{2,2} = -2\,{}_1Z_{2,2}\,, \;\; \eth^2\,{}_{-1}Z_{2,2} = -6\,{}_1Z_{2,2}\,, \;\; \eth^2\,{}_0Z_{2,2} = 2\sqrt{6}\,{}_1Z_{2,2}\,, \;\; \eth\bar{\eth}\,{}_0Z_{\ell,m} = -6\,{}_0Z_{\ell,m}\,, \\
& \eth\bar{\eth}\,{}_1Z_{\ell,m} = -6\,{}_1Z_{\ell,m}\,, \;\; \bar{\eth}^2\,{}_2Z_{2,2} = 2\sqrt{6}\,{}_0Z_{2,2}\,, \;\; \eth^2\,{}_{-2}Z_{2,2} = 2\sqrt{6}\,{}_0Z_{2,2}\,,
\end{aligned}
\tag{6.16}
$$

where the above formulas are specialized to the case $\ell = 2$. As well as the hypersurface

Eqs. (6.15), we will also need the constraints $E_{0a}$, which are

$$
\begin{aligned}
E_{00} : & -\frac{1}{2r^3}\left[12\,r\beta^{[2,2]}+24\,r\beta^{[B]}\beta^{[2,2]}-\frac{2}{r}\frac{d}{dr}\left(r^2\frac{d}{dr}\beta^{[2,2]}\right)\right.\\
& -\sqrt{6}\,r\,U^{[2,2]}\left(\frac{d}{dr}\left(\frac{W^{[B]}}{r}\right)+2\,\frac{d}{dr}\beta^{[B]}\right)\\
& -6\,r^3\,W^{[B]}\,\frac{d}{dr}\left(\frac{\beta^{[2,2]}}{r^2}\right)-2\,r^2\left(2\frac{d^2}{dr^2}\beta^{[2,2]}W^{[B]}+\frac{d}{dr}\beta^{[2,2]}\frac{d}{dr}W^{[B]}\right)\\
& -6\,r^3\,W^{[2,2]}\,\frac{d}{dr}\left(\frac{\beta^{[B]}}{r^2}\right)-2\,r^2\left(2\frac{d^2}{dr^2}\beta^{[B]}W^{[2,2]}+\frac{d}{dr}\beta^{[B]}\frac{d}{dr}W^{[2,2]}\right)\\
& +6\,W^{[2,2]}-r^2\frac{d^2}{dr^2}W^{[2,2]}-r\,W^{[2,2]}\frac{d^2}{dr^2}W^{[B]}-\,rW^{[B]}\frac{d^2}{dr^2}W^{[2,2]}-2\,i\nu\,r\,W^{[2,2]}\\
& \left.+i\,\frac{4\nu}{r^2}\frac{d}{dr}\left(r\,\beta^{[2,2]}\right)+4\,i\,\nu\,r\,\beta^{[2,2]}W^{[B]}+4\,i\,\nu\,r^2\,\frac{d}{dr}\beta^{[2,2]}W^{[B]}-2\,\sqrt{6}\,i\,\nu\,r^3\,U^{[2,2]}\right]\\
& =4\,\pi\,\left(\rho^{[2,2]}+\rho^{[B]}\frac{2\beta^{[2,2]}r+W^{[2,2]}}{r}\right),\\
E_{01} : & -\frac{1}{2r^2}\left[24\,\beta^{[B]}\beta^{[2,2]}+12\,\beta^{[2,2]}-r\frac{d^2}{dr^2}W^{[2,2]}+4\,i\nu r^2\,\frac{d}{dr}\beta^{[2,2]}\right.\\
& \left.-\frac{d}{dr}\left(2\,r^2\frac{d}{dr}\beta^{[2,2]}+2\,r\,W^{[B]}\frac{d}{dr}\beta^{[2,2]}+2\,r\,W^{[2,2]}\frac{d}{dr}\beta^{[B]}+r^2\,\sqrt{6}U^{[2,2]}\right)\right]\\
& =4\,\pi\,\left(\rho^{[2,2]}-2\,\rho^{[B]}V_1^{[2,2]}+\rho^{[B]}\frac{W^{[2,2]}}{r}\right),\\
q^A E_{0A} : & \frac{1}{2r^2}\left[4\,r^2\beta^{[B]}U^{[2,2]}+2\,\frac{d}{dr}\left(r^4\beta^{[B]}\frac{d}{dr}U^{[2,2]}\right)-2\,i\,\nu\,r^4\beta^{[B]}\,\frac{d}{dr}U^{[2,2]}\right.\\
& -\sqrt{6}\,\left(2\,r\,W^{[2,2]}\frac{d}{dr}\beta^{[B]}+\,r^2\,\frac{d}{dr}\left(\frac{W^{[2,2]}}{r}\right)-2\,i\,\nu\,r^2\,\beta^{[2,2]}\right)\\
& -2\,r^2\frac{d}{dr}W^{[B]}U^{[2,2]}-\frac{1}{r}\frac{d}{dr}\left(r^4W^{[B]}\frac{d}{dr}U^{[2,2]}\right)\\
& \left.-2\,r^2\,U^{[2,2]}-\frac{d}{dr}\left(r^4\,U^{[2,2]}\right)+i\,\nu\,r^4\,\frac{d}{dr}U^{[2,2]}+2\,i\nu\,r^2\,J^{[2,2]}\right]\\
& =4\pi\,\rho^{[B]}\left(2\,V_{ang}^{[2,2]}+U^{[2,2]}r^2\right).
\end{aligned}
\tag{6.17}
$$

The procedure for solving Eqs (6.15) and (6.17) was given in [54], and in outline is as follows. Firstly, $E_{11}$ is integrated to find $\beta^{[2,2]}(r)$; then $q^A E_{1A}$ and $E_J$ are solved together to give $J^{[2,2]}(r), U^{[2,2]}(r)$; then $h^{AB}E_{AB}$ may be integrated to give $W^{[2,2]}(r)$. The solution obtained has 6 constants of integration, 2 of which are fixed on applying the constraints $E_{00}, q^A E_{0A}$. We will see later that the matter terms can be expressed as functions of $\rho^{[B]}$ and the metric, so that Eqs. (6.15) take the form

$$
(\mathcal{M}+\rho_c\mathcal{R})(f)=0\,,
\tag{6.18}
$$

where $f$ is a multi-vector containing $\beta^{[2,2]}(r), J^{[2,2]}(r), U^{[2,2]}(r), W^{[2,2]}(r)$, and $\mathcal{M}, \mathcal{R}$ are linear differential operators with $\mathcal{M}$ being the operator when $\rho_c = 0$, i.e. when the background is Minkowski. Let $f_M$ be the solution to the homogeneous problem $\mathcal{M}(f_M) = 0$. $f_M$ was

derived in Sec 3.4.1 and is repeated here

$$\begin{aligned}
\beta^{[2,2]} =& b_0\,,\\
W^{[2,2]} =& 6i\nu r^2 C_{10} + r(12C_{10} - 10b_0) + C_{50} - \frac{12i\nu C_{40}}{r} - \frac{6C_{40}}{r^2} - C_{in0}\exp(2ir\nu)\frac{3}{r^2}\,,\\
U^{[2,2]} =& -\sqrt{6}i\nu C_{10} + \frac{2\sqrt{6}b_0}{r} + \frac{2\sqrt{6}C_{30}}{r^2} - \frac{4i\nu\sqrt{6}C_{40}}{r^4} - \frac{3\sqrt{6}C_{40}}{r^4}\\
& - C_{in0}\exp(2ir\nu)\sqrt{6}\left(i\frac{\nu}{r^3} - \frac{3}{2r^4}\right)\,,\\
J^{[2,2]} =& 2\sqrt{6}C_{10} + \frac{2\sqrt{6}C_{30}}{r} + \frac{2\sqrt{6}C_{40}}{r^3} + C_{in0}\exp(2ir\nu)\sqrt{6}\left(\frac{1}{r^3} - 2i\frac{\nu}{r^2} - \frac{\nu^2}{r}\right)\,.
\end{aligned} \tag{6.19}$$

The solution includes constants of integration $b_0, C_{in0}, C_{10}, C_{30}, C_{40}, C_{50}$, two of which are fixed on applying the constraints $E_{00}, q^A E_{0A}$ giving

$$C_{50} = 12\nu^2 C_{40}\,,\;\; C_{10} = \frac{2b_0 + i\nu C_{30} + i\nu^3 C_{40}}{3}\,. \tag{6.20}$$

The remaining Einstein equation $E_{01}$ is known as the trivial equation, since it is automatically satisfied provided all the other Einstein equations are satisfied [69]. The solution Eq. (6.19) subject to Eq. (6.20) will be denoted by $f_M$; and this may be specialized to the case of no incoming radiation by setting $C_{in0} = 0$ with the solution denoted by $f_{M0}$.

The gravitational news $\mathcal{N}$ is defined in a coordinate system that satisfies the Bondi gauge conditions $\lim_{r\to\infty} J, U, \beta, W/r = 0$, and is calculated on making the required coordinate transformation. The procedure in the general case was described in [205], which was then simplified for the linearised approximation in [54] (Sec.3.3); an explicit expression for the news was given in [92], Eq. (16). Following Ref. [54], the gravitational news is given by

$$\mathcal{N} = \Re\left[\left(-\frac{i\nu}{2}\lim_{r\infty}(r^2\partial_r J^{[2,2]}) + \frac{L_2}{4} + \sqrt{L_4}b_0\right)e^{i\nu u}\right]\,{}_2Z_{\ell,m}, \tag{6.21}$$

where,

$$J^{[2,2]}_{\infty} = \lim_{r\to\infty} J^{[2,2]}(r), \tag{6.22}$$

$$L_2 = -\ell(\ell+1), \tag{6.23}$$

and

$$L_4 = (\ell-1)\ell(\ell+2)(\ell+2). \tag{6.24}$$

So, for $\ell = 2$

$$L_2 = -\ell(\ell+1) = -2(2+1) = -6, \tag{6.25}$$

and

$$L_4 = (\ell-1)\ell(\ell+2)(\ell+2) = 24. \tag{6.26}$$

Hence, Eq. (6.21) may then be written as

$$\mathcal{N} = \Re\left(\left(-\frac{i\nu}{2}\lim_{r\infty}(r^2\partial_r J^{[2,2]}) - \frac{3}{2} + 2\sqrt{6}b_0\right)e^{i\nu u}\right)\,{}_2Z_{2,2}, \tag{6.27}$$

so that

$$\mathcal{N} = \nu^3\sqrt{6}\Re(iC_{40}e^{i\nu u})\,{}_2Z_{2,2}, \tag{6.28}$$

and

$$\partial_u\mathcal{H} = 2\mathcal{N}, \tag{6.29}$$

so that

$$\mathcal{H}_{M0} = \Re(H_{M0}\exp(i\nu u))\,{}_2Z_{2,2} \text{ with } H_{M0} = -2\sqrt{6}\nu^2 C_{40}\,. \tag{6.30}$$

$C_{40}$ is determined by the physical problem being modelled, and $b_0, C_{30}$ represent gauge freedoms; e.g., for an equal mass $m$ binary with orbital radius $r_o$, $C_{40} = 2mr_o^2\sqrt{\pi/15}$ [206].

We regard the solution $f_{M0}$ as applying when no matter shell is present, i.e. when $\rho_c = 0$, with all the constants of order $\mathcal{O}(\epsilon)$ and with $C_{40}$ fixed by the physics of the source. Then the solution in the presence of the matter shell will be $f_{M0}$ plus small corrections of order $\mathcal{O}(\epsilon\rho_c)$. We construct a solution in each of the three regions $r < r_0, r_0 < r < r_0 + \Delta, r_0 + \Delta < r$, and then apply matching conditions at the boundaries $r = r_0, r = r_0 + \Delta$.

### 6.2.1 Solution inside the shell, i.e. $r < r_0$

Perturbations in this region are on a background that is explicitly Minkowskian in $(u', r, \theta, \phi)$ coordinates; thus the solution $f_M$ applies, although the effect of boundary conditions may be to change the values of the constants by $\mathcal{O}(\epsilon\rho_c)$ from their values in $f_{M0}$. We therefore make the substitutions in Eq. (6.19) $b_0 \to b_0 + b_{0I}, C_{in0} \to C_{inI}, C_{10} \to C_{10} + C_{1I}, C_{30} \to C_{30} + C_{3I}, C_{40} \to C_{40} + C_{4I}, C_{50} \to C_{50} + C_{5I}$ with $b_{0I}$ etc. of order $\mathcal{O}(\epsilon\rho_c)$, and denote the solution as $f_{I'}$. The solution $f_I$ in global $(u, r, \theta, \phi)$ coordinates is obtained on applying the coordinate transformation Eq. (6.10) to $f_{I'}$; using computer algebra, we have evaluated $f_I$ explicitly and give the formulas in the Appendix C. Using computer algebra, the solution $f_I$ has been substituted into Eqs. (6.15) with $\beta^{[B]}, W^{[B]}$ taking the values for $r < r_0$ in Eqs. (6.8) and (6.9), and we have confirmed that the equations are satisfied. Values of the constants $C_{1I}, C_{5I}$ have been determined by substituting $f_I$ into Eqs. (6.17), and then the constraints have been re-evaluated to confirm that they are satisfied.

### 6.2.2 Solution within the shell, i.e. $r_0 < r < r_0 + \Delta$

The metric perturbations introduce perturbations into the matter fields, and these act as source terms in the Einstein equations. We evaluate the condition that the energy momentum tensor should be divergence-free, $\nabla_c T_{ab} g^{bc} = 0$, with the metric and metric connection terms evaluated using $f_{M0}$ (rather than $f$). The result is four equations for five unknowns $\rho^{[2,2]}(r), V_0^{[2,2]}(r)$, $V_1^{[2,2]}(r), V_{ang}^{[2,2]}(r)$ (note that $V_{ang}^{[2,2]}(r)$ is complex with two components), and the system is closed on applying the condition that the 4-velocity has unit norm, i.e. $V_\alpha V_\beta g^{\alpha\beta} = 1$. The resulting formulas are given in the Supplementary Material, see Appendix C, and we note that they are explicit functions of $r$ depending on the parameters $b_0, C_{10}, C_{30}, C_{40}, C_{50}, r_0, \Delta, \rho_c$. We also consider terms on the left-hand side of Eqs. (6.15) of the form ($\beta^{[B]}$ or $W^{[B]}$)×(metric perturbation) and use $f_{M0}$ rather than $f$ to evaluate the metric perturbation; thus these terms also become explicit functions of $r$ depending on known parameters.

The justification for using $f_{M0}$ instead of $f$ is that the error introduced is $\mathcal{O}(\rho_c\epsilon)$, and all such terms are multiplied by a term of $\mathcal{O}(\rho_c)$ so the total error is $\mathcal{O}(\rho_c^2\epsilon)$ which is ignorable. The result of these simplifications is that Eq. (6.18) becomes

$$\mathcal{M}f = -\rho_c\mathcal{R}_S(f_{M0})\,, \tag{6.31}$$

for which the solution to the homogeneous part has already been obtained, and there is just a particular integral that needs to be found; $\mathcal{R}_S$ denotes the specific form of the operator $\mathcal{R}$ within the shell. We denote the solution within the shell as $f_S$, and introduce additional constants $b_{0S}, C_{inS}, C_{1S}, C_{3S}, C_{4S}, C_{5S}$ similarly to what was done in Sec. 6.2.1 with $f_I$. The explicit solution for $f_S$ is obtained by means of computer algebra; it is very long and is given in the Supplementary Material, see Appendix C. Using computer algebra, we have evaluated the constraints to find expressions for $C_{1S}, C_{5S}$, and the solution $f_S$ has been confirmed by checking that it satisfies Eqs. (6.15) and (6.17) to order $\mathcal{O}(\rho_c\epsilon)$.

### 6.2.3 Solution exterior to the shell, i.e. $r_0 + \Delta < r$

In this region, the background geometry is Schwarzschild and perturbations about this background are not known analytically, but a numerical solution has been obtained [207]. Here, however, we can use the same procedure as in the previous sub-section, that is for terms of the form ($\beta^{[B]}$ or $W^{[B]}$)×(metric perturbation) we use $f_{M0}$ rather than $f$ to evaluate the metric perturbation, and Eq. (6.18) becomes $\mathcal{M}f = -\rho_c\mathcal{R}_E(f_{M0})$. We denote the solution outside the shell as $f_E$, and introduce additional constants $b_{0E}, C_{inE}, C_{1E}, C_{3E}, C_{4E}, C_{5E}$ similarly to what was done in Sec. 6.2.1 with $f_I$. The explicit solution for $f_E$ is obtained by means of computer algebra and is given in the Supplementary Material, see Appendix C. Using computer algebra, we have evaluated the constraints to find expressions for $C_{1E}, C_{5E}$, and the solution $f_E$ has been confirmed by checking that it satisfies Eqs. (6.15) and (6.17) to order $\mathcal{O}(\rho_c\epsilon)$.

Having determined the solution in the exterior region, we can now evaluate the gravitational news $\mathcal{N}^{[2,2]}$, and the formula is given in the Supplementary Material, see Appendix C. It involves $C_{40}, C_{4E}, \rho_c, r_0, \Delta$ and we need to express $C_{4E}$ in terms of the physical variables $C_{40}, \rho_c, r_0, \Delta$ so as to complete the calculation.

### 6.2.4 Matching conditions and the complete solution

After having used the constraints in each region, $f_E, f_S, f_I$ contain 12 free constants. The condition of no incoming radiation in the exterior requires that the coefficient of $\exp(2ir\nu)/r$ in $f_E$ be zero, leading to

$$C_{inE} = -4\nu\pi C_{40}M_S\,, \tag{6.32}$$

and continuity of the metric quantities $\beta, W, J, U$ at $r = r_0$ and $r = r_0 + \Delta$ imposes 8

conditions

$$\begin{aligned}
\beta^{[2,2,I]}(r=r_0) &= \beta^{[2,2,S]}(r=r_0)\,, & \beta^{[2,2,S]}(r=r_0+\Delta) &= \beta^{[2,2,E]}(r=r_0+\Delta)\,,\\
J^{[2,2,I]}(r=r_0) &= J^{[2,2,S]}(r=r_0)\,, & J^{[2,2,S]}(r=r_0+\Delta) &= J^{[2,2,E]}(r=r_0+\Delta)\,,\\
U^{[2,2,I]}(r=r_0) &= U^{[2,2,S]}(r=r_0)\,, & U^{[2,2,S]}(r=r_0+\Delta) &= U^{[2,2,E]}(r=r_0+\Delta)\,,\\
W^{[2,2,I]}(r=r_0) &= W^{[2,2,S]}(r=r_0)\,, & W^{[2,2,S]}(r=r_0+\Delta) &= W^{[2,2,E]}(r=r_0+\Delta)\,,
\end{aligned} \tag{6.33}$$

where the $I, S, E$ within the superfix indicates a quantity in the interior, shell or exterior respectively. We first solve the continuity conditions at $r = r_0 + \Delta$ to find expressions for $b_{0E}, C_{3E}, C_{4E}, C_{inS}$, and then we solve the continuity conditions at $r = r_0$ to find expressions for $b_{0S}, C_{3S}, C_{4S}, C_{inI}$; all these expressions are given in the Supplementary Material, see Appendix C. Since the Einstein hypersurface equations contain second derivatives of $J$ and $U$, we also expect $\partial_r J$, $\partial_r U$ to be continuous at $r = r_0$ and $r = r_0 + \Delta$. Using computer algebra we have checked that, provided Eqs. (6.33) are satisfied, the following conditions are also satisfied

$$\begin{aligned}
\partial_r J^{[2,2,I]}(r=r_0) &= \partial_r J^{[2,2,S]}(r=r_0)\,, & \partial_r J^{[2,2,S]}(r=r_0+\Delta) &= \partial_r J^{[2,2,E]}(r=r_0+\Delta)\,,\\
\partial_r U^{[2,2,I]}(r=r_0) &= \partial_r U^{[2,2,S]}(r=r_0)\,, & \partial_r U^{[2,2,S]}(r=r_0+\Delta) &= \partial_r U^{[2,2,E]}(r=r_0+\Delta)\,.
\end{aligned} \tag{6.34}$$

The outcome is that three degrees of freedom remain, $b_{0I}, C_{3I}, C_{4I}$, and the expression for $\mathcal{H}$ involves $C_{40}, C_{4I}$. As already discussed, the value of the constant $C_{40}$ is determined by the physics of the GW source, and we need another physical condition in order to close the system and to fix $C_{4I}$. The calculation of the perturbations from an equal mass binary assumes no incoming radiation, but the back-reaction due to the matter distribution may introduce such a term. Thus, the computer algebra script for the calculation of GWs emitted by an equal mass binary [206] has been amended with $C_{in0} \neq 0$ but $\mathcal{O}(\rho_c)$. We find

$$C_{4I} = -\frac{C_{inI}}{2}\,. \tag{6.35}$$

This result applies independently of source properties and, in particular, it applies when the mass of the orbiting binary is zero. Thus, it is reasonable to regard the result in Eq. (6.35) as general, representing the reflection at the origin of an incoming GW.
Then, finally, for all density profiles tested, the gravitational wave strain in terms of the mass of the shell $M_S$ and as measured by an observer at future null infinity, was found to be

$$\mathcal{H} = \Re\left(H_{M0}\left(1 + \frac{2M_S}{r_0} + \frac{2iM_S}{r_0^2\nu} + \frac{iM_S e^{-2ir_0\nu}}{2r_0^2\nu} + \mathcal{O}\left(\frac{M_S\Delta}{r_0^2}, \frac{M_S}{r_0^3\nu^2}\right)\right)\exp(i\nu u)\right)\,{}_2Z_{2,2}\,, \tag{6.36}$$

where $H_{M0}$ was given in Eq. (6.30). Each of the terms containing $M_S$ in Eq. (6.36) represents a correction to the wave strain in the absence of the shell, and these correction terms are discussed in Sec. 6.3 below.
The formula Eq. (6.36) was derived using quite complicated computer algebra scripts, and it is important to investigate its reliability through consistency checks:

- In each of the three regions, we confirmed using computer algebra that all 10 Einstein equations are satisfied. The four constraint equations were not used in the construction

of the solution, although they were used to fix two (in each region) constants. Note that it was found that if an error were introduced into one of the hypersurface equations, then the formulas obtained for $C_1, C_5$ were not constant but were functions of $r$. Thus, the fact that the solutions satisfy the constraints amounts to a strong consistency test.

- The solution was constructed to ensure continuity of $\beta, W, J, U$ at $r = r_0$ and $r = r_0 + \Delta$, but continuity of $\partial_r J$, $\partial_r U$ is also needed. We confirmed using computer algebra that these conditions are satisfied, which again amounts to a strong consistency test.
- As will be discussed in the next section, the formula Eq. (6.36) satisfies physical expectations, with one of the terms in the formula being derivable in an independent way.

## 6.3 Physical interpretation

We investigate the physical meaning of each of the correction terms in Eq. (6.36), in the light of the expectation that the dust shell cannot add or remove energy from the GWs:

- Correction 1, $2M_S/r_0$. In natural Minkowski coordinates $u'$ and in the absence of a matter shell, $H' = -2\nu'^2\sqrt{6}C_{40}$. From Eq. (6.10), it follows that $\nu' = \nu(1 - 2B_0))$, and thus from Eq. (6.9), $\nu' = \nu(1 + M_S/r_0))$. Thus $H' \approx -2\nu^2\sqrt{6}C_{40}(1 + 2M_S/r_0)$. This term is, therefore, a consequence of the coordinate transformation Eq. (6.9), i.e. it represents the gravitational red-shift effect of the shell.
- Correction 2, $2iM_S/(r_0^2\nu)$. The term is out of phase with the leading terms $1 + 2M_S/r_0$. Thus, to $\mathcal{O}(M_S)$, the magnitude of $\mathcal{H}$, and therefore of the energy of the GW, is not affected; but the shell does change the phase of the GW.
- Correction 3, $iM_S e^{-2ir_0\nu}/(r_0^2\nu)$. This term does affect the magnitude of $\mathcal{H}$. We have checked using computer algebra (see Appendix C) that if $\mathcal{H}$ is calculated with $C_{inI}$ set to zero the term disappears, and so it is interpreted as being an effect due to the shell generating an incoming GW. Such an incoming GW modifies the geometry near the source and affects the radiation reaction (or self-force) and thus the inspiral rate. The calculation of the self-force is a $2^{\text{nd}}$ order effect which is beyond the scope of this work. The energy change in the GW at infinity can therefore be interpreted as being caused by the modification of the self-force, rather than by energy being transferred to or from the dust cloud.

In order for Correction 1 to be a measurable, $M_S/r_0$ would need to have a significant value (but note that the results obtained here also assume that $(M_S/r_0)^2$ is negligible). For Corrections 2 and 3 to be measurable, we would also need that $r_0\nu$ should not be large, where $r_0\nu = 2\pi r_0/\lambda$ with $r_0/\lambda$ being the number of wavelengths in $r_0$; thus the shell would need to be very close to the GW source.

We now consider the case of a thick shell comprising a dust cloud of constant density ($\rho_0$) extending from near the origin to an observer at $r = r_F$, so that $\delta M_S = 4\pi r_0^2\rho_0\delta r_0$; integration gives

$$\mathcal{H} = \Re\left(H_{M0}\left(1 + 4\pi\rho_0 r_F^2 + 4i\rho_0 r_F\lambda + \mathcal{O}\left(\frac{\rho_0\log(r_F)}{\nu^2}\right)\right)\exp(i\nu u)\right)\,{}_2Z_{2,2}\,, \tag{6.37}$$

and the integral of Correction 3 is omitted since it is smaller than the order term.

## 6.4 Discussion on the results of the investigation into the effect of a thin shell of matter on a GW

Using the BS formalism, this work has investigated within linearised perturbation theory, the effect of a spherical dust shell on GWs sourced from the center of the shell. It was found that the GWs were modified, although without any energy transfer between the GWs and the shell. This finding is novel. In the context of cosmology, the effects are too small to be measurable; but the effect would be measurable if a GW event were to occur with a source surrounded by a massive shell and with the radius of the shell and the wavelength of the GWs of the same order. The computation closely follows that used in numerical calculations using the BS formalism.

There are three avenues for further work. Firstly, the matter equation of state needs to be generalized beyond dust to include shear viscosity, and perhaps other forms of dissipation. Secondly, the background spacetime without the matter shell can be changed from Minkowski to something more appropriate to cosmology. Solutions are known for de Sitter spacetime [200]; and for Einstein-de Sitter [204], although in this case the algebraic complexity of the solution may make the construction of perturbative solutions problematic. Finally, we found that a shell of matter, in effect, reflects part of an outgoing GW, and so in the context of a burst (rather than a continuous) source it is possible that an echo would be the result. Now, it should be possible to model a burst source as a Fourier sum of the eigensolutions obtained here, i.e. as something of the form $\sum_n a_n f(\nu_n)$, and in this way to investigate GW echoes, which we pursue next, in Chapter 7.

# Chapter 7

# Modifications to the signal from a gravitational wave event due to a surrounding shell of matter

In the previous chapter, Chapter 6, we developed a model for the effect of a thin matter shell around a GW source. We obtained an analytic expression for the modifications to the GWs which is a novel result. In this chapter, we apply this model to various astrophysical GW sources. The modifications found in Chapter 6 and as published in [47], included an echo. The idea of a GW echo has received much attention as being a signature of an exotic compact object (ECO), and it has also been investigated in terms of the astrophysical environment. We review these matters in Sec. 7.1.

The solution found in Chapter 6 and in our published work in Ref. [47] is for a monochromatic GW source. We discuss these findings as relevant to our investigation on echoes due to matter from various astrophysical sources. A general waveform may be decomposed into a sum of Fourier components, and the technical details are given in Sec. 7.4 on page 102. The decomposition is implemented within a Matlab script using the Fast Fourier Transform (FFT), and validation results are reported in Sec. 7.4 on page 102. In Sec. 7.5 on page 105, we investigate whether a matter shell could explain the echoes that may exist in the LIGO data of GW150914 and GW170817, using our model developed in Sec. 7.2. We discuss the possibility of finding echoes in BNS configurations with a surrounding matter shell, in general, in Sec. 7.5.2 on page 107. We extend this discussion to include the possibility of finding echoes in CCSNe with a surrounding matter shell in Sec. 7.5.3 on page 110. In discussing the consequences of results in Chapter 6 to various astrophysical scenario, we extend our considerations to implications for cosmology. The investigations make extensive use of numerical code which is available in the Appendix D on page 178. The results and conclusion are discussed in Sec. 7.6 on page 114.

## 7.1 Gravitational wave echoes

As detections of mergers of compact bodies trickle in, our understanding of compact bodies, their physics and that of the surrounding astrophysical environment, will continue to grow and at times even challenge previously long held notions. The GW event, GW190814 [208, 209], involving a BH, of mass 23 $M_\odot$ and a smaller compact body, of mass 2.6 $M_\odot$ challenged previously expected mass limits for BHs and NSs . The 2.6 $M_\odot$ body falls outside the expected lower bound for a BH and above the expected upper bound for a NS. The heaviest known NS has mass $\lesssim 2.5M_\odot$ whilst the lightest known BH has mass $\simeq 5M_\odot$. The object would then either be an extremely heavy NS, beyond the expected upper bound mass of NSs, or it could be a BH that is too light (lighter than the lower bound expected by theory). Before the merger of the two objects in the GW event, GW190814, their masses differed by an unexpected factor of 9. This makes it the most extreme mass ratio known for a GW event.

For the GW event, GW190521, reported by aLIGO and aVIRGO, the short GW signal detected has been postulated to be the consequence of the merger of a quasi-circular BBH. The resulting remnant is that of a BH of mass $M_f \sim 142\ M_\odot$, the first ever observed IMBH, at a luminosity distance $d_L \sim 5.3$ Gpc [28]. For this postulated BBH merger, at least one of the companions would have to exist in the pair-instability supernova (PISN) gap. This factor together with the faint pre-merger (*inspiral*) emission, uncharacteristic of BBH mergers, places questions on the pre-merger dynamics and on whether one or both of the colliding bodies are actually BHs. The authors of [29] have provided an alternative interpretation of GW190521 as that of the head-on collision (HOC) of two equal mass and spin horizonless vector boson stars, also known as *Proca stars* (PSs). These stars are theorised to be constituted by the hypothetical ultra-light bosonic particles and if the GW event is confirmed to be that of PSs, would be the first evidence of DM.

As we fully immerse into this era of GW detection, we will need to prepare for other expected (and unexpected) challenges. These will be at both the macroscopic and quantum level. At the quantum level, Hawking's information paradox suggests Planck-scale modifications of BH horizons such as *firewalls* [32]) and other modifications to BH structure such as *fuzzballs* [33]). Dark matter particles have been suggested surrounding star-like objects [34]. Other postulations include stars with interiors consisting of self-repulsive, de Sitter spacetime, surrounded by a shell of ordinary matter: *gravastars* [35]). Then there are *Boson stars*, which are macroscopic objects made up of scalar fields [36, 29]. All these objects may be classified as *Exotic Compact Objects* (ECOs), compact bodies mimicking BHs, but without a horizon. One consequence of these horizonless structures is that ingoing GWs produced in a merger may reflect multiple times off effective radial potential barriers. The GWs may be, in effect, trapped between effective radial potential barriers causing the waves to be "*bounced*" of these barriers several times with wave packets leaking out to infinity at regular times. These GW signals, "trailing" the main (outward bound) signal are referred to as **echoes**. [37, 38, 39]. In [39], the authors expand on the arguments for the existence of these horizonless ECOs. The ECOs which are more massive than NSs but without horizons, will have an effective surface at

$$r_0 = r_g(1+\epsilon)\,, \tag{7.1}$$

with $\epsilon \ll 1$, and $r_g$, describing the event horizon of a vacuum BH described with Schwarzschild geometry, at a location $r_g = 2GM/c^2$, where $G$ is Newton's constant, $c$ the speed of light and $M$ the BH mass or $r_g = 2M$ in geometrised units.

Light emitted from the surface of ECOs is strongly lensed back towards it. A truly relativistic feature of ECOs is that high frequency EM or GWs can orbit them in a circular motion, possible at a specific location, $r = \frac{3}{2}r_g$, which defines a surface called the *photosphere*.

A critical value for $\epsilon$ was identified by [39], where for objects satisfying

$$\epsilon \lesssim 0.0165 \tag{7.2}$$

the waves trapped at the photosphere relax away by the time that the waves from the surface hit it back. In this instance the echoes are cleary discernible. In the case where light or GWs travel from the photosphere to the object's surface and back, before dissipation of the photosphere modes occurs, then interaction with the modes will occur and there will interference in the echo signal.

The properties of the photosphere may be used to distinguish between different classes of exoctic compact objects, with those featuring photospheres referred to as *ultracompact objects* (UCOs). Furthermore, those whose reflected waves return to the photosphere after the photosphere modes have dissipated (i.e satisfying satisfy the condition (7.2)) can be said to have a "clean" photosphere. These objects are referred to as Clean Photosphere Objects *ClePhOs*. All these exotic compact objects will mimic the signal of a black hole for early times before an inbound pulse interacts with the object or the photosphere. For returning pulses to the photosphere, the signal is again partially transmitted and partially reflected and so a train of echoes will occur with diminishing amplitudes [37, 38]. It is important to mention that the main burst which is generated at the photosphere (typically), has a high frequency (of the same order as the BH modes) and a significant proportion of the main burst is carried across the potential barrier as illustrated in Fig. 7.1 on page 93.

For an exotic compact object with mass $M$, with microscopic correction at the horizon scale of size $\ell$, the delay between echoes may be approximated by $\Delta t \simeq nM \log(M/\ell)$ [38]
with $n$ a factor of order unity. This factor is determined by the nature of the exotic object :
$n = 8$ for a wormhole; $n = 6$ for a gravastar, and $n = 4$ for an empty shell of matter [38].

Generally, it is found that the time delay between echoes is much longer than the duration of the "ringdown" of a remnant. This was calculated for the first detection [210] to give delay between echoes as $\Delta t \simeq 117$ ms as compared with approximately 3ms for the ringdown. This makes the search for echoes, immediately following the main inspiral, merger and ringdown, practical.

Ref. [37] found that the ECO compactness determines the time delay with the reflective properties of the ECO influencing the decay and shape of each pulse. For less compact ECOs, with ringdowns sometimes consistent with the resonant frequencies of the ECO [38, 211], there would be no pattern for the echoes. Price and Khanna [211] argued echoes may be thought of as a superposition of the resonant modes of the ECO. Volkel and Kokkaotas provided a method to

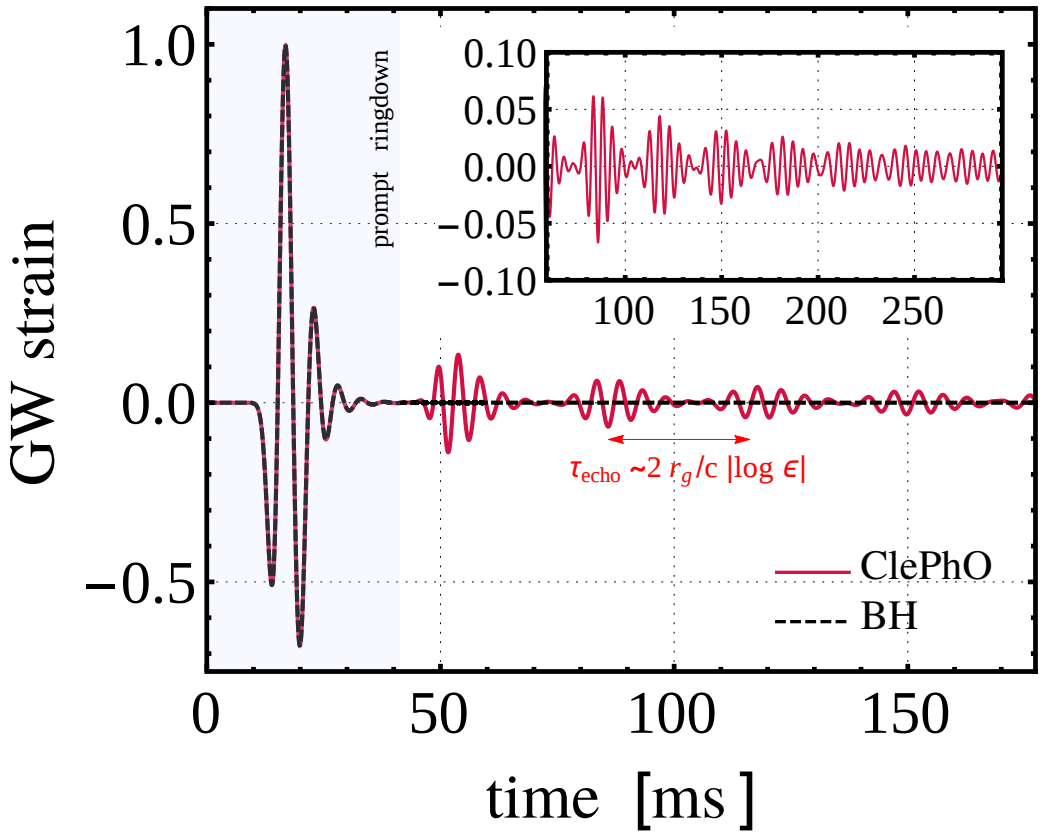


Figure 7.1: *Ringdown waveforms from black holes (black line) and ClePhOs (red line)* for objects of $60M_\odot$. For ClePhOs, there is a reflective surface at $r_0 = r_g(1+\epsilon)$, $\epsilon = 10^{-11}$. The amplitude of the GW signal (proportional to the relative strain of the interferometer's arm induced by the GW) is normalized to its peak value. The initial data describes a quadrupolar Gaussian wavepacket of axial GWs. The inset shows a zoom-in version of the waveform at late times, with each subsequent echo having a smaller frequency content. [39]

extract details of the ECO model from the ECO modes, by showing that the ECO spectrum could be used to determine the effective scattering potential the gravitational waves would experience [212].

Template-based searches proposed by [40, 42, 213], wrote the echo waveforms in terms of $\Delta t$, together with a characteristic frequency, a damping factor, and a widening factor between successive echoes. These were confined to the cases involving ECOs. Though expressions exist for echo waveforms from selected exotic objects under various assumptions [38, 39], concrete calculations have so far only been exploratory [214]. Possibilities exist that there may well be other types of objects not yet envisaged that also cause echoes. In [215], a *generic* search for echoes was conducted to enable the capture and characterisation of a wider variety waveform morphologies to allow for other classes of objects that may exhibit echoes also. Simulated signals to evaluate their method are presented in Figures 7.2 on page 94 and 7.3 on page 95.

There have been tentative claims from [40] that LIGO has observed echoes in the binary

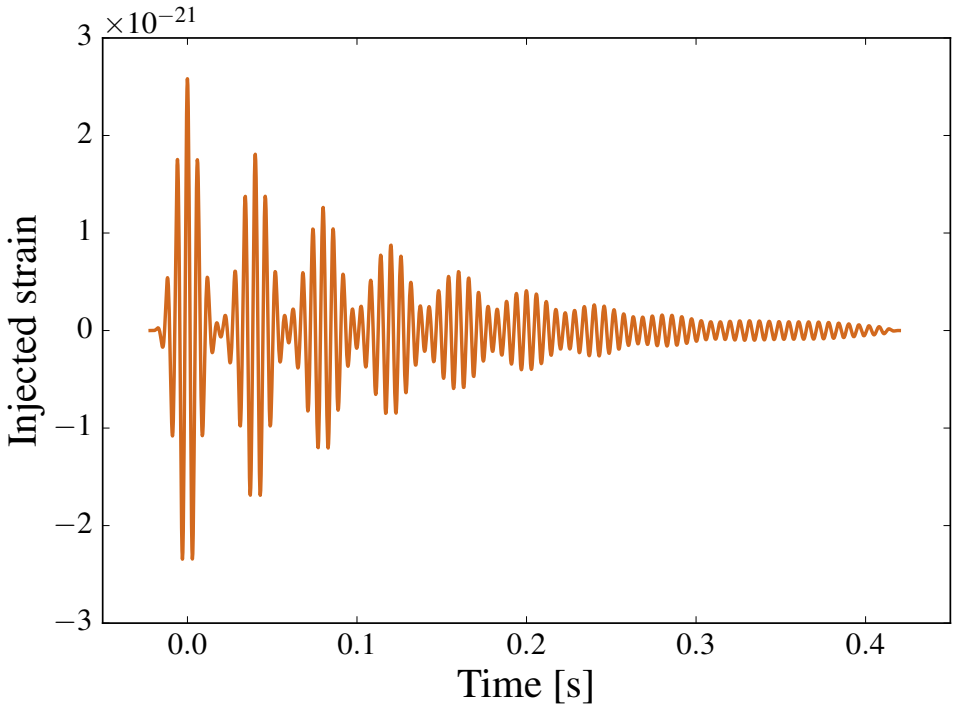


Figure 7.2: The simulated signals used to evaluate the method: A train of sine-Gaussians. [215]

black hole waveforms. These claims have been contested [41, 42], sparking a debate and responses in defence of the claims [43, 44] with further substantiations [45, 46]. In [40], the first of the tentative search for echoes, the authors find evidence for the existence of echoes in the first detection event [210] to within 99% (at false alarm rate probability of 1% or significance of $2.5\sigma$), consistent with Planckian deviations from GR. They further suggest comparable evidence for echoes by including the events GW151012 [24] (then referred to as LVT151012) and GW151226 [188]. These controversial results would challenge GR suggesting that the black hole horizon would allow post-merger repeating gravitational wave echoes and hence would not be entirely absorbing, as illustrated in Figure 7.4 on page 96. Extending their investigations to the first BNS detection GW170817 [216], the authors of [40] find evidence again of the existence of echoes in the post-merger event [45], this time with higher significance ($4.2\sigma$ significance or false alarm rate for this GW echo signal given by p-value$=1.6 \times 10^{-5}$). The echoes occur at $f_{echo} \simeq 72$ Hz, approximately 1.0 sec after the BNS merger event. Independently, Gill et al. [217], taking into account astrophysical considerations inferred from EM signals, reported a similar timeframe for the BNS collapse to a BH after merger. Figure 7.5 on page 97 illustrates the BNS merger via neutron star collapse to a black hole, producing echoes as postulated by [45]. Subsequent to the first search for gravitation echoes as conducted by [40], several other investigations followed [218, 42, 45, 219, 220, 221]. A time domain and waveform dependent strategy, similar to that used in [40], was employed in [42, 220].

A model-agnostic search using the frequency, as employed in [45] for the BNS case, was also used in [218, 221]. Morphology-independent methods were also employed by [215, 222, 219]

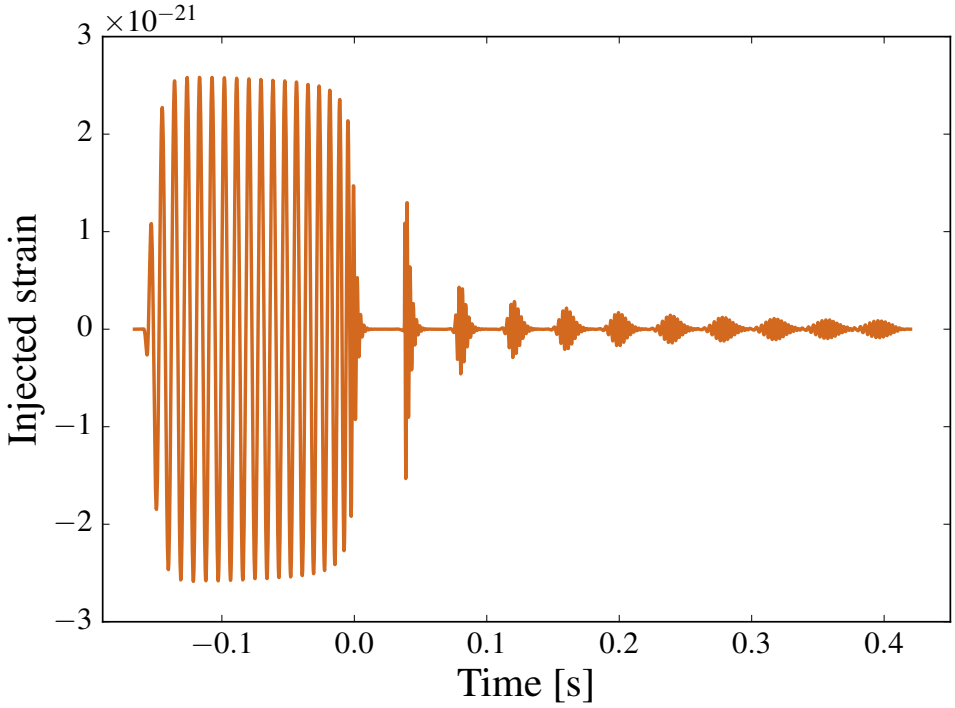


Figure 7.3: The simulated signals used to evaluate the method: the waveform from a toy model for a mass ratio $q = 1000$ inspiral of a particle in a Schwarzschild spacetime, with Neumann reflective boundary conditions just outside the horizon. [215]

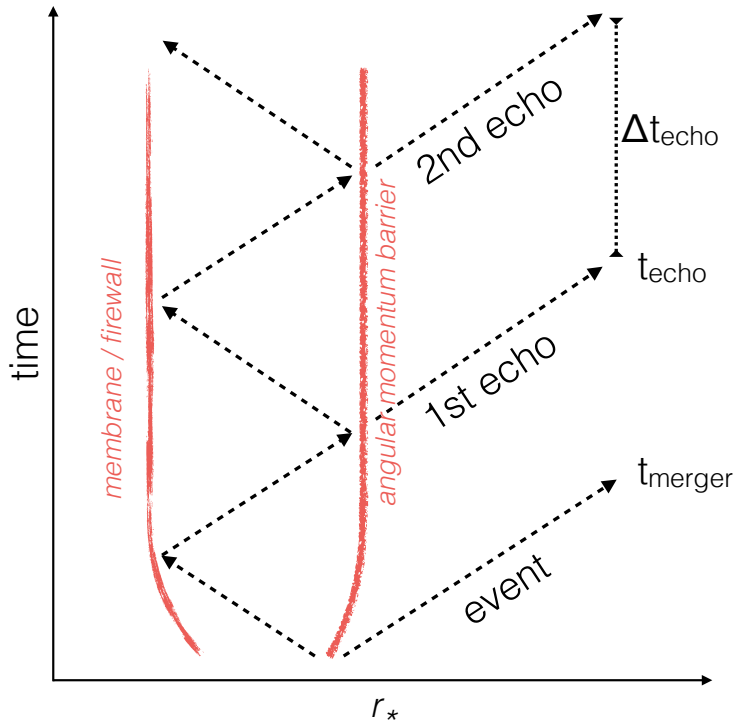


Figure 7.4: Gravitational wave echoes following a BBH merger from a cavity of membrane/firewall-angular momentum barrier [40].

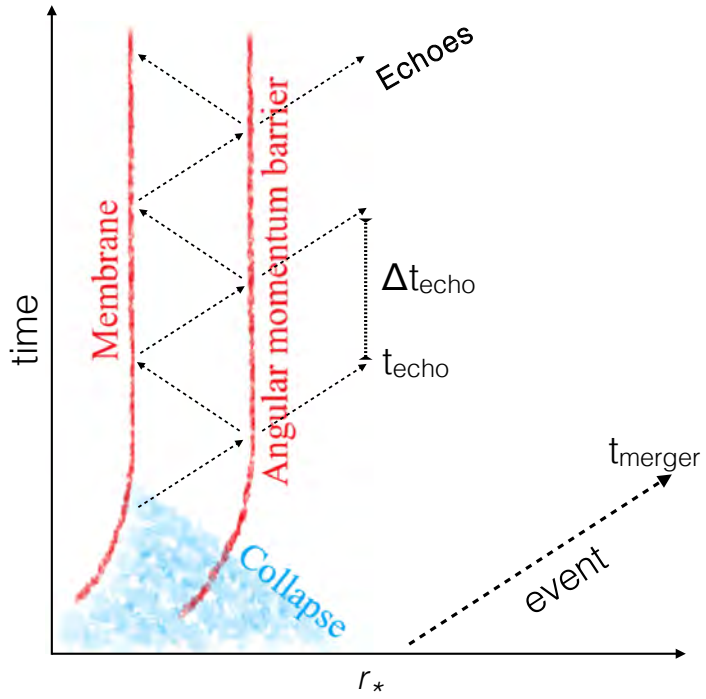


Figure 7.5: Gravitational wave echoes following a collapse of binary neutron star merger event from a cavity of membrane-angular momentum barrier [45].

Other progress was also made in modelling the echo waveform [223, 214, 213, 224, 225, 226, 227]

The evolution of test scalar fields, in lieu of gravitational perturbations, were studied by [214], allowing the use of reflecting boundary conditions in a BH spacetime. This meant that the ECO waveform could be considered as a superposition of echo pulses or as a superposition of ECO modes.

Taking the ECO as static and spherically symmetric, with an exterior Schwarzschild spacetime, (patched to a spherically symmetric interior metric at an areal radius $r = r_0$), they define the scalar, $\psi(x^\mu) = r\Phi$, in a massless scalar field $\Phi(x^\mu)$, subject to sourced, curved spacetime wave equation:

$$\Box\Phi = -\rho\,. \tag{7.3}$$

For the first echo, $\tilde{\psi}$ is a linear combination of ingoing and outgoing waves $e^{\pm i\omega x}$. Hence, close to the ECO surface $x_0 = x(r_0)$, they obtain

$$\tilde{\psi} \propto e^{-i\omega(x-x_0)} + \tilde{\mathcal{R}}(\omega)e^{i\omega(x-x_0)}, \tag{7.4}$$

where $\tilde{\mathcal{R}}(\omega)$ represents the reflectivity, which is dependent on frequency.

Wave emission, propagation and reflectivity is then considered in the ECO spacetime as il-

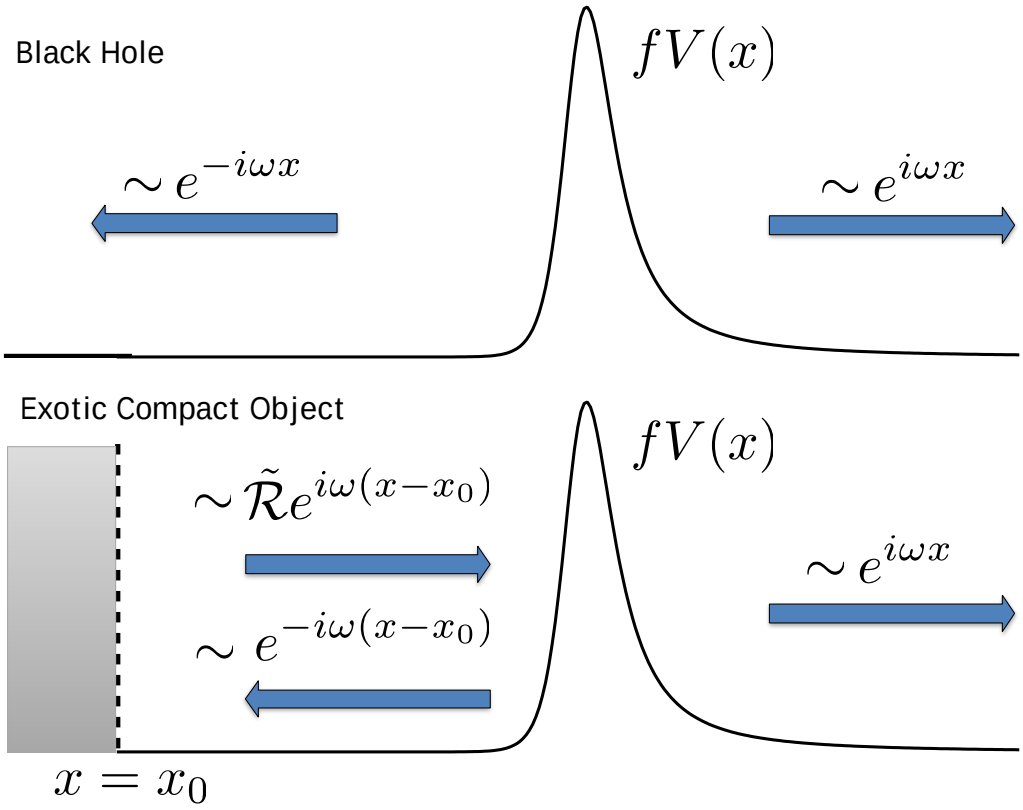


Figure 7.6: Top: The boundary conditions for waves propagating on a black hole spacetime. Bottom: The reflecting boundary conditions for the waves in the exterior of an ECO [214] .

lustrated in Fig. 7.6. Most of the early investigations into the origins of echoes did not directly relate the physical properties and parameters of the remnant to the waveforms. A first effort to construct such a template directly related to the physical properties of the ECO, was conducted by [228]. For $r > r_0$, a Schwarzschild metric is used for the background geometry:

$$ds^2 = -Adt^2 + A^{-1}dr^2 + r^2 d\Omega^2 \,, \tag{7.5}$$

with $A(r) = 1 - 2M/r$, and $M$ (total mass), $r_0$ (radius) in Schwarzschild coordinates. The reflecting membrane at $r = r_0$, is parametrised by a complex, frequency-dependent reflectivity coefficient $\mathcal{R}$ [214, 229]. Similar to [214] the stationary ECO is illustrated in Fig. 7.7 and the examples of the templates are illustrated in Fig. 7.8 on page 100. Much further discussion around GW echoes has been within the context of 'new physics' [223, 228, 225, 230, 213, 231, 232].

Echoes from a massive, thick shell were considered in [233]. This was a generalisation of the approach of [234] which was based on an infinitely thin shell. As we have shown in our Chapter 6 the case for a thin shell can be generalised to that of a thick shell by considering several concentric thin shells and integrating. [233] showed that the deviation from Schwarzschild ringdown in their astrophysical estimations were relatively small except for a large mass which indicated that, for the majority of astrophysical scenarios, the effect would be relatively small. However they did note that considerations of dark matter around black holes (or compact body mergers)

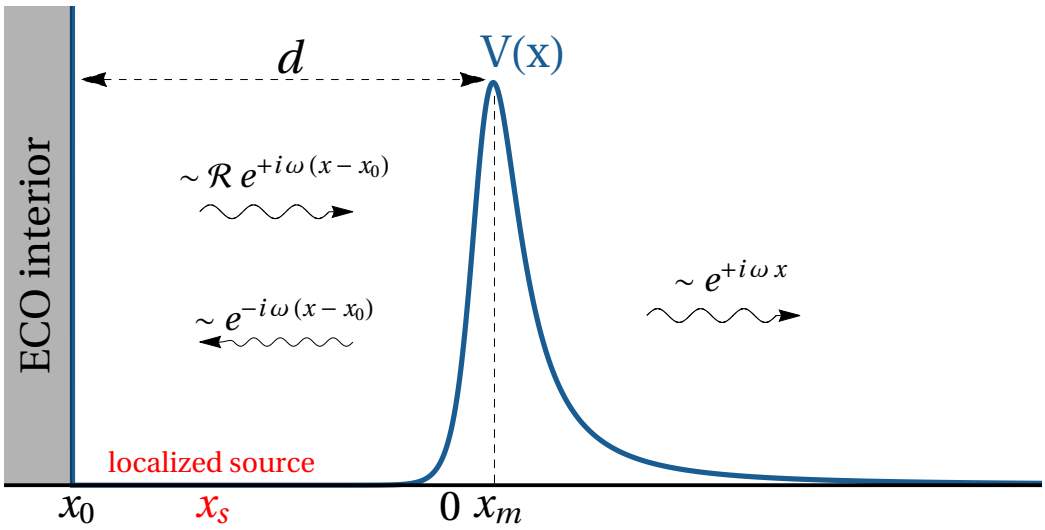


Figure 7.7: [228] description of ECO model (adapted from Ref. [214]).

| | |
|---|---|
| $M$ | total mass of the object |
| $\mathcal{A}$ | amplitude of the BH ringdown |
| $\phi$ | phase of the BH ringdown |
| $t_0$ | starting time of the BH ringdown |
| $d$ | width of the cavity ($z \sim e^{d/(4M)}$) |
| $\mathcal{R}(\omega)$ | reflection coefficient at the surface |

Table 7.1: Parameters of the ringdown+echo template presented in [228]. The first four parameters characterize the ordinary BH ringdown. The parameter $z$ is the gravitational redshift at the ECO surface.

would leave some parametric freedom for echoes as well. [31], studied both the combination of contributions of modifications of the Schwarzschild geometry near the surface, and a nonthin shell of matter surrounding the compact body/merger. They found that a massive shell at a distance could be distinguished from the purely Schwarzschild evolution of perturbations. However, for the situation of new physics near the surface of a compact object, (a wormhole in their case), the strong echoes of the surface dominate the echoes of the distant shell. Furthermore, they found that it would take an extraordinarily large mass, located sufficiently close to the wormhole, to lead to discernible changes in the main echoes of the surface and that these changes would be relatively small. The noted that even in this last case the shell would have to be extremely large comparable to the compact objects and if they were so then they would themselves have an effecton the inspiral phase it itself. They concluded that such large masses were unlikely to exist in such a scenario.

## 7.2 Effect of a shell of matter on a GW

In Chapter 6 we considered the scenario of a thin shell of matter surrounding a GW source such as a compact binary merger, as shown schematically in Fig. 6.1 on page 79. The spacetime around the GW source in Sec. 6.1 on page 78 would be otherwise empty except for the

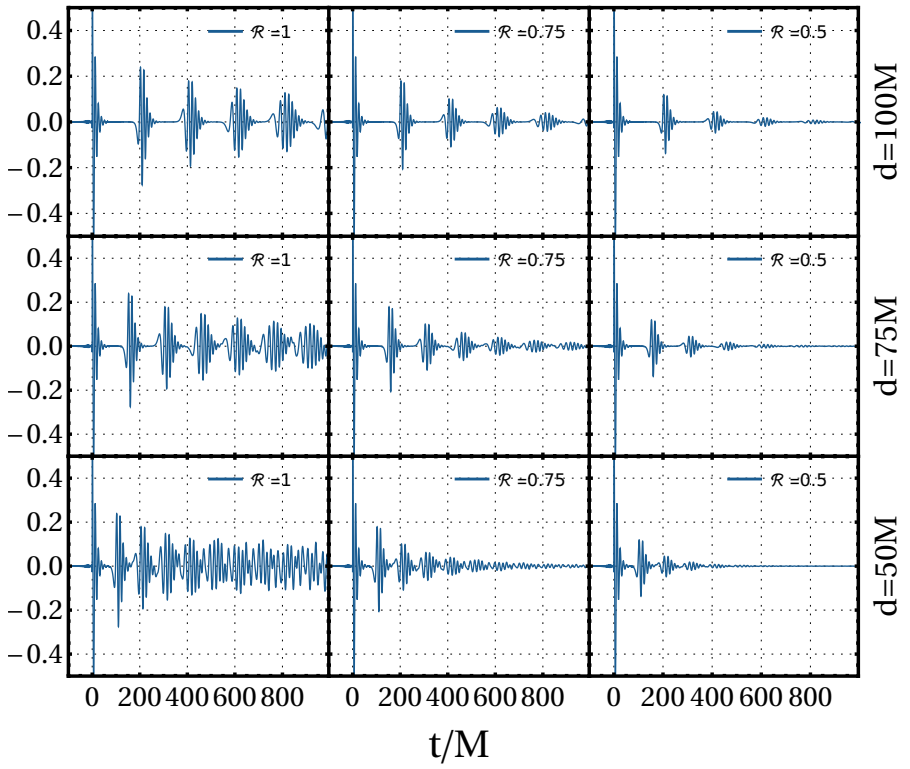


Figure 7.8: Examples of the ringdown+echo template in the time domain for different values of $d$ and $\mathcal{R}(\omega) = \text{const}$ and for scalar perturbations. From top to bottom: $d = 100M$, $d = 75M$, $d = 50M$; from left to right: $\mathcal{R} = 1$, $\mathcal{R} = 0.75$, $\mathcal{R} = 0.5$. The waveform is normalized to its peak value during the ringdown [228].

surrounding shell of matter. Confining the investigation to a thin shell does not preclude the case of a thick shell. Results can easily be applied to a series of concentric thin shells and then integrated to give the effect for a thick matter shell. The EOS is taken to be that of dust. The results in Sec. 6.1 on page 78 shows that the shell modifies the outgoing GWs in both phase and magnitude without contradicting previous results about energy transfer. The problem was set up within the BS formalism for the Einstein equations as given in Eq. 6.1 on page 78 with coordinates based on outgoing null hypersurfaces

The background solution, which may be regarded as Minkowski plus small spherically symmetric corrections of $\mathcal{O}(\rho)$, was obtained and a perturbation of the solution taken as demonstrated in Sec. 6.2 on page 80. Solutions were found: inside the shell, i.e. $r < r_0$ in Sec. 6.2.1 on page 85; within the shell, i.e. $r_0 < r < r_0 + \Delta$, in Sec. 6.2.2 on page 85 and exterior to the shell, i.e. $r_0 + \Delta < r$ in Sec. 6.2.3 on page 86. The final result of the GW strain in terms of the mass of the shell $M_S$ and as measured by an observer at future null infinity, is given in Eq. 6.36

on page 87, which we rewrite here as

$$\mathcal{H} = \Re\left(H_{M0}\left(1 + \frac{2M_S}{r_0} + \frac{iM_S}{\pi r_0^2 f} + \frac{iM_S e^{-4i\pi r_0 f}}{4\pi r_0^2 f} + \mathcal{O}\left(\frac{M_S\Delta}{r_0^2}, \frac{M_S}{r_0^3 f^2}\right)\right)\exp(2i\pi f u)\right)\,{}_2Z_{2,2}\,. \tag{7.6}$$

with the angular velocity $\nu$ replaced by the frequency $f$ with $\nu = 2\pi f$ Each of the terms containing $M_S$ in Eq. (7.6) above, represents a correction to the wave strain in the absence of the shell. Of particular interest to us, in the investigation of whether matter shells could cause echoes in astrophysical scenario, is the second correction term, containing $iM_S/(\pi r_0^2 f)$, and the third term correction, containing $\frac{iM_S e^{-4i\pi r_0 f}}{4\pi r_0^2 f}$. The presence of $e^{-4\pi i r_0 f}$ in the third term represents a time delay , i.e. and echo, and describes a change in the magnitude of $\mathcal{H}$, as verified in Chapter 6 and [47]. In this context, the modified signal would then be interpreted as an echo of the main signal. The second correction term is out of phase with the leading terms $1 + 2M_S/r_0$ and hence represents a phase shift of the GW. This term, to $\mathcal{O}(M_S)$, does not change the magnitude of $\mathcal{H}$ and hence has no effect on the energy of the GW. Hence, the echo varies from the main signal in both magnitude and phase, with the magnitude of the echo described by

$$R = \frac{M_S}{4\pi r_0^2 f}, \tag{7.7}$$

relative to the original signal.
Our attention will then turn to whether this echo will be discernible in GW signals received from various astrophysical scenario in Sections 7.4, 7.5 and 7.5.3.

## 7.3 Implications for cosmology

Calculations of GWs, both analytical and numerical, normally assume that they propagate from source to a detector on Earth in a vacuum spacetime. Although the average cosmological density of baryonic plus dark matter is small, of order $10^{-29}$g/cm$^3$, a detected GW event may be a considerable distance away from its source, up to order 1 Gpc, and the quantity of intervening matter is not negligible. As we move into an era of precision GW measurements, it is important to quantify any effects due to propagation of GWs through a non-vacuum spacetime. These issues have been investigated previously. There is a simple physical argument that an ideal fluid should not extract energy from a GW, because there is no physical mechanism for it to do so; and this idea has been given a precise expression in the work of Esposito [194], and of Ehlers *et al.* [195, 196]. However, if the matter is dissipative, e.g. through shear viscosity, then one would expect GWs to be attenuated. Hawking [235] investigated GWs in cosmological models and determined conditions for complete absorption; subsequently, the general theory of GW propagation through a viscous fluid was further developed [236, 237, 238, 239]. More recently, Goswami *et al.* [240] have investigated whether the properties of dark matter can be constrained by the attenuation effect and GW observations. Baym *et al.* [241] have extended the hydrodynamics model of the cosmological fluid to a kinetic model with low collision rates and calculated the attenuation effect.

We now consider the case of a thick shell comprising a dust cloud of constant density ($\rho_0$) extending from near the origin to an observer at $r = r_F$, so that $\delta M_S = 4\pi r_0^2 \rho_0 \delta r_0$; integration

gives

$$\mathcal{H} = \Re\left(H_{M0}\left(1 + 4\pi\rho_0 r_F^2 + 4i\rho_0 r_F\lambda + \mathcal{O}\left(\frac{\rho_0\log(r_F)}{\nu^2}\right)\right)\exp(i\nu u)\right)\,{}_2Z_{2,2}\,, \tag{7.8}$$

and the integral of Correction 3 is omitted since it is smaller than the order term. Applying Eq. (7.8) to cosmology, and taking the cosmological density as $10^{-29}\text{g/cm}^3 \approx 0.7\times10^{-8}\text{Mpc}^{-2}$ in geometric units, it is found that, apart from the gravitational redshift, no measurable effect is expected since the GW wavelength $\lambda$ is at most $\mathcal{O}(10^4)\text{km} \ll 1\text{Mpc}$.

## 7.4 Solution for a burst-like GW source using Fourier transforms

The time-delay of the echo is $2r_0$, but the echo's magnitude depends on the wave frequency $f$. The GW sources reported to date are not monochromatic but are burst-like. Such a source may be decomposed into its Fourier components and Eq. (7.6) on page 101 applied to each component, and the echo signal obtained by summing over the transformed components. Because the magnitude of the transformation is frequency-dependent, the echo signal will have a form more complicated than simply a time-delay and magnitude change to the original signal. This effect is now analysed.

We replace $\Re(H_{M0}\exp(2i\pi fu))$ in Eq. (6.30) on page 85 by $h(u)$ defined in the interval $u_0 \le u \le u_{N-1}$; and then construct a discrete representation of $h(u)$, $h_k = h(u_k)$ ($k = 0,\cdots,N-1$), with the $u_k$ on a regular grid, i.e. $u_{k+1} - u_k = \delta$ for $k = 0,\cdots,N-2$. Note that if the highest frequency that needs to be resolved is $f_m$, then $N$ should be chosen so that $(u_{N-1}-u_0)/(N-1) < 1/(2f_m)$, i.e. to satisfy the Nyquist condition. The discrete Fourier transform [242] of $\{h_k\}$ is

$$H_n = \sum_{k=0}^{N-1} h_k \exp\left(\frac{2\pi ikn}{N}\right) \quad\text{with inverse}\quad h_k = \frac{1}{N}\sum_{n=0}^{N-1} H_n \exp\left(\frac{-2\pi ikn}{N}\right). \tag{7.9}$$

Then defining $H_{2,n}$ and $H_{3,n}$ to be coefficients in the transform domain of the second (phase-shift) and third (echo) terms of Eq. (7.6) on page 101, we have

$$\begin{aligned}
&H_{2,n} = \frac{iM_S H_n}{\pi r_0^2 f_n}\,,\quad H_{3,n} = \frac{iM_S H_n\exp(-4\pi i r_0 f_n)}{4\pi r_0^2 f_n}\,,\quad n = 1,\cdots,\frac{N}{2}\,,\\
&H_{2,n} = H^*_{2,N-n}\,,\quad H_{3,n} = H^*_{3,N-n}\,,\quad n = \frac{N}{2}+1,\cdots,N-1\,,\\
&H_{2,0} = H_{3,0} = 0\,,
\end{aligned} \tag{7.10}$$

where $^*$ denotes the complex conjugate, and where we have used the condition that, in the time domain, all quantities are real. It is being assumed that $N$ is even, and normally $N = 2^m$ (with $m$ an integer) for convenience when using the fast Fourier transform; further

$$f_n = \frac{n(N-1)}{N(u_{N-1}-u_0)}\,. \tag{7.11}$$

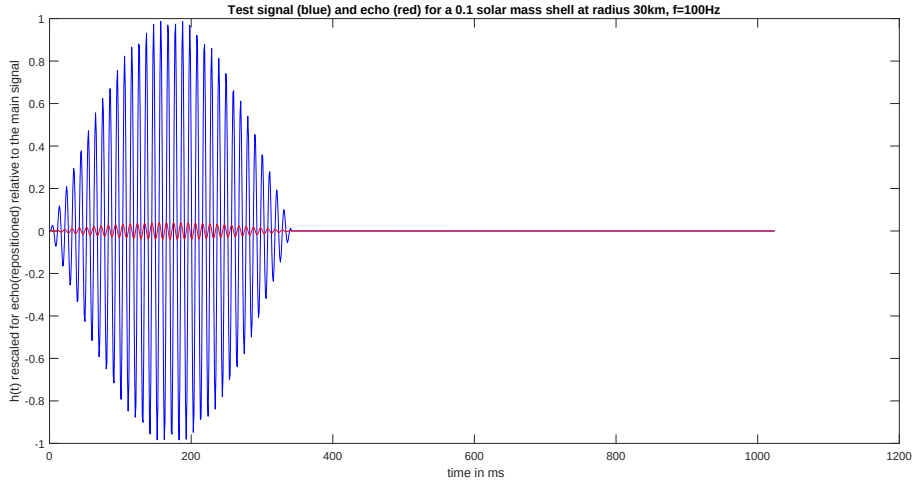


Figure 7.9: The effect of a matter shell of radius 0.1ms (about 30km) and mass 0.0005ms (about $0.1M_\odot$) on the burst signal of frequency 100Hz. The original signal is in blue the echo term in red.

Then $h_{2,k}, h_{3,k}$ are found on applying the inverse discrete Fourier transformation.
A Matlab script that implements the calculation of the previous paragraph (see Eq. (7.13) on page 103) is available in Appendix D on page 178 as a plain text file.
The script was checked by applying it to a monochromatic signal $h(u) = \Re(-i\exp(2\pi i f u))$. The errors $e_{2,k}$ in $h_{2,k}$ and $e_{3,k}$ in $h_{3,k}$ are

$$\begin{aligned} e_{2,k} &= \left| h_{2,k} - \Re\left( iM_S/(\pi r_0^2 f)\exp(2i\pi f u)\right)\right|, \\ e_{3,k} &= \left| h_{3,k} - \Re\left( iM_S/(4\pi r_0^2 f) e^{-4\pi i r_0 f}\exp(2i\pi f u)\right)\right| . \end{aligned} \tag{7.12}$$

For the case $u_0 = 0$ms, $u_{N-1} = 100$ms, $f = 1$kHz, $r_0 = 1.25$ms (≈km), and $M_S = 0.25$ms ($\approx M_\odot$), we found:

| $N$ | $\|\|e_{2,k}\|\|$ | $\|\|e_{3,k}\|\|$ |
|---|---|---|
| $2^9$ | $4.0 \times 10^{-4}$ | $1.6 \times 10^{-3}$ |
| $2^{15}$ | $1.6 \times 10^{-6}$ | $2.7 \times 10^{-5}$ |
| $2^{21}$ | $2.4 \times 10^{-8}$ | $4.3 \times 10^{-7}$ |

(7.13)

where $||e_k||$ is defined to be

$$||e_k|| = \sqrt{\frac{\sum_{k=0}^{N-1} e_k^2}{N}} . \tag{7.14}$$

Thus the errors are tending to zero, and $N$ can be chosen so as to attain a desired accuracy. Note that an error of order machine precision is achieved for special values of the frequency $f = k(N-1)/N/(u_{N-1} - u_0)$ with $k$ an integer; in this case we would have that the cyclic assumption of the discrete Fourier transform would be satisfied, i.e. $u_i = u_{i+N}$.

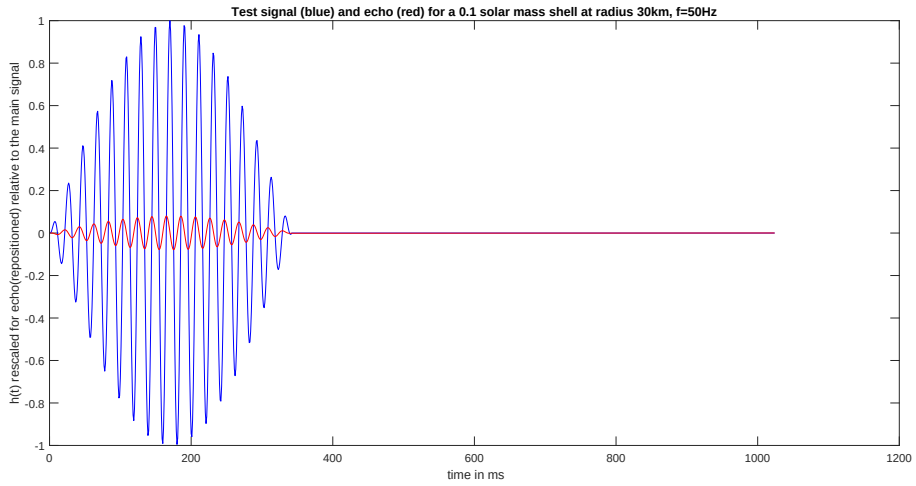


Figure 7.10: The effect of a matter shell of radius 0.1ms (about 30km) and mass 0.0005ms (about $0.1M_{\odot}$) on the burst signal of frequency 50Hz. The original signal is in blue the echo term in red.

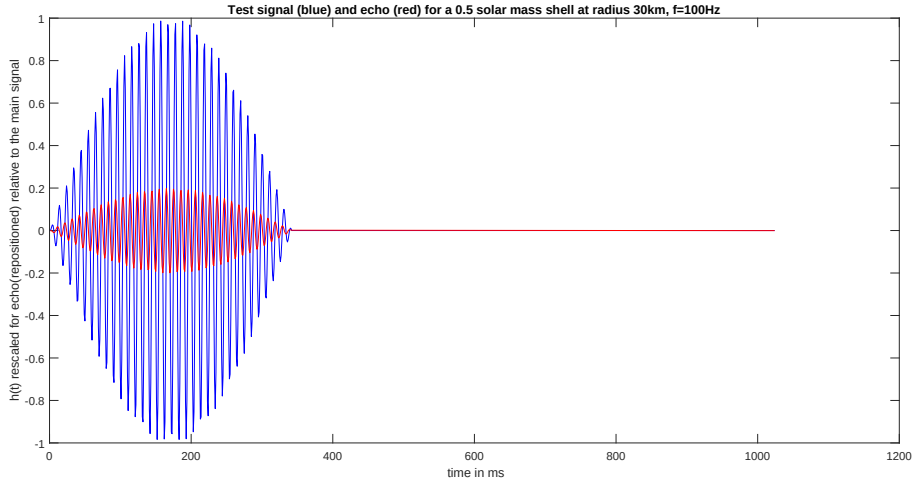


Figure 7.11: The effect of a matter shell of radius 0.1ms (about 30km) and mass 0.0025ms (about $0.5M_{\odot}$) on the burst signal of frequency 100Hz. The original signal is in blue the echo term in red.

### 7.4.1 Investigations with a test signal

We now try our test signal using various parameters.
We test the effect of a matter shell of radius 0.1ms (about 30km) and mass 0.0005ms (about $0.1M_{\odot}$) on the burst signal of frequency 100Hz as shown in Fig 7.9 . The original signal is in blue the echo term in red. We see that there is a very small echo produced. Maintaining all the parameters as in our first case illustrated in Fig. 7.9, we then only decrease the frequency from 100Hz to 50Hz as illustrated in Fig. 7.10 on page 104. The echo is clearly visible with an amplitude of almost 10%, that would significantly modify the main signal. Next, we increase the mass of the shell fourfold in as seen in Fig. 7.11 on page 104, maintaining the other parameters when compared with the case in Fig. 7.9 and notice that the echo is very clearly defined in Fig. 7.11 as compared with Fig. 7.9.

## 7.5 Could matter shells explain the GW echo claims?

In [40], the first of the tentative search for echoes, the authors find evidence for the existence of echoes in the first detection event [210] **GW150914**. They find further comparable evidence for echoes from the events GW151012 [24] (then referred to as LVT151012) and GW151226 [188]. The references report a number of echo events for GW150914, with the first occurring at about 0.3s after merger; therefore, if caused by a matter shell, the radius would be about 45,000km. The magnitude of the echo was about 0.0992 times that of the original signal. Using 132Hz for the frequency, which is its value when the amplitude was at its maximum at the end of the merger phase, and applying Eq. (7.7) on page 101, gives $\mathrm{M}_S \simeq$740,000$\mathrm{M}_{\odot}$. Such a mass within a radius of 45,000km would constitute a black hole, so the scenario of an echo caused by a shell can be discounted for GW150914.

Extending their investigations to the first BNS detection **GW170817** [216], the authors of [40] find evidence again of the existence of echoes in the postmerger event [45]. The echo was reported to occur at frequency $f_{echo} \simeq 72$ Hz, approximately 1.0 sec after the BNS merger event. The inspiral signal is at 72Hz about 4.0s before merger, so if the reported echo is caused by a matter shell it must have a radius of about 2.5s$\simeq$ 750,000km. Assuming that the magnitude of the echo signal must be at least $0.01\times$ that of the original signal and applying Eq. (7.7) on page 101, it follows that for the echo to be caused by a shell it would have a mass of approximately $10^7 M_{\odot}$. Now, a mass of $10^7 M_{\odot}$ inside a radius of 750,000km would constitute a black hole, so the scenario of an echo caused by a shell can be discounted for GW170817.

The above two examples illustrate the general difficulty of producing a GW echo by means of a matter shell. An echo, in the usual sense, is a repeat of the original signal after a short time delay, which in practice must be at least hundreds of ms, corresponding to a shell radius of at least $\sim$ 20,000km. Now, Eq. (7.7) on page 101, shows that the shell mass $M_S = 4\pi R r_0^2 f$ which, for expected values of the frequency $f$, will be large – either implying a BH and thus not feasible, or requiring an unexpected astrophysical scenario. A much smaller shell radius would avoid these difficulties, but the effect of the shell would be seen as a modification of the original signal, rather than as an echo. Some possible scenarios are presented in the next sections.

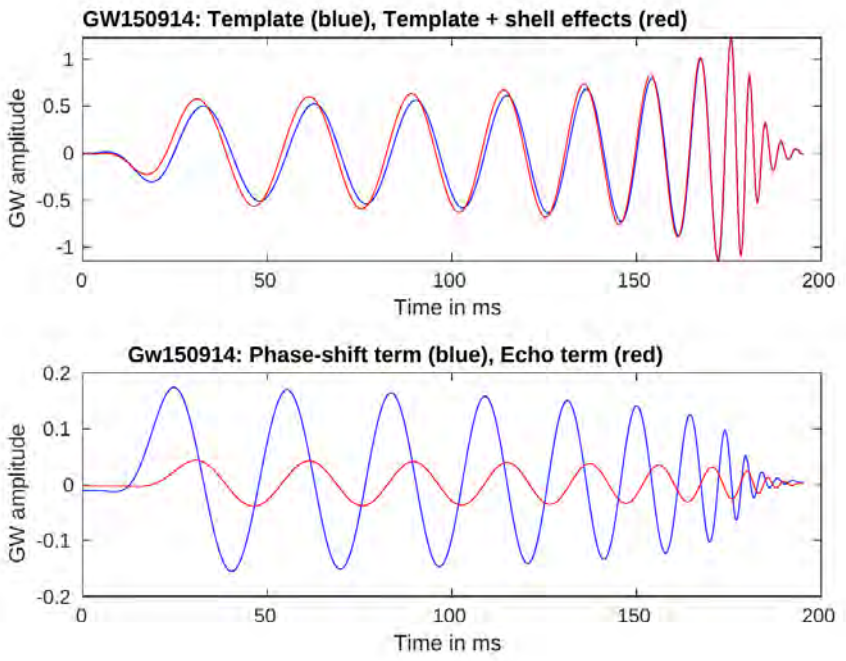


Figure 7.12: The effect of a matter shell of radius 3ms (about 900km) and mass 0.3ms (about $60M_\odot$) on the signal of GW150914. The top panel shows the original signal in blue, and the original signal plus modifications due to the shell in red. The lower panel shows the modifications due to the phase-shift term in blue, and due to the echo term in red.

### 7.5.1 GW150914 in the presence of a matter shell

Although a matter shell could not explain the echoes that might exist in GW150914 data, we now investigate how a hypothetical matter shell might modify the signal from a binary black hole merger. We consider the example case of a shell at radius 3ms (about 900km) and of mass 0.3ms (about $60M_\odot$) and the signal of GW150914 [243, 244, 245] (Of course, the astrophysical evidence does not suggest the existence of such a shell). The results are shown in Fig. 7.12 on page 106. The top panel shows that there is a small but noticeable modification to the template signal, particularly at early times; this is because the frequency is lower at early times and so the modification effects are larger. The bottom panel shows the contributions of the phase-shift term ($h_2$, blue) and the echo term ($h_3$, red); it is noticeable that, unlike the template signal, these terms decrease in magnitude as the frequency increases with time.

The signals were generated using the Matlab script BH.m which is available as a plain text files in Appendix D on page 178. The accuracy of the results presented in Fig. 7.12 on page 106 is limited since the formalism used in [47] assumed a weak field GW source, which is not the case for two black holes at merger. In particular, GWs reflected by the shell would be partially absorbed by the black holes, so reducing the magnitude of the echo contribution to the GW signal.

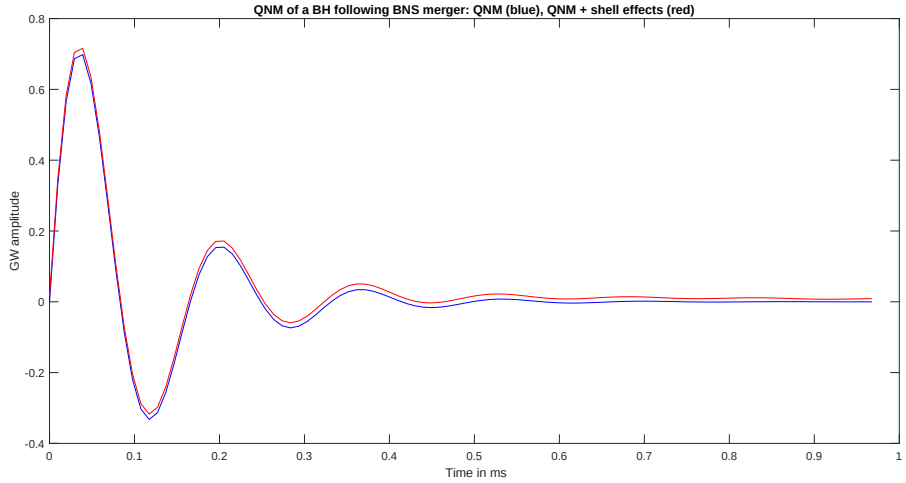


Figure 7.13: The effect of a matter shell of radius 25km and mass $0.7M_\odot$ on a quasinormal mode (QNM) signal of a $2M_\odot$ remnant of a BNS merger. The original signal is in blue, and the original signal plus modifications due to the shell is in red. The frequency is 6kHz.

### 7.5.2 Binary neutron star (BNS) mergers

BNS GW events that have been observed include GW170817 [27] and GW190425 [246]. Of these, GW170817 was at a higher signal to noise ratio and the event was observed post-merger in the electromagnetic spectrum [247], indicating that the post-merger object contained a large amount of free matter; we will therefore focus on this event.

The relevant source parameters reported for the event are [248, 249]: total mass $M_1 + M_2 = 2.74M_\odot$, and radii $R_1 = 10.8$km, $R_2 = 10.7$km. The reported GW signal increased in amplitude and frequency until 500Hz, at which stage the signal finished; i.e. the signal was observed during the inspiral phase, but ended as the two objects started to merge. The merger probably produced a central remnant of a neutron star or a black hole, in which case GWs in the lowest QNM would have been produced; however, the frequency of these GWs would be about 1.5 to 3kHz for a neutron star, or about 6kHz for a $2M_\odot$ black hole, which is outside the sensitivity band of the LIGO detectors.

In order to estimate the possible effect of matter on GWs emitted from a central remnant, we consider the model of a spherical shell of mass $M_S = 0.7M_\odot$ and radius $r_0 = 25$km around a GW source at either 6kHz or 2kHz. We find that the phase-shift term $2iM_S/(r_0^2\nu)$ evaluates to

$$\frac{iM_S}{r_0^2\pi f} = 0.0263i \;\text{ or }\; 0.0788i\,, \tag{7.15}$$

for 6kHz or 2kHz, respectively. The echo effect would be 1/4 of the above values, and the delay would be 0.1667ms, which is the same as the wave period (at 6kHz), or less than a wave period (at 2kHz). Thus, in the future if GW detectors in the kHz band are operational and if a BNS event occurs at high signal to noise ratio, then shell effects would affect the GW signal in a measurable way, although the small delay time means that it would be difficult to disentangle the echo and phase-shift effects from the main signal. The modifications to the QNM signal are

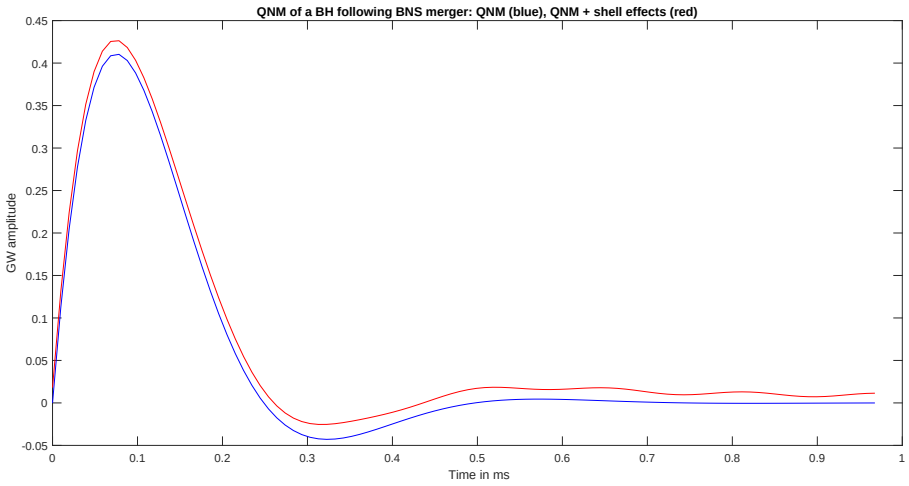


Figure 7.14: The effect of a matter shell of radius 25km and mass $0.7M_{\odot}$ on a quasinormal mode (QNM) signal of a $2M_{\odot}$ remnant of a BNS merger. Here the frequency is 2kHz.

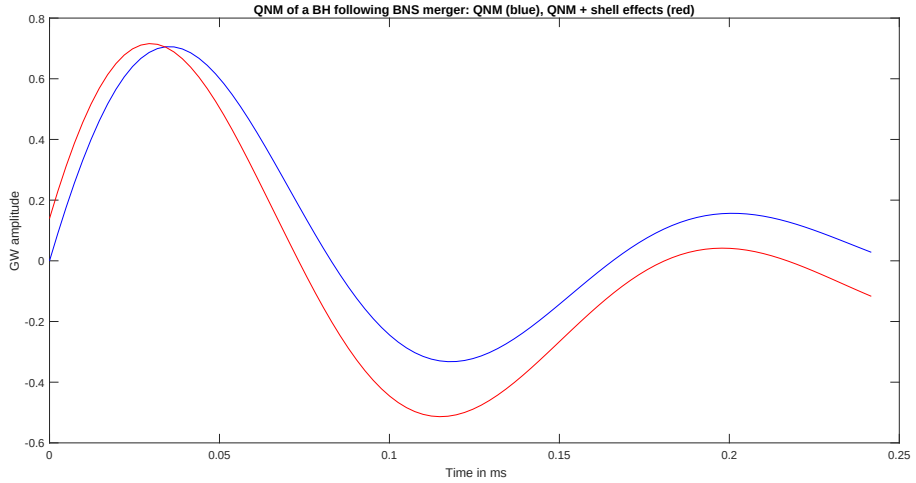


Figure 7.15: The effect of a matter shell of radius 10km and mass $1M_{\odot}$ on a quasinormal mode (QNM) signal of a $2M_{\odot}$ remnant of a BNS merger. The frequency is 6kHz

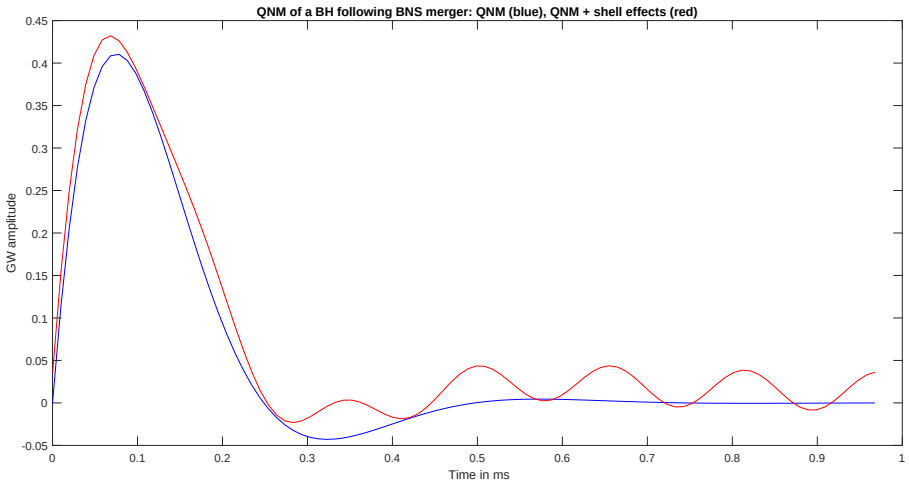


Figure 7.16: The effect of a matter shell of radius 10km and mass $1M_{\odot}$ on a quasinormal mode (QNM) signal of a $2M_{\odot}$ remnant of a BNS merger. The frequency is 2kHz

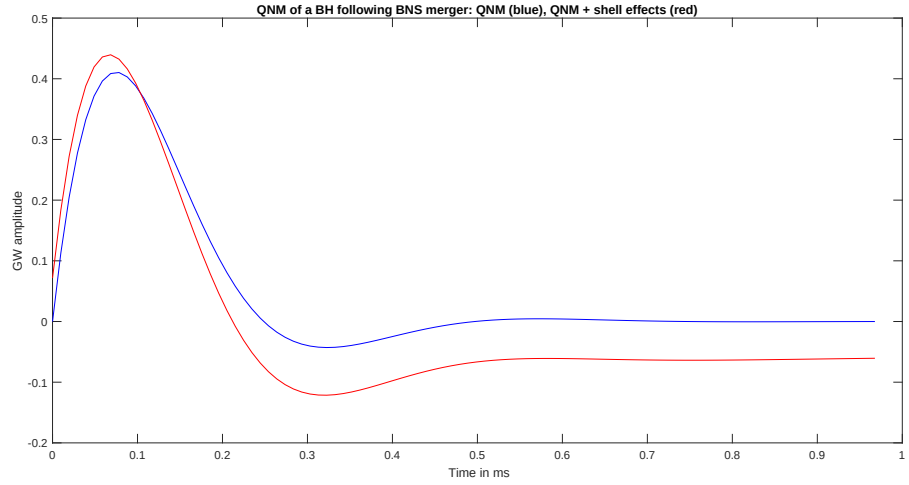


Figure 7.17: The effect of a matter shell of radius 20km and mass $1M_{\odot}$ on a quasinormal mode (QNM) signal of a $2M_{\odot}$ remnant of a BNS merger. The frequency is 2kHz

illustrated for the 6kHz case in Fig. 7.14 on page 108. However, there are a number of caveats that should be noted:

- The model in [47] assumed that the shell is static, but the aftermath of a BNS merger will be highly dynamical.
- The hypothesis of a shell forming is not supported by a detailed numerical simulation; indeed, since the system started as an inspiral, the matter outside the remnant should have a ring-like structure. Thus, Eq. (7.15) on page 107 may overestimate the matter effect for an observer on the axis of rotation of the system, but may be appropriate for an observer in the equatorial plane.
- The comment at the end of Sec. 7.5.1 on page 106 about absorption of GWs by a black hole applies here.

So the quantitative values in Eq. (7.15) on page 107 should be interpreted as indicative of the order of magnitude of the interaction of GWs with matter, rather than as precise estimates. It should also be noted that if the numerical modelling includes all the matter, and if the simulation run period includes the QNM ringdown, then shell effects would already be included in the simulation.
The Matlab script BNS.m used for the simulation is available in Appendix D on page 178 as a plain text files.

### 7.5.3 Core collapse supernovae

#### 7.5.3.1 Model for the GW modifications due to matter around the inner core

Ref. [134] presents GW waveforms from simulations of CCSNe for various zero age main sequence (ZAMS) masses in the range $9M_\odot, \cdots, 60M_\odot$. The GW signal starts with an initial burst of duration about 50ms and frequency about 100Hz, followed by a quiescent period. We model this part of the waveform as

$$\begin{aligned} &h_+ + ih_\times \sim \sin(0.2\pi u)\sin(0.02\pi u)\,{}_2Z_{2,2}\,, \;\; 0 \le u \le 50 \\ &h_+ + ih_\times = 0\,, \;\; 50 \le u \le 100\,. \end{aligned} \tag{7.16}$$

GWs are generated by aspherical motions in the inner core, commencing just after the bounce. The inner core is surrounded by the outer core, treated as a thick matter shell, and we now model its modifications to the GW signal. The shell has an inner radius $r_{in}$, an outer radius $r_{out}$, and density at $r = r_{in}$ of $\rho_0$ with density fall-off $\rho \propto r^{-1-a}$ with $1/2 \le a \le 2$. The effect of the whole shell is obtained by decomposing it into thin shells and then integrating. The result for the echo term is not a simple analytic expression and will be evaluated numerically using the Matlab script CCSN.m which is available as a plain text files in Appendix D on page 178. For, the phase shift term, we are able to obtain a simple analytic result

$$\int_{r_{in}}^{r_{out}} \frac{iM_s}{r^2\pi f}dr = i\int_{r_{in}}^{r_{out}} \frac{4\pi r^2\rho_0(r_{in})^{1+a}}{r^{1+a}r^2\pi f}dr = \frac{4i\rho_0 r_{in}}{af}\left(1-\left(\frac{r_{in}}{r_{out}}\right)^a\right), \tag{7.17}$$

where $f$ is the GW frequency. Fig. 7.18 shows the original signal given by Eq. (7.16) in blue, and the original signal plus shell modifications in red, for the case $r_{in} = 0.1$ms ($\approx 30$km),

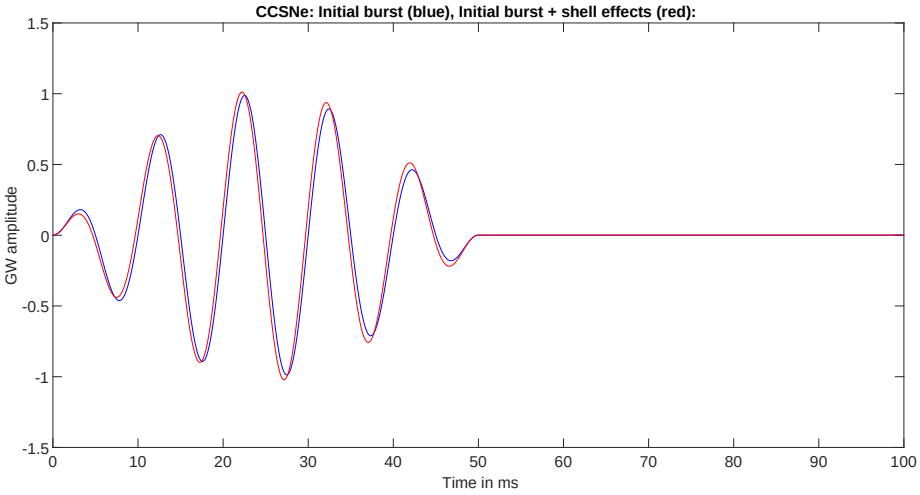


Figure 7.18: The effect of a matter shell as specified in the text, on the initial burst (Eq. (7.16) on page 110) on a CCSNe GW signal for the case $r_{in} = 0.1$ms ($\approx 30$km), $r_{out} = 0.5$ms ($\approx 150$km), $a = 1$, and $\rho_0 = 0.05/\text{ms}^2$ ($\approx 0.75 \times 10^{12}\text{g/cm}^3$). The frequency is 0.1/ms (100Hz). The mass of the shell is $0.503\text{M}\odot \sim 0.00252$ms. The original signal is in blue, and the modified signal is shown in red.

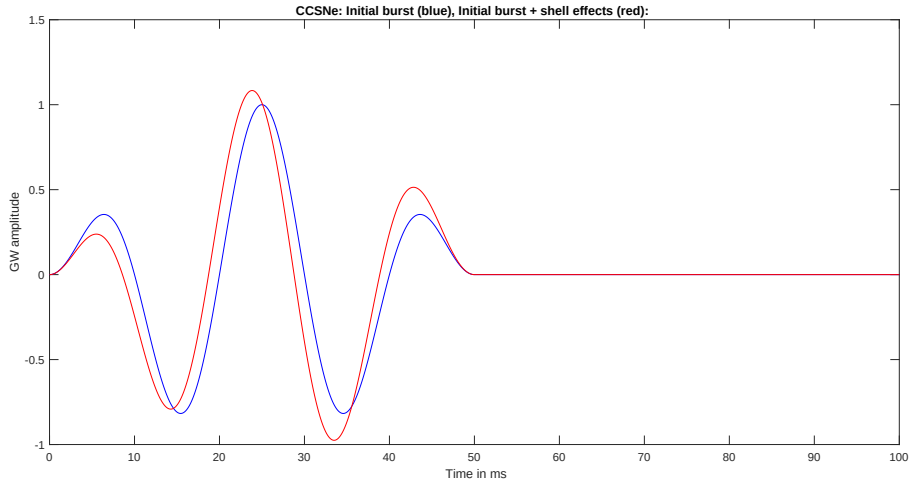


Figure 7.19: CCSN simulation with parameter values the same as in Fig. 7.18 except for the frequency changed from 100Hz to 50 Hz.

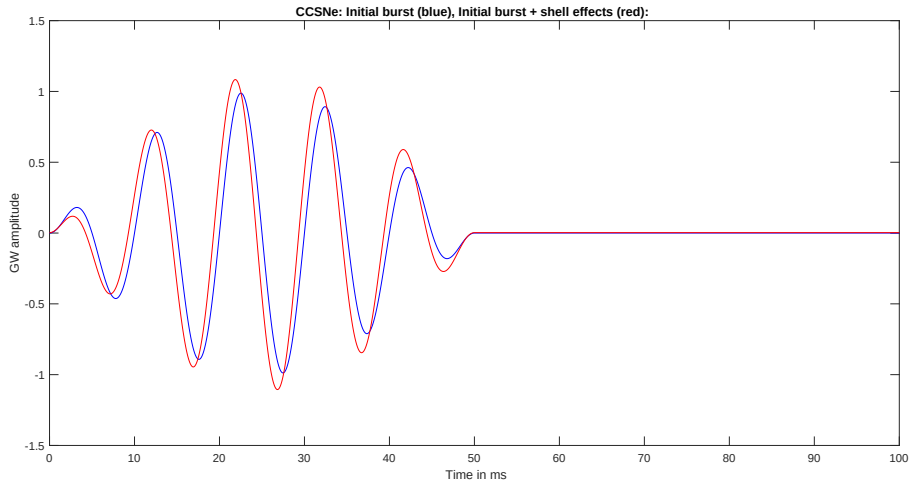


Figure 7.20: CCSN simulation with parameter values the same as in Fig. 7.18 except for the inner radius $r_{in} = 0.05$ms ($\approx 15$km), and $\rho_0 = 0.2/\text{ms}^2$ ($\approx 3 \times 10^{12}\text{g/cm}^3$). . The mass of the shell is marginally higher at $0.566\text{M}\odot \sim 0.00283$ms

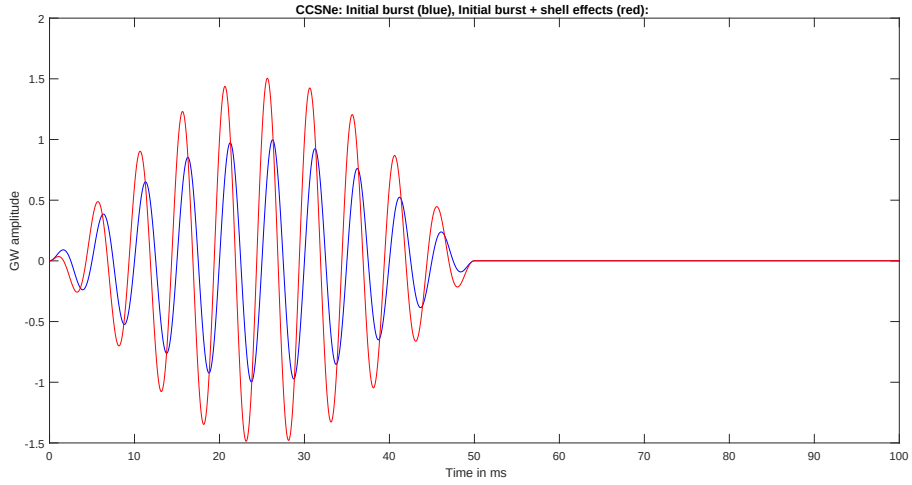


Figure 7.21: CCSN simulation with parameter values for the case $r_{in} = 1/30$ms ($\approx 10$km), $r_{out} = 2/3$ms ($\approx 200$km), $a = 1.5$, and $\rho_0 = 2/3/\text{ms}^2$ ($\approx 0.1 \times 10^{14}\text{g/cm}^3$). The frequency is 200Hz. The mass of the shell is $0.431\text{M}\odot$.

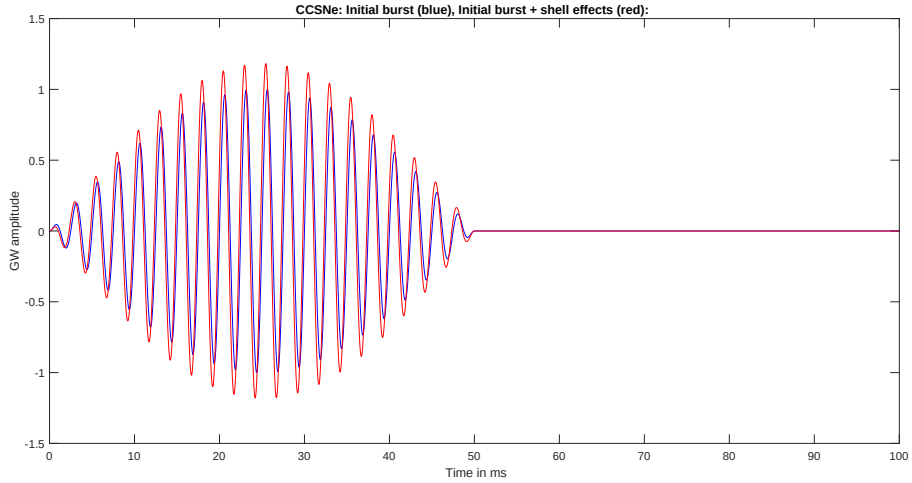


Figure 7.22: CCSN simulation with parameter values the same as in Fig. 7.21 except for the frequency changed from 200Hz to 400 Hz.

$r_{out} = 0.5$ms ($\approx$ 150km), $a = 1$, and $\rho_0 = 0.05/\text{ms}^2$ ($\approx 0.75 \times 10^{12}\text{g/cm}^3$). These values model: the inner core as a proto-neutron star (PNS) of radius 30km, and whose oscillations generate the GWs; the shock boundary as having a radius of 150km; and the density at the inner radius ($\approx 0.75 \times 10^{12}\text{g/cm}^3$) at a couple of orders below the supranuclear density. For this model, Eq. (7.17) on page 110 evaluates to $0.16i$, and the total mass of the shell to $0.503M_{\odot}$.

There is some uncertainty in the parameter values that should be used in modelling the matter shell around the inner core, and Eq. (7.17) on page 110 shows how varying the parameters would change the magnitude of the shell effect. A numerical simulation of a CCSNe entails modelling gravity as well as a number of other physical process, and requires extensive computational resources. It is not feasible to model the whole star using general relativity (GR): approximations to GR are used, and GWs may be estimated using the quadrupole formula [134]. Thus corrections to the quadrupolar signal due to shell effects are necessary.
In Fig. 7.19 on page 111 the CCSN simulation is carried out for a surrounding matter shell with inner radius $\text{r}_{in} = 30km \sim 0.1ms$ and outer radius $\text{r}_{out} = 150km \sim 2/3ms$. The frequency of the GW signal emanating from within the collapsed inner core is f$= 50Hz = 0.05ms^{-1}$ . The density at the inner radius of the matter shell is $\rho = 0.75 \times 10^{12}$ g/cm$^3$ $\sim 0.05/ms^2$ falling of as $1/\text{r}^2$. Differing from the simulation illustrated in Fig. 7.18 on page 111 only through the frequency being halved, from 100Hz to 50Hz, we see that the modification producing an increase of amplitude of almost 10% is more pronounced and clearly more discernible.

We next apply our Matlab script CCSN.m to a CCSN configuration with a surrounding matter shell extending from inner radius $\text{r}_{in} = 15km \sim 0.1ms$ to outer radius $\text{r}_{out} = 150km \sim \frac{2}{3}ms$. The frequency of the GW signal emanating from within the collapsed inner core is taken as f$= 100Hz = 0.1ms^{-1}$. The density at the inner radius of the matter shell is taken at $\rho = 3 \times 10^{12}\text{g/cm}^3 \sim 0.2/ms^2$, falling of as $1/\text{r}^2$. Compared with our original case illustrated in Fig. 7.18 on page 111, the inner radius has been halved whilst the density at the inner radius

now starts off as four times larger than in our original case We obtain the result illustrated in Fig. 7.20 on page 112. where the effect is more pronounced than the original case with a modification in both amplitude and phase that is clearly visible. We see, then, that for a matter shell closer to the source or for a lower frequency of the GW signal, the modification is more pronounced. However, we will need to restrict the range of our parameters so as to be consistent with models for the evolution of the CCSN. The mass of the surrounding matter should be such that the mass itself does not overtly effect the inspiral.

We now consider the situation of a matter shell close-in to the core at a radius of 10km from the centre of the CCSN. Within this boundary the density of the inner core is expected to reach supranuclear densities of 2 $\times 10^{14}$ g/cm$^3$ and higher. At the interface of core boundaries, density drop-off is expected to be severe. We make an estimate of the density of the inner radius of the matter shell, at the interface with the outer boundary of the inner core, $\rho = 0.1 \times 10^{14}$g/cm$^3 \sim 2/3ms^{-2}$, an order lower than that expected within the core of, falling of as $1/r^{2.5}$. Taking, then, the inner boundary of the matter shell at $r_{in} = 10km \sim 1/30$ms, we consider a matter shell extending up to the shock boundary, expected to be no further than $r_{out} = 200km \sim 2/3$ ms. The mass of the shell is $0.431M_\odot$, which should be slightly less massive than the inner iron core, expected to be around $0.5M_\odot$. As before, in our figures, the initial burst is given in blue, with the modified signal (initial burst together with the shell effects) given in red. We perform our numerical code for this configuration for two different frequencies. First, Fig. 7.21 on page 112 illustrates the case for a frequency of f= $200Hz = 0.2/ms$. Of all the cases investigated up to here, the parameter values used in Fig. 7.21 on page 112 lead to the most pronounced modification of the GW signal. The amplitude is the most enhanced of the cases we have investigated, thus far. The phase shift is also clearly visible. Fig. 7.22 on page 113 illustrates the case for the same configuration and parameter values as for the case illustrated in Fig. 7.21 on page 112 except that the frequency is increased two-fold to a frequency of f= $400Hz = 0.4/ms$. The modification to the amplitude is diminished for this increase in frequency but still discernible. The modification to the phase is not as easily discernible as the previous case. We see, then, that for lower frequencies, of around 100∼200Hz modifications are more enhanced than for higher frequencies. Frequencies of 100∼200Hz do correspond to expected frequencies of GW signals from CCSNe [134]. The inner core of CCSN is expected to reach supranuclear densities of 2 $\times 10^{14}$ g.cm$^{-3}$ and higher [128], so the choice of a density of an order lower of 0.5 $\times 10^{14}$ g.cm$^{-3}$ also seems reasonable. The values for the boundary of the inner core at $r = 10km$ and the shock boundary at $r = 200km$ is consistent with the theoretical and numerical calculations [250, 127]. The matter shell, at a mass of $\sim 0.431M\odot$ has a mass expected to be less than that of the inner core matter. This, too, is a realistic expectation and the existence of a matter shell, of such a mass, is plausible. Hence, for a GW signal emanating from the inner core of a CCSN, and passing through a surrounding matter shell with realistic parameter values (as we described above), it is reasonable to expect modifications to that signal of the kind as predicted by our codes and as illustrated in Fig. 7.21 on page 112.

## 7.6 Summary of results and conclusion

There are astrophysical scenarios which can be regarded as comprising a shell of matter around a GW source, and this chapter has investigated in what way the GW signal would be affected.

The investigation started with GW events for which echoes have been claimed to exist in the LIGO data, and it was found that such echoes could not be caused by a matter shell. Thus, an unambiguous observation of GW echoes in the future would favour the existence of ECOs.

We investigated the effect of matter shells in three specific example cases. The first was a binary black hole merger analogous to GW150914, surrounded by a hypothetical matter shell at radius 900km and mass $60M_{\odot}$. Astrophysically, such a shell is highly unlikely to exist, but this case is useful as it well illustrates some of the features of the shell effects on the waveform. The next case considered was the QNM signal from the remnant of a binary neutron star merger like GW170917. In this case, it is known that there is a substantial amount of matter around the remnant, although the extent to which the shell model is appropriate is unclear. The final case considered was that of a core collapse supernova. Although GWs from such events have not been observed, they are regarded as potential sources; and here it is clear that the PNS, in which the GWs are generated, is surrounded by shells of matter. Of the three cases, the CCSNe is that which yielded the largest shell modifications to the GWs, and for which the predictions are most reliable.

The effects of matter shells are small but measurable if the signal to noise ratio is sufficiently high. As GW observations become more accurate, through both hardware developments and, as time passes, increasing the chance of observing nearby events, these effects will need to be taken into account.

# Chapter 8

# Conclusion

In this thesis we have investigated the effect of a matter shell on the propagation of GWs. We employed the BS formalism, within the linearised perturbation theory, to investigate the effect of a spherical dust shell on GWs sourced from the center of the shell. We made the novel finding in Chapter 6 that the GWs were modified, however, without any energy transfer between the GWs and the shell. We found that the effect would be measurable if a GW event were to occur with a source surrounded by a massive shell and with the radius of the shell and the wavelength of the GWs of the same order. We also found that a shell of matter, in effect, reflects part of an outgoing GW, and so in the context of a burst (rather than a continuous) source it is possible that an echo would be the result. Taking this finding we extended our work to consider various astrophysical sources of GWs in Chapter 7. There are astrophysical scenarios which can be regarded as comprising a shell of matter around a GW source, and this thesis has investigated in what way the GW signal would be affected.

We modelled a burst source as a Fourier sum of the eigensolutions obtained to investigate possible GW echoes in the various chosen astrophysical scenarios. We investigated the effect of matter shells in three specific example cases. The investigation started with GW events for which echoes have been claimed to exist in the LIGO data. The first was a BBH merger analogous to GW150914, surrounded by a hypothetical matter shell at radius 900km and mass $60M_{\odot}$. Astrophysically, such a shell is highly unlikely to exist, but this case was useful as it illustrated some of the features of the shell effects on the waveform. It was found that such echoes could not be caused by a matter shell. Thus, an unambiguous observation of GW echoes in the future would favour the existence of ECOs. The next case considered was the QNM signal from the remnant of a BNS merger like GW170917. In this case, it is known that there is a substantial amount of matter around the remnant, although the extent to which the shell model is appropriate is unclear.

The final case considered was that of a CCSNe. Although GWs from such events have not been observed, they are regarded as potential sources; and here it is clear that the PNS, in which the GWs are generated, is surrounded by shells of matter. Of the three cases, the CCSNe is that which yielded the largest shell modifications to the GWs, and for which the predictions are most reliable. We considered various cases, varying parameters for the inner and outer radii for the

shell, the density of the shell at the innermost boundary, the density fall-off and the frequency of the GW. We found that for realistic values of these parameters, consistent with CCSNe simulations, that modifications to GWs would occur that may be discernible for detection. The effects of matter shells are small but measurable if the signal to noise ratio is sufficiently high. As GW observations become more accurate, through both hardware developments and, as time passes, the increasing chance of observing nearby events, these effects will need to be taken into account.

There are avenues for further work. This work was done for the dust case and it would be useful to extend the considerations for the matter EOS to beyond dust, including shear viscosity, and possibly other forms of dissipation. Another avenue is in relation to the background spacetime without the matter shell. In our considerations we used Minkowski spacetime and it may be also be useful to change this background spacetime to something more appropriate to cosmology. Solutions are known for the de Sitter spacetime [200] and this may present a possibility in adapting our investigations. Solutions are also known for the Einstein-de Sitter background [204], however, the algebraic complexity of the solution may make the construction of perturbative solutions problematic. A particularly appropriate background, from an astrophysical viewpoint, would be Kerr or Schwarzschild. However, expressing the Kerr metric in Bondi-Sachs form is complicated [251], and perturbations about this metric have not been investigated. Perturbations about Schwarzschild are known [207], but the solutions are complicated expressions.

In the context of cosmology, we found that the effects are too small to be measurable.

The intervening years between the postulation of Einstein's GR theory to vindication of the theory through confirmation of the existence of GWs, a consequence of the theory, is testimony to the resilience of GR and to the human condition and the qualities of perseverance and collaboration. Formulated in an environment where anti-Semitism was in the ascendency, the theory suffered prejudice itself in that it was not just a scientific theory but a scientific theory of a Jew. It is clear that the theory did not enjoy the recognition it deserved in Germany. Outside of Germany, allied nations and largely the English-speaking world who were at war with Germany were reticient towards scientific developments emanating from "enemy" territory. The theory was no more a scientific theory but a scientific theory of a German. Were it not for Eddington's Quaker roots, which informed his anti-war stance, Einstein's theory may have taken even longer to progress. The GR theory was not the only victim of the war. Whilst in the trenches on the frontline of the war doing battle on behalf of Germany, the German physicist, Karl Schwarzschild, provided within a month of Einstein announcing his equations, the first exact solution to the EFEs (albeit for a highly simplified scenario, that of a single spherical non-rotating mass). The next year he died on the Russian front.

Einstein proposed GWs as a consequence of GR [252, 11] shortly after he introduced GR in 1915. His calculations were based on the weak-field approximation resulting in a linearised version of the EFEs, which we elaborated on in Chapter 2. Whilst we have lauded Einstein for his remarkable feat of the formalisation of the GR, and justifiably so, it is important to note the thread of scientific enquiry and the effort of others. Poincaré, a decade earlier, had also postulated the existence of GWs based on his own work in special relativity. However, Poincaré had not made the leap to the four dimensions of spacetime nor did he abandon the concept of

the "aether", the thin fluid through which all objects move. It was Hermann Minkowski who took the work of Poincaré and introduced, in 1907, the four-dimensional spacetime to describe the special theory of relativity. Poincaré and Einstein, who both worked on special relativity independently, and presented their results in 1905 [253, 58], based their arguments on the postulates of Lorentz and his time transformation. Lorentz had introduced the notion of "local time" through the auxiliary quantity $t' = t - vx/c^2$ [254], leading to the Lorentz transformations on which the theory of special relativity hinges. Many have been inclined to credit Lorentz for the theory, however, Lorentz, himself, credited Einstein completely for the theory of relativity "*I considered my time transformation only as a heuristic working hypothesis. So the theory of relativity is really solely Einstein's work. And there can be no doubt that he would have conceived it even if the work of all his predecessors in the theory of this field had not been done at all. His work is in this respect independent of the previous theories.*" [255]

The works of Minkowski, Einstein, Poincaré and Lorentz in special relativity had their foundation in the 1887 experiment of Albert Michelson and Edward Morley. The Michelson-Morley experiment dispelled the long-held notion of the aether by proving that the speed of light was constant in all directions [256]. It is thus fitting that the Michelson interferometer is the principal component of the GW detector which, on 14 September 2015 [23], confirmed the existence of GWs, a consequence of the 1915 GR theory of Einstein [5].

The triumph of Einstein's GR theory, which enjoys wide acceptance a century later, and the search for GWs, predicted by the theory, is an illustration of the triumph of human spirit and endeavour. Eddington, a pacifist facing possible imprisonment for his refusal to fight for England in the war of 1914 to 1918, chose to bring Einstein, a German, to England to give public discourses on the theory of GR. Einstein's visit enjoyed widespread publicity and support from the British public. However, the most notable public affirmation of scientific achievement, the Nobel prize was never awarded to Einstein in recognition of his GR theory. The journey to the first detection spanned six decades, with three key architects of that journey, Rainer Weiss, Barry Barish and Kip Thorne, awarded the Nobel prize for Physics in 2017. Discussions reigniting GW investigations in the 1950's, initiated at the 1955 Bern conference (GR0) [55] and strengthened at the Chapel Hill conference (GR1) [17] in 1957, paved the way for the construction of GW detectors, beginning with Weber's efforts [18, 152] initiated shortly after the 1957 conference as we discussed in Chapter 5. Bondi's unambiguous mathematical discourse on the existence of GWs in 1957 [151] laid to rest doubts of the existence of GWs, at least theoretically, as we related in Chapter 3. Years of persistence and hounding of national science bodies and governments led to the securing of funds to build the detectors LIGO in the USA, VIRGO and GEO600 in Europe and TAMA300 in Japan. These detectors began their first runs around the turn of the century and went through several evolutionary changes, leading to aLIGO being the first to detect a GW on 14 September 2015 [23].

Within just a few years since the window to a new universe was opened with the discovery of GWs, challenges already exist to long-held theories and assumptions as we elaborated on in Chapter 4. The mass-gap has been filled with the discovery of a $2.6M_\odot$ compact body in the GW event, GW190814 detected by aLIGO and aVIRGO [208, 209] but there is still no confirmation on which of the candidates fill that gap: NSs, BHs or both or some other yet to be classified compact body.

For the GW event, GW190521, reported by aLIGO and aVIRGO, the short GW signal detected has been postulated to be the consequence of the merger of a quasi-circular BBH, with resulting remnant a BH of mass $M_f \sim 142\ M_\odot$, the first ever observed IMBH [28]. For this postulated BBH merger, at least one of the companions would have to exist in the PISN gap. There have been suggestions that neither of the compact bodies involved in these mergers were BHs but instead Proca stars or boson stars [29], which are DM candidates, and that their understanding would necessitate a QM approach to GR.

As discoveries of astrophysical events of GWs flow in there are likely to be many challenges to long-held notions. Ironically, the discovery of GWs, long touted, as final vindication of the theory of GR, may lead to, at the very least, a revision of the theory. It has long been suggested that until GR incorporates quantum considerations, it will remain incomplete. Perhaps the time to revise the theory will arrive sooner than expected.

# List of Tables

# List of Figures

# Appendix A

# List of abbreviations

| Abbreviation | Meaning |
|---|---|
| aLIGO | advanced LIGO |
| aVIRGO | advanced VIRGO |
| BBH | Binary Black Hole |
| BH | Black Hole |
| BNS | Binary Neutron Star |
| BS | Bondi-Sachs |
| BSG | Blue supergiant |
| C | Carbon |
| CCSN | Core Collapse Supernova |
| CCSNe | Core Collapse Supernovae |
| ClePhO | Clean Photosphere Objects |
| CNRS | Le Centre National de la Recherche Scientifique |
| DM | Dark matter |
| DNS | Double Neutron Star |
| DRFPMI | dual-recycled Fabry-Perot Michelson Interferometer |
| DRMI | dual-recycled Michelson Interferometer |
| ECO | Exotic Compact Object |
| ECSN | electron-capture supernova |
| EFE | Einstein field equations |
| EGO | European Gravitational Observatory |
| ELF | Extremely Low Frequency (Band) |
| EMF | electromagnetic field |
| EMRI | Extreme Mass-Ratio Inspiral |
| EOS | Equation of State |
| EOS | equation of state |
| ESA | European Space Agency |
| ET | Einstein Telescope |
| Fe | Iron |
| FFT | Fast Fourier Transform |
| FT | Fourier Transform |
| GR | General Relativity |
| GR1 | 1st Gravitation and General Relativity Conference; GR2, the 2nd; GR3, the third; etc. |
| GRB | Gamma-Ray Bursts |
| GW | Gravitational Wave |
| GW150914 | confirmed gravitational wave event on 15/09/2014, GW17/08/14 on 17/08/2014, etc |
| GWA | gravitational wave astronomy |

| | |
|---|---|
| H | Hydrogen |
| He | Helium |
| HF | High-Frequency (Band) |
| iLIGO | initial LIGO |
| IMBH | intermediate-mass black hole |
| INFN | Istituto Nazionale di Fisica Nucleare |
| IOFP | Institute of Field Physics |
| ISCO | Innermost Stable Circular Orbit |
| ISCO | innermost stable circular orbit |
| LCGT | Large Scale Cryogenic Gravitational Wave Telescope |
| LF | Low-Frequency (Band) |
| LIGO | Laser Interferometer Gravitational Wave Observatory |
| LISA | Laser Interferometer Space Antenna |
| LPF | LISA Pathfinder (mission) |
| LSST | Large Synoptic Survey Telescope |
| LVC | LIGO VIRGO Collaboration |
| MESA | Modules for Experiments in Stellar Astrophysics |
| Mg | Magnesium |
| MG4 | The 4th Marcel Grossman meeting; MG1, the 1st; MG2, the 2nd; etc. |
| MMA | multi-messenger astronomy |
| MT | mass transfer |
| NANOGrav | North American Nanohertz Observatory |
| Ne | Neon |
| NP | Newman-Penrose (formalism) |
| NPRO | nonplanar ring oscillator |
| NR | Numerical Relativity |
| NS | Neutron Star |
| NSBH | Neutron Star - Black Hole |
| NSF | National Science Foundation |
| PISN | pair-instability supernova (gap) |
| PN | Post-Newtonian |
| PNS | Proto neutron star |
| PRFPMI | power-recycled Fabry-Perot resonator Michelson interferometer |
| PTA | Pulsar Timing Array |
| QNM | Quasinormal mode |
| RAS | Royal Astronomical Society |
| RSG | red supergiant |
| S | Sulphur |
| SGRB | Short Gamma-Ray Burst |
| Si | Silicon |
| SKA | Square Kilometre Array |
| SMBH | super-massive black hole |
| SN | Supernova |
| SNR | signal-to-noise ratio |
| SR | Special Theory of Relativity |
| TT | Transverse Traceless (gague) |
| UCO | ultracompact object |
| UHV | Ultra-high vacuum |
| UK | United Kingdom |
| USA | United States of America |
| VLF | Very Low Frequency (Band) |
| WD | White Dwarf |
| ZAMS | zero-age main sequence |

# Appendix B

# List of symbols

## B.1 Notation

### B.1.1 Latin symbols

| | |
|---|---|
| $A_{\mu\nu}, A_+, A_\times$ | Wave amplitude tensor and coefficients |
| $A, A^A, A^u, A^\rho$ | Coefficients in transformation between Bondi and general gauges |
| $a$ | Term in Schwarzschild metric |
| $b$ | Term in Schwarzschild metric |
| $C_{abcd}$ | Weyl tensor |
| $d\Omega$ | Surface area element of a sphere |
| $E$ | Energy |
| $E_{A}^{\ell m}$ | Vector spherical harmonic |
| $\boldsymbol{A}_+, \boldsymbol{A}_\times, \boldsymbol{A}_{\text{L}}, \boldsymbol{A}_{\text{R}}$ | Polarization tensors |
| $\boldsymbol{e}_x$ | Unit vector in the direction of the coordinate $x$ |
| $F^A$ | Dyad of general Bondi-Sachs gauge metric |
| $\mathcal{F}$ | Fourier transform operator |
| $G_{ab}$ | Einstein tensor |
| $G$ | Quantity in Cauchy-perturbative matching |
| $g_{\alpha\beta}$ | four-metric |
| $\overset{0}{g}_{\mu\nu}$ | Background metric |
| $H$ | Re-scaled wave strain, i.e., $\lim_{\tilde{r}\to\infty} r(h_+ + ih_\times)$ |
| $H_0, H_1$ | Quantity in Cauchy-perturbative matching |
| $h_{AB}$ | Angular part of metric |
| $h_{\mu\nu}$ | Metric perturbation |
| $h^{\text{TT}}_{\mu\nu}$ | Metric perturbation in TT gauge |
| $\bar{h}_{\mu\nu}$ | Trace-free metric perturbation |
| $h_{A}^{(0)}, h$ | Quantity in Cauchy-perturbative matching |
| $\boldsymbol{I}_{jk}$ | Trace-less mass quadrupole |
| $\mathcal{J}^+$ | Future null infinity |
| $J$ | Bondi-Sachs metric variable |
| $J_i$ | Angular momentum |
| $K$ | Bondi-Sachs metric variable |
| $K$ | Quantity in Cauchy-perturbative matching |
| $K_{ij}$ | Extrinsic curvature |
| $k_A$ | Quantity in Cauchy-perturbative matching |
| $\mathcal{L}$ | Lie derivative operator |

| | |
|---|---|
| $L^{\ell m}, L_{A}^{\ell m}$ | Quantities in Cauchy-perturbative matching |
| $\ell^{\alpha}$ | Newman–Penrose tetrad vector, tangent to outgoing null geodesic |
| $m^{\alpha}$ | Newman–Penrose tetrad vector |
| $m^{\alpha}_{[G]}$ | Approximation to $m^{\alpha}$ |
| $\mathcal{N}$ | Gravitational news |
| $N^{\mu}_{\nu}$ | Time projection operator |
| $n^{\alpha}_{[NP]}$ | Newman–Penrose tetrad vector |
| $n^{\alpha}$ | Unit normal to $\Sigma_t$ |
| $P_i$ | three-momentum |
| $p$ | Stereographic coordinate |
| $Q^{(0)}$ | Quantity in Cauchy-perturbative matching |
| $q$ | Stereographic coordinate |
| $q^{A}$ | Complex dyad vector |
| $q_{AB}$ | Unit sphere metric |
| $R$ | "3+1" radial coordinate, $R = \sqrt{x^2 + y^2 + z^2}$ |
| $R, R_{ab}, R_{abcd}$ | Ricci scalar, Ricci tensor, Riemann tensor |
| $\mathcal{R}$ | Intrinsic 2-curvature |
| $r$ | Bondi-Sachs radial coordinate |
| $r$ | Radial coordinate in Cauchy perturbative approach |
| $S^{(0)}$ | Quantity in Cauchy-perturbative matching |
| $S_{c}^{\ell m}, S_{cd}^{\ell m}$ | Vector spherical harmonic, tensor spherical harmonic |
| $s$ | Radial like coordinate |
| $s^{i}$ | Unit normal to $S_t$ |
| $T_{ab}$ | Stress-energy tensor |
| $T^{\ell m}, T_{A}^{\ell m}$ | Quantities in Cauchy-perturbative matching |
| $t_{ab}$ | Stress-energy tensor of gravitational waves (averaged) |
| $t$ | "3 + 1" time coordinate |
| $U$ | Bondi-Sachs metric variable |
| $U^{k}(x)$ | Chebyshev polynomial of the second kind |
| $u$ | Bondi-Sachs time coordinate |
| $u^{\mu}$ | Fluid four-velocity |
| $V_{\ell}^{(0)}$ | Quantity in Cauchy-perturbative matching |
| $W$ | Lorentz factor |
| $W^{\ell m}$ | Quantities in Cauchy-perturbative matching |
| $W_{c}$ | Bondi-Sachs metric variable |
| $x^{\alpha}, x^{i}$ | Coordinates |
| $x^{\alpha}_{[B]}$ | Bondi-Sachs coordinates |
| $x^{\alpha}_{[C]}$ | Minkowski-like coordinates |
| $x^{\alpha}_{[N]}$ | Null affine coordinates |
| $X^{\ell m}$ | Quantities in Cauchy-perturbative matching |
| $Y^{\ell\, m}, {}_{s}Y^{\ell\, m}$ | Spherical harmonic, spin-weighted version |
| $Z^{\ell\, m}\ {}_{s}Z^{\ell\, m}$ | "Real" spherical harmonic, spin-weighted version |
| $Z^{\ell\, m}_{CD}$ | Tensor spherical harmonic |

### B.1.2 Greek symbols

| | |
|---|---|
| $\alpha$ | Lapse |
| $\beta$ | Bondi-Sachs metric variable |
| $\beta^i$ | Shift |
| $\Gamma$ | Extraction worldtube |
| $\gamma_{ij}$ | three-metric |
| $\delta$ | Phase factor |
| $\eta_{\mu\nu}$ | Metric of special relativity |
| $\theta$ | Spherical polar coordinate |
| $\kappa_\alpha$ | Wave propagation vector |
| $\kappa_1, \kappa_2$ | Quantities in Cauchy-perturbative matching |
| $\Lambda$ | $\ell(\ell+1)$ |
| $\lambda$ | Affine parameter |
| $\xi^\alpha$ | Vector defining gauge transformation |
| $\xi$ | $(u, q, p)$ |
| $\rho$ | Compactified radial coordinate |
| $\Sigma_t$ | Timelike slice |
| $\Phi^{(o)}, \Phi^{(e)}$ | Quantities in Cauchy-perturbative matching |
| $\phi^A$ | Angular coordinates |
| $\phi$ | Spherical polar coordinate |
| $\Upsilon$ | $-q^A \bar{q}^B \nabla_A q_B/2$, factor in definition of $\eth$ |
| $\chi$ | Quantity in Cauchy-perturbative matching |
| $\Psi^{(o)}, \Psi^{(e)}$ | Quantities in Cauchy-perturbative matching |
| $\psi_0 \cdots \psi_4$ | Newman–Penrose quantities |
| $\psi_4^0$ | Re-scaled $\psi_4$, i.e., $\lim_{r\to\infty} r\psi_4$ |
| $\Omega_\mu$ | $\nabla_\mu t$ |
| $\omega$ | Relation between the radial coordinate in the general and Bondi gauges |
| $\omega$ | Wave frequency |

### B.1.3 Operators

| | |
|---|---|
| $\nabla_\alpha$ | Covariant derivative operator |
| $\partial\alpha$ | Partial derivative operator |
| $\Box$ | Wave operator |
| $\eth$ | Spin-weighted angular derivative operator |
| $\hat{}$ | Quantity in conformally compactified gauge |
| $\hat{}$ | Index in another coordinate system |
| $\tilde{}$ | Quantity in Bondi gauge |
| $\tilde{}$ | Fourier transformed quantity |
| $\bar{}$ | Complex conjugate (except see above for $\bar{h}_{\mu\nu}$) |

### B.1.4 Indexing conventions

| | |
|---|---|
| $_{\alpha,\beta,\cdots}$ | $(0, 1, 2, 3)$ Spacetime indices |
| $_{i,j,\cdots}$ | $(1, 2, 3)$ Spacelike indices |
| $_{A,B,\cdots}$ | $(2, 3)$ Angular indices |
| $_{a,b,\cdots}$ | $(0, 1)$ Non-angular indices |
| $_{\ell m}$ | Spherical harmonic indices |

# Appendix C

# Maple code

The computer algebra scripts used in Chapter 6 are written in Maple in plain text format, and are available in this appendix.
The generated output file are not given explicitly here (except for `gamma.out`) but are all available as ancillary files in [258] (https://arxiv.org/src/1912.08289v2/anc). Note that the output files may be viewed using a plain text editor provided line-wrapping is switched off.
This appendix contains the following files:

- `backgroundShell.map`;
- `initialize.map`;
- `lin.map`;
- `paperEqs.map`;
- `ProcsRules.map`;
- `regular_0_IncomingGW.map`;
- `shell.map`;
- `shellCinI_0.map`;
- `gamma.out`;

In the Supplementary Material for Ref. [258], listed as Ancillary files in [258], the additional files relevant to Chapter 6 and Ref. [258] but not included in this appendix may be found. These include:

- `Eqs.pdf`;

- `backgroundShell.out`;
- `formulas.out`;
- `formulas.pdf`;
- `paperEqs.out`;
- `regular_0_IncomingGW.out`;
- `shell.out`;
- `shellCinI_0.out`;

The scripts `gamma.out, initialize.map, lin.map, ProcsRules.map` are not used directly, but are called by the other scripts described below. `gamma.out` contains formulas for the BS metric, its inverse and the metric connection coefficients. `lin.map` constructs the Einstein equations linearised about a given background. `ProcsRules.map` contains various procedures and rules that are used by other scripts.

The script `initialize.map` initializes various arrays etc., and sets the density profile of the matter as given in Eq. (6.4) on page 79; other density profiles tested were given by Eqs. 6.5 The script `backgroundShell.map` constructs the background (spherically symmetric) solution for the given density profile; it also checks that the metric functions are sufficiently smooth at the interface $r = r_0$, and that the solution satisfies all 10 Einstein equations. The output is in `backgroundShell.out`

The script `paperEqs.map`, with output in `paperEqs.out`, generates the formulas given in Eqs. (6.13) on page 81, (6.15) page 82 and (6.17) page 83; note that some manual simplifications have been applied to the formulas generated by the computer algebra.

The script `shell.map` uses the divergence-free condition on the energy-momentum tensor, $\nabla_a T_{bc} g^{ac} = 0$, to determine the fluid properties, i.e. density and velocity perturbations. It then constructs the metric in $r < r_0, r_0 < r < r_0 + \Delta$ and $r > r_0$, and checks that the solutions obtained satisfy all 10 Einstein equations. Finally, it constructs and solves the continuity conditions at $r = r_0, r = r_0 + \Delta$, and then evaluates the gravitational wave strain. The output is in `shell.out`.

The script `shellCinI_0.map` is the same as `shell.map` except that: on line 399 `CinI` is hard-coded to be 0, and some output has been suppressed. The output is in `shellCinI_0.out`.

The script `regular_0_IncomingGW.map` is an adaptation of the script `regular_0.map` used in [206] to calculate the GWs emitted by an equal mass binary. The adaptations are: (a) an incoming wave, as a free parameter, is included; and (b) the coefficient names have been changed to be consistent with those used in `shell.map`. The output is in `regular_0_IncomingGW.out`.

The file `formulas.pdf` is in pdf format and contains the Maple output for

$\beta^{[B]}, W^{[B]}, \beta^{[2,2,I]}, J^{[2,2,I]}, U^{[2,2,I]}, W^{[2,2,I]}, C_{1I}, C_{5I}, \rho^{[2,2]}, V_0^{[2,2]}, V_1^{[2,2]}, V_{ang}^{[2,2]}$
$\beta^{[2,2,S]}, J^{[2,2,S]}, U^{[2,2,S]}, W^{[2,2,S]}, C_{1S}, C_{5S}, \beta^{[2,2,E]}, J^{[2,2,E]}, U^{[2,2,E]}, W^{[2,2,E]}, C_{1E}, C_{5E},$
$\mathcal{N}^{[2,2]}, b_{0E}, C_{3E}, C_{4E}, C_{inS}, b_{0S}, C_{3S}, C_{4S}, C_{inI}$ .

The formulas for the above are generated during the execution of `shell.map` and written to the file `formulas.out`.

The file `Eqs.pdf` is in pdf format and includes the content of `paperEqs.out` with annotations, together with the formulas for $\beta^{[B]}, W^{[B]}$ within the matter shell extracted from `backgroundShell.out`.

## Maple output for some equations in the paper

The metric variables used in the code, together with the quantities that they represent, are:

| | |
|---|---|
| `Be` | $\beta^{[e]}$ |
| `Jb` | $\bar{J}^{[e]}$ |
| `Je` | $J^{[e]}$ |
| `Ube` | $\bar{U}^{[e]}$ |
| `Ue` | $U^{[e]}$ |
| `wn` | $W^{[e]}$ |
| `W0` | $W^{[B]}$ |
| `B0` | $\beta^{[B]}$ |
| `b22` | $\beta^{[2,2]}$ |
| `j22` | $J^{[2,2]}$ |
| `u22` | $U^{[2,2]}$ |
| `w22` | $W^{[2,2]}$ |
| `Rho0` | $\rho^{[B]}$ |
| `Rho22` | $\rho^{[2,2]}$ |
| `v220` | $V_0^{[B]}$ |
| `v221` | $V_1^{[B]}$ |
| `V22ang` | $V_{ang}^{[B]}$ |
| `omm` | $\nu$ |
| `Rhoc` | $\rho_c$ |
| `eps` | $\epsilon$ |
| `Pi` | $\pi$ |

The indices in square brackets [ ] after each quantity indicate how it is to be differentiated:

| | |
|---|---|
| `[0, 0]` | Undifferentiated |
| `[0, 1]` | $\partial_r$ |
| `[0, 2]` | $\eth$ |
| `[0, 3]` | $\bar{\eth}$ |
| `[0, 4]` | $\partial_u$ |
| `[1, 1]` | $\partial_r^2$ |
| `[1, 2]` | $\eth\partial_r$ |
| `[1, 3]` | $\bar{\eth}\partial_r$ |
| `[1, 4]` | $\partial_u\partial_r$ |
| `[2, 2]` | $\eth^2$ |
| `[2, 3]` | $\eth\bar{\eth}$ (*N.B.* Here the order is important) |
| `[2, 4]` | $\eth\partial_u$ |
| `[3, 3]` | $\bar{\eth}^2$ |
| `[3, 4]` | $\bar{\eth}\partial_u$ |
| `[4, 4]` | $\partial_u^2$ |

Note that the smallness parameters `eps, Rhoc` (equivalent to $\epsilon, \rho_c$) appear explictly in the code output, but not in the paper.

```
read `initialize.map`;
read `ProcsRules.map`:
#N.B. Basis is not sZlm but \eth Zlm, etc.

#Tab:=array(1..4,1..4);
Vu:=array([0,0,0,Vu0]):Vd:=array(1..4):
read `gamma.out`:
read `lin.map`:

t1:=prlinRhoc(pr2(g_exp[4,4]+1)):
Vu0:=prlinRhoc(subs(eps=0,(1+t1/2+3*t1^2/8))):
t2:=sum(sum(Vu[a]*Vu[b]*g_exp[a,b],a=1..4),b=1..4):
check_Vu0:=prlinRhoc(subs(eps=0,t2+1));
for a to 4 do for b to 4 do
  Tab_up_exp[a,b]:=prlinRhoc(pr2((Rhoc*Rho0)*Vu[a]*Vu[b])):
od:od:
unassign('a'):unassign('b'):
D_Tab_up:=pr_D_Tab_up(Tab_up_exp,x,C):
for a to 4 do
  Vd[a]:=sum(Vu[b]*g_exp[a,b],b=1..4):
  Vd[a]:=prlinRhoc(subs(eps=0,Vd[a])):
od:
for a to 4 do for b to 4 do
  Tab_down_exp[a,b]:=prlinRhoc(subs(eps=0,(Rhoc*Rho0)*Vd[a]*Vd[b])):
od:od:
unassign('a'):unassign('b'):
D_Tab_down:=pr_D_Tab_down(Tab_down_exp,x,C,h):
check_DTup_DTdown:=prlinRhoc(subs(eps=0,D_Tab_down[1]-sum(D_Tab_up[a2]*g[1,a2],a
2=1..4)));
for a to 4 do
  D_Tab_down[a]:=prlinRhoc(subs(eps=0,D_Tab_down[a])):
od:
unassign('a'):
print(`D_Tab_down=`,D_Tab_down);
for a to 4 do for b to 4 do
  Tab[a,b]:=subs(rule1,Tab_down_exp[a,b]):
od:od:
unassign('a'):unassign('b'):

prRHS(Tab_down_exp,g,h):
prBackInShellOut(Rhoc*rho_falloff,Rho0,B0,B1,B11,W0,W1,W11):

print(`***Shell Solution***`);
check_DE_R11:=prlinRhoc(subs(ruleBackShell,eps=0,R11e-BackRHS_R11));
check_DE_R1A:=prlinRhoc(subs(ruleBackShell,eps=0,Rqe-RHS_R1A));
check_DE_Rw:=prlinRhoc(subs(rule1,ruleBackShell,eps=0,Rwe-BackRHS_Rw));
check_DE_ev2:=prlinRhoc(subs(ruleBackShell,eps=0,ev2e-BackRHS_ev2e));
check_constraint00:=prlinRhoc(subs(rule1,ruleBackShell,eps=0,R44e-BackRHS_R00));
check_constraint01:=prlinRhoc(subs(rule1,ruleBackShell,eps=0,R14e-BackRHS_R01));
check_constraint0A:=prlinRhoc(subs(ruleBackShell,eps=0,Rq4e-BackRHS_R0A));

print(`***In Solution***`);
check_DE_R11:=prlinRhoc(subs(ruleBackIn,eps=0,R11e));
check_DE_R1A:=prlinRhoc(subs(ruleBackIn,eps=0,Rqe));
```

```
check_DE_Rw:=prlinRhoc(subs(rule1,ruleBackIn,eps=0,Rwe));
check_DE_ev2:=prlinRhoc(subs(ruleBackIn,eps=0,ev2e));
check_constraint00:=prlinRhoc(subs(rule1,ruleBackIn,eps=0,R44e));
check_constraint01:=prlinRhoc(subs(rule1,ruleBackIn,eps=0,R14e));
check_constraint0A:=prlinRhoc(subs(ruleBackIn,eps=0,Rq4e));

print(`***Out Solution***`);
check_DE_R11:=prlinRhoc(subs(ruleBackOut,eps=0,R11e));
check_DE_R1A:=prlinRhoc(subs(ruleBackOut,eps=0,Rqe));
check_DE_Rw:=prlinRhoc(subs(rule1,ruleBackOut,eps=0,Rwe));
check_DE_ev2:=prlinRhoc(subs(ruleBackOut,eps=0,ev2e));
check_constraint00:=prlinRhoc(subs(rule1,ruleBackOut,eps=0,R44e));
check_constraint01:=prlinRhoc(subs(rule1,ruleBackOut,eps=0,R14e));
check_constraint0A:=prlinRhoc(subs(ruleBackOut,eps=0,Rq4e));

insContinuousB0:=simplify(subs(r=r0,B0shell-B0in));
insContinuousB1:=simplify(subs(r=r0,B1shell-B1in));
insContinuousB11:=simplify(subs(r=r0,B11shell-B11in));
insContinuousW0:=simplify(subs(r=r0,W0shell-W0in));
insContinuousW1:=simplify(subs(r=r0,W1shell-W1in));
insContinuousW11:=simplify(subs(r=r0,W11shell-W11in));
ousContinuousB0:=simplify(subs(r=r0+del,B0out-B0shell));
ousContinuousB1:=simplify(subs(r=r0+del,B1out-B1shell));
ousContinuousB11:=simplify(subs(r=r0+del,B11out-B11shell));
ousContinuousW0:=simplify(subs(r=r0+del,W0out-W0shell));
ousContinuousW1:=simplify(subs(r=r0+del,W1out-W1shell));
ousContinuousW11:=simplify(subs(r=r0+del,W11out-W11shell));

assume(r0>0):assume(del>0):
Mshell:=factor(int(4*Pi*r^2*rho_falloff,r=r0..r0+del));
W0out:=factor(W0out);
B0out:=simplify(B0out);
W0in:=simplify(W0in);
B0in:=simplify(B0in);
W0shell:=factor(simplify(W0shell));
B0shell:=factor(simplify(B0shell));
```

```
x:=array([r,q,p,u]):
#f:= 1+p^2+q^2:
fo:=f+q*fqo+p*fpo:
fq:=fqo+q*2:
fp:=fpo+p*2:

J:=array(0..4): Jb:=array(0..4): K:=array(0..4): B:=array(0..4):
U:=array(0..4): Ub:=array(0..4): Vw:=array(0..4):
Jn:=array(0..4,0..4): Jbn:=array(0..4,0..4): Je:=array(0..4,0..4):
Jbe:=array(0..4,0..4):
Kn:=array(0..4,0..4): Bn:=array(0..4,0..4): Be:=array(0..4,0..4):
Un:=array(0..4,0..4): Ubn:=array(0..4,0..4): Ue:=array(0..4,0..4):
Ube:=array(0..4,0..4):
Va:=array(0..4,0..4): wn:=array(0..4,0..4):

C:=array(1..4,1..4,1..4):
Csum:=array(1..4):
g:=array(1..4,1..4):
h:=array(1..4,1..4):
g_exp:=array(1..4,1..4):
h_exp:=array(1..4,1..4):
R:=array(1..4,1..4):
Riem:=array(1..4,1..4,1..4,1..4):
Riemd:=array(1..4,1..4,1..4,1..4):
weyl:=array(1..4,1..4,1..4,1..4):
Ric:=array(1..4,1..4):
Tab:=array(1..4,1..4):
Tab_down_exp:=array(1..4,1..4):
Tab_up_exp:=array(1..4,1..4):
D_Tab_up:=array(1..4):
D_Tab_down:=array(1..4):

n:=2:
L2:=-n*(n+1): # \eth\bar{\eth}
L4:=L2^2+2*L2:  #\eth^2\bar{\eth}^2
alias(B0=B0(r)):alias(W0=W0(r)):
alias(Rho0=Rho0(r)):
B14:=0:B4:=0:B44:=0:W14:=0:W4:=0:W44:=0:
rho_falloff:=(1/r^3-r0/r^4)*((r0+del)/r^4-1/r^3); #For finite shell
#rho_falloff:=(1/r^2-r0/r^3)*((r0+del)/r^5-1/r^4); #For finite shell
#rho_falloff:=(1/r^2-r0/r^3)*((r0+del)/r^6-1/r^5); #For finite shell
#rho_falloff:=(1/r^3-r0/r^4)*((r0+del)^2/r^5-1/r^3): #For finite shell
#rho_falloff:=(1/r^4-r0/r^5)*((r0+del)/r^4-1/r^3): #For finite shell
```

```
  pr1(J,Jn,2):
  pr1(Jb,Jbn,-2):
  pr1(K,Kn,0):
  pr1(B,Bn,0):
  pr1(U,Un,1):
  pr1(Ub,Ubn,-1):
  pr1(Vw,Va,0):

for a7 from 1 to 4 do for b7 from 1 to 4 do
h_exp[a7,b7]:=h[a7,b7]:
g_exp[a7,b7]:=g[a7,b7]:
h[a7,b7]:=subs(rule1,h_exp[a7,b7]):
g[a7,b7]:=subs(rule1,g_exp[a7,b7]):
od; od;

R[1,1]:=prR(1,1):
R[1,2]:=prR(1,2):
R[1,3]:=prR(1,3):
Rq:=simplify(f*(R[1,2]+I*R[1,3])/2):#Rq=q^A R_{1A}
R[2,2]:=prR(2,2):
R[2,3]:=prR(2,3):
R[3,3]:=prR(3,3):
a5:=simplify(h[2,2]*R[2,2]):
a6:=simplify(2*h[2,3]*R[2,3]):
a7:=simplify(h[3,3]*R[3,3]):
Rw:=simplify(r^2*(a5+a6+a7)):#Rw=h^{AB} R_{AB}
ev1:=simplify(f^2/4*(R[2,2]-R[3,3]+2*I*R[2,3])):#ev1=q^A q^B R_{AB}
ev2:=simplify(ev1-Jn[0,0]*Rw):
R[4,4]:=prR(4,4):
R[1,4]:=prR(1,4):
R[2,4]:=prR(2,4):
R[3,4]:=prR(3,4):

prLin(Kn,Je,Jbe,Be,Ue,Ube,wn,Jn,Jbn,Bn,Un,Ubn,Va);
R11e:=simplify(pr2(R[1,1]));
Rqe:=simplify(subs(rule1,pr2(Rq)));
Rwe:=simplify(pr2(Rw));
ev1e:=simplify(subs(rule1,pr2(ev1)));
ev2e:=simplify(subs(rule1,pr2(ev2)));
R14e:=simplify(pr2(R[1,4]));
R44e:=simplify(pr2(R[4,4]));
R24e:=simplify(pr2(R[2,4])):
R34e:=simplify(pr2(R[3,4])):
Rq4e:=simplify(subs(rule1,f*(R24e+I*R34e)/2));
#check_R11e:=simplify(subs(rule2,R11e));
#check_Rqe:=simplify(subs(rule2,Rqe));
#check_Rwe:=simplify(subs(rule2,Rwe));
#check_ev2e:=simplify(subs(rule2,ev2e));
#check_R14e:=simplify(subs(rule2,R14e));
#check_R44e:=simplify(subs(rule2,R44e));
#check_Rq4e:=simplify(subs(rule2,Rq4e));

FIN;
```

```
read `initialize.map`:
read `ProcsRules.map`:
read `gamma.out`:
read `lin.map`:
#Formulas valid for $\ell=2$ ONLY

alias(b22=b22(r)):alias(j22=j22(r)):alias(u22=u22(r)):alias(w22=w22(r)):
B1:=diff(B0,r):B11:=diff(B0,r,r):W1:=diff(W0,r):W11:=diff(W0,r,r):
om:=I*omm:
S2:=sqrt(-L2):

(* #For basis \eth^s Z_{\ell,m}:
ruleconsIn:={Be[2, 3]=L2*b22, wn[2, 3]=L2*w22, wn[1, 1]=diff(w22,r,r), Be[0,
1]=diff(b22,r),Be[1, 4]=om*diff(b22,r), Be[0, 4]=om*b22,
           Ue[3, 4]=om*L2*u22,Ube[2, 4]=om*L2*u22,wn[0, 4]=om*w22, Je[3,
4]=om*(L2+2)*j22, Be[2, 4]=om*b22,Je[1,4]=om*diff(j22,r),
           Je[0,4]=om*j22,Ue[1, 4]=om*diff(u22,r),Be[1, 1]=diff(b22,r,r), wn[0,
0]=w22, wn[0, 1]=diff(w22,r), Ube[0, 2]=L2*u22,
           Ue[0, 3]=L2*u22, Ue[2, 3]=L2*u22, Ube[2, 2]=L2*u22, wn[1,
2]=diff(w22,r), wn[0, 2]=w22,  Ue[0, 0]=u22, Ue[0, 1]=diff(u22,r),
           Ue[1, 1]=diff(u22,r,r), Ube[1, 2]=L2*diff(u22,r), Ue[1, 3]
=L2*diff(u22,r),Be[0,0]=b22, Be[0,2]=b22,Be[1,2]=diff(b22,r),

Be[2,2]=b22,Je[1,3]=(L2+2)*diff(j22,r),Je[3,3]=L4*j22,Jbe[2,2]=L4*j22,Je[1,1]=di
ff(j22,r,r), Je[0,1]=diff(j22,r), Ue[0,2]=u22,
           Ue[1,2]=diff(u22,r)}:*)

#For basis {}_sZ_{\ell,m}
ruleconsIn:={Be[2, 3]=L2*b22, wn[2, 3]=L2*w22, wn[1, 1]=diff(w22,r,r), Be[0,
1]=diff(b22,r),
           Be[1, 4]=om*diff(b22,r), Be[0, 4]=om*b22,Je[1,1]=diff(j22,r,r),
           Je[0,1]=diff(j22,r),
           wn[0, 4]=om*w22,Je[1,4]=om*diff(j22,r),
           Je[0,4]=om*j22,Ue[1, 4]=om*diff(u22,r),
           Be[1, 1]=diff(b22,r,r), wn[0, 0]=w22, wn[0, 1]=diff(w22,r),  Ue[0,
0]=u22,
           Ue[0, 1]=diff(u22,r), Ue[1, 1]=diff(u22,r,r), Be[0,0]=b22,
           Ube[1, 2]=-S2*diff(u22,r), Ue[1, 3] =-S2*diff(u22,r),
           Be[0,2]=S2*b22,Be[1,2]=S2*diff(b22,r),Be[2,2]=2*S2*b22,
           Je[1,3]=(L2+2)*diff(j22,r)/2,Je[3,3]=2*S2*j22,Jbe[2,2]=2*S2*j22,
Ue[0,2]=2*u22,Ue[1,2]=2*diff(u22,r), Ue[3, 4]=-om*S2*u22,
           Ube[2, 4]=-om*S2*u22, Je[3, 4]=om*(L2+2)*j22/2, Be[2, 4]=S2*om*b22,
Ube[0, 2]=-S2*u22, Ue[0, 3]=-S2*u22,
           Ue[2, 3]=L2*u22, Ube[2, 2]=L2*u22, wn[1, 2]=S2*diff(w22,r), wn[0,
2]=S2*w22}:

Vd:=array(1..4,[-1+eps*v221,eps*(V22ang+V22angb)/fo,eps*I*(V22angb-V22ang)/fo,-1
+eps*v220]):
for a to 4 do for b to 4 do
  Tab_down[a,b]:=prlinRhoc(pr2((Rhoc*Rho0+Rhoc*eps*Rho22)*Vd[a]*Vd[b])):
od:od:
t1:=0:
for a to 4 do for b to 4 do
t1:=t1+Vd[a]*Vd[b]*h[a,b]:
```

```
 od:od:
t2:=pr2(subs(Rhoc=0,t1)):
t3:=solve(t2=-1,v220): #Set $V_0^{[2,2]}$ using the condition $V_a V_b
g^{ab}=-1$

prRHS(Tab_down,g,h):
R11e:=prlinRhoc(subs(rule1,R11e));
Rqe:=prlinRhoc(subs(rule1,Rqe));
Rwe:=prlinRhoc(subs(rule1,Rwe));
ev2e:=prlinRhoc(subs(rule1,ev2e));
E11_22:=prlinRhoc(subs(ruleconsIn,rule1,coeff(R11e,eps)))=coeff(subs(ruleconsIn,
RHS_R11),eps);
E1q_22:=prlinRhoc(subs(ruleconsIn,rule1,coeff(Rqe,eps)))=coeff(subs(ruleconsIn,R
HS_R1A),eps);
Ew_22:=prlinRhoc(subs(ruleconsIn,rule1,coeff(Rwe,eps)))=simplify(coeff(subs(v220
=t3,rule1,ruleconsIn,RHS_Rw),eps));
Eev2_22:=prlinRhoc(subs(ruleconsIn,rule1,coeff(ev2e,eps)))=coeff(subs(ruleconsIn
,RHS_ev2e),eps);
E44_22:=prlinRhoc(subs(ruleconsIn,rule1,coeff(R44e,eps)))=coeff(subs(v220=t3,rul
e1,ruleconsIn,RHS_R00),eps);
E14_22:=prlinRhoc(subs(ruleconsIn,rule1,coeff(R14e,eps)))=coeff(subs(ruleconsIn,
RHS_R01),eps);
Eq4_22:=prlinRhoc(subs(ruleconsIn,rule1,coeff(Rq4e,eps)))=coeff(subs(ruleconsIn,
RHS_R0A),eps);
```

```
rule1:={ro=r,u=0,q=0,p=0,f=1+fqo^2/4+fpo^2/4};

pr1:=proc(X,y,s)
X[0]:=y[0,0]+(r-ro)*y[0,1]+u*y[0,4]+q*(y[0,3]+y[0,2]-s*I*fp*y[0,0])/fo
          +p*(y[0,3]-y[0,2]+s*fq*y[0,0])*I/fo:

X[1]:=y[0,1]+(r-ro)*y[1,1]+u*y[1,4]+q*(y[1,3]+y[1,2]-s*I*fp*y[0,1])/fo
          +p*(y[1,3]-y[1,2]+s*fq*y[0,1])*I/fo:

X[2]:=y[0,2]+(r-ro)*y[1,2]+u*y[2,4]
          +q*(y[2,3]+2*s*y[0,0]+y[2,2]-(s+1)*I*fp*y[0,2])/fo
          +p*(y[2,3]+2*s*y[0,0]-y[2,2]+(s+1)*fq*y[0,2])*I/fo:

X[3]:=y[0,3]+(r-ro)*y[1,3]+u*y[3,4]+q*(y[3,3]+y[2,3]-(s-1)*I*fp*y[0,3])/fo
          +p*(y[3,3]-y[2,3]+(s-1)*fq*y[0,3])*I/fo:

X[4]:=y[0,4]+(r-ro)*y[1,4]+u*y[4,4]+q*(y[3,4]+y[2,4]-s*I*fp*y[0,4])/fo
          +p*(y[3,4]-y[2,4]+s*fq*y[0,4])*I/fo:
end;

pr_D_Tab_up:=proc(Tab,x,C):
  DT:=array(1..4):
  for a to 4 do
    DT[a]:=0:
    for b to 4 do
      DT[a]:=DT[a]+diff(Tab[a,b],x[b]):
      for c to 4 do
        DT[a]:=DT[a]+Tab[c,b]*C[c,b,a]+Tab[a,c]*C[c,b,b]:
    od:od:
#    DT[a]:=prlinRhoc(pr2(subs(rule1,DT[a]))):
     DT[a]:=(pr2(subs(rule1,DT[a]))):
  od:
  return(array([DT[1],DT[2],DT[3],DT[4]])):
end:

pr_D_Tab_down:=proc(Tab,x,C,h):
  DT:=array(1..4):
  for a to 4 do
    DT[a]:=0:
    for b to 4 do for c to 4 do
      DT[a]:=DT[a]+diff(Tab[a,b],x[c])*h[b,c]:
      for d to 4 do
        DT[a]:=DT[a]-(Tab[d,b]*C[a,c,d]+Tab[a,d]*C[c,b,d])*h[b,c]:
    od:od:od:
#    DT[a]:=prlinRhoc(pr2(subs(rule1,DT[a]))):
     DT[a]:=(pr2(subs(rule1,DT[a]))):
  od:
  return(array([DT[1],DT[2],DT[3],DT[4]])):
end:


prR:=proc(a,b) local a1,a2,a3,a4,a5,b2,b3,b4;
a1:=diff(C[a,b,1],x[1])+diff(C[a,b,2],x[2])+diff(C[a,b,3],x[3])
```

```
    +diff(C[a,b,4],x[4]);
a2:=-diff(Csum[a],x[b]);
a3:=sum( Csum[b2]*C[a,b,b2],b2=1..4);
a4:=-sum( sum( C[a,b3,b4]*C[b,b4,b3],b3=1..4),b4=1..4);

a1:=subs(rule1,a1);
a2:=subs(rule1,a2);
a3:=subs(rule1,a3);
a4:=subs(rule1,a4);
a5:=0:#subs(rule1,-3*alpha^2*g[a,b]);

R[a,b]:=simplify(a1+a2+a3+a4+a5);
end;

prlinRhoc:=proc(A)
t1:=simplify(subs(Rhoc=0,A))+Rhoc*simplify(subs(Rhoc=0,diff(A,Rhoc))):
return(t1):
end proc;

pr0:=proc(xns,X,s)
     xns:=X[0]+(r-ro)*X[1]+q*(X[3]+X[2]-s*I*fp*X[0])/fo
          +p*(X[3]-X[2]+s*fq*X[0])*I/fo:
end;

pr_n0:=proc(xns,X,s)
     xns:=X[0]+(r-ro)*X[1]+q*(X[3]+X[2]-s*I*fp*X[0])/fo
          +p*(X[3]-X[2]+s*fq*X[0])*I/fo+u*X[4]:
end;

pr2:=proc(A)
t1:=simplify(subs(eps=0,A))+eps*simplify(subs(eps=0,diff(A,eps))):
return(t1):
end:


prRiem:=proc(a,b,c,d) local a1,a2,a3,a4,b2,b3;
a1:=diff(C[b,d,a],x[c]);
a2:=-diff(C[b,c,a],x[d]);
a3:=sum( C[b2,c,a]*C[b,d,b2],b2=1..4);
a4:=-sum( C[b,c,b3]*C[b3,d,a],b3=1..4);
a1:=subs(rule1,a1);
a2:=subs(rule1,a2);
a3:=subs(rule1,a3);
a4:=subs(rule1,a4);
Riem[a,b,c,d]:=simplify(a1+a2+a3+a4);
end;

#jr:=sqrt(6)*((24*b0-I*(4*nu*alpha^2+nu^3)*c3+3*I*nu*c1)/18+c1/2/r-c3/r^3/6):
#ur:=sqrt(6)*((-24*I*nu*b0+3*(3*alpha^2+nu^2)*c1-nu^2*c3*(4*alpha^2+nu^2))/36
#    +2*b0/r+c1/2/r^2+c3*I*nu/3/r^3+c3/4/r^4):
#wr:=-2*b0*alpha^2*r^3+r^2/6*(24*I*nu*b0-3*c1*(nu^2+3*alpha^2)
#                             +nu^2*c3*(nu^2+4*alpha^2))
#    +r/3*(-6*b0+3*I*nu*c1-c3*I*nu*(nu^2+4*alpha^2))-c3*(nu^2+alpha^2)+c3*I*nu/r
#    +c3/2/r^2:
```

```
rule2:={wn[0,0]=wr,wn[0,1]=diff(wr,r),wn[1,1]=diff(wr,r,r),wn[0,2]=wr*sqrt(6),
        wn[1,2]=diff(wr,r)*sqrt(6),wn[2,2]=wr*2*sqrt(6),
        wn[0,4]=wr*I*nu,wn[2,3]=-6*wr,
        Ue[0,0]=ur,Ue[0,2]=2*ur,Ue[1,4]=diff(ur,r)*I*nu,Ue[2,4]=I*nu*2*ur,
        Ue[1,2]=2*diff(ur,r),
        Ue[0,1]=diff(ur,r),Ue[1,1]=diff(ur,r,r),

Ue[1,3]=-diff(ur,r)*sqrt(6),Ue[0,3]=-sqrt(6)*ur,Ue[3,4]=-sqrt(6)*I*nu*ur,
        Ue[2,3]=-6*ur,

Ube[0,2]=-sqrt(6)*ur,Ube[1,2]=-sqrt(6)*diff(ur,r),Ube[2,4]=-sqrt(6)*I*nu*ur,
        Ube[2,2]=-6*ur,
        Be[0,0]=b0,Be[0,1]=0,Be[1,1]=0,Be[1,2]=0,Be[1,4]=0,Be[0,2]=sqrt(6)*b0,
        Be[0,4]=I*nu*b0,Be[2,3]=-6*b0,
        Be[2,4]=I*nu*sqrt(6)*b0,Be[2,2]=2*sqrt(6)*b0,
        Je[0,1]=diff(jr,r),Je[0,4]=I*nu*jr,Je[4,4]=-nu^2*jr,
        Je[1,3]=-2*diff(jr,r),Je[3,4]=-2*I*nu*jr,
        Je[1,1]=diff(jr,r,r),Je[1,4]=diff(jr,r)*I*nu,Je[3,3]=2*sqrt(6)*jr,
        Jbe[2,2]=2*sqrt(6)*jr,Je[0,0]=jr
};

prLin:=proc(Kn,Je,Jbe,Be,Ue,Ube,wn,Jn,Jbn,Bn,Un,Ubn,Va)
for a from 0 to 4 do for b from a to 4 do
  Kn[a,b]:=0;
  Jn[a,b]:=eps*Je[a,b];
  Jbn[a,b]:=eps*Jbe[a,b];
  Bn[a,b]:=eps*Be[a,b];
  Un[a,b]:=eps*Ue[a,b];
  Ubn[a,b]:=eps*Ube[a,b];
  Va[a,b]:=eps*wn[a,b]/r;
od;od;
Kn[0,0]:=1;

Bn[0,0]:=Rhoc*B0+eps*Be[0,0]:
Bn[0,1]:=Rhoc*B1+eps*Be[0,1]:
Bn[1,1]:=Rhoc*B11+eps*Be[1,1]:
Bn[0,4]:=Rhoc*B4+eps*Be[0,4]:
Bn[4,4]:=Rhoc*B44+eps*Be[4,4]:
Bn[1,4]:=Rhoc*B14+eps*Be[1,4]:

#Be[1,1]:=0:
#Be[0,1]:=0: #Comment out this line to check R[1,1]=0

Va[0,0]:=1+Rhoc*W0/ro+eps*wn[0,0]/ro;
Va[0,1]:=Rhoc*W1/ro-Rhoc*W0/ro^2+(ro*eps*wn[0,1]-eps*wn[0,0])/ro^2;
Va[1,1]:=Rhoc*W11/r-2*Rhoc*W1/r^2+2*Rhoc*W0/r^3+eps*(wn[1,1]/r-2*wn[0,1]/r^2+2*w
n[0,0]/r^3);
for a from 2 to 3 do
  Va[1,a]:=eps*(wn[1,a]/r-wn[0,a]/r^2);
#  Be[1,a]:=0:
od;
Va[0,4]:=Rhoc*W4+eps*wn[0,4]/r:
Va[1,4]:=Rhoc*W14+eps*wn[1,4]/r:
```

```
Va[4,4]:=Rhoc*W44+eps*wn[4,4]/r:
#rBe:={Be[0,1]=0,Be[1,1]=0,Be[1,2]=0,Be[1,3]=0,Be[1,4]=0}:
end;

pr2sum:=proc(g,e1,e2)
local a,b:
t1:=sum(sum(g[a,b]*e1[a]*e2[b],b=1..4),a=1..4):
return(pr2(subs(rule2,t1))):
end:

pr4sum:=proc(W,e1,e2,e3,e4)
local a,b,c,d:
t1:=sum(sum(sum(sum(W[a,b,c,d]*e1[a]*e2[b]*e3[c]*e4[d],a=1..4),b=1..4),c=1..4),d
=1..4):
return(pr2(subs(rule2,t1))):
end:

prRHS:=proc(Tab_down_exp,g,h)
global T_trace,RHS_R11,RHS_R1A,RHS_Rw,RHS_ev2e,RHS_R00,RHS_R0A,RHS_R01,

BackRHS_R11,BackRHS_R1A,BackRHS_Rw,BackRHS_ev2e,BackRHS_R00,BackRHS_R0A,BackRHS_
R01:
for a to 4 do for b to 4 do
  Tab[a,b]:=simplify(subs(rule1,Tab_down_exp[a,b])):
  g[a,b]:=simplify(subs(rule1,g[a,b])):
  h[a,b]:=simplify(subs(rule1,h[a,b])):
od:od:
unassign('a'):unassign('b'):

T_trace:=prlinRhoc(pr2(sum(sum(Tab[a,b]*h[a,b],a=1..4),b=1..4))):

RHS_R11:=8*Pi*(Tab[1,1]-g[1,1]*T_trace/2):
BackRHS_R11:=prlinRhoc(subs(eps=0,RHS_R11)):
RHS_R11:=prlinRhoc(eps*coeff(pr2(RHS_R11),eps)):
RHS_R1A:=8*Pi*((Tab[1,2]-g[1,2]*T_trace/2)*fo/2+(Tab[1,3]-g[1,3]*T_trace/2)*I*fo
/2):
BackRHS_R1A:=prlinRhoc(subs(eps=0,RHS_R1A)):
RHS_R1A:=prlinRhoc(eps*subs(rule1,coeff(pr2(RHS_R1A),eps))):
RHS_Rwt:=8*Pi*((Tab[2,2]-g[2,2]*T_trace/2)*r^2*h[2,2]+2*(Tab[2,3]-g[2,3]*T_trace
/2)*r^2*h[2,3]+
              (Tab[3,3]-g[3,3]*T_trace/2)*r^2*h[3,3]):
BackRHS_Rw:=prlinRhoc(subs(eps=0,RHS_Rwt)):
RHS_Rw:=prlinRhoc(eps*coeff(pr2(RHS_Rwt),eps)):
RHS_ev2e:=8*Pi*((Tab[2,2]-g[2,2]*T_trace/2)*fo^2/4+2*(Tab[2,3]-g[2,3]*T_trace/2)
*fo^2/4*I-
              (Tab[3,3]-g[3,3]*T_trace/2)*fo^2/4)-eps*Je[0,0]*RHS_Rwt:
BackRHS_ev2e:=prlinRhoc(subs(eps=0,RHS_ev2e)):
RHS_ev2e:=prlinRhoc(eps*coeff(pr2(RHS_ev2e),eps)):
RHS_ev2e:=simplify(subs(rule1,RHS_ev2e)):
RHS_R00:=8*Pi*(Tab[4,4]-g[4,4]*T_trace/2):
BackRHS_R00:=prlinRhoc(subs(eps=0,RHS_R00)):
RHS_R00:=prlinRhoc(eps*coeff(pr2(RHS_R00),eps)):
RHS_R01:=8*Pi*(Tab[1,4]-g[1,4]*T_trace/2):
BackRHS_R01:=prlinRhoc(subs(eps=0,RHS_R01)):
```

```
RHS_R01:=prlinRhoc(eps*coeff(pr2(RHS_R01),eps)):
RHS_R0A:=8*Pi*((Tab[4,2]-g[4,2]*T_trace/2)*fo/2+(Tab[4,3]-g[4,3]*T_trace/2)*I*fo
/2):
BackRHS_R0A:=prlinRhoc(subs(eps=0,RHS_R0A)):
RHS_R0A:=prlinRhoc(eps*coeff(subs(rule1,pr2(RHS_R0A)),eps)):

end:

prBackInOut:=proc(rho_falloff,Rho0,B0,B1,B11,W0,W1,W11)
global
Back_E1,Back_E2,t1,t2,t2i,B0out,B1out,B11out,B0in,B1in,B11in,W0out,W1out,W11out,
W0in,W1in,W11in,
ruleBackIn,ruleBackOut;
Back_E1:=prlinRhoc(subs(rule1,eps=0,R11e))=BackRHS_R11:
Back_E2:=prlinRhoc(subs(rule1,eps=0,Rwe))=BackRHS_Rw:
Rho0:=rho_falloff:
t1:=solve(Back_E1,B1):
B0out:=int(t1,r):B1out:=t1:B11out:=diff(t1,r):
B0in:=subs(r=r0,B0out):B1in:=0:B11in:=0:
t2:=solve(subs(B0=B0out,Back_E2),W1):
t2i:=int(t2,r):W0out:=simplify(t2i+2*r0*B0in-subs(r=r0,t2i)):W1out:=t2:W11out:=d
iff(t2,r):
W0in:=2*r*B0in:W1in:=2*B0in:W11in:=0:
ruleBackIn:={B0=B0in,B1=B1in,B11=B11in,W0=W0in,W1=W1in,W11=W11in}:
ruleBackOut:={B0=B0out,B1=B1out,B11=B11out,W0=W0out,W1=W1out,W11=W11out}:
end;

prBackInShellOut:=proc(rho_falloff,Rho0,B0,B1,B11,W0,W1,W11)
global
Back_E1,Back_E2,t1,t2,t2i,B0out,B1out,B11out,B0shell,B1shell,B11shell,B0in,B1in,
B11in,
            W0out,W1out,W11out,W0shell,W1shell,W11shell,W0in,W1in,W11in,
            ruleBackIn,ruleBackShell,ruleBackOut;
Back_E1:=prlinRhoc(subs(rule1,eps=0,R11e))=BackRHS_R11:
Back_E2:=prlinRhoc(subs(rule1,eps=0,Rwe))=BackRHS_Rw:
Rho0:=rho_falloff:
t1:=solve(Back_E1,B1):
t11:=int(t1,r):B0shell:=t11-subs(r=r0+del,t11):B1shell:=t1:B11shell:=diff(t1,r):
B0in:=subs(r=r0,B0shell):B1in:=0:B11in:=0:
B0out:=0:B1out:=0:B11out:=0:
t2:=solve(subs(B0=B0shell,Back_E2),W1):
t2i:=int(t2,r):W0shell:=simplify(t2i+2*r0*B0in-subs(r=r0,t2i)):W1shell:=t2:W11sh
ell:=diff(t2,r):
W0in:=2*r*B0in:W1in:=2*B0in:W11in:=0:
W0out:=subs(r=r0+del,W0shell):W1out:=0:W11out:=0:
ruleBackIn:={B0=B0in,B1=B1in,B11=B11in,W0=W0in,W1=W1in,W11=W11in}:
ruleBackOut:={B0=B0out,B1=B1out,B11=B11out,W0=W0out,W1=W1out,W11=W11out}:
ruleBackShell:={B0=B0shell,B1=B1shell,B11=B11shell,W0=W0shell,W1=W1shell,W11=W11
shell}:
end;

prMakeDE:=proc()
global
D1r,D2r,tr,D1x,D2x,D3x,D1x1,D1x2,D1x3,D2x1,D2x2,D2x3,D3x1,D3x2,D3x3,st,de,de1,de
```

```
2,de3,de3a,Z0,de3b:
uses PDEtools:
D1r:=subs(rule2de,eps*coeff(prlinRhoc(Rqe),eps)=RHS_R1A);
D2r:=subs(rule2de,eps*coeff(prlinRhoc(ev2e),eps)=RHS_ev2e);
tr:={r=1/xx}:
D1x:=simplify(dchange(tr,D1r));
D2x:=simplify(dchange(tr,D2r));
D3x:=diff(D2x,xx);
D1x1:=simplify(subs(diff(Z(xx),xx,xx)=Z2,D1x)):
D1x2:=simplify(subs(diff(Z(xx),xx)=Z1,D1x1)):
D1x3:=simplify(subs(Z(xx)=Z0,D1x2)):
D2x1:=simplify(subs(diff(Z(xx),xx,xx)=Z2,D2x)):
D2x2:=simplify(subs(diff(Z(xx),xx)=Z1,D2x1)):
D2x3:=simplify(subs(Z(xx)=Z0,D2x2)):
D3x1:=simplify(subs(diff(Z(xx),xx,xx)=Z2,D3x)):
D3x2:=simplify(subs(diff(Z(xx),xx)=Z1,D3x1)):
D3x3:=simplify(subs(Z(xx)=Z0,D3x2)):
st:=solve({D1x3,D2x3,D3x3},{Z0,Z1,Z2}):

assign(st):
de:=simplify(diff(Z0,xx)-Z1)=0:
de1:=subs(diff(JJ(xx),xx$4)=diff(J2(xx),xx$2),de):
de2:=subs(diff(JJ(xx),xx$3)=diff(J2(xx),xx),de1):
de3:=subs(diff(JJ(xx),xx$2)=J2(xx),de2):
de3:=prlinRhoc(de3):
de3a:=subs(Rhoc=0,de3):de3a:=simplify(de3a);
de3b:=Rhoc*coeff(lhs(de3),Rhoc):
end:

prMakeDEInOut:=proc(ruleBack,InOutFac)
global
D1r,D2r,tr,D1x,D2x,D3x,D1x1,D1x2,D1x3,D2x1,D2x2,D2x3,D3x1,D3x2,D3x3,st,de,de1,de
2,de3,de3a,Z0,de3b:
uses PDEtools:
D1r:=subs(rule2de,ruleBack,eps*coeff(prlinRhoc(Rqe),eps)=InOutFac*RHS_R1A);
D2r:=subs(rule2de,ruleBack,eps*coeff(prlinRhoc(ev2e),eps)=InOutFac*RHS_ev2e);
tr:={r=1/xx}:
D1x:=simplify(dchange(tr,D1r));
D2x:=simplify(dchange(tr,D2r));
D3x:=diff(D2x,xx);
D1x1:=simplify(subs(diff(Z(xx),xx,xx)=Z2,D1x)):
D1x2:=simplify(subs(diff(Z(xx),xx)=Z1,D1x1)):
D1x3:=simplify(subs(Z(xx)=Z0,D1x2)):
D2x1:=simplify(subs(diff(Z(xx),xx,xx)=Z2,D2x)):
D2x2:=simplify(subs(diff(Z(xx),xx)=Z1,D2x1)):
D2x3:=simplify(subs(Z(xx)=Z0,D2x2)):
D3x1:=simplify(subs(diff(Z(xx),xx,xx)=Z2,D3x)):
D3x2:=simplify(subs(diff(Z(xx),xx)=Z1,D3x1)):
D3x3:=simplify(subs(Z(xx)=Z0,D3x2)):
st:=solve({D1x3,D2x3,D3x3},{Z0,Z1,Z2}):

assign(st):
de:=simplify(diff(Z0,xx)-Z1)=0:
de1:=subs(diff(JJ(xx),xx$4)=diff(J2(xx),xx$2),de):
```

```
de2:=subs(diff(JJ(xx),xx$3)=diff(J2(xx),xx),de1):
de3:=subs(diff(JJ(xx),xx$2)=J2(xx),de2):
de3:=prlinRhoc(de3):
de3a:=subs(Rhoc=0,de3):de3a:=simplify(de3a);
de3b:=Rhoc*coeff(lhs(de3),Rhoc):
end:


pr_Intx2:=proc(rd,ru)
global st,st_poly,st_Ei,st_Ei_t,int_st_Ei,int_st:
st:=algsubs(Ei(1,I*s)=-Ei(-I*s),st);
st_poly:=simplify(algsubs(exp(I*s)=0,st));
st_Ei:=simplify(st-st_poly);
st_Ei_t:=array(rd..ru):
for a from (rd+1) to ru do
st_Ei_t[a]:=-exp(s*I)*Ei(-I*s)*s^a*2*omm*coeff(algsubs(exp(s*I)*Ei(-I*s)=1,st_Ei
),s,a+2):
od:
int_st_Ei:=int(st_Ei_t[1]+st_Ei_t[0],s);
for a from (ru-2) by -1 to (rd+1) do
c1:=algsubs(exp(s*I)*Ei(-I*s)=1,st_Ei_t[a]);
int_st_Ei:=int_st_Ei-I*c1*(-1/a+exp(s*I)*Ei(-I*s));
st_Ei_t[a-1]:=st_Ei_t[a-1]+a*I*c1*exp(s*I)*Ei(-I*s)/s;
od;
int_st:=simplify(int_st_Ei+int(-st_poly/s^2*2*omm,s));
end:
```

```
n:=2:
Order:=2*n+4:
bin:=0:
M:=0:MM:=0:
L2:=-n*(n+1): # \eth\bar{\eth}
L4:=L2^2+2*L2:  #\eth^2\bar{\eth}^2

D1r:=4*b0+r^3*diff(Z(r),r,r)+4*r^2*diff(Z(r),r)
      +(L2+2)*r*diff(J(r),r)=0:
D2r:=-2*b0+r^2*diff(Z(r),r)+2*r*Z(r)-2*(r+M)*diff(J(r),r)
     -r*(r+2*M)*diff(J(r),r,r)+2*r^2*om*diff(J(r),r)
     +2*r*om*J(r)=0:
tr:={r=1/x}:
with(PDEtools):
D1x:=simplify(dchange(tr,D1r)):
D2x:=simplify(dchange(tr,D2r)):
D3x:=diff(D2x,x):
D1x1:=simplify(subs(diff(Z(x),x,x)=Z2,D1x)):
D1x2:=simplify(subs(diff(Z(x),x)=Z1,D1x1)):
D1x3:=simplify(subs(Z(x)=Z0,D1x2)):
D2x1:=simplify(subs(diff(Z(x),x,x)=Z2,D2x)):
D2x2:=simplify(subs(diff(Z(x),x)=Z1,D2x1)):
D2x3:=simplify(subs(Z(x)=Z0,D2x2)):
D3x1:=simplify(subs(diff(Z(x),x,x)=Z2,D3x)):
D3x2:=simplify(subs(diff(Z(x),x)=Z1,D3x1)):
D3x3:=simplify(subs(Z(x)=Z0,D3x2)):
st:=solve({D1x3,D2x3,D3x3},{Z0,Z1,Z2}):
assign(st):
de:=simplify(diff(Z0,x)-Z1)=0:
de1:=subs(diff(J(x),x$4)=diff(J2(x),x$2),de):
de2:=subs(diff(J(x),x$3)=diff(J2(x),x),de1):
de3:=subs(diff(J(x),x$2)=J2(x),de2):
s1:=dsolve(de3,J2(x)):
assign(s1):
if(limit(subs(_C2=0,J2(x)),x=0)=0) then
    J2out:=subs(_C2=CinI,_C1=C40I*6,J2(x)):
elif(limit(subs(_C1=0,J2(x)),x=0)=0) then
    J2out:=subs(_C1=CinI,_C2=C40I*6,J2(x)):
end if:

J2in:=subs(_C1=c7,_C2=c8,J2(x)):
jin:=simplify(c9+c6*x+int(int(J2in,x),x)):
zin:=simplify(subs(J(x)=jin,Z0)):
jout:=simplify(C10+C30*x+int(int(J2out,x),x)):
zout:=simplify(subs(J(x)=jout,Z0)):
om:=omm*I:
jin:=simplify(subs(x=1/r,b0=bin,jin)):
zin:=simplify(subs(x=1/r,b0=bin,zin)):
jout:=simplify(subs(x=1/r,jout));
zout:=simplify(subs(x=1/r,zout));

dwdrout:=2*b0+r^2*L2*diff(zout,r)/2+2*r*zout*L2-L2*b0
        +L4*jout/2:
woutn:=int(dwdrout,r):
```

```
wout:=woutn+C50;

R44out:=simplify(((r^2+2*M*r)*diff(wout,r,r)+L2*wout+2*(r+2*M)*L2*b0
           +M*r*2*L2*zout
           -4*r*(r+2*M)*I*omm*b0 -2*r^3*L2*I*omm*zout+2*r*I*omm*wout)
           /(2*r^3));
Rq4out:=simplify((r*diff(wout,r)-wout+4*r^3*diff(zout,r)
         +r^4*diff(zout,r,r)+2*r^2*zout
         +2*M*r^3*diff(zout,r,r)+8*M*r^2*diff(zout,r)
         +r^2*(L2+2)*I*omm*jout-r^4*I*omm*diff(zout,r)-2*r^2*I*omm*b0
         )/(2*r^2));
R14out:=simplify((r*diff(wout,r,r)+2*L2*b0
         -r^2*L2*diff(zout,r)-2*r*L2*zout)/(2*r^2));

C50:=solve(Rq4out=0,C50);
C10:=solve(R44out=0,C10);
jout:=simplify(jout):
zout:=simplify(zout):
wout:=simplify(wout):
jinf:=asympt(jout,r):

omega:=simplify(limit(jout,r=infinity)*L4/(4+2*L2)/2):
jul:=simplify(limit(-r^2*diff(jout,r),r=infinity)*I*omm/2):
news_check:=simplify(omega+b0+jul);

dwdrin:=2*bin+r^2*L2*diff(zin,r)/2+2*r*zin*L2-L2*bin
        +L4*jin/2:
winn:=int(dwdrin,r):
win:=winn+c10:


R44in:=simplify(((r^2+2*M*r)*diff(win,r,r)+L2*win+2*(r+2*M)*L2*bin
           +M*r*2*L2*zin
           -4*r*(r+2*M)*I*omm*bin -2*r^3*L2*I*omm*zin+2*r*I*omm*win)
           /(2*r^3)):
Rq4in:=simplify((r*diff(win,r)-win+4*r^3*diff(zin,r)
         +r^4*diff(zin,r,r)+2*r^2*zin
         +2*M*r^3*diff(zin,r,r)+8*M*r^2*diff(zin,r)
         +r^2*(L2+2)*I*omm*jin-r^4*I*omm*diff(zin,r)-2*r^2*I*omm*bin
         )/(2*r^2)):
R14in:=simplify((r*diff(win,r,r)+2*L2*bin
         -r^2*L2*diff(zin,r)-2*r*L2*zin)/(2*r^2)):

c10:=solve(Rq4in=0,c10):
c9:=solve(R44in=0,c9):
jin:=simplify(jin):
zin:=simplify(zin):
win:=simplify(win):
sjin:=series(jin*r^(n+1),r=0):
c8:=solve(coeff(sjin,r,n)=0,c8):
c7:=solve(coeff(sjin,r,(n-2))=0,c7):
series(jin,r):
series(zin,r):
```

```
dzout:=simplify(diff(zout,r)):
djout:=simplify(diff(jout,r)):
dzin:=simplify(diff(zin,r)):
djin:=simplify(diff(jin,r)):

e1:=subs(r=rc,jout)-subs(r=rc,jin)=0:
e3:=subs(r=rc,zout)-subs(r=rc,zin)=0:
e4:=subs(r=rc,dzout)-subs(r=rc,dzin)=xu:#2*b0/rc^2:
e5:=subs(r=rc,djout)-subs(r=rc,djin)=xj:#-b0*MM/rc^2/(1-2*MM/rc):
e2:=subs(r=rc,wout)-subs(r=rc,win)=-2*rc*b0*(1-2*MM/rc):
ss1:=solve({e1,e2,e5,e3,e4},{C30,C40I,c6,xj,xu}):

Rq4out_chk:=simplify(subs(ss1,Rq4out));
R44out_chk:=simplify(subs(ss1,R44out));
R14out_chk:=simplify(subs(ss1,R14out));
Rq4in_chk:=simplify(subs(ss1,Rq4in));
R44in_chk:=simplify(subs(ss1,R44in));
R14in_chk:=simplify(subs(ss1,R14in));

(*
jout2:=simplify(subs(ss1,jout)):
jout2:=algsubs(exp(2*I*r*omm)=0,jout2):
omega:=simplify(limit(jout2,r=infinity)*L4/(4+2*L2)/2):
jul:=simplify(limit(-r^2*diff(jout2,r),r=infinity)*I*omm/2):
news_check:=simplify(omega+b0+jul):

`Now transform to basis {}_2 Z_{ell,m} rather than eth^2 Z_{ell,m}`:
nc_s:=series(sqrt(24)*news_check,rc):
Jout_Zgauge:=simplify(sqrt(24)*jout):
Zout_Zgauge:=simplify(sqrt(6)*zout):
Wout_Zgauge:=simplify(wout):
xu1:=factor(simplify(subs(omm=V0/rc,xu))):
xj1:=factor(simplify(subs(omm=V0/rc,xj))):
*)
assign(ss1):
s_C40I:=series(C40I,rc):
s_C40:=subs(CinI=0,s_C40I);
C4I:= simplify(coeff(convert(s_C40I,polynom),CinI))*CinI;
```

```
read `initialize.map`:
read `ProcsRules.map`:

#N.B. Basis is not sZlm but \eth Zlm, etc.
rho22:=array(0..4):
v0:=array(0..4):
v1:=array(0..4):
Vang:=array(0..4):
Vangb:=array(0..4):

Tab:=array(1..4,1..4):
Vu_back:=array([0,0,0,Vu0_back]):
Vd:=array(1..4):

pr_n0(Rho22ns,rho22,0):
pr_n0(v1ns,v1,0):
pr_n0(v0ns,v0,0):
pr_n0(Vangns,Vang,1):
pr_n0(Vangbns,Vangb,-1):

read `gamma.out`:
read `lin.map`:

t1:=prlinRhoc(subs(eps=0,g_exp[4,4]+1)):
Vu0_back:=prlinRhoc(pr2(1+t1/2+3*t1^2/8)):
t2:=sum(sum(Vu_back[a]*Vu_back[b]*g_exp[a,b],a=1..4),b=1..4):
check_Vu0:=prlinRhoc(subs(eps=0,t2+1));

for a to 4 do
  Vd[a]:=sum(Vu_back[b]*g_exp[a,b],b=1..4):
  Vd[a]:=prlinRhoc(subs(eps=0,Vd[a])):
od:
Vd[1]:=Vd[1]+eps*v1ns:Vd[2]:=Vd[2]+eps*(Vangns+Vangbns)/fo:Vd[3]:=Vd[3]+eps*I*(V
angbns-Vangns)/fo:Vd[4]:=Vd[4]+eps*v0ns:

for a to 4 do for b to 4 do
  Tab_down_exp[a,b]:=prlinRhoc(pr2((Rhoc*Rho0+Rhoc*eps*Rho22ns)*Vd[a]*Vd[b])):
od:od:
unassign('a'):unassign('b'):
D_Tab_down:=pr_D_Tab_down(Tab_down_exp,x,C,h):

t3:=simplify(prlinRhoc(pr2(D_Tab_down[2]+I*D_Tab_down[3]))/2*fo):
cons_A:=simplify(subs(rule1,t3)):
cons_1:=prlinRhoc(pr2(D_Tab_down[1])):
cons_4:=prlinRhoc(pr2(D_Tab_down[4])):
cons1m4:=simplify(cons_1-cons_4):
cons1p4:=simplify(cons_1+cons_4):

t1:=subs(Rhoc=0,pr2(sum(sum(Vd[a]*Vd[b]*h_exp[a,b],a=1..4),b=1..4))):
v0_0:=solve(factor(simplify(subs(rule1,t1+1)))=0,v0[0]):
v0_1:=solve(factor(simplify(subs(rule1,diff(t1+1,r))))=0,v0[1]):
c1m4:=simplify(subs(v0[4]=v0_0*om,cons1m4)):
c1p4:=simplify(subs(v0[4]=v0_0*om,v0[0]=v0_0,v0[1]=v0_1,cons1p4)):
```

```
Vang_0:=solve(subs(Vang[4]=Vang[0]*om,wn[0,2]=wn[0,0],Be[0,2]=Be[0,0],cons_A)=0,
Vang[0]):
v1_0:=solve(subs(v1[4]=v1[0]*om,c1m4)=0,v1[0]):
t1:=subs(rho22[4]=om*rho22[0],v1[0]=v1_0,v1[4]=om*v1_0,Vang[3]=L2*Vang_0,Vangb[2
]=L2*Vang_0,c1p4):
rho22_0:=solve(t1=0,rho22[0]):

prRHS(Tab_down_exp,g,h):
RHS_R1A:=subs(Vang[0]=Vang0(r),RHS_R1A):
RHS_R0A:=subs(Vang[0]=Vang0(r),RHS_R0A):

prBackInShellOut(rho_falloff,Rho0,B0,B1,B11,W0,W1,W11):
B0r0:=B0in:

rule2de:=(Be[1,2]=diff(beta(r),r),Be[0,2]=beta(r),Be[2,2]=beta(r),

Ue[0,1]=diff(Z(r),r),Ue[1,1]=diff(Z(r),r,r),Ue[1,2]=diff(Z(r),r),Ue[0,2]=Z(r),

Je[0,1]=diff(JJ(r),r),Je[1,1]=diff(JJ(r),r,r),Je[1,4]=om*diff(JJ(r),r),Je[0,4]=o
m*JJ(r),
          Je[1,3]=(L2+2)*diff(JJ(r),r), Be[0,1]=diff(beta(r),r),
          Be[0,0]=beta(r),wn[0,0]=ww(r),Ue[0,0]=Z(r)):
DEbeta:=subs(rule2de,ruleBackShell,eps*coeff(R11e,eps)=RHS_R11):

beta(r):=b0:
prMakeDEInOut(ruleBackIn,0):
j2tin:=dsolve(de3a,J2(xx)):
jtin1:=int(int(subs(_C2=RhocCinI,_C1=(C40+Rhoc*C4I)*6,rhs(j2tin)),xx),xx)+(C30+R
hoc*C3I)*xx+C10+Rhoc*C1I:
ztin1:=simplify(subs(JJ(xx)=jtin1,Z0)):
jtin:=prlinRhoc(subs(xx=1/r,jtin1)):
ztin:=prlinRhoc(subs(xx=1/r,ztin1)):
btin:=b0:
t1:=solve(subs(rule1,ruleBackIn,Rwe)=0,wn[0,1]):
rule3in:={Be[0,0]=btin,Ube[1,2]=diff(ztin,r)*L2,Ue[1,3]=diff(ztin,r)*L2,Ube[0,2]
=ztin*L2,Ue[0,3]=ztin*L2,
        Be[2,3]=L2*btin,Je[3,3]=L4*jtin,Jbe[2,2]=L4*jtin}:
t2:=prlinRhoc(subs(rule3in,t1)):
wtin:=prlinRhoc(int(t2,r))+C50+Rhoc*C5I:

jb:=subs(Rhoc=0,jtin):zb:=subs(Rhoc=0,ztin):wb:=subs(Rhoc=0,wtin):bb:=subs(Rhoc=
0,btin):

btin:=simplify(subs(om=omm1,bb)):
btin:=subs(omm1=om*(1-2*Rhoc*B0r0),RhocCinI=Rhoc*CinI,btin):
btin:=prlinRhoc(btin):
btin:=subs(b0=b0+Rhoc*bI,btin):
jtin:=simplify(subs(om=omm1,jb)):
jtin:=subs(omm1=om*(1-2*Rhoc*B0r0),RhocCinI=Rhoc*CinI,jtin):
jtin:=subs(b0=b0+Rhoc*bI,C40=C40+Rhoc*C4I,C30=C30+Rhoc*C3I,C10=C10+Rhoc*C1I,jtin
):
jtin:=prlinRhoc(jtin):
ztin:=simplify(subs(om=omm1,zb)):
ztin:=subs(omm1=om*(1-2*Rhoc*B0r0),RhocCinI=Rhoc*CinI,ztin*(1+2*Rhoc*B0r0)):
```

```
ztin:=subs(b0=b0+Rhoc*bI,C40=C40+Rhoc*C4I,C30=C30+Rhoc*C3I,C10=C10+Rhoc*C1I,ztin
):
ztin:=prlinRhoc(ztin):
wtin:=simplify(subs(om=omm1,wb)):
wtin:=subs(omm1=om*(1-2*Rhoc*B0r0),RhocCinI=Rhoc*CinI,wtin*(1+2*Rhoc*B0r0)):
wtin:=subs(b0=b0+Rhoc*bI,C40=C40+Rhoc*C4I,C30=C30+Rhoc*C3I,C10=C10+Rhoc*C1I,C50=
C50+Rhoc*C5I,wtin):
wtin:=prlinRhoc(wtin):

writeto(`formulas.out`);
jtint:=simplify(subs(om=I*omm,jtin));
btint:=simplify(subs(om=I*omm,btin));
ztint:=simplify(subs(om=I*omm,ztin));
wtint:=simplify(subs(om=I*omm,wtin));
writeto(`terminal`);

ruleconsIn:={Be[2, 3]=L2*btin, wn[2, 3]=L2*wtin, wn[1, 1]=diff(wtin,r,r), Be[0,
1]=diff(btin,r),
           Be[1, 4]=om*diff(btin,r), Be[0, 4]=om*btin, Ue[3,
4]=om*L2*ztin,Ube[2, 4]=om*L2*ztin,
           wn[0, 4]=om*wtin, Je[3, 4]=om*(L2+2)*jtin, Be[2,
4]=om*btin,Je[1,4]=om*diff(jtin,r),
           Je[0,4]=om*jtin,Ue[1, 4]=om*diff(ztin,r),
           Be[1, 1]=diff(btin,r,r), wn[0, 0]=wtin, wn[0, 1]=diff(wtin,r), Ube[0,
2]=L2*ztin, Ue[0, 3]=L2*ztin,
           Ue[2, 3]=L2*ztin, Ube[2, 2]=L2*ztin, wn[1, 2]=diff(wtin,r), wn[0,
2]=wtin,  Ue[0, 0]=ztin,
           Ue[0, 1]=diff(ztin,r), Ue[1, 1]=diff(ztin,r,r), Ube[1,
2]=L2*diff(ztin,r), Ue[1, 3] =L2*diff(ztin,r),Be[0,0]=btin,
           Be[0,2]=btin,Be[1,2]=diff(btin,r),Be[2,2]=btin,

Je[1,3]=(L2+2)*diff(jtin,r),Je[3,3]=L4*jtin,Jbe[2,2]=L4*jtin,Je[1,1]=diff(jtin,r
,r),
           Je[0,1]=diff(jtin,r), Ue[0,2]=ztin,Ue[1,2]=diff(ztin,r)}:

check_DE_R11_In:=prlinRhoc(subs(ruleBackIn,ruleconsIn,eps*coeff(R11e,eps)));
check_DE_R1A_In:=prlinRhoc(subs(ruleBackIn,ruleconsIn,eps*coeff(Rqe,eps))):
check_DE_R1A_In:=simplify(check_DE_R1A_In);
check_DE_Rw_In:=prlinRhoc(subs(ruleBackIn,ruleconsIn,eps*coeff(Rwe,eps))):
check_DE_Rw_In:=prlinRhoc(subs(ruleBackIn,rule1,ruleconsIn,check_DE_Rw_In));
check_DE_ev2_In:=prlinRhoc(subs(ruleBackIn,ruleconsIn,eps*coeff(ev2e,eps)));

constraint00In:=prlinRhoc(subs(ruleBackIn,ruleconsIn,eps*coeff(R44e,eps))):
constraint01In:=prlinRhoc(subs(ruleBackIn,ruleconsIn,eps*coeff(R14e,eps))):
constraint0AIn:=prlinRhoc(subs(ruleBackIn,ruleconsIn,eps*coeff(Rq4e,eps))):
constraint00In:=prlinRhoc(subs(ruleBackIn,rule1,ruleconsIn,constraint00In)):
constraint01In:=prlinRhoc(subs(ruleBackIn,rule1,ruleconsIn,constraint01In));
constraint0AIn:=prlinRhoc(subs(ruleBackIn,ruleconsIn,constraint0AIn)):

C50:=solve(subs(Rhoc=0,constraint0AIn)=0,C50);
C5I:=solve(constraint0AIn=0,C5I):
C10:=solve(subs(Rhoc=0,constraint00In)=0,C10);
C1I:=solve(constraint00In=0,C1I):
constraint00In:=prlinRhoc(constraint00In);
```

```
constraint0AIn:=simplify(constraint0AIn);



beta(r):=b0+Rhoc*b0E:
bOut:=beta(r):
unassign('Z0'): unassign('Z1'): unassign('Z2'):
prMakeDEInOut(ruleBackOut,0):
jRhoc01:=subs(r=1/xx,Rhoc=0,jtin):
t1:=subs(J2(xx)=diff(jRhoc01,xx,xx),de3b):t1:=simplify(t1):
ct1:=array(1..12):
st1:=array(1..12):st1i:=array(1..12):
for a from 3 to 12 do
  st1[a]:=rhs(dsolve(lhs(de3a)+ct1[a]*xx^a,J2(xx))):
  st1[a]:=subs(_C1=0,_C2=0,st1[a]):
  ct1[a]:=coeff(t1,xx,a):
od:
unassign('a'):

st:=simplify(sum(st1[b],b=3..12)):
st:=subs(xx=2*omm/s,om=omm*I,st):
assume(s>0):
pr_Intx2(-4,1):
st:=int_st:
pr_Intx2(-5,1):
int_st_xx:=subs(s=2*om/I/xx,int_st):
t15:=simplify(diff(int_st_xx,xx,xx)):
check_2:=simplify(subs(J2(xx)=t15,omm=om/I,lhs(de3a)+t1)):
check_2:=prlinRhoc(check_2);
om:=omm*I:

jOut1:=subs(_C1=(C40+C4E*Rhoc)*6,_C2=Rhoc*CinE,int(int(rhs(j2tin),xx),xx))+(C30+
Rhoc*C3E)*xx+C10+Rhoc*C1E+int_st_xx:
zOut1:=prlinRhoc(subs(JJ(xx)=jOut1,Z0)):
jOut:=simplify(subs(xx=1/r,jOut1)):
zOut:=simplify(subs(xx=1/r,zOut1)):
rule31:={Be[0,0]=bOut,Ube[1,2]=diff(zOut,r)*L2,Ue[1,3]=diff(zOut,r)*L2,Ube[0,2]=
zOut*L2,Ue[0,3]=zOut*L2,
        Be[2,3]=L2*bOut,Je[3,3]=L4*jOut,Jbe[2,2]=L4*jOut}:
t1:=solve(coeff(subs(ruleBackOut,Rwe),eps)=0,wn[0,1]):
t2:=subs(rule1,rule31,wn[0,0]=wRhoc0,t1):
t3:=prlinRhoc(t2):
wOut:=simplify(int(t3,r))+C50+C5E*Rhoc:

appendto(`formulas.out`);
jOut:=simplify(jOut);
bOut:=simplify(bOut);
zOut:=simplify(zOut);
wOut:=simplify(wOut);
writeto(`terminal`);


rulecons1:={Be[2, 3]=L2*bOut, wn[2, 3]=L2*wOut, wn[1, 1]=diff(wOut,r,r), Be[0,
```

```
1]=diff(bOut,r),
           Be[1, 4]=om*diff(bOut,r), Be[0, 4]=om*bOut, Ue[3,
4]=om*L2*zOut,Ube[2, 4]=om*L2*zOut,
           wn[0, 4]=om*wOut, Je[3, 4]=om*(L2+2)*jOut, Be[2,
4]=om*bOut,Je[1,4]=om*diff(jOut,r),
           Je[0,4]=om*jOut,Ue[1, 4]=om*diff(zOut,r),
           Be[1, 1]=diff(bOut,r,r), wn[0, 0]=wOut, wn[0, 1]=diff(wOut,r), Ube[0,
2]=L2*zOut, Ue[0, 3]=L2*zOut,
           Ue[2, 3]=L2*zOut, Ube[2, 2]=L2*zOut, wn[1, 2]=diff(wOut,r), wn[0,
2]=wOut,  Ue[0, 0]=zOut,
           Ue[0, 1]=diff(zOut,r), Ue[1, 1]=diff(zOut,r,r), Ube[1,
2]=L2*diff(zOut,r), Ue[1, 3] =L2*diff(zOut,r),Be[0,0]=bOut,
           Be[0,2]=bOut,Be[1,2]=diff(bOut,r),Be[2,2]=bOut,

Je[1,3]=(L2+2)*diff(jOut,r),Je[3,3]=L4*jOut,Jbe[2,2]=L4*jOut,Je[1,1]=diff(jOut,r
,r),
           Je[0,1]=diff(jOut,r), Ue[0,2]=zOut,Ue[1,2]=diff(zOut,r)}:

check_DE_R11Out:=prlinRhoc(subs(ruleBackOut,rulecons1,eps*coeff(R11e,eps)));
check_DE_R1AOut:=prlinRhoc(subs(ruleBackOut,rulecons1,eps*coeff(Rqe,eps))):
check_DE_R1AOut:=simplify(check_DE_R1AOut);
check_DE_RwOut:=prlinRhoc(subs(ruleBackOut,rulecons1,eps*coeff(Rwe,eps))):
check_DE_RwOut:=prlinRhoc(subs(ruleBackOut,rule1,rulecons1,check_DE_RwOut));
check_DE_ev2Out:=prlinRhoc(subs(ruleBackOut,rulecons1,eps*coeff(ev2e,eps)));

constraint00Out:=prlinRhoc(subs(ruleBackOut,rulecons1,eps*coeff(R44e,eps))):
constraint01Out:=prlinRhoc(subs(ruleBackOut,rulecons1,eps*coeff(R14e,eps))):
constraint0AOut:=prlinRhoc(subs(ruleBackOut,rulecons1,eps*coeff(Rq4e,eps))):
constraint00Out:=prlinRhoc(subs(ruleBackOut,rule1,rulecons1,constraint00Out)):
constraint01Out:=prlinRhoc(subs(ruleBackOut,rule1,rulecons1,constraint01Out));
constraint0AOut:=prlinRhoc(subs(ruleBackOut,rulecons1,constraint0AOut)):

C5E:=solve(constraint0AOut=0,C5E):
C1E:=solve(constraint00Out=0,C1E):
constraint00Out:=simplify(constraint00Out);
constraint0AOut:=simplify(constraint0AOut);




unassign('om'):




beta(r):=b0+Rhoc*betaRhoc(r):
unassign('Z0'): unassign('Z1'): unassign('Z2'):
prMakeDEInOut(ruleBackShell,1):
bshell:=subs(Rhoc=0,beta(r)):
rulecons:={Be[2, 3]=L2*btin, wn[2, 3]=L2*wtin, wn[1, 1]=diff(wtin,r,r), Be[0,
1]=diff(btin,r),
           Be[1, 4]=om*diff(btin,r), Be[0, 4]=om*btin, Ue[3,
4]=om*L2*ztin,Ube[2, 4]=om*L2*ztin,
           wn[0, 4]=om*wtin, Je[3, 4]=om*(L2+2)*jtin, Be[2,
```

```
4]=om*btin,Je[1,4]=om*diff(jtin,r),
           Je[0,4]=om*jtin,Ue[1, 4]=om*diff(ztin,r),
           Be[1, 1]=diff(btin,r,r), wn[0, 0]=wtin, wn[0, 1]=diff(wtin,r), Ube[0,
2]=L2*ztin, Ue[0, 3]=L2*ztin,
           Ue[2, 3]=L2*ztin, Ube[2, 2]=L2*ztin, wn[1, 2]=diff(wtin,r), wn[0,
2]=wtin,  Ue[0, 0]=ztin,
           Ue[0, 1]=diff(ztin,r), Ue[1, 1]=diff(ztin,r,r), Ube[1,
2]=L2*diff(ztin,r), Ue[1, 3] =L2*diff(ztin,r),Be[0,0]=btin,
           Be[0,2]=btin,Be[1,2]=diff(btin,r),Be[2,2]=btin,

Je[1,3]=(L2+2)*diff(jtin,r),Je[3,3]=L4*jtin,Jbe[2,2]=L4*jtin,Je[1,1]=diff(jtin,r
,r),
           Je[0,1]=diff(jtin,r), Ue[0,2]=ztin,Ue[1,2]=diff(ztin,r)}:

jRhoc01:=subs(r=1/xx,Rhoc=0,jtin):
wRhoc0:=subs(Rhoc=0,wtin):
Vang[0]:=simplify(subs(rule2de,rulecons,ww(r)=wRhoc0,Rhoc=0,Vang_0)):
Vang0(r):=Vang[0]:
Vang0(xx):=subs(r=1/xx,Vang0(r)):
v0[0]:=v0_0:
v1[0]:=simplify(subs(rule2de,rulecons,ww(r)=wRhoc0,Rhoc=0,v1_0)):
v1[1]:=simplify(diff(v1[0],r)):
rho22[0]:=simplify(subs(rule2de,rulecons,ww(r)=wRhoc0,Rhoc=0,rho22_0)):

appendto(`formulas.out`);
v10:=simplify(subs(om=I*omm,v1[0]));
v00:=simplify(subs(om=I*omm,v0[0])):
v00:=simplify(subs(Rhoc=0,subs(ruleconsIn,v00)));
vang0:=simplify(subs(om=I*omm,Vang[0]));
rho220:=simplify(subs(om=I*omm,rho22[0]));
writeto(`terminal`);


betaRhoc(r):=int(rhs(DEbeta)*r/4/eps/Rhoc,r)+b0S:
bshell:=b0+Rhoc*betaRhoc(r):#beta(r):

t1:=subs(J2(xx)=diff(jRhoc01,xx,xx),JJ(xx)=jRhoc01,betaRhoc(xx)=subs(r=1/xx,beta
Rhoc(r)),de3b):simplify(t1):
t1:=simplify(subs(r=1/xx,t1)):
ct1:=array(1..12):
st1:=array(1..12):st1i:=array(1..12):
for a from 3 to 12 do
  st1[a]:=rhs(dsolve(lhs(de3a)+ct1[a]*xx^a,J2(xx))):
  st1[a]:=subs(_C1=0,_C2=0,st1[a]):
  ct1[a]:=coeff(t1,xx,a):
od:
unassign('a'):

st:=simplify(sum(st1[b],b=3..12)):
st:=subs(xx=2*omm/s,om=omm*I,st):
#assume(s>0):
pr_Intx2(-4,1):
st:=int_st:
pr_Intx2(-5,1):
```

```
int_st_xx:=subs(s=2*om/I/xx,int_st):
t15:=simplify(diff(int_st_xx,xx,xx)):
check_2:=simplify(subs(J2(xx)=t15,omm=om/I,lhs(de3a)+t1));

om:=omm*I:

jshell1:=subs(_C1=(C40+C4S*Rhoc)*6,_C2=CinS*Rhoc,int(int(rhs(j2tin),xx),xx))+(C3
0+Rhoc*C3S)*xx+C10+Rhoc*C1S+int_st_xx:
zshell1:=prlinRhoc(subs(JJ(xx)=jshell1,Z0)):
zshell1:=simplify(subs(betaRhoc(xx)=subs(r=1/xx,betaRhoc(r)),zshell1)):
jshell:=simplify(subs(xx=1/r,jshell1)):
zshell:=simplify(subs(xx=1/r,zshell1)):

rule31:={Be[0,0]=bshell,Ube[1,2]=diff(zshell,r)*L2,Ue[1,3]=diff(zshell,r)*L2,Ube
[0,2]=zshell*L2,Ue[0,3]=zshell*L2,
        Be[2,3]=L2*bshell,Je[3,3]=L4*jshell,Jbe[2,2]=L4*jshell}:
t1:=solve(coeff(subs(ruleBackShell,Rwe-RHS_Rw),eps)=0,wn[0,1]):
t2:=subs(rule1,rule31,wn[0,0]=wRhoc0,t1):
t3:=prlinRhoc(t2):
wshell:=simplify(int(t3,r))+C50+C5S*Rhoc:

appendto(`formulas.out`);
jshell:=simplify(jshell);
bshell:=simplify(bshell);
zshell:=simplify(zshell);
wshell:=simplify(wshell);
writeto(`terminal`);

#Formally identical to rulecons, but it needs to be re-eveluated since jshell
etc have changed
rulecons1:={Be[2, 3]=L2*bshell, wn[2, 3]=L2*wshell, wn[1, 1]=diff(wshell,r,r),
Be[0, 1]=diff(bshell,r),
           Be[1, 4]=om*diff(bshell,r), Be[0, 4]=om*bshell, Ue[3,
4]=om*L2*zshell,Ube[2, 4]=om*L2*zshell,
           wn[0, 4]=om*wshell, Je[3, 4]=om*(L2+2)*jshell, Be[2,
4]=om*bshell,Je[1,4]=om*diff(jshell,r),
           Je[0,4]=om*jshell,Ue[1, 4]=om*diff(zshell,r),
           Be[1, 1]=diff(bshell,r,r), wn[0, 0]=wshell, wn[0, 1]=diff(wshell,r),
Ube[0, 2]=L2*zshell, Ue[0, 3]=L2*zshell,
           Ue[2, 3]=L2*zshell, Ube[2, 2]=L2*zshell, wn[1, 2]=diff(wshell,r),
wn[0, 2]=wshell,  Ue[0, 0]=zshell,
           Ue[0, 1]=diff(zshell,r), Ue[1, 1]=diff(zshell,r,r), Ube[1,
2]=L2*diff(zshell,r), Ue[1, 3] =L2*diff(zshell,r),Be[0,0]=bshell,
           Be[0,2]=bshell,Be[1,2]=diff(bshell,r),Be[2,2]=bshell,

Je[1,3]=(L2+2)*diff(jshell,r),Je[3,3]=L4*jshell,Jbe[2,2]=L4*jshell,Je[1,1]=diff(
jshell,r,r),
           Je[0,1]=diff(jshell,r), Ue[0,2]=zshell,Ue[1,2]=diff(zshell,r)}:

check_DE_R11_shell:=prlinRhoc(subs(ruleBackShell,rulecons1,eps*coeff(R11e-RHS_R1
1,eps)));
check_DE_R1A_shell:=prlinRhoc(subs(ruleBackShell,rulecons1,eps*coeff(Rqe-RHS_R1A
,eps))):
check_DE_R1A_shell:=simplify(check_DE_R1A_shell);
```

```
check_DE_Rw_shell:=prlinRhoc(subs(ruleBackShell,rulecons1,eps*coeff(Rwe-RHS_Rw,e
ps))):
check_DE_Rw_shell:=prlinRhoc(subs(ruleBackShell,rule1,rulecons1,check_DE_Rw_shel
l));
check_DE_ev2_shell:=prlinRhoc(subs(ruleBackShell,rulecons1,eps*coeff(ev2e-RHS_ev
2e,eps)));

constraint00shell:=prlinRhoc(subs(ruleBackShell,rulecons1,eps*coeff(R44e-RHS_R00
,eps))):
constraint01shell:=prlinRhoc(subs(ruleBackShell,rulecons1,eps*coeff(R14e-RHS_R01
,eps))):
constraint0Ashell:=prlinRhoc(subs(ruleBackShell,rulecons1,eps*coeff(Rq4e-RHS_R0A
,eps))):
constraint00shell:=prlinRhoc(subs(ruleBackShell,rule1,rulecons1,constraint00shel
l)):
constraint01shell:=prlinRhoc(subs(ruleBackShell,rule1,rulecons1,constraint01shel
l));
constraint0Ashell:=prlinRhoc(subs(ruleBackShell,rulecons1,constraint0Ashell)):

C5S:=solve(constraint0Ashell=0,C5S):
C1S:=solve(constraint00shell=0,C1S):
constraint00shell:=simplify(constraint00shell);
constraint0Ashell:=simplify(constraint0Ashell);

appendto(`formulas.out`);
C1I:=simplify(C1I);
C5I:=simplify(C5I);
C1E:=simplify(C1E);
C5E:=simplify(C5E);
C1S:=simplify(C1S);
C5S:=simplify(C5S);
writeto(`terminal`);


ebIS:=simplify(subs(r=r0,btin-bshell)):
b0S:=solve(ebIS=0,b0S):
ejIS:=simplify(subs(r=r0,jtin-jshell)):
ezIS:=simplify(subs(r=r0,ztin-zshell)):
ewIS:=simplify(subs(r=r0,wtin-wshell)):
sol_jzwIS:=solve({ejIS=0,ezIS=0,ewIS=0},{C3S,C4S,CinI}):
ejdIS:=simplify(subs(r=r0,sol_jzwIS,diff(jtin-jshell,r)));
ezdIS:=simplify(subs(r=r0,sol_jzwIS,diff(ztin-zshell,r)));

ebSE:=simplify(subs(r=r0+del,bOut-bshell)):
b0E:=solve(ebSE=0,b0E):
ejSE:=simplify(subs(r=r0+del,jOut-jshell)):
ezSE:=simplify(subs(r=r0+del,zOut-zshell)):
ewSE:=simplify(subs(r=r0+del,wOut-wshell)):
sol_jzwSE:=solve({ejSE=0,ezSE=0,ewSE=0},{C3E,C4E,CinS}):
ejdSE:=simplify(subs(r=r0+del,sol_jzwSE,diff(jOut-jshell,r)));
ezdSE:=simplify(subs(r=r0+del,sol_jzwSE,diff(zOut-zshell,r)));

assume(r>0):assume(omm>0):
t1:=algsubs(exp(2*I*r*omm)=exp2rom,jOut):
```

```
t2:=algsubs(Ei(-2*I*r*omm)=limit(Ei(-2*I*r*omm),r=infinity),t1):
t3:=coeff(t2,exp2rom):
t4:=coeff(t3,r,-1):
CinE:=solve(t4=0,CinE):

appendto(`formulas.out`);
b0E:=simplify(b0E);
CinE:=simplify(CinE);
b0S:=simplify(b0S);
sol_jzwIS[1];
sol_jzwIS[2];
sol_jzwIS[3];
sol_jzwSE[1];
sol_jzwSE[2];
sol_jzwSE[3];
writeto(`terminal`);

t5:=simplify(subs(exp2rom=0,t1)):
omega:=coeff(t5,r,0)*L4/(4+2*L2)/2:
jul:=coeff(t5,r,-1)*I*omm/2:
bOut_inf:=simplify(limit(bOut,r=infinity)):
news_check:=simplify(omega+bOut_inf+jul):
news_check1:=prlinRhoc(subs(sol_jzwSE,news_check)):
news_check2:=prlinRhoc(subs(sol_jzwIS,news_check1)):
news0:=simplify(sqrt(24)*news_check);

CinI:=subs(sol_jzwIS,CinI):CinI:=subs(sol_jzwSE,CinI):
as20:=asympt(Ei(-2*I*ommr0),ommr0,20):
t1:=convert(series(exp(2*I*(r0+del)*omm),del,16),polynom):
t2:=convert(series(Ei(-2*I*(r0+del)*omm),del,16),polynom):
t3:=convert(series(exp(-2*I*(r0+del)*omm),del,16),polynom):
t4:=convert(series(exp(-2*I*del*omm),del,16),polynom):

CinI:=algsubs(exp(2*I*(r0+del)*omm)=t1,CinI):
CinI:=algsubs(Ei(-2*I*(r0+del)*omm)=t2,CinI):
CinI:=algsubs(exp(-2*I*(r0+del)*omm)=t3,CinI):
CinI:=simplify(algsubs(exp(-2*I*omm*(del+r0))=t3,CinI)):
CinI:=simplify(algsubs(exp(-2*I*r0*omm)=1/e2iromm,CinI)):
CinI:=simplify(algsubs(exp(2*I*r0*omm)=e2ir0mm,CinI)):
CinI:=simplify(algsubs(exp(-2*I*omm*(del+r0))=t3,CinI)):
CinI:=subs(omm=ommr0/r0,CinI):
CinIt:=factor(convert(simplify(algsubs(Ei(-2*I*ommr0)=as20,CinI)),polynom)):

CinIt:=simplify(subs(ommr0=omm*r0,CinIt)):
CinIt:=algsubs(exp(-2*I*(r0+del)*omm)=t3,CinIt):
CinIt:=algsubs(exp(-2*I*del*omm)=t4,CinIt):
CinIt:=simplify(algsubs(exp(-2*I*r0*omm)=1/e2iromm,CinIt)):
CinIt:=simplify(algsubs(exp(2*I*r0*omm)=e2ir0mm,CinIt)):

C4I:=-CinIt/2: #From regular_0_IncomingGW.map
news:=simplify(sqrt(24)*news_check2):

assume(r0>0):assume(del>0):
mas:=int(4*Pi*r^2*Rhoc*rho_falloff,r=r0..r0+del):
```

```
Rhoc1:=solve(mas=mass,Rhoc):
#news:=subs(Rhoc=Rhoc1,news):
strain:=subs(Rhoc=Rhoc1,2*news/I/omm):

strain_del[0]:=factor(simplify(subs(del=0,strain))):
for a to 8 do
  strain_del[a]:=factor(simplify(del^a*subs(del=0,diff(strain,del$a)))):
od:
straindel:=simplify(sum(strain_del[b],b=0..8)):

strain_r0_0:=coeff(straindel,r0,0);
strain_r0_m1:=coeff(straindel,r0,-1);
strain_r0_m2:=simplify(coeff(coeff(straindel,r0,-2),del,0));

T1:=simplify(strain_r0_m1/r0/strain_r0_0);
T2:=expand(simplify(strain_r0_m2/r0^2/strain_r0_0));

CinE:=simplify(subs(Rhoc=Rhoc1,Rhoc*CinE));
```

```
read `initialize.map`:
read `ProcsRules.map`:

#N.B. Basis is not sZlm but \eth Zlm, etc.
rho22:=array(0..4):
v0:=array(0..4):
v1:=array(0..4):
Vang:=array(0..4):
Vangb:=array(0..4):

Tab:=array(1..4,1..4):
Vu_back:=array([0,0,0,Vu0_back]):
Vd:=array(1..4):

pr_n0(Rho22ns,rho22,0):
pr_n0(v1ns,v1,0):
pr_n0(v0ns,v0,0):
pr_n0(Vangns,Vang,1):
pr_n0(Vangbns,Vangb,-1):

read `gamma.out`:
read `lin.map`:

t1:=prlinRhoc(subs(eps=0,g_exp[4,4]+1)):
Vu0_back:=prlinRhoc(pr2(1+t1/2+3*t1^2/8)):
t2:=sum(sum(Vu_back[a]*Vu_back[b]*g_exp[a,b],a=1..4),b=1..4):
check_Vu0:=prlinRhoc(subs(eps=0,t2+1));

for a to 4 do
  Vd[a]:=sum(Vu_back[b]*g_exp[a,b],b=1..4):
  Vd[a]:=prlinRhoc(subs(eps=0,Vd[a])):
od:
Vd[1]:=Vd[1]+eps*v1ns:Vd[2]:=Vd[2]+eps*(Vangns+Vangbns)/fo:Vd[3]:=Vd[3]+eps*I*(V
angbns-Vangns)/fo:Vd[4]:=Vd[4]+eps*v0ns:

for a to 4 do for b to 4 do
  Tab_down_exp[a,b]:=prlinRhoc(pr2((Rhoc*Rho0+Rhoc*eps*Rho22ns)*Vd[a]*Vd[b])):
od:od:
unassign('a'):unassign('b'):
D_Tab_down:=pr_D_Tab_down(Tab_down_exp,x,C,h):

t3:=simplify(prlinRhoc(pr2(D_Tab_down[2]+I*D_Tab_down[3]))/2*fo):
cons_A:=simplify(subs(rule1,t3)):
cons_1:=prlinRhoc(pr2(D_Tab_down[1])):
cons_4:=prlinRhoc(pr2(D_Tab_down[4])):
cons1m4:=simplify(cons_1-cons_4):
cons1p4:=simplify(cons_1+cons_4):

t1:=subs(Rhoc=0,pr2(sum(sum(Vd[a]*Vd[b]*h_exp[a,b],a=1..4),b=1..4))):
v0_0:=solve(factor(simplify(subs(rule1,t1+1)))=0,v0[0]):
v0_1:=solve(factor(simplify(subs(rule1,diff(t1+1,r))))=0,v0[1]):
c1m4:=simplify(subs(v0[4]=v0_0*om,cons1m4)):
c1p4:=simplify(subs(v0[4]=v0_0*om,v0[0]=v0_0,v0[1]=v0_1,cons1p4)):
```

```
Vang_0:=solve(subs(Vang[4]=Vang[0]*om,wn[0,2]=wn[0,0],Be[0,2]=Be[0,0],cons_A)=0,
Vang[0]):
v1_0:=solve(subs(v1[4]=v1[0]*om,c1m4)=0,v1[0]):
t1:=subs(rho22[4]=om*rho22[0],v1[0]=v1_0,v1[4]=om*v1_0,Vang[3]=L2*Vang_0,Vangb[2
]=L2*Vang_0,c1p4):
rho22_0:=solve(t1=0,rho22[0]):

prRHS(Tab_down_exp,g,h):
RHS_R1A:=subs(Vang[0]=Vang0(r),RHS_R1A):
RHS_R0A:=subs(Vang[0]=Vang0(r),RHS_R0A):

prBackInShellOut(rho_falloff,Rho0,B0,B1,B11,W0,W1,W11):
B0r0:=B0in:

rule2de:=(Be[1,2]=diff(beta(r),r),Be[0,2]=beta(r),Be[2,2]=beta(r),

Ue[0,1]=diff(Z(r),r),Ue[1,1]=diff(Z(r),r,r),Ue[1,2]=diff(Z(r),r),Ue[0,2]=Z(r),

Je[0,1]=diff(JJ(r),r),Je[1,1]=diff(JJ(r),r,r),Je[1,4]=om*diff(JJ(r),r),Je[0,4]=o
m*JJ(r),
          Je[1,3]=(L2+2)*diff(JJ(r),r), Be[0,1]=diff(beta(r),r),
          Be[0,0]=beta(r),wn[0,0]=ww(r),Ue[0,0]=Z(r)):
DEbeta:=subs(rule2de,ruleBackShell,eps*coeff(R11e,eps)=RHS_R11):

beta(r):=b0:
prMakeDEInOut(ruleBackIn,0):
j2tin:=dsolve(de3a,J2(xx)):
jtin1:=int(int(subs(_C2=RhocCinI,_C1=(C40+Rhoc*C4I)*6,rhs(j2tin)),xx),xx)+(C30+R
hoc*C3I)*xx+C10+Rhoc*C1I:
ztin1:=simplify(subs(JJ(xx)=jtin1,Z0)):
jtin:=prlinRhoc(subs(xx=1/r,jtin1)):
ztin:=prlinRhoc(subs(xx=1/r,ztin1)):
btin:=b0:
t1:=solve(subs(rule1,ruleBackIn,Rwe)=0,wn[0,1]):
rule3in:={Be[0,0]=btin,Ube[1,2]=diff(ztin,r)*L2,Ue[1,3]=diff(ztin,r)*L2,Ube[0,2]
=ztin*L2,Ue[0,3]=ztin*L2,
        Be[2,3]=L2*btin,Je[3,3]=L4*jtin,Jbe[2,2]=L4*jtin}:
t2:=prlinRhoc(subs(rule3in,t1)):
wtin:=prlinRhoc(int(t2,r))+C50+Rhoc*C5I:

jb:=subs(Rhoc=0,jtin):zb:=subs(Rhoc=0,ztin):wb:=subs(Rhoc=0,wtin):bb:=subs(Rhoc=
0,btin):

btin:=simplify(subs(om=omm1,bb)):
btin:=subs(omm1=om*(1-2*Rhoc*B0r0),RhocCinI=Rhoc*CinI,btin):
btin:=prlinRhoc(btin):
btin:=subs(b0=b0+Rhoc*bI,btin):
jtin:=simplify(subs(om=omm1,jb)):
jtin:=subs(omm1=om*(1-2*Rhoc*B0r0),RhocCinI=Rhoc*CinI,jtin):
jtin:=subs(b0=b0+Rhoc*bI,C40=C40+Rhoc*C4I,C30=C30+Rhoc*C3I,C10=C10+Rhoc*C1I,jtin
):
jtin:=prlinRhoc(jtin):
ztin:=simplify(subs(om=omm1,zb)):
ztin:=subs(omm1=om*(1-2*Rhoc*B0r0),RhocCinI=Rhoc*CinI,ztin*(1+2*Rhoc*B0r0)):
```

```
ztin:=subs(b0=b0+Rhoc*bI,C40=C40+Rhoc*C4I,C30=C30+Rhoc*C3I,C10=C10+Rhoc*C1I,ztin
):
ztin:=prlinRhoc(ztin):
wtin:=simplify(subs(om=omm1,wb)):
wtin:=subs(omm1=om*(1-2*Rhoc*B0r0),RhocCinI=Rhoc*CinI,wtin*(1+2*Rhoc*B0r0)):
wtin:=subs(b0=b0+Rhoc*bI,C40=C40+Rhoc*C4I,C30=C30+Rhoc*C3I,C10=C10+Rhoc*C1I,C50=
C50+Rhoc*C5I,wtin):
wtin:=prlinRhoc(wtin):

(* writeto(`formulas.out`);
jtint:=simplify(subs(om=I*omm,jtin));
btint:=simplify(subs(om=I*omm,btin));
ztint:=simplify(subs(om=I*omm,ztin));
wtint:=simplify(subs(om=I*omm,wtin));
writeto(`terminal`); *)

ruleconsIn:={Be[2, 3]=L2*btin, wn[2, 3]=L2*wtin, wn[1, 1]=diff(wtin,r,r), Be[0,
1]=diff(btin,r),
           Be[1, 4]=om*diff(btin,r), Be[0, 4]=om*btin, Ue[3,
4]=om*L2*ztin,Ube[2, 4]=om*L2*ztin,
           wn[0, 4]=om*wtin, Je[3, 4]=om*(L2+2)*jtin, Be[2,
4]=om*btin,Je[1,4]=om*diff(jtin,r),
           Je[0,4]=om*jtin,Ue[1, 4]=om*diff(ztin,r),
           Be[1, 1]=diff(btin,r,r), wn[0, 0]=wtin, wn[0, 1]=diff(wtin,r), Ube[0,
2]=L2*ztin, Ue[0, 3]=L2*ztin,
           Ue[2, 3]=L2*ztin, Ube[2, 2]=L2*ztin, wn[1, 2]=diff(wtin,r), wn[0,
2]=wtin,  Ue[0, 0]=ztin,
           Ue[0, 1]=diff(ztin,r), Ue[1, 1]=diff(ztin,r,r), Ube[1,
2]=L2*diff(ztin,r), Ue[1, 3] =L2*diff(ztin,r),Be[0,0]=btin,
           Be[0,2]=btin,Be[1,2]=diff(btin,r),Be[2,2]=btin,

Je[1,3]=(L2+2)*diff(jtin,r),Je[3,3]=L4*jtin,Jbe[2,2]=L4*jtin,Je[1,1]=diff(jtin,r
,r),
           Je[0,1]=diff(jtin,r), Ue[0,2]=ztin,Ue[1,2]=diff(ztin,r)}:

check_DE_R11_In:=prlinRhoc(subs(ruleBackIn,ruleconsIn,eps*coeff(R11e,eps)));
check_DE_R1A_In:=prlinRhoc(subs(ruleBackIn,ruleconsIn,eps*coeff(Rqe,eps))):
check_DE_R1A_In:=simplify(check_DE_R1A_In);
check_DE_Rw_In:=prlinRhoc(subs(ruleBackIn,ruleconsIn,eps*coeff(Rwe,eps))):
check_DE_Rw_In:=prlinRhoc(subs(ruleBackIn,rule1,ruleconsIn,check_DE_Rw_In));
check_DE_ev2_In:=prlinRhoc(subs(ruleBackIn,ruleconsIn,eps*coeff(ev2e,eps)));

constraint00In:=prlinRhoc(subs(ruleBackIn,ruleconsIn,eps*coeff(R44e,eps))):
constraint01In:=prlinRhoc(subs(ruleBackIn,ruleconsIn,eps*coeff(R14e,eps))):
constraint0AIn:=prlinRhoc(subs(ruleBackIn,ruleconsIn,eps*coeff(Rq4e,eps))):
constraint00In:=prlinRhoc(subs(ruleBackIn,rule1,ruleconsIn,constraint00In)):
constraint01In:=prlinRhoc(subs(ruleBackIn,rule1,ruleconsIn,constraint01In));
constraint0AIn:=prlinRhoc(subs(ruleBackIn,ruleconsIn,constraint0AIn)):

C50:=solve(subs(Rhoc=0,constraint0AIn)=0,C50);
C5I:=solve(constraint0AIn=0,C5I):
C10:=solve(subs(Rhoc=0,constraint00In)=0,C10);
C1I:=solve(constraint00In=0,C1I):
constraint00In:=prlinRhoc(constraint00In);
```

```
constraint0AIn:=simplify(constraint0AIn);



beta(r):=b0+Rhoc*b0E:
bOut:=beta(r):
unassign('Z0'): unassign('Z1'): unassign('Z2'):
prMakeDEInOut(ruleBackOut,0):
jRhoc01:=subs(r=1/xx,Rhoc=0,jtin):
t1:=subs(J2(xx)=diff(jRhoc01,xx,xx),de3b):t1:=simplify(t1):
ct1:=array(1..12):
st1:=array(1..12):st1i:=array(1..12):
for a from 3 to 12 do
  st1[a]:=rhs(dsolve(lhs(de3a)+ct1[a]*xx^a,J2(xx))):
  st1[a]:=subs(_C1=0,_C2=0,st1[a]):
  ct1[a]:=coeff(t1,xx,a):
od:
unassign('a'):

st:=simplify(sum(st1[b],b=3..12)):
st:=subs(xx=2*omm/s,om=omm*I,st):
assume(s>0):
pr_Intx2(-4,1):
st:=int_st:
pr_Intx2(-5,1):
int_st_xx:=subs(s=2*om/I/xx,int_st):
t15:=simplify(diff(int_st_xx,xx,xx)):
check_2:=simplify(subs(J2(xx)=t15,omm=om/I,lhs(de3a)+t1)):
check_2:=prlinRhoc(check_2);
om:=omm*I:

jOut1:=subs(_C1=(C40+C4E*Rhoc)*6,_C2=Rhoc*CinE,int(int(rhs(j2tin),xx),xx))+(C30+
Rhoc*C3E)*xx+C10+Rhoc*C1E+int_st_xx:
zOut1:=prlinRhoc(subs(JJ(xx)=jOut1,Z0)):
jOut:=simplify(subs(xx=1/r,jOut1)):
zOut:=simplify(subs(xx=1/r,zOut1)):
rule31:={Be[0,0]=bOut,Ube[1,2]=diff(zOut,r)*L2,Ue[1,3]=diff(zOut,r)*L2,Ube[0,2]=
zOut*L2,Ue[0,3]=zOut*L2,
        Be[2,3]=L2*bOut,Je[3,3]=L4*jOut,Jbe[2,2]=L4*jOut}:
t1:=solve(coeff(subs(ruleBackOut,Rwe),eps)=0,wn[0,1]):
t2:=subs(rule1,rule31,wn[0,0]=wRhoc0,t1):
t3:=prlinRhoc(t2):
wOut:=simplify(int(t3,r))+C50+C5E*Rhoc:

(* appendto(`formulas.out`);
jOut:=simplify(jOut);
bOut:=simplify(bOut);
zOut:=simplify(zOut);
wOut:=simplify(wOut);
writeto(`terminal`); *)


rulecons1:={Be[2, 3]=L2*bOut, wn[2, 3]=L2*wOut, wn[1, 1]=diff(wOut,r,r), Be[0,
```

```
1]=diff(bOut,r),
           Be[1, 4]=om*diff(bOut,r), Be[0, 4]=om*bOut, Ue[3,
4]=om*L2*zOut,Ube[2, 4]=om*L2*zOut,
           wn[0, 4]=om*wOut, Je[3, 4]=om*(L2+2)*jOut, Be[2,
4]=om*bOut,Je[1,4]=om*diff(jOut,r),
           Je[0,4]=om*jOut,Ue[1, 4]=om*diff(zOut,r),
           Be[1, 1]=diff(bOut,r,r), wn[0, 0]=wOut, wn[0, 1]=diff(wOut,r), Ube[0,
2]=L2*zOut, Ue[0, 3]=L2*zOut,
           Ue[2, 3]=L2*zOut, Ube[2, 2]=L2*zOut, wn[1, 2]=diff(wOut,r), wn[0,
2]=wOut,  Ue[0, 0]=zOut,
           Ue[0, 1]=diff(zOut,r), Ue[1, 1]=diff(zOut,r,r), Ube[1,
2]=L2*diff(zOut,r), Ue[1, 3] =L2*diff(zOut,r),Be[0,0]=bOut,
           Be[0,2]=bOut,Be[1,2]=diff(bOut,r),Be[2,2]=bOut,

Je[1,3]=(L2+2)*diff(jOut,r),Je[3,3]=L4*jOut,Jbe[2,2]=L4*jOut,Je[1,1]=diff(jOut,r
,r),
           Je[0,1]=diff(jOut,r), Ue[0,2]=zOut,Ue[1,2]=diff(zOut,r)}:

check_DE_R11Out:=prlinRhoc(subs(ruleBackOut,rulecons1,eps*coeff(R11e,eps)));
check_DE_R1AOut:=prlinRhoc(subs(ruleBackOut,rulecons1,eps*coeff(Rqe,eps))):
check_DE_R1AOut:=simplify(check_DE_R1AOut);
check_DE_RwOut:=prlinRhoc(subs(ruleBackOut,rulecons1,eps*coeff(Rwe,eps))):
check_DE_RwOut:=prlinRhoc(subs(ruleBackOut,rule1,rulecons1,check_DE_RwOut));
check_DE_ev2Out:=prlinRhoc(subs(ruleBackOut,rulecons1,eps*coeff(ev2e,eps)));

constraint00Out:=prlinRhoc(subs(ruleBackOut,rulecons1,eps*coeff(R44e,eps))):
constraint01Out:=prlinRhoc(subs(ruleBackOut,rulecons1,eps*coeff(R14e,eps))):
constraint0AOut:=prlinRhoc(subs(ruleBackOut,rulecons1,eps*coeff(Rq4e,eps))):
constraint00Out:=prlinRhoc(subs(ruleBackOut,rule1,rulecons1,constraint00Out)):
constraint01Out:=prlinRhoc(subs(ruleBackOut,rule1,rulecons1,constraint01Out));
constraint0AOut:=prlinRhoc(subs(ruleBackOut,rulecons1,constraint0AOut)):

C5E:=solve(constraint0AOut=0,C5E):
C1E:=solve(constraint00Out=0,C1E):
constraint00Out:=simplify(constraint00Out);
constraint0AOut:=simplify(constraint0AOut);




unassign('om'):




beta(r):=b0+Rhoc*betaRhoc(r):
unassign('Z0'): unassign('Z1'): unassign('Z2'):
prMakeDEInOut(ruleBackShell,1):
bshell:=subs(Rhoc=0,beta(r)):
rulecons:={Be[2, 3]=L2*btin, wn[2, 3]=L2*wtin, wn[1, 1]=diff(wtin,r,r), Be[0,
1]=diff(btin,r),
           Be[1, 4]=om*diff(btin,r), Be[0, 4]=om*btin, Ue[3,
4]=om*L2*ztin,Ube[2, 4]=om*L2*ztin,
           wn[0, 4]=om*wtin, Je[3, 4]=om*(L2+2)*jtin, Be[2,
```

```
4]=om*btin,Je[1,4]=om*diff(jtin,r),
           Je[0,4]=om*jtin,Ue[1, 4]=om*diff(ztin,r),
           Be[1, 1]=diff(btin,r,r), wn[0, 0]=wtin, wn[0, 1]=diff(wtin,r), Ube[0,
2]=L2*ztin, Ue[0, 3]=L2*ztin,
           Ue[2, 3]=L2*ztin, Ube[2, 2]=L2*ztin, wn[1, 2]=diff(wtin,r), wn[0,
2]=wtin,  Ue[0, 0]=ztin,
           Ue[0, 1]=diff(ztin,r), Ue[1, 1]=diff(ztin,r,r), Ube[1,
2]=L2*diff(ztin,r), Ue[1, 3] =L2*diff(ztin,r),Be[0,0]=btin,
           Be[0,2]=btin,Be[1,2]=diff(btin,r),Be[2,2]=btin,

Je[1,3]=(L2+2)*diff(jtin,r),Je[3,3]=L4*jtin,Jbe[2,2]=L4*jtin,Je[1,1]=diff(jtin,r
,r),
           Je[0,1]=diff(jtin,r), Ue[0,2]=ztin,Ue[1,2]=diff(ztin,r)}:

jRhoc01:=subs(r=1/xx,Rhoc=0,jtin):
wRhoc0:=subs(Rhoc=0,wtin):
Vang[0]:=simplify(subs(rule2de,rulecons,ww(r)=wRhoc0,Rhoc=0,Vang_0)):
Vang0(r):=Vang[0]:
Vang0(xx):=subs(r=1/xx,Vang0(r)):
v0[0]:=v0_0:
v1[0]:=simplify(subs(rule2de,rulecons,ww(r)=wRhoc0,Rhoc=0,v1_0)):
v1[1]:=simplify(diff(v1[0],r)):
rho22[0]:=simplify(subs(rule2de,rulecons,ww(r)=wRhoc0,Rhoc=0,rho22_0)):

(* appendto(`formulas.out`);
v10:=simplify(subs(om=I*omm,v1[0]));
v00:=simplify(subs(om=I*omm,v0[0])):
v00:=simplify(subs(Rhoc=0,subs(ruleconsIn,v00)));
vang0:=simplify(subs(om=I*omm,Vang[0]));
rho220:=simplify(subs(om=I*omm,rho22[0]));
writeto(`terminal`); *)


betaRhoc(r):=int(rhs(DEbeta)*r/4/eps/Rhoc,r)+b0S:
bshell:=b0+Rhoc*betaRhoc(r):#beta(r):

t1:=subs(J2(xx)=diff(jRhoc01,xx,xx),JJ(xx)=jRhoc01,betaRhoc(xx)=subs(r=1/xx,beta
Rhoc(r)),de3b):simplify(t1):
t1:=simplify(subs(r=1/xx,t1)):
ct1:=array(1..12):
st1:=array(1..12):st1i:=array(1..12):
for a from 3 to 12 do
  st1[a]:=rhs(dsolve(lhs(de3a)+ct1[a]*xx^a,J2(xx))):
  st1[a]:=subs(_C1=0,_C2=0,st1[a]):
  ct1[a]:=coeff(t1,xx,a):
od:
unassign('a'):

st:=simplify(sum(st1[b],b=3..12)):
st:=subs(xx=2*omm/s,om=omm*I,st):
#assume(s>0):
pr_Intx2(-4,1):
st:=int_st:
pr_Intx2(-5,1):
```

```
int_st_xx:=subs(s=2*om/I/xx,int_st):
t15:=simplify(diff(int_st_xx,xx,xx)):
check_2:=simplify(subs(J2(xx)=t15,omm=om/I,lhs(de3a)+t1));

om:=omm*I:

jshell1:=subs(_C1=(C40+C4S*Rhoc)*6,_C2=CinS*Rhoc,int(int(rhs(j2tin),xx),xx))+(C3
0+Rhoc*C3S)*xx+C10+Rhoc*C1S+int_st_xx:
zshell1:=prlinRhoc(subs(JJ(xx)=jshell1,Z0)):
zshell1:=simplify(subs(betaRhoc(xx)=subs(r=1/xx,betaRhoc(r)),zshell1)):
jshell:=simplify(subs(xx=1/r,jshell1)):
zshell:=simplify(subs(xx=1/r,zshell1)):

rule31:={Be[0,0]=bshell,Ube[1,2]=diff(zshell,r)*L2,Ue[1,3]=diff(zshell,r)*L2,Ube
[0,2]=zshell*L2,Ue[0,3]=zshell*L2,
        Be[2,3]=L2*bshell,Je[3,3]=L4*jshell,Jbe[2,2]=L4*jshell}:
t1:=solve(coeff(subs(ruleBackShell,Rwe-RHS_Rw),eps)=0,wn[0,1]):
t2:=subs(rule1,rule31,wn[0,0]=wRhoc0,t1):
t3:=prlinRhoc(t2):
wshell:=simplify(int(t3,r))+C50+C5S*Rhoc:

(* appendto(`formulas.out`);
jshell:=simplify(jshell);
bshell:=simplify(bshell);
zshell:=simplify(zshell);
wshell:=simplify(wshell);
writeto(`terminal`); *)

#Formally identical to rulecons, but it needs to be re-eveluated since jshell
etc have changed
rulecons1:={Be[2, 3]=L2*bshell, wn[2, 3]=L2*wshell, wn[1, 1]=diff(wshell,r,r),
Be[0, 1]=diff(bshell,r),
           Be[1, 4]=om*diff(bshell,r), Be[0, 4]=om*bshell, Ue[3,
4]=om*L2*zshell,Ube[2, 4]=om*L2*zshell,
           wn[0, 4]=om*wshell, Je[3, 4]=om*(L2+2)*jshell, Be[2,
4]=om*bshell,Je[1,4]=om*diff(jshell,r),
           Je[0,4]=om*jshell,Ue[1, 4]=om*diff(zshell,r),
           Be[1, 1]=diff(bshell,r,r), wn[0, 0]=wshell, wn[0, 1]=diff(wshell,r),
Ube[0, 2]=L2*zshell, Ue[0, 3]=L2*zshell,
           Ue[2, 3]=L2*zshell, Ube[2, 2]=L2*zshell, wn[1, 2]=diff(wshell,r),
wn[0, 2]=wshell,  Ue[0, 0]=zshell,
           Ue[0, 1]=diff(zshell,r), Ue[1, 1]=diff(zshell,r,r), Ube[1,
2]=L2*diff(zshell,r), Ue[1, 3] =L2*diff(zshell,r),Be[0,0]=bshell,
           Be[0,2]=bshell,Be[1,2]=diff(bshell,r),Be[2,2]=bshell,

Je[1,3]=(L2+2)*diff(jshell,r),Je[3,3]=L4*jshell,Jbe[2,2]=L4*jshell,Je[1,1]=diff(
jshell,r,r),
           Je[0,1]=diff(jshell,r), Ue[0,2]=zshell,Ue[1,2]=diff(zshell,r)}:

check_DE_R11_shell:=prlinRhoc(subs(ruleBackShell,rulecons1,eps*coeff(R11e-RHS_R1
1,eps)));
check_DE_R1A_shell:=prlinRhoc(subs(ruleBackShell,rulecons1,eps*coeff(Rqe-RHS_R1A
,eps))):
check_DE_R1A_shell:=simplify(check_DE_R1A_shell);
```

```
check_DE_Rw_shell:=prlinRhoc(subs(ruleBackShell,rulecons1,eps*coeff(Rwe-RHS_Rw,e
ps))):
check_DE_Rw_shell:=prlinRhoc(subs(ruleBackShell,rule1,rulecons1,check_DE_Rw_shel
l));
check_DE_ev2_shell:=prlinRhoc(subs(ruleBackShell,rulecons1,eps*coeff(ev2e-RHS_ev
2e,eps)));

constraint00shell:=prlinRhoc(subs(ruleBackShell,rulecons1,eps*coeff(R44e-RHS_R00
,eps))):
constraint01shell:=prlinRhoc(subs(ruleBackShell,rulecons1,eps*coeff(R14e-RHS_R01
,eps))):
constraint0Ashell:=prlinRhoc(subs(ruleBackShell,rulecons1,eps*coeff(Rq4e-RHS_R0A
,eps))):
constraint00shell:=prlinRhoc(subs(ruleBackShell,rule1,rulecons1,constraint00shel
l)):
constraint01shell:=prlinRhoc(subs(ruleBackShell,rule1,rulecons1,constraint01shel
l));
constraint0Ashell:=prlinRhoc(subs(ruleBackShell,rulecons1,constraint0Ashell)):

C5S:=solve(constraint0Ashell=0,C5S):
C1S:=solve(constraint00shell=0,C1S):
constraint00shell:=simplify(constraint00shell);
constraint0Ashell:=simplify(constraint0Ashell);

(* appendto(`formulas.out`);
C1I:=simplify(C1I);
C5I:=simplify(C5I);
C1E:=simplify(C1E);
C5E:=simplify(C5E);
C1S:=simplify(C1S);
C5S:=simplify(C5S);
writeto(`terminal`); *)


ebIS:=simplify(subs(r=r0,btin-bshell)):
b0S:=solve(ebIS=0,b0S):
ejIS:=simplify(subs(r=r0,jtin-jshell)):
ezIS:=simplify(subs(r=r0,ztin-zshell)):
ewIS:=simplify(subs(r=r0,wtin-wshell)):
sol_jzwIS:=solve({ejIS=0,ezIS=0,ewIS=0},{C3S,C4S,CinI}):
ejdIS:=simplify(subs(r=r0,sol_jzwIS,diff(jtin-jshell,r)));
ezdIS:=simplify(subs(r=r0,sol_jzwIS,diff(ztin-zshell,r)));

ebSE:=simplify(subs(r=r0+del,bOut-bshell)):
b0E:=solve(ebSE=0,b0E):
ejSE:=simplify(subs(r=r0+del,jOut-jshell)):
ezSE:=simplify(subs(r=r0+del,zOut-zshell)):
ewSE:=simplify(subs(r=r0+del,wOut-wshell)):
sol_jzwSE:=solve({ejSE=0,ezSE=0,ewSE=0},{C3E,C4E,CinS}):
ejdSE:=simplify(subs(r=r0+del,sol_jzwSE,diff(jOut-jshell,r)));
ezdSE:=simplify(subs(r=r0+del,sol_jzwSE,diff(zOut-zshell,r)));

assume(r>0):assume(omm>0):
t1:=algsubs(exp(2*I*r*omm)=exp2rom,jOut):
```

```
t2:=algsubs(Ei(-2*I*r*omm)=limit(Ei(-2*I*r*omm),r=infinity),t1):
t3:=coeff(t2,exp2rom):
t4:=coeff(t3,r,-1):
CinE:=solve(t4=0,CinE):

(* appendto(`formulas.out`);
b0E:=simplify(b0E);
CinE:=simplify(CinE);
b0S:=simplify(b0S);
sol_jzwIS[1];
sol_jzwIS[2];
sol_jzwIS[3];
sol_jzwSE[1];
sol_jzwSE[2];
sol_jzwSE[3];
writeto(`terminal`); *)

t5:=simplify(subs(exp2rom=0,t1)):
omega:=coeff(t5,r,0)*L4/(4+2*L2)/2:
jul:=coeff(t5,r,-1)*I*omm/2:
bOut_inf:=simplify(limit(bOut,r=infinity)):
news_check:=simplify(omega+bOut_inf+jul):
news_check1:=prlinRhoc(subs(sol_jzwSE,news_check)):
news_check2:=prlinRhoc(subs(sol_jzwIS,news_check1)):
news0:=simplify(sqrt(24)*news_check):

CinI:=0; #CinI:=subs(sol_jzwIS,CinI):CinI:=subs(sol_jzwSE,CinI):
as20:=asympt(Ei(-2*I*ommr0),ommr0,20):
t1:=convert(series(exp(2*I*(r0+del)*omm),del,16),polynom):
t2:=convert(series(Ei(-2*I*(r0+del)*omm),del,16),polynom):
t3:=convert(series(exp(-2*I*(r0+del)*omm),del,16),polynom):
t4:=convert(series(exp(-2*I*del*omm),del,16),polynom):

CinI:=algsubs(exp(2*I*(r0+del)*omm)=t1,CinI):
CinI:=algsubs(Ei(-2*I*(r0+del)*omm)=t2,CinI):
CinI:=algsubs(exp(-2*I*(r0+del)*omm)=t3,CinI):
CinI:=simplify(algsubs(exp(-2*I*omm*(del+r0))=t3,CinI)):
CinI:=simplify(algsubs(exp(-2*I*r0*omm)=1/e2iromm,CinI)):
CinI:=simplify(algsubs(exp(2*I*r0*omm)=e2ir0mm,CinI)):
CinI:=simplify(algsubs(exp(-2*I*omm*(del+r0))=t3,CinI)):
CinI:=subs(omm=ommr0/r0,CinI):
CinIt:=factor(convert(simplify(algsubs(Ei(-2*I*ommr0)=as20,CinI)),polynom)):

CinIt:=simplify(subs(ommr0=omm*r0,CinIt)):
CinIt:=algsubs(exp(-2*I*(r0+del)*omm)=t3,CinIt):
CinIt:=algsubs(exp(-2*I*del*omm)=t4,CinIt):
CinIt:=simplify(algsubs(exp(-2*I*r0*omm)=1/e2iromm,CinIt)):
CinIt:=simplify(algsubs(exp(2*I*r0*omm)=e2ir0mm,CinIt)):

C4I:=-CinIt/2: #From regular_0_IncomingGW.map
news:=simplify(sqrt(24)*news_check2):

assume(r0>0):assume(del>0):
mas:=int(4*Pi*r^2*Rhoc*rho_falloff,r=r0..r0+del):
```

```
Rhoc1:=solve(mas=mass,Rhoc):
#news:=subs(Rhoc=Rhoc1,news):
strain:=subs(Rhoc=Rhoc1,2*news/I/omm):

strain_del[0]:=factor(simplify(subs(del=0,strain))):
for a to 8 do
  strain_del[a]:=factor(simplify(del^a*subs(del=0,diff(strain,del$a)))):
od:
straindel:=simplify(sum(strain_del[b],b=0..8)):

strain_r0_0:=coeff(straindel,r0,0);
strain_r0_m1:=coeff(straindel,r0,-1);
strain_r0_m2:=simplify(coeff(coeff(straindel,r0,-2),del,0));

T1:=simplify(strain_r0_m1/r0/strain_r0_0);
T2:=expand(simplify(strain_r0_m2/r0^2/strain_r0_0));

CinE:=simplify(subs(Rhoc=Rhoc1,Rhoc*CinE));
```

```
g[   1   ,   1   ]:=   0   :
h[   1   ,   1   ]:=   exp(-2*B[0])*Vw[0]   :
g[   1   ,   2   ]:=   0   :
h[   1   ,   2   ]:=   -1/4*fo*(U[0]+Ub[0])*exp(-2*B[0])   :
g[   1   ,   3   ]:=   0   :
h[   1   ,   3   ]:=   1/4*I*(-Ub[0]*exp(-2*B[0])*fo+U[0]*exp(-2*B[0])*fo)   :
g[   1   ,   4   ]:=   -exp(2*B[0])   :
h[   1   ,   4   ]:=   -exp(-2*B[0])   :
g[   2   ,   1   ]:=   0   :
h[   2   ,   1   ]:=   -1/4*fo*(U[0]+Ub[0])*exp(-2*B[0])   :
g[   2   ,   2   ]:=   2*r^2/fo^2*(2*K[0]+J[0]+Jb[0])   :
h[   2   ,   2   ]:=   -1/8*fo^2*(-2*K[0]+J[0]+Jb[0])/r^2   :
g[   2   ,   3   ]:=   -2*I*r^2*(-Jb[0]+J[0])/fo^2   :
h[   2   ,   3   ]:=   1/8*I*fo^2*(-Jb[0]+J[0])/r^2   :
g[   2   ,   4   ]:=   -r^2*(K[0]*U[0]+K[0]*Ub[0]+J[0]*Ub[0]+Jb[0]*U[0])/fo   :
h[   2   ,   4   ]:=   0   :
g[   3   ,   1   ]:=   0   :
h[   3   ,   1   ]:=   1/4*I*(-Ub[0]*exp(-2*B[0])*fo+U[0]*exp(-2*B[0])*fo)   :
g[   3   ,   2   ]:=   -2*I*r^2*(-Jb[0]+J[0])/fo^2   :
h[   3   ,   2   ]:=   1/8*I*fo^2*(-Jb[0]+J[0])/r^2   :
g[   3   ,   3   ]:=   -2*r^2*(-2*K[0]+J[0]+Jb[0])/fo^2   :
h[   3   ,   3   ]:=   1/8*fo^2*(2*K[0]+J[0]+Jb[0])/r^2   :
g[   3   ,   4   ]:=   I*r^2*(-K[0]*Ub[0]+K[0]*U[0]+J[0]*Ub[0]-Jb[0]*U[0])/fo
   :
h[   3   ,   4   ]:=   0   :
g[   4   ,   1   ]:=   -exp(2*B[0])   :
h[   4   ,   1   ]:=   -exp(-2*B[0])   :
g[   4   ,   2   ]:=   -r^2*(K[0]*U[0]+K[0]*Ub[0]+J[0]*Ub[0]+Jb[0]*U[0])/fo   :
h[   4   ,   2   ]:=   0   :
g[   4   ,   3   ]:=   I*r^2*(-K[0]*Ub[0]+K[0]*U[0]+J[0]*Ub[0]-Jb[0]*U[0])/fo
   :
h[   4   ,   3   ]:=   0   :
g[   4   ,   4   ]:=   -exp(2*B[0])*Vw[0]+r^2*K[0]*U[0]*Ub[0]+1/2*r^2*J[0]*Ub[0
]^2+1/2*r^2*Jb[0]*U[0]^2   :
h[   4   ,   4   ]:=   0   :
Csum[   1   ]:=   -1/2*(-4*B[1]*r-4*K[0]^2-2*K[0]*r*K[1]+4*J[0]*Jb[0]+J[0]*r*Jb
[1]+Jb[0]*r*J[1])/r   :
Csum[   2   ]:=   1/2*(4*J[0]*fq*Jb[0]+4*B[3]+4*B[2]-Jb[0]*J[3]-J[0]*Jb[2]-Jb[0
]*J[2]+2*K[0]*K[3]-4*fq*K[0]^2-J[0]*Jb[3]+2*K[0]*K[2])/fo   :
Csum[   3   ]:=   -1/2*I*(Jb[0]*J[3]-J[0]*Jb[2]-Jb[0]*J[2]+2*K[0]*K[2]-2*K[0]*K
[3]+J[0]*Jb[3]+4*B[2]-4*B[3]-4*I*fp*K[0]^2+4*I*Jb[0]*fp*J[0])/fo   :
Csum[   4   ]:=   2*B[4]-1/2*J[0]*Jb[4]+K[0]*K[4]-1/2*Jb[0]*J[4]   :
C[   1   ,   1   ,   1   ]:=   2*B[1]   :
C[   1   ,   1   ,   2   ]:=   0   :
C[   1   ,   1   ,   3   ]:=   0   :
C[   1   ,   1   ,   4   ]:=   0   :
C[   1   ,   2   ,   1   ]:=   1/2*(r^2*K[0]*U[1]+r^2*K[0]*Ub[1]+r^2*J[0]*Ub[1]
+r^2*Jb[0]*U[1]+2*exp(2*B[0])*B[3]+2*exp(2*B[0])*B[2])/fo*exp(-2*B[0])   :
C[   1   ,   2   ,   2   ]:=   -1/4*(-4*K[0]^2-2*K[0]*r*K[1]-K[0]*r*J[1]-K[0]*r
*Jb[1]+4*J[0]*Jb[0]+J[0]*r*K[1]+J[0]*r*Jb[1]+Jb[0]*r*K[1]+Jb[0]*r*J[1])/r   :
C[   1   ,   2   ,   3   ]:=   1/4*I*(-Jb[0]*K[1]-Jb[0]*J[1]+J[0]*K[1]+J[0]*Jb[
1]+K[0]*Jb[1]-K[0]*J[1])   :
C[   1   ,   2   ,   4   ]:=   0   :
C[   1   ,   3   ,   1   ]:=   -1/2*I/fo*(r^2*K[0]*U[1]-r^2*K[0]*Ub[1]+r^2*J[0]
```

```
*Ub[1]-r^2*Jb[0]*U[1]-2*exp(2*B[0])*B[3]+2*exp(2*B[0])*B[2])*exp(-2*B[0])   :
C[   1   ,   3   ,   2   ]:=   -1/4*I*(-K[0]*Jb[1]+K[0]*J[1]+J[0]*Jb[1]-Jb[0]*J
[1]+Jb[0]*K[1]-J[0]*K[1])   :
C[   1   ,   3   ,   3   ]:=   -1/4*(4*J[0]*Jb[0]+Jb[0]*r*J[1]+J[0]*r*Jb[1]-4*K
[0]^2-2*K[0]*r*K[1]+K[0]*r*J[1]+K[0]*r*Jb[1]-J[0]*r*K[1]-Jb[0]*r*K[1])/r   :
C[   1   ,   3   ,   4   ]:=   0   :
C[   1   ,   4   ,   1   ]:=   -1/4*(-4*B[1]*exp(2*B[0])*Vw[0]-2*exp(2*B[0])*Vw
[1]+2*U[0]*exp(2*B[0])*B[3]+2*Ub[0]*exp(2*B[0])*B[2]+r^2*K[0]*U[0]*Ub[1]+r^2*K[
0]*Ub[0]*U[1]+r^2*J[0]*Ub[0]*Ub[1]+r^2*Jb[0]*U[0]*U[1])*exp(-2*B[0])   :
C[   1   ,   4   ,   2   ]:=   1/8*fo*(-K[0]*r^2*J[1]*Ub[0]-K[0]*r^2*Jb[1]*U[0]
+Jb[0]*r^2*K[1]*U[0]-2*r*K[0]^2*U[0]-2*r*K[0]^2*Ub[0]-r^2*K[0]^2*U[1]-r^2*K[0]^
2*Ub[1]+2*K[0]*exp(2*B[0])*B[3]+2*K[0]*exp(2*B[0])*B[2]-2*J[0]*exp(2*B[0])*B[3]
-2*Jb[0]*exp(2*B[0])*B[2]-K[0]*r^2*K[1]*U[0]-K[0]*r^2*K[1]*Ub[0]+2*J[0]*r*Jb[0]
*U[0]+J[0]*r^2*K[1]*Ub[0]+J[0]*r^2*Jb[1]*U[0]+J[0]*r^2*Jb[0]*U[1]+2*Jb[0]*r*J[0
]*Ub[0]+Jb[0]*r^2*J[1]*Ub[0]+Jb[0]*r^2*J[0]*Ub[1])/r^2   :
C[   1   ,   4   ,   3   ]:=   -1/8*I*(-Ub[0]*J[1]*r^2*K[0]*fo+U[0]*Jb[1]*r^2*K
[0]*fo-U[0]*K[1]*r^2*Jb[0]*fo-2*B[3]*exp(2*B[0])*K[0]*fo+2*B[2]*exp(2*B[0])*K[0
]*fo+2*B[2]*exp(2*B[0])*Jb[0]*fo-2*B[3]*exp(2*B[0])*J[0]*fo-2*U[0]*K[0]^2*r*fo+
2*Ub[0]*K[0]^2*r*fo-U[1]*K[0]^2*r^2*fo+Ub[1]*K[0]^2*r^2*fo-U[0]*K[1]*r^2*K[0]*
fo+Ub[0]*K[1]*r^2*K[0]*fo+2*U[0]*Jb[0]*r*J[0]*fo+Ub[0]*K[1]*r^2*J[0]*fo+U[0]*Jb
[1]*r^2*J[0]*fo+U[1]*Jb[0]*r^2*J[0]*fo-2*Ub[0]*J[0]*r*Jb[0]*fo-Ub[0]*J[1]*r^2*
Jb[0]*fo-Ub[1]*J[0]*r^2*Jb[0]*fo)/r^2   :
C[   1   ,   4   ,   4   ]:=   0   :
C[   2   ,   1   ,   1   ]:=   1/2*(r^2*K[0]*U[1]+r^2*K[0]*Ub[1]+r^2*J[0]*Ub[1]
+r^2*Jb[0]*U[1]+2*exp(2*B[0])*B[3]+2*exp(2*B[0])*B[2])/fo*exp(-2*B[0])   :
C[   2   ,   1   ,   2   ]:=   -1/4*(-4*K[0]^2-2*K[0]*r*K[1]-K[0]*r*J[1]-K[0]*r
*Jb[1]+4*J[0]*Jb[0]+J[0]*r*K[1]+J[0]*r*Jb[1]+Jb[0]*r*K[1]+Jb[0]*r*J[1])/r   :
C[   2   ,   1   ,   3   ]:=   1/4*I*(-Jb[0]*K[1]-Jb[0]*J[1]+J[0]*K[1]+J[0]*Jb[
1]+K[0]*Jb[1]-K[0]*J[1])   :
C[   2   ,   1   ,   4   ]:=   0   :
C[   2   ,   2   ,   1   ]:=   1/2*r*(-4*Vw[0]*r*K[1]-2*Vw[0]*r*J[1]-2*Vw[0]*r*
Jb[1]+2*r*K[3]*U[0]+r*J[3]*U[0]+r*Jb[3]*U[0]+2*r*K[2]*Ub[0]+r*J[2]*Ub[0]+r*Jb[2
]*Ub[0]+2*r*K[0]*U[3]+2*r*K[0]*U[2]+2*r*K[0]*Ub[3]+2*r*K[0]*Ub[2]+2*r*J[0]*Ub[3
]+2*r*J[0]*Ub[2]+2*r*Jb[0]*U[3]+2*r*Jb[0]*U[2]-8*Vw[0]*K[0]-4*Vw[0]*J[0]-4*Vw[0
]*Jb[0]+2*r*J[4]+2*r*Jb[4]+4*r*K[4])*exp(-2*B[0])/fo^2   :
C[   2   ,   2   ,   2   ]:=   1/4*(exp(2*B[0])*K[0]*Jb[2]+exp(2*B[0])*K[0]*Jb[
3]+4*exp(2*B[0])*J[0]*fq*Jb[0]+exp(2*B[0])*K[0]*J[2]-2*exp(2*B[0])*Jb[0]*J[3]-2
*exp(2*B[0])*J[0]*Jb[2]+exp(2*B[0])*Jb[0]*Jb[2]-exp(2*B[0])*Jb[0]*J[2]+2*exp(2*
B[0])*K[0]*K[3]-4*exp(2*B[0])*fq*K[0]^2-2*exp(2*B[0])*Jb[0]*K[3]-exp(2*B[0])*J[
0]*Jb[3]+exp(2*B[0])*K[0]*J[3]+2*exp(2*B[0])*K[0]*K[2]-2*exp(2*B[0])*J[0]*K[2]+
exp(2*B[0])*J[0]*J[3]+2*Ub[0]*r^2*K[1]+Ub[0]*r^2*J[1]+2*U[0]*r^2*K[1]+U[0]*r^2*
J[1]+U[0]*r^2*Jb[1]+2*r*Ub[0]*J[0]+2*r*Ub[0]*Jb[0]+2*r*U[0]*J[0]+2*r*U[0]*Jb[0]
+4*r*Ub[0]*K[0]+Ub[0]*r^2*Jb[1]+4*r*U[0]*K[0])/fo*exp(-2*B[0])   :
C[   2   ,   2   ,   3   ]:=   -1/4*I*(-3*exp(2*B[0])*K[0]*Jb[2]-exp(2*B[0])*K[
0]*Jb[3]+exp(2*B[0])*K[0]*J[2]+2*exp(2*B[0])*Jb[0]*J[3]-2*exp(2*B[0])*J[0]*Jb[2
]-exp(2*B[0])*Jb[0]*Jb[2]+exp(2*B[0])*Jb[0]*J[2]+2*exp(2*B[0])*K[0]*K[3]+2*exp(
2*B[0])*Jb[0]*K[3]-exp(2*B[0])*J[0]*Jb[3]+3*exp(2*B[0])*K[0]*J[3]-2*exp(2*B[0])
*K[0]*K[2]-2*exp(2*B[0])*J[0]*K[2]+exp(2*B[0])*J[0]*J[3]-4*I*exp(2*B[0])*Jb[0]*
fp*J[0]+4*I*exp(2*B[0])*fp*K[0]^2-2*Ub[0]*r^2*K[1]-Ub[0]*r^2*J[1]+2*U[0]*r^2*K[
1]+U[0]*r^2*J[1]+U[0]*r^2*Jb[1]-2*r*Ub[0]*J[0]-2*r*Ub[0]*Jb[0]+2*r*U[0]*J[0]+2*
r*U[0]*Jb[0]-4*r*Ub[0]*K[0]-Ub[0]*r^2*Jb[1]+4*r*U[0]*K[0])/fo*exp(-2*B[0])   :
C[   2   ,   2   ,   4   ]:=   exp(-2*B[0])*r*(4*K[0]+2*J[0]+2*Jb[0]+2*r*K[1]+r
*J[1]+r*Jb[1])/fo^2   :
C[   2   ,   3   ,   1   ]:=   -1/2*I*(-U[0]*Jb[3]*exp(-2*B[0])*r^2+2*Jb[1]*Vw[
```

```
0]*exp(-2*B[0])*r^2-2*U[3]*Jb[0]*exp(-2*B[0])*r^2+2*J[4]*exp(-2*B[0])*r^2+2*U[2
]*K[0]*exp(-2*B[0])*r^2-2*Ub[3]*K[0]*exp(-2*B[0])*r^2+2*Ub[2]*J[0]*exp(-2*B[0])
*r^2+U[0]*J[3]*exp(-2*B[0])*r^2-Ub[0]*Jb[2]*exp(-2*B[0])*r^2-2*J[1]*Vw[0]*exp(-
2*B[0])*r^2-2*Jb[4]*exp(-2*B[0])*r^2+4*Jb[0]*Vw[0]*exp(-2*B[0])*r-4*J[0]*Vw[0]*
exp(-2*B[0])*r+Ub[0]*J[2]*exp(-2*B[0])*r^2)/fo^2   :
C[   2   ,   3   ,   2   ]:=   -1/4*I*(-2*r*Ub[0]*Jb[0]-2*r*U[0]*Jb[0]+2*r*U[0]
*J[0]-U[0]*r^2*Jb[1]+U[0]*r^2*J[1]-2*exp(2*B[0])*J[0]*K[2]+exp(2*B[0])*J[0]*J[3
]+exp(2*B[0])*J[0]*Jb[3]-exp(2*B[0])*Jb[0]*J[2]-exp(2*B[0])*Jb[0]*Jb[2]+2*exp(2
*B[0])*K[0]*K[2]-exp(2*B[0])*K[0]*J[3]+exp(2*B[0])*K[0]*J[2]-exp(2*B[0])*K[0]*
Jb[3]+exp(2*B[0])*K[0]*Jb[2]-2*exp(2*B[0])*K[0]*K[3]+2*exp(2*B[0])*Jb[0]*K[3]+4
*I*exp(2*B[0])*Jb[0]*fp*J[0]-4*I*exp(2*B[0])*fp*K[0]^2+2*r*Ub[0]*J[0]-Ub[0]*r^2
*Jb[1]+Ub[0]*r^2*J[1])/fo*exp(-2*B[0])   :
C[   2   ,   3   ,   3   ]:=   -1/4*(-Ub[0]*r^2*J[1]+U[0]*r^2*J[1]-U[0]*r^2*Jb[
1]-2*r*Ub[0]*J[0]+2*r*Ub[0]*Jb[0]+2*r*U[0]*J[0]-2*r*U[0]*Jb[0]+Ub[0]*r^2*Jb[1]+
exp(2*B[0])*Jb[0]*Jb[2]-2*exp(2*B[0])*J[0]*K[2]+exp(2*B[0])*J[0]*J[3]+exp(2*B[0
])*J[0]*Jb[3]-2*exp(2*B[0])*Jb[0]*K[3]+exp(2*B[0])*Jb[0]*J[2]-2*exp(2*B[0])*K[0
]*K[3]-2*exp(2*B[0])*K[0]*K[2]+exp(2*B[0])*K[0]*J[3]+exp(2*B[0])*K[0]*Jb[3]+4*
exp(2*B[0])*fq*K[0]^2+exp(2*B[0])*K[0]*J[2]+exp(2*B[0])*K[0]*Jb[2]-4*exp(2*B[0]
)*J[0]*fq*Jb[0])*exp(-2*B[0])/fo   :
C[   2   ,   3   ,   4   ]:=   -I*(-2*Jb[0]*exp(-2*B[0])*r+2*J[0]*exp(-2*B[0])*
r-Jb[1]*exp(-2*B[0])*r^2+J[1]*exp(-2*B[0])*r^2)/fo^2   :
C[   2   ,   4   ,   1   ]:=   -1/4*(r^2*U[0]*K[0]*U[3]+r^2*Ub[0]*Jb[2]*U[0]+2*
r^2*U[0]*Jb[4]+2*r^2*Ub[0]*K[4]+2*r^2*Ub[0]*J[4]-4*Vw[0]*r*Ub[0]*K[0]-4*Vw[0]*r
*Ub[0]*J[0]-4*Vw[0]*r*U[0]*Jb[0]-2*Vw[0]*U[0]*r^2*K[1]-2*Vw[0]*Ub[0]*r^2*K[1]-2
*Vw[0]*Ub[0]*r^2*J[1]-2*Vw[0]*U[0]*r^2*Jb[1]-2*Vw[0]*r^2*K[0]*U[1]-2*Vw[0]*r^2*
K[0]*Ub[1]-2*Vw[0]*r^2*J[0]*Ub[1]-2*Vw[0]*r^2*Jb[0]*U[1]+2*r^2*U[0]*K[4]-4*Vw[0
]*r*U[0]*K[0]+r^2*K[3]*U[0]*Ub[0]+2*r^2*K[0]*U[0]*Ub[3]+r^2*K[0]*U[0]*Ub[2]+r^2
*K[0]*Ub[0]*U[3]+2*r^2*K[0]*Ub[0]*U[2]+r^2*Ub[0]*J[0]*Ub[3]+2*r^2*Ub[0]*J[0]*Ub
[2]+2*r^2*U[0]*Jb[0]*U[3]+r^2*U[0]*Jb[0]*U[2]+r^2*K[2]*U[0]*Ub[0]+r^2*Jb[3]*U[0
]^2+r^2*J[2]*Ub[0]^2-2*exp(2*B[0])*Vw[3]-2*exp(2*B[0])*Vw[2]+r^2*Ub[0]*K[0]*Ub[
2]+r^2*Ub[0]*Jb[0]*U[2]+r^2*U[0]*J[0]*Ub[3]+r^2*U[0]*J[3]*Ub[0]+r^2*K[2]*Ub[0]^
2+r^2*K[3]*U[0]^2)*exp(-2*B[0])/fo   :
C[   2   ,   4   ,   2   ]:=   -1/8*(r^2*K[0]*U[0]*Ub[1]+r^2*K[0]*Ub[0]*U[1]+r^
2*J[0]*Ub[0]*Ub[1]+r^2*Jb[0]*U[0]*U[1]+Ub[0]*r^2*Jb[0]*U[1]+2*Ub[0]*r*U[0]*Jb[0
]+Ub[0]*U[0]*r^2*Jb[1]+Ub[0]*r^2*K[0]*Ub[1]+4*U[0]*r*Ub[0]*K[0]+2*U[0]*r*Ub[0]*
J[0]+2*U[0]*Ub[0]*r^2*K[1]+U[0]*Ub[0]*r^2*J[1]+U[0]*r^2*K[0]*U[1]+U[0]*r^2*J[0]
*Ub[1]+2*r*Ub[0]^2*K[0]+2*r*Ub[0]^2*J[0]+Ub[0]^2*r^2*K[1]+Ub[0]^2*r^2*J[1]-2*U[
0]*exp(2*B[0])*B[3]-2*Ub[0]*exp(2*B[0])*B[2]+2*r*U[0]^2*K[0]+2*r*U[0]^2*Jb[0]+U
[0]^2*r^2*K[1]+U[0]^2*r^2*Jb[1]+2*exp(2*B[0])*Jb[0]*J[4]-2*U[0]*exp(2*B[0])*B[2
]-2*Ub[0]*exp(2*B[0])*B[3]-4*exp(2*B[0])*K[0]*K[4]-2*exp(2*B[0])*K[0]*J[4]-2*
exp(2*B[0])*K[0]*Jb[4]+2*exp(2*B[0])*J[0]*K[4]+2*exp(2*B[0])*J[0]*Jb[4]+2*exp(2
*B[0])*Jb[0]*K[4]-exp(2*B[0])*Jb[0]*K[3]*U[0]+exp(2*B[0])*Jb[0]*K[0]*Ub[2]-exp(
2*B[0])*Jb[0]*J[0]*Ub[3]-exp(2*B[0])*Jb[0]*K[0]*U[3]+exp(2*B[0])*J[0]*K[0]*U[3]
+exp(2*B[0])*Jb[0]*K[2]*Ub[0]-exp(2*B[0])*Jb[0]*J[3]*Ub[0]+exp(2*B[0])*J[0]^2*
Ub[3]+exp(2*B[0])*Jb[0]^2*U[2]+exp(2*B[0])*J[0]*J[3]*Ub[0]+exp(2*B[0])*J[0]*K[3
]*U[0]-exp(2*B[0])*J[0]*K[2]*Ub[0]-exp(2*B[0])*J[0]*Jb[0]*U[2]-exp(2*B[0])*J[0]
*K[0]*Ub[2]+exp(2*B[0])*Jb[0]*Jb[2]*U[0]-exp(2*B[0])*J[0]*Jb[2]*U[0])*exp(-2*B[
0])   :
C[   2   ,   4   ,   3   ]:=   1/8*I*(2*exp(2*B[0])*K[0]^2*U[3]-2*exp(2*B[0])*K
[0]^2*Ub[2]+2*exp(2*B[0])*K[0]*J[3]*Ub[0]+2*exp(2*B[0])*K[0]*J[0]*Ub[3]-2*exp(2
*B[0])*K[0]*Jb[0]*U[2]-2*exp(2*B[0])*K[0]*Jb[2]*U[0]+2*exp(2*B[0])*K[0]*K[3]*U[
0]+r^2*K[0]*U[0]*Ub[1]-r^2*K[0]*Ub[0]*U[1]-r^2*J[0]*Ub[0]*Ub[1]+r^2*Jb[0]*U[0]*
U[1]-Ub[0]*r^2*Jb[0]*U[1]-2*Ub[0]*r*U[0]*Jb[0]-Ub[0]*U[0]*r^2*Jb[1]-Ub[0]*r^2*K
[0]*Ub[1]+2*U[0]*r*Ub[0]*J[0]+U[0]*Ub[0]*r^2*J[1]+U[0]*r^2*K[0]*U[1]+U[0]*r^2*J
```

```
[0]*Ub[1]-2*r*Ub[0]^2*K[0]-2*r*Ub[0]^2*J[0]-Ub[0]^2*r^2*K[1]-Ub[0]^2*r^2*J[1]-2
*U[0]*exp(2*B[0])*B[3]+2*Ub[0]*exp(2*B[0])*B[2]+2*r*U[0]^2*K[0]+2*r*U[0]^2*Jb[0
]+U[0]^2*r^2*K[1]+U[0]^2*r^2*Jb[1]-2*exp(2*B[0])*K[0]*K[2]*Ub[0]-2*exp(2*B[0])*
Jb[0]*J[4]-2*U[0]*exp(2*B[0])*B[2]+2*Ub[0]*exp(2*B[0])*B[3]-2*exp(2*B[0])*K[0]*
J[4]+2*exp(2*B[0])*K[0]*Jb[4]+2*exp(2*B[0])*J[0]*K[4]+2*exp(2*B[0])*J[0]*Jb[4]-
2*exp(2*B[0])*Jb[0]*K[4]+exp(2*B[0])*Jb[0]*K[3]*U[0]-exp(2*B[0])*Jb[0]*K[0]*Ub[
2]+exp(2*B[0])*Jb[0]*J[0]*Ub[3]+exp(2*B[0])*Jb[0]*K[0]*U[3]+exp(2*B[0])*J[0]*K[
0]*U[3]-exp(2*B[0])*Jb[0]*K[2]*Ub[0]+exp(2*B[0])*Jb[0]*J[3]*Ub[0]+exp(2*B[0])*J
[0]^2*Ub[3]-exp(2*B[0])*Jb[0]^2*U[2]+exp(2*B[0])*J[0]*J[3]*Ub[0]+exp(2*B[0])*J[
0]*K[3]*U[0]-exp(2*B[0])*J[0]*K[2]*Ub[0]-exp(2*B[0])*J[0]*Jb[0]*U[2]-exp(2*B[0]
)*J[0]*K[0]*Ub[2]-exp(2*B[0])*Jb[0]*Jb[2]*U[0]-exp(2*B[0])*J[0]*Jb[2]*U[0])*exp
(-2*B[0])   :
C[   2   ,   4   ,   4   ]:=   -1/2*(-2*exp(2*B[0])*B[3]-2*exp(2*B[0])*B[2]+2*r
*U[0]*K[0]+2*r*Ub[0]*K[0]+2*r*Ub[0]*J[0]+2*r*U[0]*Jb[0]+U[0]*r^2*K[1]+Ub[0]*r^2
*K[1]+Ub[0]*r^2*J[1]+U[0]*r^2*Jb[1]+r^2*K[0]*U[1]+r^2*K[0]*Ub[1]+r^2*J[0]*Ub[1]
+r^2*Jb[0]*U[1])*exp(-2*B[0])/fo   :
C[   3   ,   1   ,   1   ]:=   -1/2*I/fo*(r^2*K[0]*U[1]-r^2*K[0]*Ub[1]+r^2*J[0]
*Ub[1]-r^2*Jb[0]*U[1]-2*exp(2*B[0])*B[3]+2*exp(2*B[0])*B[2])*exp(-2*B[0])   :
C[   3   ,   1   ,   2   ]:=   -1/4*I*(-K[0]*Jb[1]+K[0]*J[1]+J[0]*Jb[1]-Jb[0]*J
[1]+Jb[0]*K[1]-J[0]*K[1])   :
C[   3   ,   1   ,   3   ]:=   -1/4*(4*J[0]*Jb[0]+Jb[0]*r*J[1]+J[0]*r*Jb[1]-4*K
[0]^2-2*K[0]*r*K[1]+K[0]*r*J[1]+K[0]*r*Jb[1]-J[0]*r*K[1]-Jb[0]*r*K[1])/r   :
C[   3   ,   1   ,   4   ]:=   0   :
C[   3   ,   2   ,   1   ]:=   -1/2*I*(-U[0]*Jb[3]*exp(-2*B[0])*r^2+2*Jb[1]*Vw[
0]*exp(-2*B[0])*r^2-2*U[3]*Jb[0]*exp(-2*B[0])*r^2+2*J[4]*exp(-2*B[0])*r^2+2*U[2
]*K[0]*exp(-2*B[0])*r^2-2*Ub[3]*K[0]*exp(-2*B[0])*r^2+2*Ub[2]*J[0]*exp(-2*B[0])
*r^2+U[0]*J[3]*exp(-2*B[0])*r^2-Ub[0]*Jb[2]*exp(-2*B[0])*r^2-2*J[1]*Vw[0]*exp(-
2*B[0])*r^2-2*Jb[4]*exp(-2*B[0])*r^2+4*Jb[0]*Vw[0]*exp(-2*B[0])*r-4*J[0]*Vw[0]*
exp(-2*B[0])*r+Ub[0]*J[2]*exp(-2*B[0])*r^2)/fo^2   :
C[   3   ,   2   ,   2   ]:=   -1/4*I*(-2*r*Ub[0]*Jb[0]-2*r*U[0]*Jb[0]+2*r*U[0]
*J[0]-U[0]*r^2*Jb[1]+U[0]*r^2*J[1]-2*exp(2*B[0])*J[0]*K[2]+exp(2*B[0])*J[0]*J[3
]+exp(2*B[0])*J[0]*Jb[3]-exp(2*B[0])*Jb[0]*J[2]-exp(2*B[0])*Jb[0]*Jb[2]+2*exp(2
*B[0])*K[0]*K[2]-exp(2*B[0])*K[0]*J[3]+exp(2*B[0])*K[0]*J[2]-exp(2*B[0])*K[0]*
Jb[3]+exp(2*B[0])*K[0]*Jb[2]-2*exp(2*B[0])*K[0]*K[3]+2*exp(2*B[0])*Jb[0]*K[3]+4
*I*exp(2*B[0])*Jb[0]*fp*J[0]-4*I*exp(2*B[0])*fp*K[0]^2+2*r*Ub[0]*J[0]-Ub[0]*r^2
*Jb[1]+Ub[0]*r^2*J[1])/fo*exp(-2*B[0])   :
C[   3   ,   2   ,   3   ]:=   -1/4*(-Ub[0]*r^2*J[1]+U[0]*r^2*J[1]-U[0]*r^2*Jb[
1]-2*r*Ub[0]*J[0]+2*r*Ub[0]*Jb[0]+2*r*U[0]*J[0]-2*r*U[0]*Jb[0]+Ub[0]*r^2*Jb[1]+
exp(2*B[0])*Jb[0]*Jb[2]-2*exp(2*B[0])*J[0]*K[2]+exp(2*B[0])*J[0]*J[3]+exp(2*B[0
])*J[0]*Jb[3]-2*exp(2*B[0])*Jb[0]*K[3]+exp(2*B[0])*Jb[0]*J[2]-2*exp(2*B[0])*K[0
]*K[3]-2*exp(2*B[0])*K[0]*K[2]+exp(2*B[0])*K[0]*J[3]+exp(2*B[0])*K[0]*Jb[3]+4*
exp(2*B[0])*fq*K[0]^2+exp(2*B[0])*K[0]*J[2]+exp(2*B[0])*K[0]*Jb[2]-4*exp(2*B[0]
)*J[0]*fq*Jb[0])*exp(-2*B[0])/fo   :
C[   3   ,   2   ,   4   ]:=   -I*(-2*Jb[0]*exp(-2*B[0])*r+2*J[0]*exp(-2*B[0])*
r-Jb[1]*exp(-2*B[0])*r^2+J[1]*exp(-2*B[0])*r^2)/fo^2   :
C[   3   ,   3   ,   1   ]:=   1/2*r*(-4*Vw[0]*r*K[1]+2*Vw[0]*r*J[1]+2*Vw[0]*r*
Jb[1]+2*r*K[3]*U[0]-r*J[3]*U[0]-r*Jb[3]*U[0]+2*r*K[2]*Ub[0]-r*J[2]*Ub[0]-r*Jb[2
]*Ub[0]+2*r*K[0]*U[3]-2*r*K[0]*U[2]-2*r*K[0]*Ub[3]+2*r*K[0]*Ub[2]+2*r*J[0]*Ub[3
]-2*r*J[0]*Ub[2]-2*r*Jb[0]*U[3]+2*r*Jb[0]*U[2]-8*Vw[0]*K[0]+4*Vw[0]*J[0]+4*Vw[0
]*Jb[0]-2*r*J[4]-2*r*Jb[4]+4*r*K[4])*exp(-2*B[0])/fo^2   :
C[   3   ,   3   ,   2   ]:=   -1/4*(-3*exp(2*B[0])*K[0]*Jb[2]+exp(2*B[0])*K[0]
*Jb[3]+4*exp(2*B[0])*J[0]*fq*Jb[0]+exp(2*B[0])*K[0]*J[2]+2*exp(2*B[0])*Jb[0]*J[
3]+2*exp(2*B[0])*J[0]*Jb[2]+exp(2*B[0])*Jb[0]*Jb[2]-exp(2*B[0])*Jb[0]*J[2]+2*
exp(2*B[0])*K[0]*K[3]-4*exp(2*B[0])*fq*K[0]^2-2*exp(2*B[0])*Jb[0]*K[3]-exp(2*B[
```

```
0])*J[0]*Jb[3]-3*exp(2*B[0])*K[0]*J[3]+2*exp(2*B[0])*K[0]*K[2]-2*exp(2*B[0])*J[
0]*K[2]+exp(2*B[0])*J[0]*J[3]-2*Ub[0]*r^2*K[1]+Ub[0]*r^2*J[1]-2*U[0]*r^2*K[1]+U
[0]*r^2*J[1]+U[0]*r^2*Jb[1]+2*r*Ub[0]*J[0]+2*r*Ub[0]*Jb[0]+2*r*U[0]*J[0]+2*r*U[
0]*Jb[0]-4*r*Ub[0]*K[0]+Ub[0]*r^2*Jb[1]-4*r*U[0]*K[0])*exp(-2*B[0])/fo   :
C[   3   ,   3   ,   3   ]:=   1/4*I*(exp(2*B[0])*K[0]*Jb[2]-exp(2*B[0])*K[0]*
Jb[3]+exp(2*B[0])*K[0]*J[2]-2*exp(2*B[0])*Jb[0]*J[3]+2*exp(2*B[0])*J[0]*Jb[2]-
exp(2*B[0])*Jb[0]*Jb[2]+exp(2*B[0])*Jb[0]*J[2]+2*exp(2*B[0])*K[0]*K[3]+2*exp(2*
B[0])*Jb[0]*K[3]-exp(2*B[0])*J[0]*Jb[3]-exp(2*B[0])*K[0]*J[3]-2*exp(2*B[0])*K[0
]*K[2]-2*exp(2*B[0])*J[0]*K[2]+exp(2*B[0])*J[0]*J[3]-4*I*exp(2*B[0])*Jb[0]*fp*J
[0]+4*I*exp(2*B[0])*fp*K[0]^2+2*Ub[0]*r^2*K[1]-Ub[0]*r^2*J[1]-2*U[0]*r^2*K[1]+U
[0]*r^2*J[1]+U[0]*r^2*Jb[1]-2*r*Ub[0]*J[0]-2*r*Ub[0]*Jb[0]+2*r*U[0]*J[0]+2*r*U[
0]*Jb[0]+4*r*Ub[0]*K[0]-Ub[0]*r^2*Jb[1]-4*r*U[0]*K[0])/fo*exp(-2*B[0])   :
C[   3   ,   3   ,   4   ]:=   -exp(-2*B[0])*r*(-4*K[0]+2*J[0]+2*Jb[0]-2*r*K[1]
+r*J[1]+r*Jb[1])/fo^2   :
C[   3   ,   4   ,   1   ]:=   1/4*I*(r^2*U[0]*K[0]*U[3]-r^2*Ub[0]*Jb[2]*U[0]-2
*r^2*U[0]*Jb[4]-2*r^2*Ub[0]*K[4]+2*r^2*Ub[0]*J[4]+4*Vw[0]*r*Ub[0]*K[0]-4*Vw[0]*
r*Ub[0]*J[0]+4*Vw[0]*r*U[0]*Jb[0]-2*Vw[0]*U[0]*r^2*K[1]+2*Vw[0]*Ub[0]*r^2*K[1]-
2*Vw[0]*Ub[0]*r^2*J[1]+2*Vw[0]*U[0]*r^2*Jb[1]-2*Vw[0]*r^2*K[0]*U[1]+2*Vw[0]*r^2
*K[0]*Ub[1]-2*Vw[0]*r^2*J[0]*Ub[1]+2*Vw[0]*r^2*Jb[0]*U[1]+2*r^2*U[0]*K[4]-4*Vw[
0]*r*U[0]*K[0]-r^2*K[3]*U[0]*Ub[0]-2*r^2*K[0]*U[0]*Ub[3]+r^2*K[0]*U[0]*Ub[2]-r^
2*K[0]*Ub[0]*U[3]+2*r^2*K[0]*Ub[0]*U[2]-r^2*Ub[0]*J[0]*Ub[3]+2*r^2*Ub[0]*J[0]*
Ub[2]-2*r^2*U[0]*Jb[0]*U[3]+r^2*U[0]*Jb[0]*U[2]+r^2*K[2]*U[0]*Ub[0]-r^2*Jb[3]*U
[0]^2+r^2*J[2]*Ub[0]^2+2*exp(2*B[0])*Vw[3]-2*exp(2*B[0])*Vw[2]-r^2*Ub[0]*K[0]*
Ub[2]-r^2*Ub[0]*Jb[0]*U[2]+r^2*U[0]*J[0]*Ub[3]+r^2*U[0]*J[3]*Ub[0]-r^2*K[2]*Ub[
0]^2+r^2*K[3]*U[0]^2)*exp(-2*B[0])/fo   :
C[   3   ,   4   ,   2   ]:=   1/8*I*(-2*exp(2*B[0])*K[0]^2*U[3]+2*exp(2*B[0])*
K[0]^2*Ub[2]-2*exp(2*B[0])*K[0]*J[3]*Ub[0]-2*exp(2*B[0])*K[0]*J[0]*Ub[3]+2*exp(
2*B[0])*K[0]*Jb[0]*U[2]+2*exp(2*B[0])*K[0]*Jb[2]*U[0]-2*exp(2*B[0])*K[0]*K[3]*U
[0]-r^2*K[0]*U[0]*Ub[1]+r^2*K[0]*Ub[0]*U[1]+r^2*J[0]*Ub[0]*Ub[1]-r^2*Jb[0]*U[0]
*U[1]-Ub[0]*r^2*Jb[0]*U[1]-2*Ub[0]*r*U[0]*Jb[0]-Ub[0]*U[0]*r^2*Jb[1]-Ub[0]*r^2*
K[0]*Ub[1]+2*U[0]*r*Ub[0]*J[0]+U[0]*Ub[0]*r^2*J[1]+U[0]*r^2*K[0]*U[1]+U[0]*r^2*
J[0]*Ub[1]-2*r*Ub[0]^2*K[0]+2*r*Ub[0]^2*J[0]-Ub[0]^2*r^2*K[1]+Ub[0]^2*r^2*J[1]+
2*U[0]*exp(2*B[0])*B[3]-2*Ub[0]*exp(2*B[0])*B[2]+2*r*U[0]^2*K[0]-2*r*U[0]^2*Jb[
0]+U[0]^2*r^2*K[1]-U[0]^2*r^2*Jb[1]+2*exp(2*B[0])*K[0]*K[2]*Ub[0]+2*exp(2*B[0])
*Jb[0]*J[4]-2*U[0]*exp(2*B[0])*B[2]+2*Ub[0]*exp(2*B[0])*B[3]-2*exp(2*B[0])*K[0]
*J[4]+2*exp(2*B[0])*K[0]*Jb[4]+2*exp(2*B[0])*J[0]*K[4]-2*exp(2*B[0])*J[0]*Jb[4]
-2*exp(2*B[0])*Jb[0]*K[4]+exp(2*B[0])*Jb[0]*K[3]*U[0]-exp(2*B[0])*Jb[0]*K[0]*Ub
[2]+exp(2*B[0])*Jb[0]*J[0]*Ub[3]+exp(2*B[0])*Jb[0]*K[0]*U[3]+exp(2*B[0])*J[0]*K
[0]*U[3]-exp(2*B[0])*Jb[0]*K[2]*Ub[0]+exp(2*B[0])*Jb[0]*J[3]*Ub[0]+exp(2*B[0])*
J[0]^2*Ub[3]-exp(2*B[0])*Jb[0]^2*U[2]+exp(2*B[0])*J[0]*J[3]*Ub[0]+exp(2*B[0])*J
[0]*K[3]*U[0]-exp(2*B[0])*J[0]*K[2]*Ub[0]-exp(2*B[0])*J[0]*Jb[0]*U[2]-exp(2*B[0
])*J[0]*K[0]*Ub[2]-exp(2*B[0])*Jb[0]*Jb[2]*U[0]-exp(2*B[0])*J[0]*Jb[2]*U[0])*
exp(-2*B[0])   :
C[   3   ,   4   ,   3   ]:=   1/8*(-r^2*K[0]*U[0]*Ub[1]-r^2*K[0]*Ub[0]*U[1]-r^
2*J[0]*Ub[0]*Ub[1]-r^2*Jb[0]*U[0]*U[1]+Ub[0]*r^2*Jb[0]*U[1]+2*Ub[0]*r*U[0]*Jb[0
]+Ub[0]*U[0]*r^2*Jb[1]+Ub[0]*r^2*K[0]*Ub[1]-4*U[0]*r*Ub[0]*K[0]+2*U[0]*r*Ub[0]*
J[0]-2*U[0]*Ub[0]*r^2*K[1]+U[0]*Ub[0]*r^2*J[1]+U[0]*r^2*K[0]*U[1]+U[0]*r^2*J[0]
*Ub[1]+2*r*Ub[0]^2*K[0]-2*r*Ub[0]^2*J[0]+Ub[0]^2*r^2*K[1]-Ub[0]^2*r^2*J[1]+2*U[
0]*exp(2*B[0])*B[3]+2*Ub[0]*exp(2*B[0])*B[2]+2*r*U[0]^2*K[0]-2*r*U[0]^2*Jb[0]+U
[0]^2*r^2*K[1]-U[0]^2*r^2*Jb[1]-2*exp(2*B[0])*Jb[0]*J[4]-2*U[0]*exp(2*B[0])*B[2
]-2*Ub[0]*exp(2*B[0])*B[3]+4*exp(2*B[0])*K[0]*K[4]-2*exp(2*B[0])*K[0]*J[4]-2*
exp(2*B[0])*K[0]*Jb[4]+2*exp(2*B[0])*J[0]*K[4]-2*exp(2*B[0])*J[0]*Jb[4]+2*exp(2
*B[0])*Jb[0]*K[4]-exp(2*B[0])*Jb[0]*K[3]*U[0]+exp(2*B[0])*Jb[0]*K[0]*Ub[2]-exp(
2*B[0])*Jb[0]*J[0]*Ub[3]-exp(2*B[0])*Jb[0]*K[0]*U[3]+exp(2*B[0])*J[0]*K[0]*U[3]
```

```
+exp(2*B[0])*Jb[0]*K[2]*Ub[0]-exp(2*B[0])*Jb[0]*J[3]*Ub[0]+exp(2*B[0])*J[0]^2*
Ub[3]+exp(2*B[0])*Jb[0]^2*U[2]+exp(2*B[0])*J[0]*J[3]*Ub[0]+exp(2*B[0])*J[0]*K[3
]*U[0]-exp(2*B[0])*J[0]*K[2]*Ub[0]-exp(2*B[0])*J[0]*Jb[0]*U[2]-exp(2*B[0])*J[0]
*K[0]*Ub[2]+exp(2*B[0])*Jb[0]*Jb[2]*U[0]-exp(2*B[0])*J[0]*Jb[2]*U[0])*exp(-2*B[
0])   :
C[   3   ,   4   ,   4   ]:=   1/2*I*(2*exp(2*B[0])*B[3]-2*exp(2*B[0])*B[2]-2*r
*Ub[0]*K[0]+2*r*U[0]*K[0]+2*r*Ub[0]*J[0]-2*r*U[0]*Jb[0]-Ub[0]*r^2*K[1]+U[0]*r^2
*K[1]+Ub[0]*r^2*J[1]-U[0]*r^2*Jb[1]-r^2*K[0]*Ub[1]+r^2*K[0]*U[1]+r^2*J[0]*Ub[1]
-r^2*Jb[0]*U[1])*exp(-2*B[0])/fo   :
C[   4   ,   1   ,   1   ]:=   -1/4*(-4*B[1]*exp(2*B[0])*Vw[0]-2*exp(2*B[0])*Vw
[1]+2*U[0]*exp(2*B[0])*B[3]+2*Ub[0]*exp(2*B[0])*B[2]+r^2*K[0]*U[0]*Ub[1]+r^2*K[
0]*Ub[0]*U[1]+r^2*J[0]*Ub[0]*Ub[1]+r^2*Jb[0]*U[0]*U[1])*exp(-2*B[0])   :
C[   4   ,   1   ,   2   ]:=   1/8*fo*(-K[0]*r^2*J[1]*Ub[0]-K[0]*r^2*Jb[1]*U[0]
+Jb[0]*r^2*K[1]*U[0]-2*r*K[0]^2*U[0]-2*r*K[0]^2*Ub[0]-r^2*K[0]^2*U[1]-r^2*K[0]^
2*Ub[1]+2*K[0]*exp(2*B[0])*B[3]+2*K[0]*exp(2*B[0])*B[2]-2*J[0]*exp(2*B[0])*B[3]
-2*Jb[0]*exp(2*B[0])*B[2]-K[0]*r^2*K[1]*U[0]-K[0]*r^2*K[1]*Ub[0]+2*J[0]*r*Jb[0]
*U[0]+J[0]*r^2*K[1]*Ub[0]+J[0]*r^2*Jb[1]*U[0]+J[0]*r^2*Jb[0]*U[1]+2*Jb[0]*r*J[0
]*Ub[0]+Jb[0]*r^2*J[1]*Ub[0]+Jb[0]*r^2*J[0]*Ub[1])/r^2   :
C[   4   ,   1   ,   3   ]:=   -1/8*I*(-Ub[0]*J[1]*r^2*K[0]*fo+U[0]*Jb[1]*r^2*K
[0]*fo-U[0]*K[1]*r^2*Jb[0]*fo-2*B[3]*exp(2*B[0])*K[0]*fo+2*B[2]*exp(2*B[0])*K[0
]*fo+2*B[2]*exp(2*B[0])*Jb[0]*fo-2*B[3]*exp(2*B[0])*J[0]*fo-2*U[0]*K[0]^2*r*fo+
2*Ub[0]*K[0]^2*r*fo-U[1]*K[0]^2*r^2*fo+Ub[1]*K[0]^2*r^2*fo-U[0]*K[1]*r^2*K[0]*
fo+Ub[0]*K[1]*r^2*K[0]*fo+2*U[0]*Jb[0]*r*J[0]*fo+Ub[0]*K[1]*r^2*J[0]*fo+U[0]*Jb
[1]*r^2*J[0]*fo+U[1]*Jb[0]*r^2*J[0]*fo-2*Ub[0]*J[0]*r*Jb[0]*fo-Ub[0]*J[1]*r^2*
Jb[0]*fo-Ub[1]*J[0]*r^2*Jb[0]*fo)/r^2   :
C[   4   ,   1   ,   4   ]:=   0   :
C[   4   ,   2   ,   1   ]:=   -1/4*(r^2*U[0]*K[0]*U[3]+r^2*Ub[0]*Jb[2]*U[0]+2*
r^2*U[0]*Jb[4]+2*r^2*Ub[0]*K[4]+2*r^2*Ub[0]*J[4]-4*Vw[0]*r*Ub[0]*K[0]-4*Vw[0]*r
*Ub[0]*J[0]-4*Vw[0]*r*U[0]*Jb[0]-2*Vw[0]*U[0]*r^2*K[1]-2*Vw[0]*Ub[0]*r^2*K[1]-2
*Vw[0]*Ub[0]*r^2*J[1]-2*Vw[0]*U[0]*r^2*Jb[1]-2*Vw[0]*r^2*K[0]*U[1]-2*Vw[0]*r^2*
K[0]*Ub[1]-2*Vw[0]*r^2*J[0]*Ub[1]-2*Vw[0]*r^2*Jb[0]*U[1]+2*r^2*U[0]*K[4]-4*Vw[0
]*r*U[0]*K[0]+r^2*K[3]*U[0]*Ub[0]+2*r^2*K[0]*U[0]*Ub[3]+r^2*K[0]*U[0]*Ub[2]+r^2
*K[0]*Ub[0]*U[3]+2*r^2*K[0]*Ub[0]*U[2]+r^2*Ub[0]*J[0]*Ub[3]+2*r^2*Ub[0]*J[0]*Ub
[2]+2*r^2*U[0]*Jb[0]*U[3]+r^2*U[0]*Jb[0]*U[2]+r^2*K[2]*U[0]*Ub[0]+r^2*Jb[3]*U[0
]^2+r^2*J[2]*Ub[0]^2-2*exp(2*B[0])*Vw[3]-2*exp(2*B[0])*Vw[2]+r^2*Ub[0]*K[0]*Ub[
2]+r^2*Ub[0]*Jb[0]*U[2]+r^2*U[0]*J[0]*Ub[3]+r^2*U[0]*J[3]*Ub[0]+r^2*K[2]*Ub[0]^
2+r^2*K[3]*U[0]^2)*exp(-2*B[0])/fo   :
C[   4   ,   2   ,   2   ]:=   -1/8*(r^2*K[0]*U[0]*Ub[1]+r^2*K[0]*Ub[0]*U[1]+r^
2*J[0]*Ub[0]*Ub[1]+r^2*Jb[0]*U[0]*U[1]+Ub[0]*r^2*Jb[0]*U[1]+2*Ub[0]*r*U[0]*Jb[0
]+Ub[0]*U[0]*r^2*Jb[1]+Ub[0]*r^2*K[0]*Ub[1]+4*U[0]*r*Ub[0]*K[0]+2*U[0]*r*Ub[0]*
J[0]+2*U[0]*Ub[0]*r^2*K[1]+U[0]*Ub[0]*r^2*J[1]+U[0]*r^2*K[0]*U[1]+U[0]*r^2*J[0]
*Ub[1]+2*r*Ub[0]^2*K[0]+2*r*Ub[0]^2*J[0]+Ub[0]^2*r^2*K[1]+Ub[0]^2*r^2*J[1]-2*U[
0]*exp(2*B[0])*B[3]-2*Ub[0]*exp(2*B[0])*B[2]+2*r*U[0]^2*K[0]+2*r*U[0]^2*Jb[0]+U
[0]^2*r^2*K[1]+U[0]^2*r^2*Jb[1]+2*exp(2*B[0])*Jb[0]*J[4]-2*U[0]*exp(2*B[0])*B[2
]-2*Ub[0]*exp(2*B[0])*B[3]-4*exp(2*B[0])*K[0]*K[4]-2*exp(2*B[0])*K[0]*J[4]-2*
exp(2*B[0])*K[0]*Jb[4]+2*exp(2*B[0])*J[0]*K[4]+2*exp(2*B[0])*J[0]*Jb[4]+2*exp(2
*B[0])*Jb[0]*K[4]-exp(2*B[0])*Jb[0]*K[3]*U[0]+exp(2*B[0])*Jb[0]*K[0]*Ub[2]-exp(
2*B[0])*Jb[0]*J[0]*Ub[3]-exp(2*B[0])*Jb[0]*K[0]*U[3]+exp(2*B[0])*J[0]*K[0]*U[3]
+exp(2*B[0])*Jb[0]*K[2]*Ub[0]-exp(2*B[0])*Jb[0]*J[3]*Ub[0]+exp(2*B[0])*J[0]^2*
Ub[3]+exp(2*B[0])*Jb[0]^2*U[2]+exp(2*B[0])*J[0]*J[3]*Ub[0]+exp(2*B[0])*J[0]*K[3
]*U[0]-exp(2*B[0])*J[0]*K[2]*Ub[0]-exp(2*B[0])*J[0]*Jb[0]*U[2]-exp(2*B[0])*J[0]
*K[0]*Ub[2]+exp(2*B[0])*Jb[0]*Jb[2]*U[0]-exp(2*B[0])*J[0]*Jb[2]*U[0])*exp(-2*B[
0])   :
C[   4   ,   2   ,   3   ]:=   1/8*I*(2*exp(2*B[0])*K[0]^2*U[3]-2*exp(2*B[0])*K
```

```
[0]^2*Ub[2]+2*exp(2*B[0])*K[0]*J[3]*Ub[0]+2*exp(2*B[0])*K[0]*J[0]*Ub[3]-2*exp(2
*B[0])*K[0]*Jb[0]*U[2]-2*exp(2*B[0])*K[0]*Jb[2]*U[0]+2*exp(2*B[0])*K[0]*K[3]*U[
0]+r^2*K[0]*U[0]*Ub[1]-r^2*K[0]*Ub[0]*U[1]-r^2*J[0]*Ub[0]*Ub[1]+r^2*Jb[0]*U[0]*
U[1]-Ub[0]*r^2*Jb[0]*U[1]-2*Ub[0]*r*U[0]*Jb[0]-Ub[0]*U[0]*r^2*Jb[1]-Ub[0]*r^2*K
[0]*Ub[1]+2*U[0]*r*Ub[0]*J[0]+U[0]*Ub[0]*r^2*J[1]+U[0]*r^2*K[0]*U[1]+U[0]*r^2*J
[0]*Ub[1]-2*r*Ub[0]^2*K[0]-2*r*Ub[0]^2*J[0]-Ub[0]^2*r^2*K[1]-Ub[0]^2*r^2*J[1]-2
*U[0]*exp(2*B[0])*B[3]+2*Ub[0]*exp(2*B[0])*B[2]+2*r*U[0]^2*K[0]+2*r*U[0]^2*Jb[0
]+U[0]^2*r^2*K[1]+U[0]^2*r^2*Jb[1]-2*exp(2*B[0])*K[0]*K[2]*Ub[0]-2*exp(2*B[0])*
Jb[0]*J[4]-2*U[0]*exp(2*B[0])*B[2]+2*Ub[0]*exp(2*B[0])*B[3]-2*exp(2*B[0])*K[0]*
J[4]+2*exp(2*B[0])*K[0]*Jb[4]+2*exp(2*B[0])*J[0]*K[4]+2*exp(2*B[0])*J[0]*Jb[4]-
2*exp(2*B[0])*Jb[0]*K[4]+exp(2*B[0])*Jb[0]*K[3]*U[0]-exp(2*B[0])*Jb[0]*K[0]*Ub[
2]+exp(2*B[0])*Jb[0]*J[0]*Ub[3]+exp(2*B[0])*Jb[0]*K[0]*U[3]+exp(2*B[0])*J[0]*K[
0]*U[3]-exp(2*B[0])*Jb[0]*K[2]*Ub[0]+exp(2*B[0])*Jb[0]*J[3]*Ub[0]+exp(2*B[0])*J
[0]^2*Ub[3]-exp(2*B[0])*Jb[0]^2*U[2]+exp(2*B[0])*J[0]*J[3]*Ub[0]+exp(2*B[0])*J[
0]*K[3]*U[0]-exp(2*B[0])*J[0]*K[2]*Ub[0]-exp(2*B[0])*J[0]*Jb[0]*U[2]-exp(2*B[0]
)*J[0]*K[0]*Ub[2]-exp(2*B[0])*Jb[0]*Jb[2]*U[0]-exp(2*B[0])*J[0]*Jb[2]*U[0])*exp
(-2*B[0])   :
C[   4   ,   2   ,   4   ]:=   -1/2*(-2*exp(2*B[0])*B[3]-2*exp(2*B[0])*B[2]+2*r
*U[0]*K[0]+2*r*Ub[0]*K[0]+2*r*Ub[0]*J[0]+2*r*U[0]*Jb[0]+U[0]*r^2*K[1]+Ub[0]*r^2
*K[1]+Ub[0]*r^2*J[1]+U[0]*r^2*Jb[1]+r^2*K[0]*U[1]+r^2*K[0]*Ub[1]+r^2*J[0]*Ub[1]
+r^2*Jb[0]*U[1])*exp(-2*B[0])/fo   :
C[   4   ,   3   ,   1   ]:=   1/4*I*(r^2*U[0]*K[0]*U[3]-r^2*Ub[0]*Jb[2]*U[0]-2
*r^2*U[0]*Jb[4]-2*r^2*Ub[0]*K[4]+2*r^2*Ub[0]*J[4]+4*Vw[0]*r*Ub[0]*K[0]-4*Vw[0]*
r*Ub[0]*J[0]+4*Vw[0]*r*U[0]*Jb[0]-2*Vw[0]*U[0]*r^2*K[1]+2*Vw[0]*Ub[0]*r^2*K[1]-
2*Vw[0]*Ub[0]*r^2*J[1]+2*Vw[0]*U[0]*r^2*Jb[1]-2*Vw[0]*r^2*K[0]*U[1]+2*Vw[0]*r^2
*K[0]*Ub[1]-2*Vw[0]*r^2*J[0]*Ub[1]+2*Vw[0]*r^2*Jb[0]*U[1]+2*r^2*U[0]*K[4]-4*Vw[
0]*r*U[0]*K[0]-r^2*K[3]*U[0]*Ub[0]-2*r^2*K[0]*U[0]*Ub[3]+r^2*K[0]*U[0]*Ub[2]-r^
2*K[0]*Ub[0]*U[3]+2*r^2*K[0]*Ub[0]*U[2]-r^2*Ub[0]*J[0]*Ub[3]+2*r^2*Ub[0]*J[0]*
Ub[2]-2*r^2*U[0]*Jb[0]*U[3]+r^2*U[0]*Jb[0]*U[2]+r^2*K[2]*U[0]*Ub[0]-r^2*Jb[3]*U
[0]^2+r^2*J[2]*Ub[0]^2+2*exp(2*B[0])*Vw[3]-2*exp(2*B[0])*Vw[2]-r^2*Ub[0]*K[0]*
Ub[2]-r^2*Ub[0]*Jb[0]*U[2]+r^2*U[0]*J[0]*Ub[3]+r^2*U[0]*J[3]*Ub[0]-r^2*K[2]*Ub[
0]^2+r^2*K[3]*U[0]^2)*exp(-2*B[0])/fo   :
C[   4   ,   3   ,   2   ]:=   1/8*I*(-2*exp(2*B[0])*K[0]^2*U[3]+2*exp(2*B[0])*
K[0]^2*Ub[2]-2*exp(2*B[0])*K[0]*J[3]*Ub[0]-2*exp(2*B[0])*K[0]*J[0]*Ub[3]+2*exp(
2*B[0])*K[0]*Jb[0]*U[2]+2*exp(2*B[0])*K[0]*Jb[2]*U[0]-2*exp(2*B[0])*K[0]*K[3]*U
[0]-r^2*K[0]*U[0]*Ub[1]+r^2*K[0]*Ub[0]*U[1]+r^2*J[0]*Ub[0]*Ub[1]-r^2*Jb[0]*U[0]
*U[1]-Ub[0]*r^2*Jb[0]*U[1]-2*Ub[0]*r*U[0]*Jb[0]-Ub[0]*U[0]*r^2*Jb[1]-Ub[0]*r^2*
K[0]*Ub[1]+2*U[0]*r*Ub[0]*J[0]+U[0]*Ub[0]*r^2*J[1]+U[0]*r^2*K[0]*U[1]+U[0]*r^2*
J[0]*Ub[1]-2*r*Ub[0]^2*K[0]+2*r*Ub[0]^2*J[0]-Ub[0]^2*r^2*K[1]+Ub[0]^2*r^2*J[1]+
2*U[0]*exp(2*B[0])*B[3]-2*Ub[0]*exp(2*B[0])*B[2]+2*r*U[0]^2*K[0]-2*r*U[0]^2*Jb[
0]+U[0]^2*r^2*K[1]-U[0]^2*r^2*Jb[1]+2*exp(2*B[0])*K[0]*K[2]*Ub[0]+2*exp(2*B[0])
*Jb[0]*J[4]-2*U[0]*exp(2*B[0])*B[2]+2*Ub[0]*exp(2*B[0])*B[3]-2*exp(2*B[0])*K[0]
*J[4]+2*exp(2*B[0])*K[0]*Jb[4]+2*exp(2*B[0])*J[0]*K[4]-2*exp(2*B[0])*J[0]*Jb[4]
-2*exp(2*B[0])*Jb[0]*K[4]+exp(2*B[0])*Jb[0]*K[3]*U[0]-exp(2*B[0])*Jb[0]*K[0]*Ub
[2]+exp(2*B[0])*Jb[0]*J[0]*Ub[3]+exp(2*B[0])*Jb[0]*K[0]*U[3]+exp(2*B[0])*J[0]*K
[0]*U[3]-exp(2*B[0])*Jb[0]*K[2]*Ub[0]+exp(2*B[0])*Jb[0]*J[3]*Ub[0]+exp(2*B[0])*
J[0]^2*Ub[3]-exp(2*B[0])*Jb[0]^2*U[2]+exp(2*B[0])*J[0]*J[3]*Ub[0]+exp(2*B[0])*J
[0]*K[3]*U[0]-exp(2*B[0])*J[0]*K[2]*Ub[0]-exp(2*B[0])*J[0]*Jb[0]*U[2]-exp(2*B[0
])*J[0]*K[0]*Ub[2]-exp(2*B[0])*Jb[0]*Jb[2]*U[0]-exp(2*B[0])*J[0]*Jb[2]*U[0])*
exp(-2*B[0])   :
C[   4   ,   3   ,   3   ]:=   1/8*(-r^2*K[0]*U[0]*Ub[1]-r^2*K[0]*Ub[0]*U[1]-r^
2*J[0]*Ub[0]*Ub[1]-r^2*Jb[0]*U[0]*U[1]+Ub[0]*r^2*Jb[0]*U[1]+2*Ub[0]*r*U[0]*Jb[0
]+Ub[0]*U[0]*r^2*Jb[1]+Ub[0]*r^2*K[0]*Ub[1]-4*U[0]*r*Ub[0]*K[0]+2*U[0]*r*Ub[0]*
J[0]-2*U[0]*Ub[0]*r^2*K[1]+U[0]*Ub[0]*r^2*J[1]+U[0]*r^2*K[0]*U[1]+U[0]*r^2*J[0]
```

```
*Ub[1]+2*r*Ub[0]^2*K[0]-2*r*Ub[0]^2*J[0]+Ub[0]^2*r^2*K[1]-Ub[0]^2*r^2*J[1]+2*U[
0]*exp(2*B[0])*B[3]+2*Ub[0]*exp(2*B[0])*B[2]+2*r*U[0]^2*K[0]-2*r*U[0]^2*Jb[0]+U
[0]^2*r^2*K[1]-U[0]^2*r^2*Jb[1]-2*exp(2*B[0])*Jb[0]*J[4]-2*U[0]*exp(2*B[0])*B[2
]-2*Ub[0]*exp(2*B[0])*B[3]+4*exp(2*B[0])*K[0]*K[4]-2*exp(2*B[0])*K[0]*J[4]-2*
exp(2*B[0])*K[0]*Jb[4]+2*exp(2*B[0])*J[0]*K[4]-2*exp(2*B[0])*J[0]*Jb[4]+2*exp(2
*B[0])*Jb[0]*K[4]-exp(2*B[0])*Jb[0]*K[3]*U[0]+exp(2*B[0])*Jb[0]*K[0]*Ub[2]-exp(
2*B[0])*Jb[0]*J[0]*Ub[3]-exp(2*B[0])*Jb[0]*K[0]*U[3]+exp(2*B[0])*J[0]*K[0]*U[3]
+exp(2*B[0])*Jb[0]*K[2]*Ub[0]-exp(2*B[0])*Jb[0]*J[3]*Ub[0]+exp(2*B[0])*J[0]^2*
Ub[3]+exp(2*B[0])*Jb[0]^2*U[2]+exp(2*B[0])*J[0]*J[3]*Ub[0]+exp(2*B[0])*J[0]*K[3
]*U[0]-exp(2*B[0])*J[0]*K[2]*Ub[0]-exp(2*B[0])*J[0]*Jb[0]*U[2]-exp(2*B[0])*J[0]
*K[0]*Ub[2]+exp(2*B[0])*Jb[0]*Jb[2]*U[0]-exp(2*B[0])*J[0]*Jb[2]*U[0])*exp(-2*B[
0])   :
C[   4   ,   3   ,   4   ]:=   1/2*I*(2*exp(2*B[0])*B[3]-2*exp(2*B[0])*B[2]-2*r
*Ub[0]*K[0]+2*r*U[0]*K[0]+2*r*Ub[0]*J[0]-2*r*U[0]*Jb[0]-Ub[0]*r^2*K[1]+U[0]*r^2
*K[1]+Ub[0]*r^2*J[1]-U[0]*r^2*Jb[1]-r^2*K[0]*Ub[1]+r^2*K[0]*U[1]+r^2*J[0]*Ub[1]
-r^2*Jb[0]*U[1])*exp(-2*B[0])/fo   :
C[   4   ,   4   ,   1   ]:=   1/8*(2*Ub[0]*r^2*K[0]*U[0]*Ub[2]+2*Ub[0]*r^2*U[0
]*Jb[0]*U[2]+Ub[0]*r^2*Jb[2]*U[0]^2+2*r^2*K[0]*U[0]^2*Ub[3]+2*r^2*U[0]^2*Jb[0]*
U[3]+r^2*J[2]*Ub[0]^3+2*r^2*K[3]*U[0]^2*Ub[0]+2*r^2*K[0]*Ub[0]^2*U[2]+2*r^2*Ub[
0]^2*J[0]*Ub[2]+2*r^2*K[2]*U[0]*Ub[0]^2+U[0]*r^2*J[3]*Ub[0]^2+2*U[0]*r^2*K[0]*
Ub[0]*U[3]+2*U[0]*r^2*Ub[0]*J[0]*Ub[3]-8*Vw[0]*U[0]*r*Ub[0]*K[0]-4*Vw[0]*r*Ub[0
]^2*J[0]-4*Vw[0]*r*U[0]^2*Jb[0]-4*Vw[0]*r^2*K[0]*U[0]*Ub[1]-4*Vw[0]*U[0]*Ub[0]*
r^2*K[1]-4*Vw[0]*r^2*Jb[0]*U[0]*U[1]-4*Vw[0]*r^2*J[0]*Ub[0]*Ub[1]+r^2*Jb[3]*U[0
]^3-4*Vw[0]*r^2*K[0]*Ub[0]*U[1]-2*Vw[0]*U[0]^2*r^2*Jb[1]-2*Vw[0]*Ub[0]^2*r^2*J[
1]+4*r^2*K[4]*U[0]*Ub[0]+2*r^2*J[4]*Ub[0]^2+2*r^2*Jb[4]*U[0]^2-2*U[0]*exp(2*B[0
])*Vw[3]-2*Ub[0]*exp(2*B[0])*Vw[2]+8*B[1]*exp(2*B[0])*Vw[0]^2+4*Vw[0]*exp(2*B[0
])*Vw[1]+4*exp(2*B[0])*Vw[4]-8*B[4]*exp(2*B[0])*Vw[0]-4*Ub[0]*exp(2*B[0])*Vw[0]
*B[2]-4*U[0]*exp(2*B[0])*Vw[0]*B[3])*exp(-2*B[0])   :
C[   4   ,   4   ,   2   ]:=   1/16*fo*(4*r^3*U[0]^2*Ub[0]*K[0]+2*r^4*K[0]*U[0]
^2*Ub[1]+2*r^4*U[0]^2*Ub[0]*K[1]+2*r^4*Jb[0]*U[0]^2*U[1]+4*r^3*U[0]*Ub[0]^2*K[0
]+2*r^4*K[0]*Ub[0]^2*U[1]+2*r^4*U[0]*Ub[0]^2*K[1]+2*r^4*J[0]*Ub[0]^2*Ub[1]+2*r^
3*U[0]*Ub[0]^2*J[0]+2*r^4*U[0]*K[0]*Ub[0]*U[1]+r^4*U[0]*Ub[0]^2*J[1]+r^4*Ub[0]*
U[0]^2*Jb[1]+2*r^4*Ub[0]*K[0]*U[0]*Ub[1]+2*r^4*Ub[0]*Jb[0]*U[0]*U[1]+2*r^3*Ub[0
]*U[0]^2*Jb[0]+2*r^4*U[0]*J[0]*Ub[0]*Ub[1]+2*r^3*U[0]^3*Jb[0]+r^4*U[0]^3*Jb[1]+
2*r^3*Ub[0]^3*J[0]+r^4*Ub[0]^3*J[1]-4*Jb[0]*exp(4*B[0])*Vw[0]*B[2]+2*K[0]*exp(4
*B[0])*Vw[2]+8*r^2*Ub[0]*B[4]*exp(2*B[0])-2*r^2*Ub[0]*exp(2*B[0])*Vw[1]+8*r^2*U
[0]*B[4]*exp(2*B[0])-2*r^2*U[0]*exp(2*B[0])*Vw[1]-4*r^2*Ub[0]*B[1]*exp(2*B[0])*
Vw[0]-4*r^2*U[0]*B[1]*exp(2*B[0])*Vw[0]+2*exp(2*B[0])*J[0]*r^2*K[3]*U[0]*Ub[0]+
2*exp(2*B[0])*J[0]*r^2*K[0]*U[0]*Ub[3]+2*exp(2*B[0])*J[0]*r^2*K[0]*Ub[0]*U[3]-4
*exp(2*B[0])*r^2*K[0]^2*U[4]-exp(2*B[0])*K[0]*r^2*Jb[3]*U[0]^2+2*exp(2*B[0])*J[
0]*r^2*U[0]*Jb[0]*U[3]-exp(2*B[0])*K[0]*r^2*J[3]*Ub[0]^2+4*exp(2*B[0])*J[0]*r^2
*U[0]*Jb[4]+4*exp(2*B[0])*J[0]*r^2*Ub[0]*K[4]-exp(2*B[0])*K[0]*r^2*Jb[2]*U[0]^2
-exp(2*B[0])*K[0]*r^2*J[2]*Ub[0]^2-4*exp(2*B[0])*r^2*K[0]^2*Ub[4]-2*exp(2*B[0])
*r^2*K[0]^2*Ub[0]*U[3]-2*exp(2*B[0])*r^2*K[0]^2*U[0]*Ub[2]+4*exp(2*B[0])*Jb[0]*
r^2*Ub[0]*J[4]+2*exp(2*B[0])*r^2*Ub[0]*J[0]^2*Ub[3]-2*exp(2*B[0])*r^2*K[0]^2*U[
0]*Ub[3]+exp(2*B[0])*J[0]*r^2*Jb[3]*U[0]^2+4*exp(2*B[0])*J[0]*r^2*Jb[0]*U[4]-2*
exp(2*B[0])*r^2*K[0]^2*Ub[0]*U[2]+4*exp(2*B[0])*Jb[0]*r^2*J[0]*Ub[4]+exp(2*B[0]
)*Jb[0]*r^2*Jb[2]*U[0]^2+exp(2*B[0])*J[0]*r^2*J[3]*Ub[0]^2+2*exp(2*B[0])*Jb[0]*
r^2*K[2]*U[0]*Ub[0]+exp(2*B[0])*Jb[0]*r^2*J[2]*Ub[0]^2+2*exp(2*B[0])*Jb[0]*r^2*
K[0]*Ub[0]*U[2]+2*exp(2*B[0])*Jb[0]*r^2*K[0]*U[0]*Ub[2]+2*exp(2*B[0])*Jb[0]*r^2
*Ub[0]*J[0]*Ub[2]-2*exp(2*B[0])*K[0]*r^2*K[2]*U[0]*Ub[0]-2*exp(2*B[0])*K[0]*r^2
*U[0]*Jb[0]*U[2]-2*exp(2*B[0])*K[0]*r^2*Ub[0]*J[0]*Ub[2]-2*exp(2*B[0])*K[0]*r^2
*U[0]*Jb[0]*U[3]-4*exp(2*B[0])*K[0]*r^2*Ub[0]*J[4]-4*exp(2*B[0])*K[0]*r^2*Ub[0]
*K[4]-4*exp(2*B[0])*K[0]*r^2*U[0]*K[4]-2*exp(2*B[0])*K[0]*r^2*K[3]*U[0]*Ub[0]+2
```

```
*exp(2*B[0])*r^2*U[0]*Jb[0]^2*U[2]-4*exp(2*B[0])*K[0]*r^2*U[0]*Jb[4]+4*exp(2*B[
0])*Jb[0]*r^2*U[0]*K[4]-2*J[0]*exp(4*B[0])*Vw[3]+2*K[0]*exp(4*B[0])*Vw[3]-2*Jb[
0]*exp(4*B[0])*Vw[2]+4*K[0]*exp(4*B[0])*Vw[0]*B[3]-4*J[0]*exp(4*B[0])*Vw[0]*B[3
]+4*K[0]*exp(4*B[0])*Vw[0]*B[2]-2*exp(2*B[0])*K[0]*r^2*Ub[0]*J[0]*Ub[3])*exp(-2
*B[0])/r^2   :
C[   4   ,   4   ,   3   ]:=   -1/16*I*(-2*Vw[3]*exp(4*B[0])*J[0]*fo-4*B[3]*Vw[
0]*exp(4*B[0])*J[0]*fo+4*B[2]*Vw[0]*exp(4*B[0])*K[0]*fo-4*B[3]*Vw[0]*exp(4*B[0]
)*K[0]*fo+2*Vw[2]*exp(4*B[0])*K[0]*fo-2*Vw[3]*exp(4*B[0])*K[0]*fo+2*Vw[2]*exp(4
*B[0])*Jb[0]*fo+4*B[2]*Vw[0]*exp(4*B[0])*Jb[0]*fo-Ub[0]^2*J[2]*r^2*K[0]*exp(2*B
[0])*fo+2*U[3]*Jb[0]*U[0]*r^2*K[0]*exp(2*B[0])*fo-2*Ub[2]*J[0]*Ub[0]*r^2*Jb[0]*
exp(2*B[0])*fo-Ub[0]^2*J[2]*r^2*Jb[0]*exp(2*B[0])*fo-2*U[2]*Jb[0]*U[0]*r^2*K[0]
*exp(2*B[0])*fo-2*Ub[2]*J[0]*Ub[0]*r^2*K[0]*exp(2*B[0])*fo-8*exp(2*B[0])*B[4]*
Ub[0]*r^2*fo-U[0]^2*Jb[2]*r^2*K[0]*exp(2*B[0])*fo+2*U[3]*Jb[0]*U[0]*r^2*J[0]*
exp(2*B[0])*fo+2*Ub[3]*U[0]*K[0]^2*r^2*exp(2*B[0])*fo+U[0]^2*Jb[3]*r^2*J[0]*exp
(2*B[0])*fo+4*U[4]*Jb[0]*r^2*J[0]*exp(2*B[0])*fo+8*exp(2*B[0])*B[4]*U[0]*r^2*fo
-2*Vw[1]*exp(2*B[0])*U[0]*r^2*fo+4*Vw[0]*exp(2*B[0])*B[1]*Ub[0]*r^2*fo-4*Vw[0]*
exp(2*B[0])*B[1]*U[0]*r^2*fo-4*J[4]*Ub[0]*r^2*Jb[0]*exp(2*B[0])*fo-2*Ub[0]*U[0]
*K[2]*r^2*Jb[0]*exp(2*B[0])*fo-2*U[2]*Ub[0]*K[0]*r^2*Jb[0]*exp(2*B[0])*fo+Ub[0]
^2*J[3]*r^2*J[0]*exp(2*B[0])*fo-2*Ub[2]*U[0]*K[0]^2*r^2*exp(2*B[0])*fo+2*Vw[1]*
exp(2*B[0])*Ub[0]*r^2*fo+2*Ub[0]*U[0]*K[3]*r^2*J[0]*exp(2*B[0])*fo-2*U[2]*Ub[0]
*K[0]^2*r^2*exp(2*B[0])*fo-4*Ub[4]*J[0]*r^2*Jb[0]*exp(2*B[0])*fo+2*U[3]*Ub[0]*K
[0]^2*r^2*exp(2*B[0])*fo+2*Ub[3]*U[0]*K[0]*r^2*J[0]*exp(2*B[0])*fo+2*U[3]*Ub[0]
*K[0]*r^2*J[0]*exp(2*B[0])*fo-4*U[4]*K[0]^2*r^2*exp(2*B[0])*fo+4*Jb[4]*U[0]*r^2
*K[0]*exp(2*B[0])*fo-4*K[4]*U[0]*r^2*Jb[0]*exp(2*B[0])*fo-2*Ub[0]*U[0]*K[2]*r^2
*K[0]*exp(2*B[0])*fo+2*Ub[3]*J[0]*Ub[0]*r^2*K[0]*exp(2*B[0])*fo+U[0]^2*Jb[3]*r^
2*K[0]*exp(2*B[0])*fo+2*Ub[3]*J[0]^2*Ub[0]*r^2*exp(2*B[0])*fo-2*Ub[2]*U[0]*K[0]
*r^2*Jb[0]*exp(2*B[0])*fo-U[0]^2*Jb[2]*r^2*Jb[0]*exp(2*B[0])*fo+Ub[0]^2*J[3]*r^
2*K[0]*exp(2*B[0])*fo+4*Jb[4]*U[0]*r^2*J[0]*exp(2*B[0])*fo+4*K[4]*Ub[0]*r^2*J[0
]*exp(2*B[0])*fo+4*Ub[4]*K[0]^2*r^2*exp(2*B[0])*fo-4*J[4]*Ub[0]*r^2*K[0]*exp(2*
B[0])*fo+4*K[4]*Ub[0]*r^2*K[0]*exp(2*B[0])*fo-4*K[4]*U[0]*r^2*K[0]*exp(2*B[0])*
fo+2*Ub[0]*U[0]*K[3]*r^2*K[0]*exp(2*B[0])*fo-2*U[2]*Jb[0]^2*U[0]*r^2*exp(2*B[0]
)*fo+J[1]*Ub[0]^2*U[0]*r^4*fo-2*Ub[1]*U[0]*K[0]*Ub[0]*r^4*fo-2*U[1]*U[0]*Jb[0]*
Ub[0]*r^4*fo-2*Jb[0]*U[0]^2*Ub[0]*r^3*fo+2*Ub[1]*U[0]^2*K[0]*r^4*fo-J[1]*Ub[0]^
3*r^4*fo-Jb[1]*U[0]^2*Ub[0]*r^4*fo-2*K[1]*Ub[0]^2*U[0]*r^4*fo-2*Ub[1]*Ub[0]^2*J
[0]*r^4*fo+2*J[0]*Ub[0]^2*U[0]*r^3*fo+2*U[1]*Ub[0]*K[0]*U[0]*r^4*fo+2*Ub[1]*Ub[
0]*J[0]*U[0]*r^4*fo+Jb[1]*U[0]^3*r^4*fo-2*J[0]*Ub[0]^3*r^3*fo+2*K[1]*Ub[0]*U[0]
^2*r^4*fo+2*U[1]*U[0]^2*Jb[0]*r^4*fo-4*K[0]*Ub[0]^2*U[0]*r^3*fo+2*Jb[0]*U[0]^3*
r^3*fo-2*U[1]*Ub[0]^2*K[0]*r^4*fo+4*K[0]*Ub[0]*U[0]^2*r^3*fo)*exp(-2*B[0])/r^2
   :
C[   4   ,   4   ,   4   ]:=   1/4*(8*B[4]*exp(2*B[0])-4*B[1]*exp(2*B[0])*Vw[0]
-2*exp(2*B[0])*Vw[1]+4*U[0]*r*Ub[0]*K[0]+2*r*Ub[0]^2*J[0]+2*r*U[0]^2*Jb[0]+2*r^
2*K[0]*Ub[0]*U[1]+U[0]^2*r^2*Jb[1]+2*r^2*K[0]*U[0]*Ub[1]+Ub[0]^2*r^2*J[1]+2*U[0
]*Ub[0]*r^2*K[1]+2*r^2*Jb[0]*U[0]*U[1]+2*r^2*J[0]*Ub[0]*Ub[1])*exp(-2*B[0])   :
```

# Appendix D

# Matlab code

This appendix contains the Matlab scripts NormTest.m (see Eq. (7.13)), BH.m used in Sec. 7.5.1, BNS.m used in Sec. 7.5.2, and CCSN.m used in Sec. 7.5.3.1. The data file clean.xlsx is also included and represents the data from the LIGO reading for GW150914 as provided in Ref. [244].

```
%Units used are milliseconds (ms)
%Time domain comprises N0 points, with non-zero burst in first N points;
%fac is the sampling interval (in ms)
%Model of shell, radius r0 ms, mass Ms ms. 1 ms ~ 300 km ~ 200 Msun
%T_Total is the whole time interval; EnvelopeWidth is the burst duration;
%freq is the wave frequency during the burst, set by the integer freq_int
'Parameters:'
r0=3 %about 900km
Ms=0.3 % about 60 Msun
T_Total=1000
N=879
N0=2^12
fac=T_Total/(N0-1);
K=1:N;
T=fac*(K-1);
K0=1:N0;
%T0=fac*(K0-1);
K1=1:800;
T0=fac*(K1-1);

y=0*K0;
y(1:N)=xlsread('Clean.xlsx','A:A');

y_ff=fft(y,N0); % FFT of the burst
for a=1:N0/2+1
    nu(a)=(a-1)*2*pi/N0/fac;
end
y_ff2(1)=0;y_ff1(1)=0;%Terms 1 and 2 in the Fourier transform domain
for a=2:N0/2+1
    y_ff1(a)=2*1i*Ms*y_ff(a)/(r0^2*nu(a));
    y_ff2(a)=1i*Ms*y_ff(a)/(2*r0^2*nu(a))*exp(-2*1i*r0*nu(a));
end
for a=N0/2+2:N0
    y_ff1(a)=conj(y_ff1(N0-a+2));
    y_ff2(a)=conj(y_ff2(N0-a+2));
end

iy1=ifft(y_ff1);
iy2=ifft(y_ff2);

tiledlayout(2,1)

% Top plot
ax1 = nexttile;
plot(ax1,T0,y(K1),'b',T0,y(K1)+real(iy1(K1))+real(iy2(K1)),'r')
title(ax1,'GW150914: Template (blue), Template + shell effects (red)')
ylabel(ax1,'GW amplitude')
xlabel(ax1,' Time in ms')

% Bottom plot
ax2 = nexttile;
plot(ax2,T0,real(iy1(K1)),'b',T0,real(iy2(K1)),'r')
title(ax2,'Gw150914: Phase-shift term (blue), Echo term (red)')
ylabel(ax2,'GW amplitude')
```

```
xlabel(ax2,' Time in ms')
```

```
%Units used are milliseconds (ms)
%Time domain comprises N0 points, with non-zero burst in first N points;
%fac is the sampling interval (in ms)
%Model of shell, radius r0 ms, mass Ms ms. 1 ms ~ 300 km ~ 200 Msun
%T_Total is the whole time interval; EnvelopeWidth is the burst duration;
%freq is the wave frequency during the burst, set by the integer freq_int
'Parameters:'
r0=0.0833 %about 25km
Ms=0.0035 % about 0.7 Msun
T_Total=10
N0=2^12
fac=T_Total/(N0-1);
K0=1:N0;
T0=fac*(K0-1);

y=sin(6.036*2*pi*T0).*exp(-T0/0.11);

y_ff=fft(y,N0); % FFT of the signal
for a=1:N0/2+1
    nu(a)=(a-1)*2*pi/N0/fac;
end
y_ff2(1)=0;y_ff1(1)=0;%Terms 1 and 2 in the Fourier transform domain
for a=2:N0/2+1
    y_ff1(a)=2*1i*Ms*y_ff(a)/(r0^2*nu(a));
    y_ff2(a)=1i*Ms*y_ff(a)/(2*r0^2*nu(a))*exp(-2*1i*r0*nu(a));
end
for a=N0/2+2:N0
    y_ff1(a)=conj(y_ff1(N0-a+2));
    y_ff2(a)=conj(y_ff2(N0-a+2));
end

iy1=ifft(y_ff1);
iy2=ifft(y_ff2);
K1=1:100;
plot(T0(K1),y(K1),'b',T0(K1),y(K1)+real(iy1(K1))+real(iy2(K1)),'r')
title('QNM of a BH following BNS merger: QNM (blue), QNM + shell effects (red)')
ylabel('GW amplitude')
xlabel(' Time in ms')
```

```
%Units used are milliseconds (ms); 1 ms ~ 300 km ~ 200 Msun
%Time domain comprises N0 points, with non-zero burst in first N points;
%fac is the sampling interval (in ms)
%T_Total is the whole time interval (in ms)
%EnvelopeWidth is the burst duration (in ms)
%freq is the wave frequency during the burst (in kHz)
%Looking at Radice et al., we model the initial GWs as a burst
%of duration 60ms, and of frequency 100Hz
%The shell exists between rin and rout
%rho0 is the density (in (ms)^(-2)) of the shell at r=rin
%The density falls off as 1/r^(1+aa)

rin=0.1 %about 30km
rout=0.5 %about 150km
rho0=0.05 %about 3/4 of 10^12 g/cm^3
aa=1 %Density falls off as 1/r^2
Mshell_ms=4*pi*rho0*rin^(1+aa)*(rout^(2-aa)-rin^(2-aa))/(2-aa)
Mshell_Msun=Mshell_ms*200
T_Total=100
N0=2^12
fac=T_Total/(N0-1);
K0=1:N0;
T0=fac*(K0-1);

freq=0.1
om=freq*2*pi;
EnvelopeWidth=50;
N=round(EnvelopeWidth/T_Total*N0);
K=1:N;
T=fac*(K-1);

y=0*K0;
y(1:N)=-1i*exp(1i*om*T).*sin(T*pi/EnvelopeWidth);
yr=real(y);

y_ff=fft(yr,N0); % FFT of the burst
for a=1:N0/2+1
    nu(a)=(a-1)*2*pi/N0/fac;
end
y_ff2(1)=0;y_ff1(1)=0;%Terms 1 and 2 in the Fourier transform domain
for a=2:N0/2+1
    f=@(r) exp(-2*1i*r*nu(a))./r.^(1+aa);
    y_ff1(a)=4*1i*rho0*rin/(nu(a)/2/pi/aa)*y_ff(a)*(1-(rin/rout)^aa);
    y_ff2(a)=1i*rho0*rin^2*2*pi/nu(a)*quadgk(f,rin,rout)*y_ff(a);
end
for a=N0/2+2:N0
    y_ff1(a)=conj(y_ff1(N0-a+2));
    y_ff2(a)=conj(y_ff2(N0-a+2));
end

iy0=ifft(y_ff);
iy1=ifft(y_ff1);
iy2=ifft(y_ff2);
```

```
%plot(T0,yr,'r',T0,real(iy1),'b',T0,real(iy2),'m')
plot(T0,yr,'b',T0,(yr+real(iy1)+real(iy2)),'r')
ylabel('GW amplitude')
xlabel(' Time in ms')
```

```
%Units used are milliseconds (ms)
%Time domain comprises N0 points, with non-zero burst in first N points;
%fac is the sampling interval (in ms)
%Model of shell, radius r0 ms, mass Ms ms. 1 ms ~ 300 km ~ 200 Msun
%T_Total is the whole time interval;
%freq is the wave frequency
'Parameters:'
r0=1.25
Ms=0.25
T_Total=100
for k=1:3
    N0=2^(3+6*k)
    fac=T_Total/(N0-1);
    K0=1:N0;
    T0=fac*(K0-1);

    freq=1; %Wave frequency in cycles per ms, i.e. x10^3Hz
    %freq=100*(N0-1)/N0/T_Total; %So that y(N0+1)=y(1)
    om=freq*2*pi;
    y=-1i*exp(1i*om*T0); %Constant frequency source
    yr=real(y);

    y_ff=fft(yr,N0); % FFT
    for a=1:N0/2+1
        nu(a)=(a-1)*2*pi/N0/fac;
    end
    y_ff2(1)=0;y_ff1(1)=0;%Terms 1 and 2 in the Fourier transform domain
    for a=2:N0/2+1
        y_ff1(a)=2*1i*Ms*y_ff(a)/(r0^2*nu(a));
        y_ff2(a)=1i*Ms*y_ff(a)/(2*r0^2*nu(a))*exp(-2*1i*r0*nu(a));
    end
    for a=N0/2+2:N0
        y_ff1(a)=conj(y_ff1(N0-a+2));
        y_ff2(a)=conj(y_ff2(N0-a+2));
    end

    iy1=ifft(y_ff1);
    iy2=ifft(y_ff2);
    y1=real(2*1i*Ms/(r0^2*om)*y);
    y2=real(1i*Ms/(2*r0^2*om)*exp(-2*1i*r0*om)*y);
    norm1=sqrt(sum((y1-real(iy1)).^2)/N0)
    norm2=sqrt(sum((y2-real(iy2)).^2)/N0)
end%for
```

| | | | | | |
|---|---|---|---|---|---|
| 0 | -0,095227722 | -0,028371816 | 0,343510269 | -0,501632181 | 0,491573625 |
| 0 | -0,104279261 | -0,005543383 | 0,325596826 | -0,495991085 | 0,500686158 |
| 0 | -0,114822803 | 0,016219497 | 0,306032019 | -0,48951189 | 0,508158435 |
| 0 | -0,124380084 | 0,039687485 | 0,286498964 | -0,481269387 | 0,514456456 |
| 0 | -0,135387524 | 0,061949809 | 0,265425103 | -0,472209312 | 0,519073912 |
| 0 | -0,145285583 | 0,085732449 | 0,24446149 | -0,461434746 | 0,522469723 |
| 0 | -0,156578364 | 0,10816429 | 0,222075154 | -0,44987706 | 0,524160397 |
| 0 | -0,166630711 | 0,131924871 | 0,199885544 | -0,436667122 | 0,524598249 |
| 0 | -0,178010318 | 0,154187534 | 0,176397926 | -0,422722113 | 0,523322689 |
| 0 | -0,188012298 | 0,177583856 | 0,153200519 | -0,407200121 | 0,520779811 |
| 0 | -0,199263924 | 0,19933631 | 0,12883547 | -0,391004227 | 0,516531926 |
| 9,91E-05 | -0,208996638 | 0,222027206 | 0,104860072 | -0,373319109 | 0,511019194 |
| 0,000339263 | -0,219893353 | 0,242932652 | 0,079851995 | -0,355033763 | 0,503826737 |
| 0,00080679 | -0,229128062 | 0,264584569 | 0,055337847 | -0,335358764 | 0,495388973 |
| 0,001311473 | -0,239435427 | 0,284317004 | 0,029929465 | -0,315168953 | 0,485313653 |
| 0,002079333 | -0,247938329 | 0,304610507 | 0,005122947 | -0,293700056 | 0,47402954 |
| 0,00277209 | -0,257419342 | 0,322861124 | -0,020437048 | -0,271812617 | 0,46116674 |
| 0,003754025 | -0,264956646 | 0,341497175 | -0,045284805 | -0,248766711 | 0,447148349 |
| 0,004542215 | -0,273376914 | 0,358010409 | -0,070744187 | -0,225408364 | 0,431626461 |
| 0,005637566 | -0,279720077 | 0,374898176 | -0,095379775 | -0,201021151 | 0,415018389 |
| 0,00641544 | -0,286853108 | 0,389720275 | -0,120485282 | -0,1764363 | 0,396997755 |
| 0,007512042 | -0,291784131 | 0,404817922 | -0,144655543 | -0,150959982 | 0,377975874 |
| 0,008164025 | -0,297416612 | 0,417803571 | -0,169155423 | -0,125408283 | 0,357647343 |
| 0,009141566 | -0,300733269 | 0,430964582 | -0,192609997 | -0,099109035 | 0,336417168 |
| 0,009545835 | -0,304670227 | 0,441974745 | -0,216256568 | -0,07286278 | 0,314000277 |
| 0,010279538 | -0,306191103 | 0,453069867 | -0,238750458 | -0,046018035 | 0,290794961 |
| 0,010311833 | -0,308260803 | 0,461983544 | -0,261302662 | -0,019359353 | 0,266535756 |
| 0,010676351 | -0,307830024 | 0,470902196 | -0,282598769 | 0,007745069 | 0,241613738 |
| 0,010213935 | -0,307888513 | 0,47761775 | -0,303824685 | 0,034527153 | 0,215782247 |
| 0,010087354 | -0,305380053 | 0,484269263 | -0,323696298 | 0,061600048 | 0,189424565 |
| 0,009013039 | -0,303315214 | 0,48870557 | -0,343375605 | 0,088212675 | 0,162311954 |
| 0,008280891 | -0,298636667 | 0,493020259 | -0,361608819 | 0,114960564 | 0,134819248 |
| 0,006487013 | -0,294371695 | 0,495117682 | -0,379535163 | 0,141110181 | 0,106734686 |
| 0,005046193 | -0,287467419 | 0,497047722 | -0,395931197 | 0,167240484 | 0,078423926 |
| 0,002438443 | -0,280963621 | 0,496768888 | -0,41191445 | 0,192636045 | 0,049691181 |
| 0,000200937 | -0,271817163 | 0,49628899 | -0,426291836 | 0,217860291 | 0,020892148 |
| -0,003298055 | -0,263076008 | 0,493619358 | -0,440160221 | 0,242216471 | -0,008154041 |
| -0,006401744 | -0,25171175 | 0,490727239 | -0,452356853 | 0,266253514 | -0,037102486 |
| -0,010849166 | -0,240776099 | 0,485675459 | -0,463958902 | 0,289293911 | -0,066120227 |
| -0,014866973 | -0,227260062 | 0,48039209 | -0,473833906 | 0,311873106 | -0,094874038 |
| -0,020297015 | -0,214214546 | 0,472990139 | -0,483040239 | 0,333333389 | -0,123518252 |
| -0,025252741 | -0,198654316 | 0,465359773 | -0,490475651 | 0,354197704 | -0,15173222 |
| -0,0316743 | -0,183624826 | 0,455662869 | -0,497180553 | 0,373828677 | -0,179658707 |
| -0,037565591 | -0,1661686 | 0,445752838 | -0,502082786 | 0,392737698 | -0,206990564 |
| -0,044960543 | -0,149320884 | 0,43383912 | -0,506205554 | 0,410308237 | -0,23386013 |
| -0,051757477 | -0,13015562 | 0,421739411 | -0,508506627 | 0,427041036 | -0,259974683 |
| -0,060079602 | -0,111693011 | 0,407709401 | -0,509992681 | 0,442340876 | -0,285457274 |
| -0,067723934 | -0,091041724 | 0,393532001 | -0,5096512 | 0,456698702 | -0,310030526 |
| -0,076898509 | -0,07120202 | 0,377507831 | -0,508472935 | 0,469541031 | -0,333809323 |
| -0,085303616 | -0,049320257 | 0,361385844 | -0,505474815 | 0,481349797 | -0,356532534 |

| | | | | | |
|---|---|---|---|---|---|
| -0,378307961 | 0,243426158 | -0,150971314 | 0,146423267 | -0,269852711 | 0,538175192 |
| -0,398891589 | 0,271781039 | -0,184418008 | 0,183425759 | -0,309056184 | 0,567591986 |
| -0,418385181 | 0,299347811 | -0,2171026 | 0,22006356 | -0,346523 | 0,594361303 |
| -0,436562661 | 0,325925786 | -0,24924357 | 0,255613523 | -0,382856427 | 0,617253001 |
| -0,453520742 | 0,351532781 | -0,280371894 | 0,290493258 | -0,417069558 | 0,637146963 |
| -0,469052055 | 0,375963575 | -0,310719158 | 0,323975363 | -0,449786822 | 0,652837816 |
| -0,483249182 | 0,399251932 | -0,33981216 | 0,356492453 | -0,480025552 | 0,665254084 |
| -0,495924159 | 0,42118944 | -0,367897434 | 0,387315521 | -0,508435231 | 0,67322004 |
| -0,507166279 | 0,441827021 | -0,394499456 | 0,416894825 | -0,534041186 | 0,677717513 |
| -0,516807597 | 0,460954343 | -0,419881504 | 0,444502347 | -0,557521682 | 0,677604558 |
| -0,524934871 | 0,478640632 | -0,443567531 | 0,470608561 | -0,577913582 | 0,673920179 |
| -0,531400703 | 0,494674822 | -0,465839291 | 0,494488934 | -0,595927417 | 0,665559484 |
| -0,536289965 | 0,509145495 | -0,486221925 | 0,516636606 | -0,610614843 | 0,653621582 |
| -0,539476234 | 0,521841944 | -0,505017287 | 0,536332887 | -0,622721806 | 0,637040912 |
| -0,54104304 | 0,532873054 | -0,521753305 | 0,554095875 | -0,631317647 | 0,616978566 |
| -0,54088525 | 0,542029447 | -0,536753437 | 0,569214895 | -0,637186484 | 0,592409468 |
| -0,539085479 | 0,549441136 | -0,549549853 | 0,582235085 | -0,639417791 | 0,56455741 |
| -0,53556009 | 0,554900914 | -0,560488962 | 0,592455731 | -0,638836137 | 0,532437742 |
| -0,530391081 | 0,558560612 | -0,569108462 | 0,600450845 | -0,634553069 | 0,497336421 |
| -0,523516393 | 0,560215882 | -0,575778886 | 0,605531343 | -0,62743535 | 0,458307883 |
| -0,515017581 | 0,560040912 | -0,580044556 | 0,608301653 | -0,616617963 | 0,416698404 |
| -0,504854116 | 0,557834751 | -0,582301099 | 0,608085678 | -0,603011004 | 0,371598827 |
| -0,493107153 | 0,553794315 | -0,582100345 | 0,605519482 | -0,585773635 | 0,324412564 |
| -0,479757514 | 0,547722417 | -0,57986376 | 0,599940967 | -0,565859775 | 0,274262837 |
| -0,46488586 | 0,539838904 | -0,575151331 | 0,592018694 | -0,542452828 | 0,222605666 |
| -0,448494055 | 0,529950535 | -0,568410873 | 0,581105202 | -0,516550343 | 0,168591286 |
| -0,430662037 | 0,518300117 | -0,559210925 | 0,567902014 | -0,487359325 | 0,113722484 |
| -0,411412272 | 0,504698355 | -0,548025901 | 0,551776542 | -0,455920041 | 0,057169857 |
| -0,390823611 | 0,489410852 | -0,534433026 | 0,533463338 | -0,421461733 | 0,000475871 |
| -0,368938552 | 0,472252074 | -0,518933294 | 0,512344501 | -0,385065746 | -0,05717637 |
| -0,34583436 | 0,453510068 | -0,501112475 | 0,489187244 | -0,345981461 | -0,114212947 |
| -0,321572871 | 0,433002681 | -0,481497851 | 0,463387735 | -0,305328935 | -0,171447181 |
| -0,296229137 | 0,411039868 | -0,459683314 | 0,435745045 | -0,262374864 | -0,227282925 |
| -0,269883515 | 0,387442283 | -0,43622186 | 0,405668354 | -0,218274942 | -0,282539772 |
| -0,242608099 | 0,362541065 | -0,410714798 | 0,373987356 | -0,172309659 | -0,335609385 |
| -0,21450083 | 0,336158918 | -0,383739989 | 0,340122749 | -0,125666589 | -0,387328197 |
| -0,185629986 | 0,308647258 | -0,354905177 | 0,304933185 | -0,077635843 | -0,436086322 |
| -0,156110053 | 0,279829902 | -0,324811955 | 0,267848961 | -0,029432501 | -0,48274808 |
| -0,126004528 | 0,250077461 | -0,293073249 | 0,229755607 | 0,019648486 | -0,525713027 |
| -0,095443305 | 0,219213756 | -0,260312996 | 0,190090688 | 0,068369487 | -0,565884637 |
| -0,06448404 | 0,187627353 | -0,226147783 | 0,149764134 | 0,117436026 | -0,601682968 |
| -0,033270821 | 0,155140809 | -0,191222248 | 0,108218071 | 0,165593352 | -0,634061841 |
| -0,001854321 | 0,122159248 | -0,155154879 | 0,066383992 | 0,213553207 | -0,661472636 |
| 0,029608471 | 0,088502551 | -0,118609139 | 0,023705537 | 0,260049528 | -0,684930325 |
| 0,061075067 | 0,054590871 | -0,081203433 | -0,018867396 | 0,305806358 | -0,702927872 |
| 0,092376927 | 0,020239872 | -0,043617964 | -0,061893008 | 0,349552421 | -0,716551474 |
| 0,12348101 | -0,014116909 | -0,005468872 | -0,104406431 | 0,392030381 | -0,724345034 |
| 0,154208613 | -0,04866968 | 0,032549171 | -0,146971316 | 0,431970011 | -0,72747498 |
| 0,184537438 | -0,082973263 | 0,070824641 | -0,188611484 | 0,470138983 | -0,724544263 |
| 0,214280032 | -0,117225474 | 0,108650813 | -0,229899841 | 0,505274367 | -0,716807132 |

| | | | | | |
|---|---|---|---|---|---|
| -0,702932114 | -0,313641648 | -0,756211331 | -0,43534278 | -0,019543264 | 5,22E-05 |
| -0,684267128 | -0,39848675 | -0,893768989 | -0,318404553 | -0,018238306 | -0,000259238 |
| -0,659550891 | -0,478898964 | -1,006060755 | -0,17283569 | -0,013139076 | 5,69E-05 |
| -0,630228792 | -0,555526206 | -1,089969135 | -0,023099667 | -0,008743272 | -0,000197478 |
| -0,59511215 | -0,625604965 | -1,138374871 | 0,114347128 | -0,002208569 | 9,26E-05 |
| -0,555745291 | -0,68984459 | -1,149463679 | 0,220662332 | 0,002060442 | -0,000127867 |
| -0,511012089 | -0,745535135 | -1,117914774 | 0,289010962 | 0,00709627 | 0,000117185 |
| -0,462554706 | -0,793503358 | -1,044343829 | 0,312191674 | 0,008913829 | -8,09E-05 |
| -0,409326856 | -0,831149943 | -0,92638341 | 0,295445921 | 0,010934981 | 0,000114197 |
| -0,353064691 | -0,859477671 | -0,768208353 | 0,242298202 | 0,009681621 | -6,01E-05 |
| -0,292786227 | -0,876056309 | -0,571432698 | 0,166415338 | 0,008924125 | 9,06E-05 |
| -0,230314899 | -0,882123303 | -0,344629142 | 0,076528146 | 0,00555995 | -5,22E-05 |
| -0,16472459 | -0,875474472 | -0,093932624 | -0,011698715 | 0,003490173 | 6,18E-05 |
| -0,097916409 | -0,85763749 | 0,167564114 | -0,090735992 | -0,000260829 | -4,37E-05 |
| -0,029008778 | -0,82668637 | 0,429631489 | -0,148566765 | -0,001925153 | 3,75E-05 |
| 0,04003197 | -0,784487927 | 0,675754538 | -0,183392105 | -0,004574515 | -2,94E-05 |
| 0,110056998 | -0,729437902 | 0,893485931 | -0,189948385 | -0,004750196 | 1,92E-05 |
| 0,179049904 | -0,663780524 | 1,065605354 | -0,173487588 | -0,005711026 | -1,22E-05 |
| 0,247848147 | -0,586264 | 1,181004862 | -0,135049492 | -0,004328795 | 4,17E-06 |
| 0,314402858 | -0,499533262 | 1,226056725 | -0,084956659 | -0,003986455 | 0 |
| 0,37955679 | -0,402702461 | 1,195819025 | -0,027394844 | -0,001775228 | 0 |
| 0,441248288 | -0,298820998 | 1,08525617 | 0,026151648 | -0,0010461 | 0 |
| 0,500346265 | -0,18736067 | 0,900273403 | 0,072501434 | 0,001044841 | 0 |
| 0,55479756 | -0,071755208 | 0,648177385 | 0,102907016 | 0,001325314 | 0 |
| 0,605519437 | 0,04820025 | 0,347872786 | 0,118342231 | 0,002673713 | 0 |
| 0,650489527 | 0,16873573 | 0,01891322 | 0,114841598 | 0,00215644 | 0 |
| 0,690696335 | 0,289796785 | -0,309645366 | 0,098233576 | 0,002687588 | 0 |
| 0,724170903 | 0,407356463 | -0,611846129 | 0,068675816 | 0,001540554 | 0 |
| 0,751995818 | 0,521197369 | -0,857172348 | 0,034983652 | 0,001595078 | 0 |
| 0,772277702 | 0,627147919 | -1,024202119 | -0,001277614 | 0,000255751 | |
| 0,786215188 | 0,724957606 | -1,093059312 | -0,03143221 | 0,000283529 | |
| 0,792011309 | 0,81045588 | -1,058635053 | -0,055530879 | -0,000849803 | |
| 0,791000924 | 0,883521485 | -0,921437192 | -0,067530983 | -0,000553762 | |
| 0,781502048 | 0,940161446 | -0,69871964 | -0,070714151 | -0,001308495 | |
| 0,765003203 | 0,980574542 | -0,412397452 | -0,062265778 | -0,000697557 | |
| 0,739952714 | 1,001146851 | -0,097383091 | -0,048270047 | -0,001130668 | |
| 0,708006492 | 1,002608315 | 0,213295561 | -0,0278863 | -0,000339212 | |
| 0,667754279 | 0,981940005 | 0,481876145 | -0,008188577 | -0,000624734 | |
| 0,621028403 | 0,940621517 | 0,681628185 | 0,011699146 | 0,000162809 | |
| 0,566565957 | 0,87644368 | 0,789447824 | 0,025608948 | -0,000139496 | |
| 0,506379092 | 0,791842987 | 0,799842707 | 0,035943808 | 0,000515533 | |
| 0,439352115 | 0,685611638 | 0,71436908 | 0,038379916 | 0,000116503 | |
| 0,367673945 | 0,561313395 | 0,552212995 | 0,037152004 | 0,000605863 | |
| 0,290369128 | 0,418880963 | 0,335902869 | 0,029523173 | 0,000120855 | |
| 0,209793133 | 0,263106042 | 0,099124838 | 0,020847688 | 0,000486041 | |
| 0,125096303 | 0,095112307 | -0,129580551 | 0,009004951 | -2,26E-05 | |
| 0,038782757 | -0,079089223 | -0,319294289 | -0,000597229 | 0,000286419 | |
| -0,049893666 | -0,257264815 | -0,452273789 | -0,010436548 | -0,000180651 | |
| -0,13830605 | -0,432347002 | -0,51414568 | -0,015832158 | 0,000124299 | |
| -0,227127359 | -0,601250008 | -0,506801317 | -0,020114157 | -0,000265164 | |

# Appendix E

# Catalogue of GW detections

Listed in this appendix is the first the complete O1 and O2 runs and the partial O3 run together with specific data. Data was obtained form the Gravitational Wave Open Science Center hosted by LVC [257].

Mass $M_1$ is the more massive of the masses in the binary before merger. $M_f$ is the final mass, that is, the mass of the remnant.

Table E.1: List of events in O1 and O2 run for GW detection. Data from [257]

| Event | $M_1$ in M$\odot$ | $M_2$ in M$\odot$ | $M_f$ in M$\odot$ |
|---|---|---|---|
| **GW150914** | $35.6^{+4.7}_{-3.1}$ | $30.6^{+3.0}_{-4.4}$ | $63.1^{+3.4}_{-3.0}$ |
| **GW151012** | $23.2^{+14.9}_{-5.5}$ | $13.6^{+4.1}_{-4.8}$ | $35.6^{+10.8}_{-3.8}$ |
| **GW151226** | $13.7^{+8.8}_{-3.2}$ | $7.7^{+2.2}_{-2.5}$ | $20.5^{+6.4}_{-1.5}$ |
| **GW170104** | $30.8^{+7.3}_{-5.6}$ | $20.0^{+4.9}_{-4.6}$ | $48.9^{+5.1}_{-4.0}$ |
| **GW170608** | $11.0^{+5.5}_{-1.7}$ | $7.6^{+1.4}_{-2.2}$ | $17.8^{+3.4}_{-0.7}$ |
| **GW170729** | $50.2^{+16.2}_{-10.2}$ | $34.0^{+9.1}_{-10.1}$ | $79.5^{+14.7}_{-10.2}$ |
| **GW170809** | $35.0^{+8.3}_{-5.9}$ | $23.8^{+5.1}_{-5.2}$ | $56.3^{+5.2}_{-3.8}$ |
| **GW170814** | $30.6^{+5.6}_{-3.0}$ | $25.2^{+2.8}_{-4.0}$ | $53.2^{+3.2}_{-2.4}$ |
| **GW170817** | $1.46^{+0.12}_{-0.1}$ | $1.27^{+0.09}_{-0.09}$ | 2.8 |
| **GW170818** | $35.4^{+7.5}_{-4.7}$ | $26.7^{+4.3}_{-5.2}$ | $59.4^{+4.9}_{-3.8}$ |
| **GW170823** | $39.5^{+11.2}_{-6.7}$ | $29.0^{+6.7}_{-7.8}$ | $65.4^{+10.1}_{-7.4}$ |

Table E.2: List of events in O3 run for GW detection. Data from [257]

| Event | $M_1$ in M$\odot$ | $M_2$ in M$\odot$ | $(M_1 + M_2)$ in M$\odot$ | $M_f$ in M$\odot$ |
|---|---|---|---|---|
| **GW190408_181802** | $24.6^{+5.1}_{-3.4}$ | $18.4^{+3.3}_{-3.6}$ | $43.0^{+4.2}_{-3.0}$ | $41.1^{+3.9}_{-2.8}$ |
| **GW190412** | $30.1^{+4.7}_{-5.1}$ | $8.3^{+1.6}_{-0.9}$ | $38.4^{+3.8}_{-3.7}$ | $37.3^{+3.9}_{-3.8}$ |
| **GW190413_052954** | $34.7^{+12.6}_{-8.1}$ | $23.7^{+7.3}_{-6.7}$ | $58.6^{+13.3}_{-9.7}$ | $56.0^{+12.5}_{-9.2}$ |
| **GW190413_134308** | $47.5^{+13.5}_{-10.7}$ | $31.8^{+11.7}_{-10.8}$ | $78.8^{+17.4}_{-11.9}$ | $75.5^{+16.4}_{-11.4}$ |
| **GW190421_213856** | $41.3^{+10.4}_{-6.9}$ | $31.9^{+8.0}_{-8.8}$ | $72.9^{+13.4}_{-9.2}$ | $69.7^{+12.5}_{-8.7}$ |
| **GW190424_180648** | $40.5^{+11.1}_{-7.3}$ | $31.8^{+7.6}_{-7.7}$ | $72.6^{+13.3}_{-10.7}$ | $68.9^{+12.4}_{-10.1}$ |
| **GW190425** | $2.0^{+0.6}_{-0.3}$ | $1.4^{+0.3}_{-0.3}$ | | $3.4^{+0.3}_{-0.1}$ |
| **GW190426_152155** | $5.7^{+3.9}_{-2.3}$ | $1.5^{+0.8}_{-0.5}$ | | $7.2^{+3.5}_{-1.5}$ |
| **GW190503_185404** | $43.3^{+9.2}_{-8.1}$ | $28.4^{+7.7}_{-8.0}$ | $71.7^{+9.4}_{-8.3}$ | $68.6^{+8.8}_{-7.7}$ |
| **GW190512_180714** | $23.3^{+5.3}_{-5.8}$ | $12.6^{+3.6}_{-2.5}$ | $35.9^{+3.8}_{-3.5}$ | $34.5^{+3.8}_{-3.5}$ |
| **GW190513_205428** | $35.7^{+9.5}_{-9.2}$ | $18.0^{+7.7}_{-4.1}$ | $53.9^{+8.6}_{-5.9}$ | $51.6^{+8.2}_{-5.8}$ |
| **GW190514_065416** | $39.0^{+14.7}_{-8.2}$ | $28.4^{+9.3}_{-8.8}$ | $67.2^{+18.7}_{-10.8}$ | $64.5^{+17.9}_{-10.4}$ |
| **GW190517_055101** | $37.4^{+11.7}_{-7.6}$ | $25.3^{+7.0}_{-7.3}$ | $63.5^{+9.6}_{-9.6}$ | $59.3^{+9.1}_{-8.9}$ |
| **GW190519_153544** | $66.0^{+10.7}_{-12.0}$ | $40.5^{+11.0}_{-11.1}$ | $106.6^{+13.5}_{-14.8}$ | $101.0^{+12.4}_{-13.8}$ |
| **GW190521** | $95.3^{+28.7}_{-18.9}$ | $69.0^{+22.7}_{-23.1}$ | $163.9^{+39.2}_{-23.5}$ | $156.3^{+36.8}_{-22.4}$ |
| **GW190521_074359** | $42.2^{+5.9}_{-4.8}$ | $32.8^{+5.4}_{-6.4}$ | $74.7^{+7.0}_{-4.8}$ | $71.0^{+6.5}_{-4.4}$ |
| **GW190527_092055** | $36.5^{+16.4}_{-9.0}$ | $22.6^{+10.5}_{-8.1}$ | $59.1^{+21.3}_{-9.8}$ | $56.4^{+20.2}_{-9.3}$ |
| **GW190602_175927** | $69.1^{+15.7}_{-13.0}$ | $47.8^{+14.3}_{-17.4}$ | $116.3^{+19.0}_{-15.6}$ | $110.9^{+17.7}_{-14.9}$ |
| **GW190620_030421** | $57.1^{+16.0}_{-12.7}$ | $35.5^{+12.2}_{-12.3}$ | $92.1^{+18.5}_{-13.1}$ | $87.2^{+16.8}_{-12.1}$ |
| **GW190630_185205** | $35.1^{+6.9}_{-5.6}$ | $23.7^{+5.2}_{-5.1}$ | $59.1^{+4.6}_{-4.8}$ | $56.4^{+4.4}_{-4.6}$ |
| **GW190701_203306** | $53.9^{+11.8}_{-8.0}$ | $40.8^{+8.7}_{-12.0}$ | $94.3^{+12.1}_{-9.5}$ | $90.2^{+11.3}_{-8.9}$ |
| **GW190706_222641** | $67.0^{+14.6}_{-16.2}$ | $38.2^{+14.6}_{-13.3}$ | $104.1^{+20.2}_{-13.9}$ | $99.0^{+18.3}_{-13.5}$ |
| **GW190707_093326** | $11.6^{+3.3}_{-1.7}$ | $8.4^{+1.4}_{-1.7}$ | $20.1^{+1.9}_{-1.3}$ | $19.2^{+1.9}_{-1.3}$ |
| **GW190708_232457** | $17.6^{+4.7}_{-2.3}$ | $13.2^{+2.0}_{-2.7}$ | $30.9^{+2.5}_{-1.8}$ | $29.5^{+2.5}_{-1.8}$ |
| **GW190719_215514** | $36.5^{+18.0}_{-10.3}$ | $20.8^{+9.0}_{-7.2}$ | $57.8^{+18.3}_{-10.7}$ | $54.9^{+17.3}_{-10.2}$ |
| **GW190720_000836** | $13.4^{+6.7}_{-3.0}$ | $7.8^{+2.3}_{-2.2}$ | $21.5^{+4.3}_{-2.3}$ | $20.4^{+4.5}_{-2.2}$ |
| **GW190727_060333** | $38.0^{+9.5}_{-6.2}$ | $29.4^{+7.1}_{-8.4}$ | $67.1^{+11.7}_{-8.0}$ | $63.8^{+10.9}_{-7.5}$ |
| **GW190728_064510** | $12.3^{+7.2}_{-2.2}$ | $8.1^{+1.7}_{-2.6}$ | $20.6^{+4.5}_{-1.3}$ | $19.6^{+4.7}_{-1.3}$ |
| **GW190731_140936** | $41.5^{+12.2}_{-9.0}$ | $28.8^{+9.7}_{-9.5}$ | $70.1^{+15.8}_{-11.3}$ | $67.0^{+14.6}_{-10.8}$ |
| **GW190803_022701** | $37.3^{+10.6}_{-7.0}$ | $27.3^{+7.8}_{-8.2}$ | $64.5^{+12.6}_{-9.0}$ | $61.7^{+11.8}_{-8.5}$ |
| **GW190814** | $23.2^{+1.1}_{-1.0}$ | $2.59^{+0.08}_{-0.09}$ | $25.8^{+1.0}_{-0.9}$ | $25.6^{+1.1}_{-0.9}$ |
| **GW190828_063405** | $32.1^{+5.8}_{-4.0}$ | $26.2^{+4.6}_{-4.8}$ | $58.0^{+7.7}_{-4.8}$ | $54.9^{+7.2}_{-4.3}$ |
| **GW190828_065509** | $24.1^{+7.0}_{-7.2}$ | $10.2^{+3.6}_{-2.1}$ | $34.4^{+5.4}_{-4.4}$ | $33.1^{+5.5}_{-4.5}$ |
| **GW190909_114149** | $45.8^{+52.7}_{-13.3}$ | $28.3^{+13.4}_{-12.7}$ | $75.0^{+55.9}_{-17.6}$ | $72.0^{+54.9}_{-16.8}$ |
| **GW190910_112807** | $43.9^{+7.6}_{-6.1}$ | $35.6^{+6.3}_{-7.2}$ | $79.6^{+9.3}_{-9.1}$ | $75.8^{+8.5}_{-8.6}$ |
| **GW190915_235702** | $35.3^{+9.5}_{-6.4}$ | $24.4^{+5.6}_{-6.1}$ | $59.9^{+7.5}_{-6.4}$ | $57.2^{+7.1}_{-6.0}$ |
| **GW190924_021846** | $8.9^{+7.0}_{-2.0}$ | $5.0^{+1.4}_{-1.9}$ | $13.9^{+5.1}_{-1.0}$ | $13.3^{+5.2}_{-1.0}$ |
| **GW190929_012149** | $80.8^{+33.0}_{-33.2}$ | $24.1^{+19.3}_{-10.6}$ | $104.3^{+34.9}_{-25.2}$ | $101.5^{+33.6}_{-25.3}$ |
| **GW190930_133541** | $12.3^{+12.4}_{-2.3}$ | $7.8^{+1.7}_{-3.3}$ | $20.3^{+8.9}_{-1.5}$ | $19.4^{+9.2}_{-1.5}$ |

# Bibliography


[1] S. Abiko, Einstein's Kyoto Address: "How I Created the Theory of Relativity", Historical Studies in the Physical and Biological Sciences **31**(1), 1 (2000). DOI 10.2307/27757844

[2] A. Einstein, Zur algemeinen relativitätstheorie, Preuss. Akad. Wiss. Berlin, Sitzungsber. pp. 778–786 (1915)

[3] A. Einstein, Zur Allgemeinen Relativitätstheorie, Sitzungsber. Preuss. Akad. Wiss. Berlin (Math. Phys. ) **1915**, 778 (1915). [Addendum: Sitzungsber.Preuss.Akad.Wiss.Berlin (Math.Phys.) 1915, 799–801 (1915)]

[4] A. Einstein, Explanation of the Perihelion Motion of Mercury from the General Theory of Relativity, Sitzungsber. Preuss. Akad. Wiss. Berlin (Math. Phys. ) **1915**, 831 (1915)

[5] A. Einstein, The Field Equations of Gravitation, Sitzungsber. Preuss. Akad. Wiss. Berlin (Math. Phys. ) **1915**, 844 (1915)

[6] F.W. Dyson, A.S. Eddington, C. Davidson, A Determination of the Deflection of Light by the Sun's Gravitational Field, from Observations Made at the Total Eclipse of May 29, 1919, Phil. Trans. Roy. Soc. Lond. A **220**, 291 (1920). DOI 10.1098/rsta.1920.0009

[7] A.S. Eddington, The propagation of gravitational waves, Proc. Roy. Soc. Lond. **A102**, 268 (1922)

[8] A. Pais, How Einstein Got the Nobel Prize, American Scientist **70**(4), 358 (1982)

[9] R.V. Pound, G.A. Rebka, Jr., Apparent Weight of Photons, Phys. Rev. Lett. **4**, 337 (1960). DOI 10.1103/PhysRevLett.4.337

[10] A. Einstein, Approximative Integration of the Field Equations of Gravitation, Sitzungsber. Preuss. Akad. Wiss. Berlin (Math. Phys. ) **1916**, 688 (1916)

[11] A. Einstein, Über Gravitationswellen, Sitzungsberichte der Königlich Preussischen Akademie der Wissenschaften (Berlin) **1918**, 154 (1918)

[12] A. Einstein, N. Rosen, On gravitational waves, J. Franklin. Inst. **223**, 43 (1937). DOI 10.1016/S0016-0032(37)90583-0

[13] A. Einstein, N. Rosen, Two-Body Problem in General Relativity Theory, Phys. Rev. **49**, 404 (1936). DOI 10.1103/PhysRev.49.404.2

[14] S. Chandrasekhar, The maximum mass of ideal white dwarfs, Astrophys. J. **74**, 81 (1931). DOI 10.1086/143324

[15] K.C. Wali, Chandrasekhar vs. Eddington–an unanticipated confrontation, Physics Today **35**(10), 33 (1982). DOI 10.1063/1.2914790. URL `https://ui.adsabs.harvard.edu/abs/1982PhT....35j..33W`

[16] A.I. Miller, K. Wali, Empire of the Stars: Obsession, Friendship, and Betrayal in the Quest for Black Holes, Physics Today **59**(2), 53 (2006). DOI 10.1063/1.2186283

[17] C.M. De Witt (ed.). *Proceedings: Conference on the Role of Gravitation in Physics, Chapel Hill, North Carolina, Jan 18-23, 1957* (1957)

[18] J. Weber, Detection and Generation of Gravitational Waves, Phys. Rev. **117**, 306 (1960). DOI 10.1103/PhysRev.117.306

[19] A. Rudiger, W. Winkler, K. Maischberger, R. Schilling, L. Schnupp, D. Shoemaker, in *4th Marcel Grossmann Meeting on the Recent Developments of General Relativity* (1985), pp. 621–630

[20] J. Hough, B.J. Meers, G.P. Newton, N.A. Robertson, H. Ward, B.F. Schutz, R.W.P. Drever, R. Mason, C. Pollard, R. Tolcher, D.W. Bellenger, J.R.J. Bennett, I.F. Corbett, M.D. Percival, A British long baseline gravitational wave observatory., Rutherford Appleton Laboratory Report **1** (1986)

[21] K. Danzmann, H. Lück, A. Rüdiger, R. Schilling, M. Schrempel, W. Winkler, J. Hough, G.P. Newton, N.A. Robertson, H. Ward, A.M. Campbell, J.E. Logan, D.I. Robertson, K.A. Strain, J.R.J. Bennett, V. Kose, M. Kühne, B.F. Schutz, D. Nicholson, J. Shuttleworth, H. Welling, P. Aufmuth, R. Rinkleff, A. Tünnermann, B. Willke, GEO 600 - a 600 m laser interferometric gravitational wave antenna., First Edoardo Amaldi Conference on Gravitational Wave Experiments p. 100 (1995). URL `https://ui.adsabs.harvard.edu/abs/1995gwe..conf..100D`

[22] B.C. Barish, in *American Physical Society (APS) Meeting of the Division of Particles and Fields (DPF 99)* (1999)

[23] J. Aasi, et al., Advanced LIGO, Class. Quant. Grav. **32**, 074001 (2015). DOI 10.1088/0264-9381/32/7/074001

[24] A.H. Nitz, C. Capano, A.B. Nielsen, S. Reyes, R. White, D.A. Brown, B. Krishnan, 1-OGC: The first open gravitational-wave catalog of binary mergers from analysis of public Advanced LIGO data, Astrophys. J. **872**(2), 195 (2019). DOI 10.3847/1538-4357/ab0108

[25] B. Abbott, et al., GWTC-1: A Gravitational-Wave Transient Catalog of Compact Binary Mergers Observed by LIGO and Virgo during the First and Second Observing Runs, Phys. Rev. X **9**(3), 031040 (2019). DOI 10.1103/PhysRevX.9.031040

[26] B. Abbott, et al., GW170814: A Three-Detector Observation of Gravitational Waves from a Binary Black Hole Coalescence, Phys. Rev. Lett. **119**(14), 141101 (2017). DOI 10.1103/PhysRevLett.119.141101

[27] B. Abbott, et al., GW170817: Observation of Gravitational Waves from a Binary Neutron Star Inspiral, Phys. Rev. Lett. **119**(16), 161101 (2017). DOI 10.1103/PhysRevLett.119.161101

[28] D. Shoemaker, LIGO Scientific Collaboration, Gravitational wave astronomy with LIGO and similar detectors in the next decade, Bulletin of the American Astronomical Society **51**(3), 452 (2019)

[29] J. Calderón Bustillo, N. Sanchis-Gual, A. Torres-Forné, J.A. Font, A. Vajpeyi, R. Smith, C. Herdeiro, E. Radu, S.H.W. Leong, GW190521 as a merger of Proca stars: a potential new vector boson of $8.7 \times 10^{-13}$ eV, Phys. Rev. Lett. **126**(8), 081101 (2021). DOI 10.1103/PhysRevLett.126.081101

[30] R.S. Conklin, B. Holdom, J. Ren, Gravitational wave echoes through new windows, Phys. Rev. D **98**, 044021 (2018). DOI 10.1103/PhysRevD.98.044021. URL https://link.aps.org/doi/10.1103/PhysRevD.98.044021

[31] R.A. Konoplya, Z. Stuchlík, A. Zhidenko, Echoes of compact objects: New physics near the surface and matter at a distance, Phys. Rev. D **99**, 024007 (2019). DOI 10.1103/PhysRevD.99.024007. URL https://link.aps.org/doi/10.1103/PhysRevD.99.024007

[32] A. Almheiri, D. Marolf, J. Polchinski, J. Sully, Black Holes: Complementarity or Firewalls?, JHEP **02**, 062 (2013). DOI 10.1007/JHEP02(2013)062

[33] O. Lunin, S.D. Mathur, AdS / CFT duality and the black hole information paradox, Nucl. Phys. B **623**, 342 (2002). DOI 10.1016/S0550-3213(01)00620-4

[34] G.F. Giudice, M. McCullough, A. Urbano, Hunting for Dark Particles with Gravitational Waves, JCAP **10**, 001 (2016). DOI 10.1088/1475-7516/2016/10/001

[35] P.O. Mazur, E. Mottola, Gravitational vacuum condensate stars, Proc. Nat. Acad. Sci. **101**, 9545 (2004). DOI 10.1073/pnas.0402717101

[36] S.L. Liebling, C. Palenzuela, Dynamical Boson Stars, Living Rev. Rel. **20**(1), 5 (2017). DOI 10.12942/lrr-2012-6

[37] V. Cardoso, E. Franzin, P. Pani, Is the gravitational-wave ringdown a probe of the event horizon?, Phys. Rev. Lett. **116**(17), 171101 (2016). DOI 10.1103/PhysRevLett.116.171101. [Erratum: Phys.Rev.Lett. 117, 089902 (2016)]

[38] V. Cardoso, S. Hopper, C.F.B. Macedo, C. Palenzuela, P. Pani, Gravitational-wave signatures of exotic compact objects and of quantum corrections at the horizon scale, Phys. Rev. D **94**(8), 084031 (2016). DOI 10.1103/PhysRevD.94.084031

[39] V. Cardoso, P. Pani, Tests for the existence of black holes through gravitational wave echoes, Nature Astron. **1**(9), 586 (2017). DOI 10.1038/s41550-017-0225-y

[40] J. Abedi, H. Dykaar, N. Afshordi, Echoes from the Abyss: Tentative evidence for Planck-scale structure at black hole horizons, Phys. Rev. D **96**(8), 082004 (2017). DOI 10.1103/PhysRevD.96.082004

[41] G. Ashton, O. Birnholtz, M. Cabero, C. Capano, T. Dent, B. Krishnan, G.D. Meadors, A.B. Nielsen, A. Nitz, J. Westerweck. Comments on: "Echoes from the abyss: Evidence for Planck-scale structure at black hole horizons" (2016)

[42] J. Westerweck, A. Nielsen, O. Fischer-Birnholtz, M. Cabero, C. Capano, T. Dent, B. Krishnan, G. Meadors, A.H. Nitz, Low significance of evidence for black hole echoes in gravitational wave data, Phys. Rev. D **97**(12), 124037 (2018). DOI 10.1103/PhysRevD.97.124037

[43] J. Abedi, H. Dykaar, N. Afshordi, Echoes from the Abyss: The Holiday Edition!, arXiv e-prints arXiv:1701.03485 (2017)

[44] J. Abedi, H. Dykaar, N. Afshordi, Comment on: "Low significance of evidence for black hole echoes in gravitational wave data", arXiv e-prints arXiv:1803.08565 (2018). URL https://ui.adsabs.harvard.edu/abs/2018arXiv180308565A

[45] J. Abedi, N. Afshordi, Echoes from the Abyss: A highly spinning black hole remnant for the binary neutron star merger GW170817, JCAP **11**, 010 (2019). DOI 10.1088/1475-7516/2019/11/010

[46] J. Abedi, N. Afshordi, Echoes from the Abyss: A Status Update, arXiv e-prints arXiv:2001.00821 (2020). URL https://ui.adsabs.harvard.edu/abs/2020arXiv200100821A

[47] N.T. Bishop, P.J. van der Walt, M. Naidoo, Effect of a low density dust shell on the propagation of gravitational waves, Gen. Rel. Grav. **52**(9), 92 (2020). DOI 10.1007/s10714-020-02740-9

[48] M. Naidoo, N.T. Bishop, P.J. van der Walt, Modifications to the signal from a gravitational wave event due to a surrounding shell of matter, arXiv e-prints arXiv:2102.00060 (2021). URL https://ui.adsabs.harvard.edu/abs/2021arXiv210200060N

[49] B.F. Schutz, *A First Course in General Relativity* (Cambridge Univ. Pr., Cambridge, UK, 1985)

[50] R.M. Wald, *General relativity* (The University of Chicago Press, Chicago, 1984)

[51] J. Foster, J.D. Nightingale, *A Short Course in General Relativity* (2006). DOI 10.1007/978-0-387-27583-3. URL https://ui.adsabs.harvard.edu/abs/2006asci.book.....F

[52] S. Weinberg, *Gravitation and Cosmology: Principles and Applications of the General Theory of Relativity* (John Wiley and Sons, New York, 1972)

[53] N. Bishop, R. Gómez, P. Holvorcem, R. Matzner, P. Papadopoulos, J. Winicour, Cauchy-characteristic evolution and waveforms, J. Comput. Phys. **136**, 140 (1997). DOI 10.1006/jcph.1997.5754

[54] N.T. Bishop, Linearized solutions of the Einstein equations within a Bondi-Sachs framework, and implications for boundary conditions in numerical simulations, Class. Quantum Grav. **22**(12), 2393 (2005). DOI 10.1088/0264-9381/22/12/006

[55] A. Mercier, M. Kervaire (eds.). *Helvetica Physica Acta Supplementum IV* (Birkhauser, 1956)

[56] C. Kiefer, Space and Time 62 Years after the Berne Conference, Einstein Stud. **15**, 1 (2020). DOI 10.1007/978-3-030-47782-0_1

[57] A.S. Eddington, The Physical Society of London Report on the Relativity Theory of Gravitation, Nature **103** (1919). DOI https://doi.org/10.1038/103002a0

[58] A. Einstein, Zur elektrodynamik bewegter körper, Ann. Phys. **17**, 891 (1905)

[59] A. Einstein, Ist die trägheit eines körpers von seinem energieinhalt abhängig?, Ann. Phys. **18**, 639 (1905)

[60] J.L. Cervantes-Cota, S. Galindo-Uribarri, G.F. Smoot, A Brief History of Gravitational Waves, Universe **2**(3), 22 (2016). DOI 10.3390/universe2030022

[61] S.M. Carroll, Lecture Notes on General Relativity, arXiv e-prints gr-qc/9712019 (1997). URL https://ui.adsabs.harvard.edu/abs/1997gr.qc....12019C

[62] S.M. Carroll, A no-nonsense introduction to general relativity (2001). URL http://pancake.uchicago.edu/~carroll/notes/grtiny.pdf

[63] N.T. Bishop, Introduction to gravitational wave astronomy, arXiv e-prints arXiv:2103.07675 (2021)

[64] A. Ashtekar, B. Bonga, On the ambiguity in the notion of transverse traceless modes of gravitational waves, Gen. Rel. Grav. **49**(9), 122 (2017). DOI 10.1007/s10714-017-2290-z

[65] H. Bondi, *Science, Churchill and Me* (Pergamon, Oxford, 1990). DOI https://doi.org/10.1016/C2009-0-07936-7

[66] H. Bondi, Gravitational waves in general relativity, Nature **186**, 535 (1960). DOI 10.1038/186535a0

[67] R. Sachs, Gravitational waves in general relativity VIII. Waves in asymptotically flat space-time, Proc. Roy. Soc. London **A270**, 103 (1962)

[68] E. Newman, R. Penrose, An Approach to gravitational radiation by a method of spin coefficients, J. Math. Phys. **3**, 566 (1962). DOI 10.1063/1.1724257

[69] H. Bondi, M.G.J. van der Burg, A.W.K. Metzner, Gravitational waves in general relativity VII. Waves from axi-symmetric isolated systems, Proc. R. Soc. London **A269**, 21 (1962)

[70] J. Winicour, Characteristic Evolution and Matching, Living Reviews in Relativity **8**, 10 (2005)

[71] N.T. Bishop, L. Rezzolla, Extraction of gravitational waves in numerical relativity, Living Rev. Relativ. **19**, 1 (2016). DOI DOI10.1007/s41114-016-0001-9. URL `http://dx.doi.org/10.1007/s41114-016-0001-9`

[72] T. Mädler, J. Winicour, Bondi-Sachs Formalism, Scholarpedia **11**, 33528 (2016). DOI 10.4249/scholarpedia.33528

[73] N.T. Bishop, Numerical relativity: Combining the Cauchy and characteristic initial value problem, Class. Quantum Grav. **10**, 333 (1993)

[74] N.T. Bishop, C. Reisswig, The gravitational wave strain in the characteristic formalism of numerical relativity, Gen. Rel. Grav. **46**, 1643 (2014)

[75] J. Winicour, Characteristic Evolution and Matching, Living Reviews in Relativity **15**, 2 (2012). DOI 10.12942/lrr-2012-2

[76] J. Winicour, in *Yukawa Meeting 1999*. Gr-qc/9911106

[77] J. Winicour, Characteristic Evolution and Matching, Living Rev. Rel. **12**, 3 (2009). DOI 10.12942/lrr-2009-3

[78] H. Bondi, M.G.J. van der Burg, A.W.K. Metzner, Gravitational waves in general relativity. 7. Waves from axisymmetric isolated systems, Proc. Roy. Soc. Lond. A **269**, 21 (1962). DOI 10.1098/rspa.1962.0161

[79] R. Sachs, Proc. Roy. Soc. London **A264**, 309 (1961)

[80] E.T. Newman, R. Penrose, An approach to gravitational radiation by a method of spin coefficients, J. Math. Phys. **3**(3), 566 (1962). DOI 10.1063/1.1724257. Erratum in J. Math. Phys. 4, 998 (1963)

[81] P.J. van der Walt, N.T. Bishop, Observational cosmology using characteristic numerical relativity, Phys. Rev. D **82**, 084001 (2010). DOI 10.1103/PhysRevD.82.084001

[82] P.J. van der Walt, N.T. Bishop, Observational cosmology using characteristic numerical relativity: Characteristic formalism on null geodesics, Phys. Rev. D **85**, 044016 (2012). DOI 10.1103/PhysRevD.85.044016

[83] H.L. Bester, J. Larena, N.T. Bishop, Towards the geometry of the universe from data, Mon. Not. Roy. Astron. Soc. **453**(3), 2364 (2015). DOI 10.1093/mnras/stv1672

[84] J. Winicour, Affine-null metric formulation of Einstein's equations, Phys. Rev. D **87**(12), 124027 (2013). DOI 10.1103/PhysRevD.87.124027

[85] E.T. Newman, R. Penrose, Note on the bondi-metzner-sachs group, Journal of Mathematical Physics **7**(5), 863 (1966). DOI 10.1063/1.1931221. URL `https://doi.org/10.1063/1.1931221`

[86] J.N. Goldberg, A.J. MacFarlane, E.T. Newman, F. Rohrlich, E.C.G. Sudarshan, Spin-$s$ spherical harmonics and $\eth$, J. Math. Phys. **8**(11), 2155 (1967). DOI 10.1063/1.1705135

[87] R. Gómez, L. Lehner, P. Papadopoulos, J. Winicour, The eth formalism in numerical relativity, Class. Quantum Grav. **14**(4), 977 (1997)

[88] C. Reisswig, N.T. Bishop, D. Pollney, B. Szilagyi, Characteristic extraction in numerical relativity: binary black hole merger waveforms at null infinity (2009)

[89] C. Reisswig, N.T. Bishop, D. Pollney, B. Szilagyi, Characteristic extraction in numerical relativity: binary black hole merger waveforms at null infinity, Class. Quantum Grav. **27**, 075014 (2010)

[90] N.T. Bishop, L. Rezzolla, Extraction of Gravitational Waves in Numerical Relativity, Living Rev. Rel. **19**, 2 (2016). DOI 10.1007/s41114-016-0001-9

[91] N.T. Bishop, R. Isaacson, M. Maharaj, J. Winicour, Black hole data via a Kerr-Schild approach, Phys. Rev. D **57**, 6113 (1998)

[92] C. Reisswig, N.T. Bishop, C.W. Lai, J. Thornburg, B. Szilagyi, Characteristic evolutions in numerical relativity using six angular patches, Classical and Quantum Gravity **24**, 327 (2007). DOI 10.1088/0264-9381/24/12/S21

[93] B.S. Sathyaprakash, B.F. Schutz, Physics, Astrophysics and Cosmology with Gravitational Waves, Living Rev. Relativ. **12**, 2 (2009)

[94] K. Riles, Gravitational Waves: Sources, Detectors and Searches, Prog. Part. Nucl. Phys. **68**, 1 (2013). DOI 10.1016/j.ppnp.2012.08.001

[95] F. Pretorius, Evolution of binary black hole spacetimes, Phys. Rev. Lett. **95**, 121101 (2005)

[96] M. Campanelli, C.O. Lousto, P. Marronetti, Y. Zlochower, Accurate evolutions of orbiting black-hole binaries without excision, Phys. Rev. Lett. **96**, 111101 (2006)

[97] J.G. Baker, J. Centrella, D.I. Choi, M. Koppitz, J. van Meter, Gravitational wave extraction from an inspiraling configuration of merging black holes, Phys. Rev. Lett. **96**, 111102 (2006)

[98] M. Shibata, K. Uryū, Computation of gravitational waves from inspiraling binary neutron stars in quasiequilibrium circular orbits: Formulation and calibration, Phys. Rev. D **64**, 104017 (2001)

[99] M. Shibata, K. Uryū, Gravitational Waves from Merger of Binary Neutron Stars in Fully General Relativistic Simulation, Progress of Theoretical Physics **107**, 265 (2002). DOI 10.1143/PTP.107.265

[100] M. Shibata, K. Taniguchi, K. Uryū, Merger of binary neutron stars with realistic equations of state in full general relativity, Phys. Rev. D **71**(8), 084021 (2005). DOI 10.1103/PhysRevD.71.084021

[101] M. Shibata, K. Taniguchi, Merger of binary neutron stars to a black hole: Disk mass, short gamma-ray bursts, and quasinormal mode ringing, Phys. Rev. D **73**(6), 064027 (2006). DOI 10.1103/PhysRevD.73.064027

[102] M. Shibata, K. Uryu, Merger of black hole-neutron star binaries: nonspinning black hole case, Phys. Rev. D **74**, 121503 (R) (2006). DOI 10.1103/PhysRevD.74.121503

[103] F. García, A.S. Bunzel, S. Chaty, E. Porter, E. Chassande-Mottin. Progenitors of low-mass binary black-hole mergers in the isolated binary evolution scenario (2021)

[104] P.C. Peters, Gravitational Radiation and the Motion of Two Point Masses, Phys. Rev. **136**, B1224 (1964). DOI 10.1103/PhysRev.136.B1224

[105] L. Zwick, P.R. Capelo, E. Bortolas, L. Mayer, P. Amaro-Seoane, Improved gravitational radiation time-scales: significance for LISA and LIGO-Virgo sources, Mon. Not. Roy. Astron. Soc. **495**(2), 2321 (2020). DOI 10.1093/mnras/staa1314

[106] J.A. Faber, F.A. Rasio, Binary neutron star mergers, Living Reviews in Relativity **15**(8) (2012). URL `http://www.livingreviews.org/lrr-2012-8`

[107] R. Abbott, et al. Population Properties of Compact Objects from the Second LIGO-Virgo Gravitational-Wave Transient Catalog (2020)

[108] I. Mandel, S.E. de Mink, Merging binary black holes formed through chemically homogeneous evolution in short-period stellar binaries, Mon. Not. Roy. Astron. Soc. **458**(3), 2634 (2016). DOI 10.1093/mnras/stw379

[109] C.L. Rodriguez, M. Morscher, B. Pattabiraman, S. Chatterjee, C.J. Haster, F.A. Rasio, Binary Black Hole Mergers from Globular Clusters: Implications for Advanced LIGO, Phys. Rev. Lett. **115**(5), 051101 (2015). DOI 10.1103/PhysRevLett.115.051101. [Erratum: Phys.Rev.Lett. 116, 029901 (2016)]

[110] J. Riley, I. Mandel, P. Marchant, E. Butler, K. Nathaniel, C. Neijssel, S. Shortt, A. Vigna-Gomez. Chemically Homogeneous Evolution: A rapid population synthesis approach (2020)

[111] C.L. Fryer, K. Belczynski, G. Wiktorowicz, M. Dominik, V. Kalogera, D.E. Holz, Compact remnant mass function: Dependence on the explosion mechanism and metallicity, The Astrophysical Journal **749**(1), 91 (2012). DOI 10.1088/0004-637x/749/1/91. URL `http://dx.doi.org/10.1088/0004-637X/749/1/91`

[112] E. Burns, Neutron Star Mergers and How to Study Them, Living Rev. Rel. **23**(1), 4 (2020). DOI 10.1007/s41114-020-00028-7

[113] E. Burns, A. Tohuvavohu, J. Buckley, T.D. Canton, B. Cenko, J. Conklin, F. D'ammando, D. Eichler, C. Fryer, A. van der Horst, M. Kamionkowski, M. Kasliwal, R. Margutti, B. Metzger, K. Murase, S. Nissanke, D. Radice, J. Tomsick, C. Wilson-Hodge, B. Zhang, A Summary of Multimessenger Science with Neutron Star Mergers, Bulletin of the American Astronomical Society **51**(3), 38 (2019). URL `https://ui.adsabs.harvard.edu/abs/2019BAAS...51c..38B`

[114] G. Raaijmakers, et al. The Challenges Ahead for Multimessenger Analyses of Gravitational Waves and Kilonova: a Case Study on GW190425 (2021)

[115] D. Chattopadhyay, S. Stevenson, J.R. Hurley, M. Bailes, F. Broekgaarden. Modelling Neutron Star-Black Hole Binaries: Future Pulsar Surveys and Gravitational Wave Detectors (2020)

[116] D. Chattopadhyay, S. Stevenson, J.R. Hurley, L.J. Rossi, C. Flynn, Modelling Double Neutron Stars: Radio and Gravitational Waves, Mon. Not. Roy. Astron. Soc. **494**(2), 1587 (2020). DOI 10.1093/mnras/staa756

[117] F. Foucart, A brief overview of black hole-neutron star mergers, Front. Astron. Space Sci. **7**, 46 (2020). DOI 10.3389/fspas.2020.00046

[118] D.R. Lorimer, Binary and millisecond pulsars at the new millennium, Living Rev. Rel. **4**, 5 (2001). DOI 10.12942/lrr-2001-5

[119] J.A. Faber, F.A. Rasio, Binary Neutron Star Mergers, Living Rev. Rel. **15**, 8 (2012). DOI 10.12942/lrr-2012-8

[120] K. Belczynski, G. Wiktorowicz, C.L. Fryer, D.E. Holz, V. Kalogera, Missing black holes unveil the supernova explosion mechanism, The Astrophysical Journal **757**(1), 91 (2012). DOI 10.1088/0004-637x/757/1/91. URL `http://dx.doi.org/10.1088/0004-637X/757/1/91`

[121] R. Hulse, J. Taylor, Discovery of a pulsar in a binary system, Astrophys. J. **195**, L51 (1975)

[122] P.C. Peters, J. Mathews, Gravitational radiation from point masses in a Keplerian orbit, Phys. Rev. **131**, 435 (1963)

[123] B. Müller, Hydrodynamics of core-collapse supernovae and their progenitors, Astrophysics **6**, 3 (2020). DOI 10.1007/s41115-020-0008-5

[124] E. Abdikamalov, G. Pagliaroli, D. Radice. Gravitational Waves from Core-Collapse Supernovae (2020)

[125] A. Heger, C.L. Fryer, S.E. Woosley, N. Langer, D.H. Hartmann, How Massive Single Stars End Their Life, Astrophys. J. **591**, 288 (2003). DOI 10.1086/375341

[126] S.E. Woosley, A. Heger, T.A. Weaver, The evolution and explosion of massive stars, Rev. Mod. Phys. **74**, 1015 (2002)

[127] S.E. Woosley, A. Heger, The Progenitor Stars of Gamma-Ray Bursts, Astrophys. J. **637**, 914 (2006). DOI 10.1086/498500

[128] S. Woosley, T. Janka, The physics of core-collapse supernovae, Nature Phys. **1**, 147 (2005). DOI 10.1038/nphys172

[129] H.T. Janka, F. Hanke, L. Huedepohl, A. Marek, B. Mueller, M. Obergaulinger. Core-collapse supernovae: Reflections and directions (2012)

[130] B. Paxton, et al., Modules for Experiments in Stellar Astrophysics (MESA): Binaries, Pulsations, and Explosions, Astrophys. J. Suppl. **220**(1), 15 (2015). DOI 10.1088/0067-0049/220/1/15

[131] C. Fields, S. Couch, On The Development of Multidimensional Progenitor Models For Core-collapse Supernovae, Astrophys. J. **901**(1), 33 (2020). DOI 10.3847/1538-4357/abada7

[132] H. Andresen, B. Müller, E. Müller, H.T. Janka, Gravitational Wave Signals from 3D Neutrino Hydrodynamics Simulations of Core-Collapse Supernovae, Mon. Not. Roy. Astron. Soc. **468**(2), 2032 (2017). DOI 10.1093/mnras/stx618

[133] H. Andresen, E. Müller, H. Janka, A. Summa, K. Gill, M. Zanolin, Gravitational waves from 3D core-collapse supernova models: The impact of moderate progenitor rotation, Mon. Not. Roy. Astron. Soc. **486**(2), 2238 (2019). DOI 10.1093/mnras/stz990

[134] D. Radice, V. Morozova, A. Burrows, D. Vartanyan, H. Nagakura, Characterizing the Gravitational Wave Signal from Core-Collapse Supernovae, Astrophys. J. Lett. **876**(1), L9 (2019). DOI 10.3847/2041-8213/ab191a

[135] S. Shibagaki, T. Kuroda, K. Kotake, T. Takiwaki, A New Gravitational Wave Signature of Low-$T/|W|$ Instability in Rapidly Rotating Stellar Core Collapse, Mon. Not. Roy. Astron. Soc. **493**(1), L138 (2020). DOI 10.1093/mnrasl/slaa021

[136] J.M. Weisberg, J.H. Taylor, L.A. Fowler, GRAVITATIONAL RADIATION FROM PULSAR PSR-1913+16. (IN GERMAN), Spektrum Wiss. **12**, 53 (1981)

[137] J.M. Weisberg, J.H. Taylor, Observations of Post-Newtonian Timing Effects in the Binary Pulsar PSR 1913+16, Phys. Rev. Lett. **52**, 1348 (1984). DOI 10.1103/PhysRevLett.52.1348

[138] J.H. Taylor, J.M. Weisberg, Further experimental tests of relativistic gravity using the binary pulsar PSR 1913+16, Astrophys. J. **345**, 434 (1989). DOI 10.1086/167917

[139] V.R. Pandharipande, D. Pines, R.A. Smith, Neutron star structure: Theory observation, and speculation, Astrophys. J. **208**, 550 (1976). DOI 10.1086/154637

[140] M. Zimmermann, Revised Estimate of Gravitational Radiation from Crab and Vela Pulsars, Nature **271**, 524 (1978). DOI 10.1038/271524a0

[141] J.L. Friedman, S.M. Morsink, Axial instability of rotating relativistic stars, Astrophys. J. **502**, 714 (1998). DOI 10.1086/305920

[142] N. Andersson, A New class of unstable modes of rotating relativistic stars, Astrophys. J. **502**, 708 (1998). DOI 10.1086/305919

[143] M.F. Alam, et al., The NANOGrav 12.5 yr Data Set: Observations and Narrowband Timing of 47 Millisecond Pulsars, Astrophys. J. Suppl. **252**(1), 4 (2021). DOI 10.3847/1538-4365/abc6a0

[144] B.F. Schutz, Gravitational Wave Astronomy: Delivering on the Promises, Phil. Trans. Roy. Soc. Lond. A **376**(2120), 20170279 (2018). DOI 10.1098/rsta.2017.0279

[145] K.L. Dooley, H. Grote, J. van den Brand, Terrestrial Laser Interferometers, arXiv e-prints arXiv:2103.01740 (2021). URL `https://ui.adsabs.harvard.edu/abs/2021arXiv210301740D`

[146] S.L. Cacciatori, Gravitational waves, 100 years later, arXiv e-prints arXiv:2005.03989 (2020). URL `https://ui.adsabs.harvard.edu/abs/2020arXiv200503989C`

[147] H. Grote, *Gravitational Waves: A History of Discovery* (Taylor and Francis group / CRC Press, 2019). DOI https://doi.org/10.1201/9780429028045. `https://doi.org/10.1201/9780429028045`

[148] P.S. Shawhan, Gravitational waves and the effort to detect them: A worldwide network of detectors may soon measure subtle ripples in spacetime itself, ushering in a new era of astrophysical research, American Scientist **92**(4), 350 (2004). URL http://www.jstor.org/stable/27858424

[149] F.A.E. Pirani, On the Physical significance of the Riemann tensor, Acta. Phys. Polon. **15**, 389 (1956). DOI 10.1007/s10714-009-0787-9

[150] G. Weinstein, Einstein and Gravitational Waves 1936-1938, arXiv e-prints arXiv:1602.04674 (2016). URL https://ui.adsabs.harvard.edu/abs/2016arXiv160204674W

[151] H. Bondi, Plane gravitational waves in general relativity, Nature **179**, 1072 (1957). DOI 10.1038/1791072a0

[152] J. Weber, Evidence for discovery of gravitational radiation, Phys. Rev. Lett. **22**, 1320 (1969). DOI 10.1103/PhysRevLett.22.1320

[153] J. Hough, K.D. *et al.*, Geo 600 – proposal for a 600 m laser-interferometric gravitational wave antenna (1994). Proposal to the PPARC, 1994

[154] F. Acernese, et al., Advanced Virgo: a second-generation interferometric gravitational wave detector, Class. Quant. Grav. **32**(2), 024001 (2015). DOI 10.1088/0264-9381/32/2/024001

[155] nasa.gov.goddard. public nasa (2021). URL https://www.nasa.gov/goddard

[156] A.A. Abramovici, W. Althouse, R.P. Drever, Y. Gursel, S. Kawamura, F. Raab, D. Shoemaker, L. Sievers, R. Spero, K.S. Thorne, R. Vogt, R. Weiss, S. Whitcomb, M. Zuker, LIGO: The Laser Interferometer Gravitational-Wave Observatory, Science **256**, 325 (1992)

[157] T.J. Kane, R.L. Byer, Monolithic, unidirectional single-mode Nd:YAG ring laser, Opt. Lett. **10**(2), 65 (1985)

[158] The Virgo Collaboration. Instrumentspayloads/suspensions/mirrors (2021). URL http://public.virgo-gw.eu/wp-content/grand-media/image/201412_BSpayload_IMG_5971.jpg. [Online; accessed April 7, 2021]

[159] The LIGO Laboratory. Ligo hanford laser and vacuum equipment area (2021). URL https://www.ligo.caltech.edu/image/ligo20150731i. [Online; accessed April 7, 2021]

[160] F. Matichard, B. Lantz, R. Mittleman, K. Mason, J. Kissel, B. Abbott, S. Biscans, J. McIver, R. Abbott, S. Abbott, E. Allwine, S. Barnum, J. Birch, C. Celerier, D. Clark, D. Coyne, D. DeBra, R. DeRosa, M. Evans, S. Foley, P. Fritschel, J.A. Giaime, C. Gray, G. Grabeel, J. Hanson, C. Hardham, M. Hillard, W. Hua, C. Kucharczyk, M. Landry, A.L. Roux, V. Lhuillier, D. Macleod, M. Macinnis, R. Mitchell, B. O'Reilly, D. Ottaway, H. Paris, A. Pele, M. Puma, H. Radkins, C. Ramet, M. Robinson, L. Ruet, P. Sarin, D. Shoemaker, A. Stein, J. Thomas, M. Vargas, K. Venkateswara, J. Warner, S. Wen, Seismic isolation of advanced LIGO: Review of strategy, instrumentation and performance, Classical and Quantum Gravity **32**(18), 185003 (2015). DOI 10.1088/0264-9381/32/18/185003

[161] T. Accadia, F. Acernese, et al., The seismic superattenuators of the virgo gravitational waves interferometer, Journal of Low Frequency Noise Vibration and Active Control **30**, 63 (2011). DOI 10.1260/0263-0923.30.1.63

[162] The LIGO Laboratory. Virgosuperattenuatorvacuumtower (2021). URL http://public.virgo-gw.eu/wp-content/grand-media/image/VirgoSuperAttenuator_VacuumTower_Sketch.jpg. [Online; accessed April 7, 2021]

[163] A. Freise, et al., *FINESSE*. http://gwoptics.org

[164] M. Evans, et al., *Optickle*. https://github.com/Optickle/Optickle

[165] G. Vajente, Fast modal simulation of paraxial optical systems: the MIST open source toolbox, Classical and Quantum Gravity **30**(7), 075014 (2013). DOI 10.1088/0264-9381/30/7/075014

[166] L. Sun, E. Goetz, J.S. Kissel, J. Betzwieser, S. Karki, A. Viets, M. Wade, D. Bhattacharjee, V. Bossilkov, P.B. Covas, L.E.H. Datrier, R. Gray, S. Kandhasamy, Y.K. Lecoeuche, G. Mendell, T. Mistry, E. Payne, R.L. Savage, A.J. Weinstein, S. Aston, A. Buikema, C. Cahillane, J.C. Driggers, S.E. Dwyer, R. Kumar, A. Urban, Characterization of systematic error in Advanced LIGO calibration, Classical and Quantum Gravity **37**(22), 225008 (2020). DOI 10.1088/1361-6382/abb14e. URL https://doi.org/10.1088%2F1361-6382%2Fabb14e

[167] M. Maggiore, C.V.D. Broeck, N. Bartolo, E. Belgacem, D. Bertacca, M.A. Bizouard, M. Branchesi, S. Clesse, S. Foffa, J. García-Bellido, S. Grimm, J. Harms, T. Hinderer, S. Matarrese, C. Palomba, M. Peloso, A. Ricciardone, M. Sakellariadou, Science case for the Einstein Telescope, Journal of Cosmology and Astroparticle Physics **2020**(03), 050 (2020). DOI 10.1088/1475-7516/2020/03/050. URL https://doi.org/10.1088%2F1475-7516%2F2020%2F03%2F050

[168] C.M. Caves, Quantum-mechanical noise in an interferometer, Phys. Rev. D **23**, 1693 (1981). DOI 10.1103/PhysRevD.23.1693. URL https://link.aps.org/doi/10.1103/PhysRevD.23.1693

[169] H. Grote, K. Danzmann, K.L. Dooley, R. Schnabel, J. Slutsky, H. Vahlbruch, First long-term application of squeezed states of light in a gravitational-wave observatory, Phys. Rev. Lett. **110**, 181101 (2013). DOI 10.1103/PhysRevLett.110.181101. URL https://link.aps.org/doi/10.1103/PhysRevLett.110.181101

[170] M. Tse, et. al., Quantum-enhanced advanced ligo detectors in the era of gravitational-wave astronomy, Phys. Rev. Lett. **123**, 231107 (2019). DOI 10.1103/PhysRevLett.123.231107. URL https://link.aps.org/doi/10.1103/PhysRevLett.123.231107

[171] Virgo Collaboration, Increasing the astrophysical reach of the advanced virgo detector via the application of squeezed vacuum states of light, Phys. Rev. Lett. **123**, 231108 (2019). DOI 10.1103/PhysRevLett.123.231108. URL https://link.aps.org/doi/10.1103/PhysRevLett.123.231108

[172] L. McCuller, C. Whittle, D. Ganapathy, K. Komori, M. Tse, A. Fernandez-Galiana, L. Barsotti, P. Fritschel, M. MacInnis, F. Matichard, K. Mason, N. Mavalvala, R. Mittleman, H. Yu, M.E. Zucker, M. Evans, Frequency-dependent squeezing for advanced ligo, Phys. Rev. Lett. **124**, 171102 (2020). DOI 10.1103/PhysRevLett.124.171102. URL https://link.aps.org/doi/10.1103/PhysRevLett.124.171102

[173] Y. Levin, Internal thermal noise in the ligo test masses: A direct approach, Phys. Rev. D **57**, 659 (1998). DOI 10.1103/PhysRevD.57.659

[174] M. Evans, S. Ballmer, M. Fejer, P. Fritschel, G. Harry, G. Ogin, Thermo-optic noise in coated mirrors for high-precision optical measurements, Phys. Rev. D **78**, 102003

(2008). DOI 10.1103/PhysRevD.78.102003. URL https://link.aps.org/doi/10.1103/PhysRevD.78.102003

[175] R. Weiss, Quarterly Progress Report, Research Laboratory of Electronics, MIT. **105** (1972). http://dspace.mit.edu/handle/1721.1/56271

[176] P.R. Saulson, Terrestrial gravitational noise on a gravitational wave antenna, Phys. Rev. D **30**, 732 (1984). DOI 10.1103/PhysRevD.30.732. URL https://link.aps.org/doi/10.1103/PhysRevD.30.732

[177] The LIGO Laboratory. Ligo livingston (2021). URL https://www.ligo.caltech.edu/image/ligo20150731c. [Online; accessed April 7, 2021]

[178] The LIGO Laboratory. Virgo observatory (2021). URL https://www.ligo.caltech.edu/system/avm_image_sqls/binaries/85/page/Virgo_aerial_view_01.jpg?1506540063. [Online; accessed April 7, 2021]

[179] KAGRA. Kagra's arm tunnel (2021). URL https://gwcenter.icrr.u-tokyo.ac.jp/wp-content/uploads/2019/11/DSC_0802.jpg. [Online; accessed April 7, 2021]

[180] G. Janssen, et al., Gravitational wave astronomy with the SKA, PoS **AASKA14**, 037 (2015). DOI 10.22323/1.215.0037

[181] J.A. Tyson, Large synoptic survey telescope: Overview, Proc. SPIE Int. Soc. Opt. Eng. **4836**, 10 (2002). DOI 10.1117/12.456772

[182] J.I. Thorpe, J. Ziemer, I. Thorpe, J. Livas, J.W. Conklin, R. Caldwell, E. Berti, S.T. McWilliams, R. Stebbins, D. Shoemaker, E.C. Ferrara, S.L. Larson, D. Shoemaker, J.S. Key, M. Vallisneri, M. Eracleous, J. Schnittman, B. Kamai, J. Camp, G. Mueller, J. Bellovary, N. Rioux, J. Baker, P.L. Bender, C. Cutler, N. Cornish, C. Hogan, S. Manthripragada, B. Ware, P. Natarajan, K. Numata, S.R. Sankar, B.J. Kelly, K. McKenzie, J. Slutsky, R. Spero, M. Hewitson, S. Francis, R. DeRosa, A. Yu, A. Hornschemeier, P. Wass, in *Bulletin of the American Astronomical Society*, vol. 51 (2019), vol. 51, p. 77. URL https://ui.adsabs.harvard.edu/abs/2019BAAS...51g..77T

[183] LISA Pathfinder: First steps to observing gravitational waves from space, J. Phys. Conf. Ser. **840**(1), 012001 (2017). DOI 10.1088/1742-6596/840/1/012001

[184] S. Kawamura, et al., Current status of space gravitational wave antenna DECIGO and B-DECIGO, arXiv e-prints arXiv:2006.13545 (2020). URL https://ui.adsabs.harvard.edu/abs/2020arXiv200613545K

[185] Y.L. Wu, Hyperunified field theory and Taiji program in space for GWD, Int. J. Mod. Phys. A **33**(31), 1844014 (2018). DOI 10.1142/S0217751X18440141

[186] B. P. Abbott et. al., Observation of Gravitational Waves from a Binary Black Hole Merger, Phys. Rev. Lett. **116**, 061102 (2016). DOI 10.1103/PhysRevLett.116.061102

[187] R. Abbott, et al., GWTC-2: Compact Binary Coalescences Observed by LIGO and Virgo During the First Half of the Third Observing Run, arXiv e-prints arXiv:2010.14527 (2020). URL https://ui.adsabs.harvard.edu/abs/2020arXiv201014527A

[188] B.P. Abbott, et al., GW151226: Observation of Gravitational Waves from a 22-Solar-Mass Binary Black Hole Coalescence, Phys. Rev. Lett. **116**(24), 241103 (2016). DOI 10.1103/PhysRevLett.116.241103

[189] B.P. Abbott, et al., Multi-messenger Observations of a Binary Neutron Star Merger, Astrophys. J. Lett. **848**(2), L12 (2017). DOI 10.3847/2041-8213/aa91c9

[190] The LIGO Laboratory. Virgo observatory (2021). URL https://www.ligo.caltech.edu/system/media_files/binaries/481/large/O3_detection_count.png?1585251129. [Online; accessed April 7, 2021]

[191] The LIGO Laboratory. Masses of dead stars (2021). URL https://ligo.northwestern.edu/media/mass-plot/index.html. [Online; accessed April 7, 2021]

[192] The LIGO Laboratory. Gw150914 factsheet (2021). URL https://ligo.org/detections/GW150914/fact-sheet.pdf. [Online; accessed April 7, 2021]

[193] The LIGO Laboratory. Gw170817factsheet (2021). URL https://www.ligo.caltech.edu/system/avm_image_sqls/binaries/99/page/GW170817_Factsheet.jpg?1508114118. [Online; accessed April 7, 2021]

[194] F.P. Esposito, Interaction of Gravitational Radiation with an Inviscid Fluid in Simple Motion, The Astrophysical Journal **168**, 495 (1971). DOI 10.1086/151103

[195] J. Ehlers, A.R. Prasanna, R.A. Breuer, Propagation of gravitational waves through pressureless matter, Classical and Quantum Gravity **4**(2), 253 (1987). DOI 10.1088/0264-9381/4/2/009. URL https://doi.org/10.1088%2F0264-9381%2F4%2F2%2F009

[196] J. Ehlers, A.R. Prasanna, A WKB formalism for multicomponent fields and its application to gravitational and sound waves in perfect fluids, Classical and Quantum Gravity **13**(8), 2231 (1996). DOI 10.1088/0264-9381/13/8/016. URL https://doi.org/10.1088%2F0264-9381%2F13%2F8%2F016

[197] J. Winicour, Newtonian gravity on the null cone, Journal of Mathematical Physics **24**, 1193 (1983)

[198] N.T. Bishop, R. Gómez, L. Lehner, J. Winicour, Cauchy-characteristic extraction in numerical relativity, Phys. Rev. D **54**, 6153 (1996)

[199] R. Isaacson, S. Welling, J, J. Winicour, Gravitational radiation from dust, Journal of Mathematical Physics **26**(5), 2859 (1985). DOI 10.1063/1.526712

[200] N.T. Bishop, Gravitational waves in a de sitter universe, Phys. Rev. D **93**, 044025 (2016). DOI 10.1103/PhysRevD.93.044025. URL https://link.aps.org/doi/10.1103/PhysRevD.93.044025

[201] A. Ashtekar, B. Bonga, A. Kesavan, Asymptotics with a positive cosmological constant: II. Linear fields on de Sitter space-time , Phys. Rev. D **92**, 044011 (2015)

[202] A. Ashtekar, B. Bonga, A. Kesavan, Asymptotics with a positive cosmological constant: Iii. the quadrupole formula, Phys. Rev. D **92**, 10432 (2015)

[203] R. Isaacson, J. Welling, J. Winicour, Null cone computation of gravitational radiation, J. Math. Phys. **24**, 1824 (1983)

[204] P.J. van der Walt, N.T. Bishop, Observational cosmology using characteristic numerical relativity, Phys. Rev. D **82**, 084001 (2010). DOI 10.1103/PhysRevD.82.084001. URL https://link.aps.org/doi/10.1103/PhysRevD.82.084001

[205] N.T. Bishop, R. Gómez, L. Lehner, M. Maharaj, J. Winicour, High-powered gravitational news, Phys. Rev. D **56**, 6298 (1997). DOI 10.1103/PhysRevD.56.6298

[206] N.T. Bishop, D. Pollney, C. Reisswig, Initial data transients in binary black hole evolutions, Class. Quantum Grav. **28**, 155019 (2011)

[207] N.T. Bishop, A.S. Kubeka, Quasinormal modes of a schwarzschild white hole, Phys. Rev. D **80**, 064011 (2009). DOI 10.1103/PhysRevD.80.064011. URL https://link.aps.org/doi/10.1103/PhysRevD.80.064011

[208] R. Abbott, et al., GW190814: Gravitational Waves from the Coalescence of a 23 Solar Mass Black Hole with a 2.6 Solar Mass Compact Object, Astrophys. J. **896**(2), L44 (2020). DOI 10.3847/2041-8213/ab960f

[209] B.P. Abbott, R. Abbott, T.D. Abbott, S. Abraham, F. Acernese, K. Ackley, C. Adams, R.X. Adhikari, V.B. Adya, C. Affeldt, et al., Gw190425: Observation of a compact binary coalescence with total mass 3.4 solar mass, The Astrophysical Journal **892**(1), L3 (2020). DOI 10.3847/2041-8213/ab75f5. URL http://dx.doi.org/10.3847/2041-8213/ab75f5

[210] B. Abbott, et al., Observation of Gravitational Waves from a Binary Black Hole Merger, Phys. Rev. Lett. **116**(6), 061102 (2016). DOI 10.1103/PhysRevLett.116.061102

[211] R.H. Price, G. Khanna, Gravitational wave sources: reflections and echoes, Classical and Quantum Gravity **34**(22), 225005 (2017). DOI 10.1088/1361-6382/aa8f29. URL https://doi.org/10.1088%2F1361-6382%2Faa8f29

[212] S.H. Völkel, K.D. Kokkotas, Ultra Compact Stars: Reconstructing the Perturbation Potential, Class. Quant. Grav. **34**(17), 175015 (2017). DOI 10.1088/1361-6382/aa82de

[213] A. Maselli, S.H. Völkel, K.D. Kokkotas, Parameter estimation of gravitational wave echoes from exotic compact objects, Phys. Rev. D **96**(6), 064045 (2017). DOI 10.1103/PhysRevD.96.064045

[214] Z. Mark, A. Zimmerman, S.M. Du, Y. Chen, A recipe for echoes from exotic compact objects, Phys. Rev. D **96**(8), 084002 (2017). DOI 10.1103/PhysRevD.96.084002

[215] K.W. Tsang, M. Rollier, A. Ghosh, A. Samajdar, M. Agathos, K. Chatziioannou, V. Cardoso, G. Khanna, C. Van Den Broeck, A morphology-independent data analysis method for detecting and characterizing gravitational wave echoes, Phys. Rev. D **98**(2), 024023 (2018). DOI 10.1103/PhysRevD.98.024023

[216] B. Abbott, R. Abbott, T. Abbott, F. Acernese, K. Ackley, C. Adams, T. Adams, P. Addesso, R. Adhikari, V. Adya, et al., Gw170817: Observation of gravitational waves from a binary neutron star inspiral, Physical Review Letters **119**(16) (2017). DOI 10.1103/physrevlett.119.161101. URL http://dx.doi.org/10.1103/PhysRevLett.119.161101

[217] R. Gill, A. Nathanail, L. Rezzolla, When Did the Remnant of GW170817 Collapse to a Black Hole?, Astrophys. J. **876**(2), 139 (2019). DOI 10.3847/1538-4357/ab16da

[218] R.S. Conklin, B. Holdom, J. Ren, Gravitational wave echoes through new windows, Phys. Rev. D **98**, 044021 (2018). DOI 10.1103/PhysRevD.98.044021. URL https://link.aps.org/doi/10.1103/PhysRevD.98.044021

[219] F. Salemi, E. Milotti, G. Prodi, G. Vedovato, C. Lazzaro, S. Tiwari, S. Vinciguerra, M. Drago, S. Klimenko, Wider look at the gravitational-wave transients from GWTC-1 using an unmodeled reconstruction method, Phys. Rev. D **100**(4), 042003 (2019). DOI 10.1103/PhysRevD.100.042003

[220] N. Uchikata, H. Nakano, T. Narikawa, N. Sago, H. Tagoshi, T. Tanaka, Searching for black hole echoes from the ligo-virgo catalog gwtc-1, Physical Review D **100**(6) (2019). DOI 10.1103/physrevd.100.062006. URL http://dx.doi.org/10.1103/PhysRevD.100.062006

[221] B. Holdom, Not quite black holes at LIGO, Phys. Rev. D **101**(6), 064063 (2020). DOI 10.1103/PhysRevD.101.064063

[222] K.W. Tsang, A. Ghosh, A. Samajdar, K. Chatziioannou, S. Mastrogiovanni, M. Agathos, C. Van Den Broeck, A morphology-independent search for gravitational wave echoes in data from the first and second observing runs of Advanced LIGO and Advanced Virgo, Phys. Rev. D **101**(6), 064012 (2020). DOI 10.1103/PhysRevD.101.064012

[223] H. Nakano, N. Sago, H. Tagoshi, T. Tanaka, Black hole ringdown echoes and howls, Progress of Theoretical and Experimental Physics **2017**(7) (2017). DOI 10.1093/ptep/ptx093. URL `http://dx.doi.org/10.1093/ptep/ptx093`

[224] P. Bueno, P.A. Cano, F. Goelen, T. Hertog, B. Vercnocke, Echoes of kerr-like wormholes, Physical Review D **97**(2) (2018). DOI 10.1103/physrevd.97.024040. URL `http://dx.doi.org/10.1103/PhysRevD.97.024040`

[225] Y.T. Wang, Z.P. Li, J. Zhang, S.Y. Zhou, Y.S. Piao, Are gravitational wave ringdown echoes always equal-interval?, Eur. Phys. J. C **78**(6), 482 (2018). DOI 10.1140/epjc/s10052-018-5974-y

[226] M.R. Correia, V. Cardoso, Characterization of echoes: A Dyson-series representation of individual pulses, Phys. Rev. D **97**(8), 084030 (2018). DOI 10.1103/PhysRevD.97.084030

[227] Q. Wang, N. Afshordi, Black hole echology: The observer's manual, Physical Review D **97**(12) (2018). DOI 10.1103/physrevd.97.124044. URL `http://dx.doi.org/10.1103/PhysRevD.97.124044`

[228] A. Testa, P. Pani, Analytical template for gravitational-wave echoes: signal characterization and prospects of detection with current and future interferometers, Phys. Rev. D **98**(4), 044018 (2018). DOI 10.1103/PhysRevD.98.044018

[229] E. Maggio, P. Pani, V. Ferrari, Exotic Compact Objects and How to Quench their Ergoregion Instability, Phys. Rev. D **96**(10), 104047 (2017). DOI 10.1103/PhysRevD.96.104047

[230] P. Bueno, P.A. Cano, F. Goelen, T. Hertog, B. Vercnocke, Echoes of Kerr-like wormholes, Phys. Rev. D **97**(2), 024040 (2018). DOI 10.1103/PhysRevD.97.024040

[231] C. Barceló, R. Carballo-Rubio, L.J. Garay, Gravitational wave echoes from macroscopic quantum gravity effects, JHEP **05**, 054 (2017). DOI 10.1007/JHEP05(2017)054

[232] R. Carballo-Rubio, F. Di Filippo, S. Liberati, M. Visser, Phenomenological aspects of black holes beyond general relativity, Phys. Rev. D **98**(12), 124009 (2018). DOI 10.1103/PhysRevD.98.124009

[233] E. Barausse, V. Cardoso, P. Pani, Can environmental effects spoil precision gravitational-wave astrophysics?, Phys. Rev. D **89**(10), 104059 (2014). DOI 10.1103/PhysRevD.89.104059

[234] P. Leung, Y. Liu, W. Suen, C. Tam, K. Young, Quasinormal modes of dirty black holes, Phys. Rev. Lett. **78**, 2894 (1997). DOI 10.1103/PhysRevLett.78.2894

[235] S.W. Hawking, Perturbations of an Expanding Universe, The Astrophysical Journal **145**, 544 (1966). DOI 10.1086/148793

[236] F.P. Esposito, Absorption of Gravitational Energy by a Viscous Compressible Fluid, The Astrophysical Journal **165**, 165 (1971). DOI 10.1086/150884

[237] J. Madore, The absorption of gravitational radiation by a dissipative fluid, Communications in Mathematical Physics **30**(4), 335 (1973). DOI 10.1007/BF01645508. URL https://doi.org/10.1007/BF01645508

[238] A.M. Anile, V. Pirronello, High-frequency gravitational waves in a dissipative fluid, Il Nuovo Cimento B (1971-1996) **48**(1), 90 (1978). DOI 10.1007/BF02748651. URL https://doi.org/10.1007/BF02748651

[239] A. Prasanna, Propagation of gravitational waves through a dispersive medium, Physics Letters A **257**(3), 120 (1999). DOI https://doi.org/10.1016/S0375-9601(99)00313-8. URL http://www.sciencedirect.com/science/article/pii/S0375960199003138

[240] G. Goswami, G.K. Chakravarty, S. Mohanty, A.R. Prasanna, Constraints on cosmological viscosity and self-interacting dark matter from gravitational wave observations, Phys. Rev. D **95**, 103509 (2017). DOI 10.1103/PhysRevD.95.103509. URL https://link.aps.org/doi/10.1103/PhysRevD.95.103509

[241] G. Baym, S.P. Patil, C.J. Pethick, Damping of gravitational waves by matter, Phys. Rev. D **96**, 084033 (2017). DOI 10.1103/PhysRevD.96.084033. URL https://link.aps.org/doi/10.1103/PhysRevD.96.084033

[242] W.H. Press, B.P. Flannery, S.A. Teukolsky, W.T. Vetterling, *Numerical Recipes*, 2nd edn. (Cambridge University Press, New York, 1992)

[243] B.P. Abbott, et al., A guide to LIGO–Virgo detector noise and extraction of transient gravitational-wave signals, Class. Quant. Grav. **37**(5), 055002 (2020). DOI 10.1088/1361-6382/ab685e

[244] G.W.O.S. Center. GW150914 Template Data. https://www.gw-openscience.org/GW150914data

[245] G.W.O.S. Center. Binary Black Hole Signals in LIGO Open Data. https://losc.ligo.org/s/events/GW150914/LOSC_Event_tutorial_GW150914.html

[246] B. Abbott, et al., GW190425: Observation of a Compact Binary Coalescence with Total Mass $\sim 3.4 M_\odot$, Astrophys. J. Lett. **892**(1), L3 (2020). DOI 10.3847/2041-8213/ab75f5

[247] B. P. Abbott et. al., Multi-messenger Observations of a Binary Neutron Star Merger, Astrophys. J. Lett. **848**, L12 (2017). DOI 10.3847/2041-8213/aa91c9

[248] B. Abbott, et al., Observing gravitational-wave transient GW150914 with minimal assumptions, Phys. Rev. D **93**(12), 122004 (2016). DOI 10.1103/PhysRevD.93.122004. [Addendum: Phys.Rev.D 94, 069903 (2016)]

[249] B. Abbott, et al., GW170817: Measurements of neutron star radii and equation of state, Phys. Rev. Lett. **121**(16), 161101 (2018). DOI 10.1103/PhysRevLett.121.161101

[250] A.I. MacFadyen, S.E. Woosley, A. Heger, Supernovae, Jets, and Collapsars, Astrophys. J. **550**, 410 (2001). DOI 10.1086/319698

[251] L.R. Venter, N.T. Bishop, Numerical validation of the Kerr metric in Bondi-Sachs form, Phys. Rev. D **73**, 084023 (2006). DOI 10.1103/PhysRevD.73.084023

[252] A. Einstein, Naherungsweise Integration der Feldgleichungen der Gravitation, Sitzungsberichte der Königlich Preussischen Akademie der Wissenschaften (Berlin) **1916**, 688 (1916)

[253] H. Poincaré, Sur la dynamique de l'électron, Rendiconti del Circolo matematico di Palermo **21**, 129 (1906). DOI 10.1007/BF03013466

[254] J.P. Hsu, Y.Z. Zhang. Lorentz And Poincaré Invariance. Lorentz And Poincaré Invariance. Series: Advanced Series on Theoretical Physical Science (2001). DOI 10.1142/4785. URL https://ui.adsabs.harvard.edu/abs/2001ASTPS...8.....H

[255] A.A. Michelson, H.A. Lorentz, D.C. Miller, R.J. Kennedy, E.R. Hedrick, P.S. Epstein, Conference on the Michelson-Morley Experiment Held at Mount Wilson, February, 1927, Astrophysical Journal **68**, 341 (1928). DOI 10.1086/143148

[256] A.A. Michelson, E.W. Morley, On the Relative Motion of the Earth and of the Luminiferous Ether, Sidereal Messenger **6**, 306 (1887)

[257] G.W.O.S. Center. Gravitational Wave Transient Catalogue. https://www.gw-openscience.org/eventapi/html/GWTC/

[258] N.T. Bishop, P.J. van der Walt, M. Naidoo. Supplementary material for effect of a low density dust shell on the propagation of gravitational waves (2020). URL https://arxiv.org/src/1912.08289v2/anc